This is to certify that the

dissertation entitled

"A Study of Soil-Tire Interactions Using Finite Element Method"

presented by

Adman Degirmencioglu

has been accepted towards fulfillment
of the requirements for

Ph.D. degree in Agricultural Engineering

Major professor

Date 8/25/97

A STUDY OF SOIL-TIRE INTERACTIONS USING FINITE ELEMENT METHOD

VOLUME I

By

ADNAN DEGIRMENCIOGLU

A DISSERTATION

Submitted to
Michigan State University
in partial fulfillment of the requirements
for the degree of

DOCTOR OF PHILOSOPHY

Department of Agricultural Engineering

1997

Tract

and soil. T

anisotropic

tire and the

related studi

behavior in

interface pre

related varia

was a high

interface pre

the finite ele

pressure dist

high axle loa

been studied

on the result

methodology

Element Met

ABSTRACT

A STUDY OF SOIL-TIRE INTERACTIONS USING FINITE ELEMENT METHOD

By

Adnan Degirmencioglu

Traction that can be developed by a tire is a result of the interaction between tire and soil. Tires are complex with respect to the incompressibility of rubber and the anisotropic properties of cord-rubber laminates. The complicated geometrical shape of a tire and the distribution of the loads on the tire have been limiting factors for traction and related studies. Nevethless, considerable progress has been made to understand tire behavior in studies focused on tire-rigid surface interactions. In this study the soil-tire interface pressures were measured and it was found that tires, their size and construction related variables and initial soil conditions are responsible for interface pressures. There was a high correlation between the tire variables and interface pressures. The highest interface pressures from the statistical analysis was found to be at the edge of the tire and the finite element method verified this information. Studies in the past assumed a uniform pressure distribution under a tractor tire. However this is not the case when tires carry a high axle load. Due to the complex nature of the soils, the soil-tire interaction has usually been studied experimentally. The traction models created in the past were usually based on the results of cone measurements that were hard to correlate with soil conditions. A methodology to study soil-tire interaction was developed in this study and a Finite Element Method based study was conducted. The results were used to develop a traction

model that uses

dynamic behavio

the necessary soi

model that uses a dimensionless number called the Rigidity Index which represents the dynamic behavior of the soil under load. In the compact form, the rigidity index includes the necessary soil and tire variables.

This dissertat

DEDICATION

This dissertation is dedicated to my wife, Kadriye and my daughter, Ceylin Degirmencioglu

"To the memory of those years we missed each other"

with my tears..

I wo

Wilkinson fo

I am

member of r

guidance to

encouraged

I wo

Engineering

guidance to

I wa

member. Civ

and for his s

the knowledg

I am

his suggestio

My s

Auburn, Alab

for providing

I wou

Department f

I exte

ACKNOWLEDGEMENTS

I would like to express my sincere thanks to my major professor Dr. Robert H. Wilkinson for his technical, personal guidance and endless support during my studies.

I am grateful to Dr. Ajit K. Srivastava, Agricultural Engineering Department, a member of my committee whose help is appreciated to finish up my studies. His personal guidance to solve many technical problems. His personality has played a vital role and encouraged and lead me to bring this study to an end.

I would like to extend my deepest gratitude to Prof.Larry J.Segerlind, Agricultural Engineering Department for his serving as a member of my committee for his support and guidance to solve my finite element based thesis problem.

I want to also extent my appreciation to Dr. Thomas F. Wolff, a committee member, Civil Engineering Department for his technical support to conduct triaxial tests and for his suggestions to understand the soil mechanics and soil behavior and incorporate the knowledge into this study.

I am grateful to Dr. Alvin J. M. Smucker, Crop and Soil Science Department, for his suggestions to obtain the data and analysis.

My special thanks to the United States Department of Agriculture Personnel in Auburn, Alabama. Drs. Eddie Burt, Alvin Bailey and Thomas Way for their kind support for providing me the data and making this study possible.

I would like to thank Dr. Von Bernuth, Chairperson, Agricultural Engineering Department for his kind support and financial aid to finalize my studies.

I extent my special thanks to the Department of Farm Machinery Personnel for

assisting me. The
thank my friends
Nuray Unlu, Ceyl
James Schaper fo

assisting me. Their encouragement and support for my studies is highly appreciated. I also thank my friends, Ahmet Kizilay, Cem Akyol, Sait Akgun, Gulten Akgun, Oktay Unlu Nuray Unlu, Ceyda Tekin, Salih Armagan, Ali Berker, Ismail Kavdir, Yasemin Kavdir and James Schaper for their help.

TABLE OF CONTENTS

LIST OF TABLES

Page

Table 5.11 I

LIST OF FIGURES

LIST OF APPENDICES

APPENDIX D

APPENDIX E

APPENDIX F

APPENDIX G

APPENDIX H

APPENDIX I

1.1 Economi

An inc

thousand barr

an oil-depend

efficiency of f

Therefore any

agricultural pr

Any at

A basic unders

information wh

has long been

tire in service

determined in

through a se

modifications

The use of an

limited in scop

beyond the dom

Due to i

Chapter 1

INTRODUCTION

1.1 Economic Significance and Magnitude of The Problem

An increasing world oil supply (67680 thousand barrels per day in 1993 and 69397 thousand barrels per day in 1995, US Department of Energy Report) is a natural result of an oil-dependent world. An estimate of annual fuel loss in the U.S. due to poor tractive efficiency of farm units is 575 million liters (Gill and VandenBerg, 1968; Wulfson, 1987). Therefore any improvement that can be made in traction directly affects the efficiency of agricultural production and conservation of fuel energy.

Any attempt to improve traction must also consider the soil compaction problem. A basic understanding of the soil-tire interaction and the soil compaction effect is valuable information when considering and matching of agricultural equipment. The pneumatic tire has long been considered as a simple component. A closer look, however shows that the tire in service is subjected to severe stresses and deformations whose quantities must be determined in order to accurately predict tire performance. Modern tire structures evolved through a series of modifications of the original pneumatic rubber tire. These modifications were based on field experiences and experimental studies of tire behavior. The use of analytical techniques to calculate tire stresses and deformations remained limited in scope for a long time because the complexity of the tire structure placed it beyond the domain of available methods of analysis (Ridha, 1980).

Due to increasing heavy machinery use in recent years, researchers have attempted

to investigate
of tractors an
viewpoints. I
implement inte
to soil propert
the soil in proc
load on the tra
to the soil con
to model a tire
inflation press
wheel-soil inte
tire can be pr
inflation pressu

1.2 Objectives

This di
interaction and
distribution in t

1. To understa
load, inflatio
2. To study the
obtain the de
3. To study the
axle load to c

to investigate the soil-vehicle interaction in greater depth. The selection and management of tractors and implements is a major factor from both the economical and technical viewpoints. In the process of selecting a tractor, information on how the tractor and implement interacts with the soil is important. The information of performance as related to soil properties is key to two areas (Clark,1984) : 1. how the tractor tires interact with the soil in producing traction, and 2. how the implement interacts with the soil in placing load on the tractor. Since the tractor tires and the traffic on soil are the main contributors to the soil compaction, understanding the wheel-soil interaction and results will enable us to model a tire or choose the correct tire variables, such as size and construction, load and inflation pressure to reduce soil compaction. Another important result from modeling wheel-soil interaction is that when interface pressures are known, the traction of a tractor tire can be predicted in a way that is sensitive to soil properties affected by load and inflation pressure.

1.2 Objectives

This dissertation is mainly focused on developing a traction model, the soil-tire interaction and understanding soil-tire interface pressure distribution as well as the stress distribution in the soil under various tire and soil conditions. The specific objectives were:

1. To understand the effects of soil (soft or firm) and tire variables (size, construction, load, inflation pressure and slip) on soil-tire interface pressures.
2. To study the deformations that take place in tires under inflation pressure axle load to obtain the deformations.
3. To study the tire behaviour on a rigid surface varying both the inflation pressure and the axle load to obtain the deformations.

4. To simulate t

5. To develop a

6. To develop

behavior of

7. To understa

4. To simulate tire-soil interaction under different tire operating and initial soil conditions.
5. To develop a methodology to study the soil-tire interaction.
6. To develop and test a theory based traction model by incorporating the elasto-plastic behavior of the soil.
7. To understand the effects of soil and tire variables on traction.

Soil

topics for

agricultural

been condu

distributed

variability

variables c

experiment

computer

that use th

problems s

most reser

stressed th

non-linear

soil compa

from a hugg

no model i

Chapter 2

LITERATURE REVIEW

Soil-tire interaction problem has been one of the most challenging and studied topics for many researchers in the past. Due to the complex nature of the pneumatic agricultural tire and difficulty of modeling soil behavior under load, separate studies have been conducted. Most studies have used the assumption that the tire load is uniformly distributed over the contact area. The use of radial tires in agriculture along with the variability of sizes available has complicated the investigation of the effect of tire and soil variables on soil compaction and traction. The cost and time requirement of such experiments are also limiting factors for investigations. These factors suggest that the computer model may be an expedient way to study this problem. Computer based studies that use the theory of elasticity and plasticity have been successfully applied to some problems separately. The finite element method as a numerical method is the one that most reserachers suggested to study the soil and tire behavior. Schafer et al. (1992) stressed the importance of this by mentioning that the finite element method, modified for non-linear stress-strain behavior, may be an important link between "traction models and soil compaction models. Wood et al. (1988) found that the surface pressure distribution from a lugged tire is not uniform and varies with soil conditions. Wood also implied that no model incorporates the surface pressure distribution.

2.1 Tr

2.1.1 T

Flotatic

Load.

support

This fo

Load, s

surface

and zer

Load tr

vehicle

Motion

Motion

traction

Power,

direction

Power, i

a tractio

Power, o

device.

Pull, draw

2.1 Traction and Traction Modeling

2.1.1 Traction Terminology

Flotation: Ability to resist sinkage into the medium being traversed.

Load, dynamic [W]: Total force normal to the reference plane of the predisturbed supporting surface exerted by the traction or transport device under operating conditions. This force may result from ballast and/or applied mechanical forces (Figure 2.1).

Load, static: Total force normal to the reference plane of the predisturbed supporting surface exerted by the traction or transport device while stationary with zero net traction and zero input torque.

Load transfer: The change in normal forces on the traction and transport devices of the vehicle under operating conditions, as compared to those for the static vehicle.

Motion resistance ratio [p= MR/W]: Ratio between motion resistance and dynamic load.

Motion resistance of transport device [MR= GT - NT]: The difference between gross traction and net traction (Figure 2.2).

Power, drawbar [DP= p.V]: The product of drawbar pull and vehicle velocity in the direction of travel.

Power, input [T.]: The product of input torque and angular velocity of the driving axle of a traction device.

Power, output [NT.V]: The product of net traction and forward velocity of a traction device.

Pull, drawbar [P]: Force in the direction of travel produced by the vehicle at the drawbar.

Figure 2.1 Basic v
force (

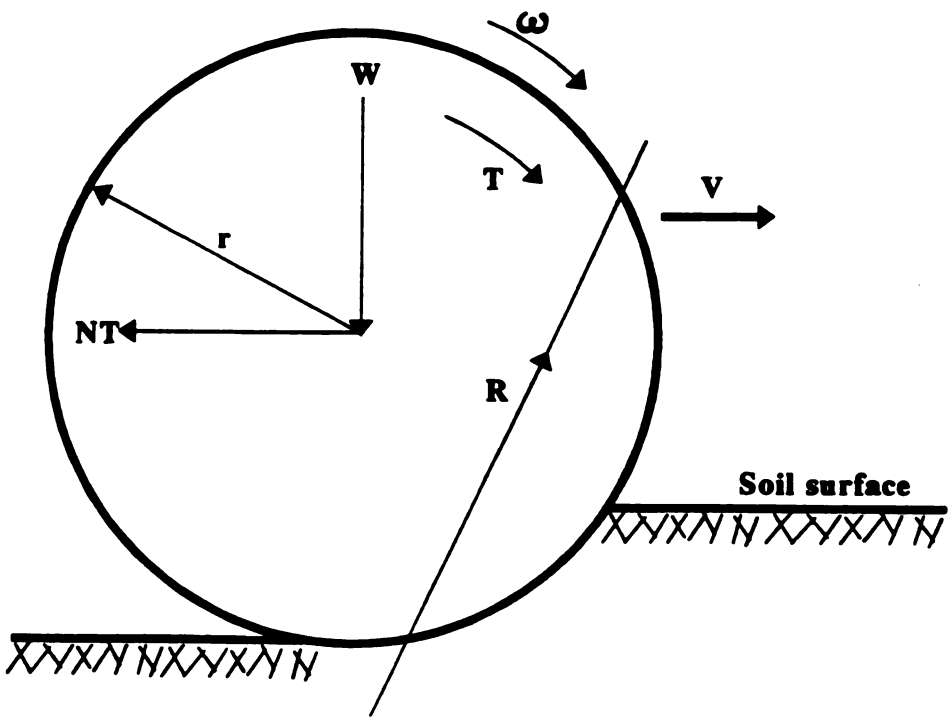

Figure 2.1 Basic velocities and forces on a single wheel with resultant soil reaction force (ASAE Standard:ASAE S296.3,1994)

Figure 2.2

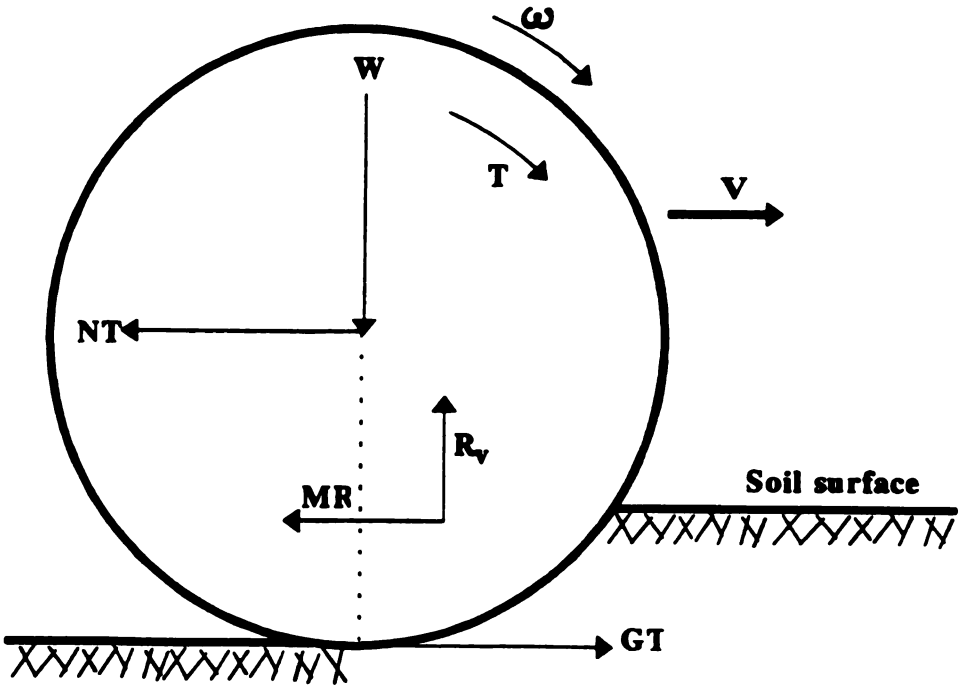

Figure 2.2 Basic velocities and forces on a single wheel with component soil reaction forces (MR and Rv act at soil-tire interface, ASAE Standard:ASAE S296.3, 1994)

Rolling c

device w

determine

Rolling ra

specified)

Slip [s]: A

transport

one minus

condition

Soil reacti

in the supp

Thrust: To

measureme

Torque [T]

Traction, n

torque by th

2.1.2 Tire T

Bias-ply tire

(Figure 2.3).

Breaker plies

Cinch band o

Rolling circumference, zero conditions: Distance traveled per revolution of the traction device when operating at the specified zero condition. Rolling circumference may be determined on the test surface or another surface.

Rolling radius [r]: Rolling circumference divided by 2π (r_o when zero conditions are specified).

Slip [s]: A measure of relative movement at the mutual contact surface of the traction or transport device and the surface which supports it, expressed in percent and computed as one minus the travel ratio when the rolling circumference is defined at the self-propelled condition on a hard surface or test surface at the test load and inflation pressure.

Soil reaction force [R]: The resultant of all forces acting on the traction device originating in the supporting surface (Figure 2.1)

Thrust: Total force in the direction of travel as determined from tangential stress measurements at the soil-traction interface.

Torque [T]: The driving moment in the axle of the traction device (Figure 2.1).

Traction, net [$GT= T/r_o$]: Total force in the direction of travel as defined by the input torque by the rolling radius, at a specified zero condition.

2.1.2 Tire Terminology

Bias-ply tire: A tire in which the cords of the body plies run diagonally from bead to bead (Figure 2.3).

Breaker plies: Plies of cord material, in bias-ply tires, that do not tie into the beads.

Cinch band or belt: Plies of cord material under the tread area of a tire having the cords

nearly p

beads bu

Deflecti

Deflecti

beyond t

End-of-l

follows (

Inflation

any posit

and with

Loaded r

tire when

recomme

Lug angl

(Figure 2.

Lug base

planes of

section A-

Lug face:

Lug fillet:

2.4, sectio

nearly parallel to the centerline of the tire (Figure 2.4). These cords do not tie into the tire beads but furnish circumferential strength for the tire.

Deflection, tire: [=(tire diameter/2)-(radius at a static load)] (Figure 2.5).

Deflection, percent tire: Tire deflection divided by that portion of the tire section height beyond the rim flange, expressed as a percentage.

End-of-lug clearance: Distance from trailing side of a lug to the end of the lug that follows (Figure 2.4).

Inflation Pressure: For air-filled tires, it is the gauge pressure measured with the valve in any position. For tires containing liquid, it is the gauge measured with an air-water gauge and with the valve in the bottom position.

Loaded radius (static): Distance from the center of the axle to the supporting surface for a tire when inflated to recommended pressure, mounted on an approved rim and carrying recommended load (Figure 2.5).

Lug angle: The angle between the centerline of the lug face and the centerline of the tire (Figure 2.4).

Lug base: The projected thickness of width of the lug at the points where projected planes of the leading and trailing sides meet the projected undertread face (Figure 2.4, section A-A).

Lug face: The outermost surface of the lug (Figure 2.4, section A-A).

Lug fillet: The curved section which blends the lug sides into the undertread face (Figure 2.4, section A-A).

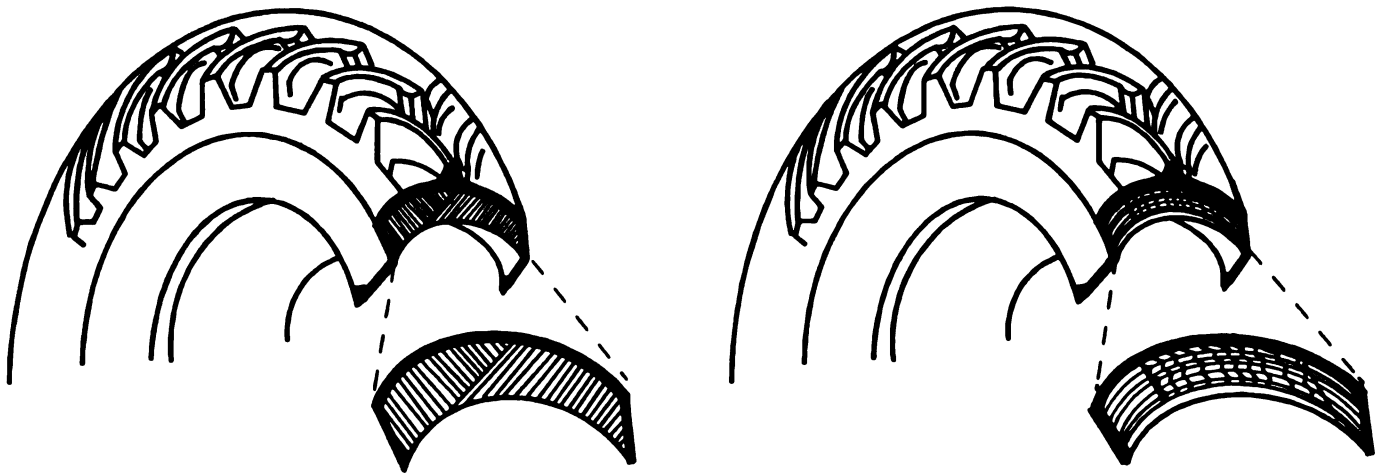

Bias-ply tire

Radial tire

Figure 2.3 Bias-ply and radial agricultural tires.

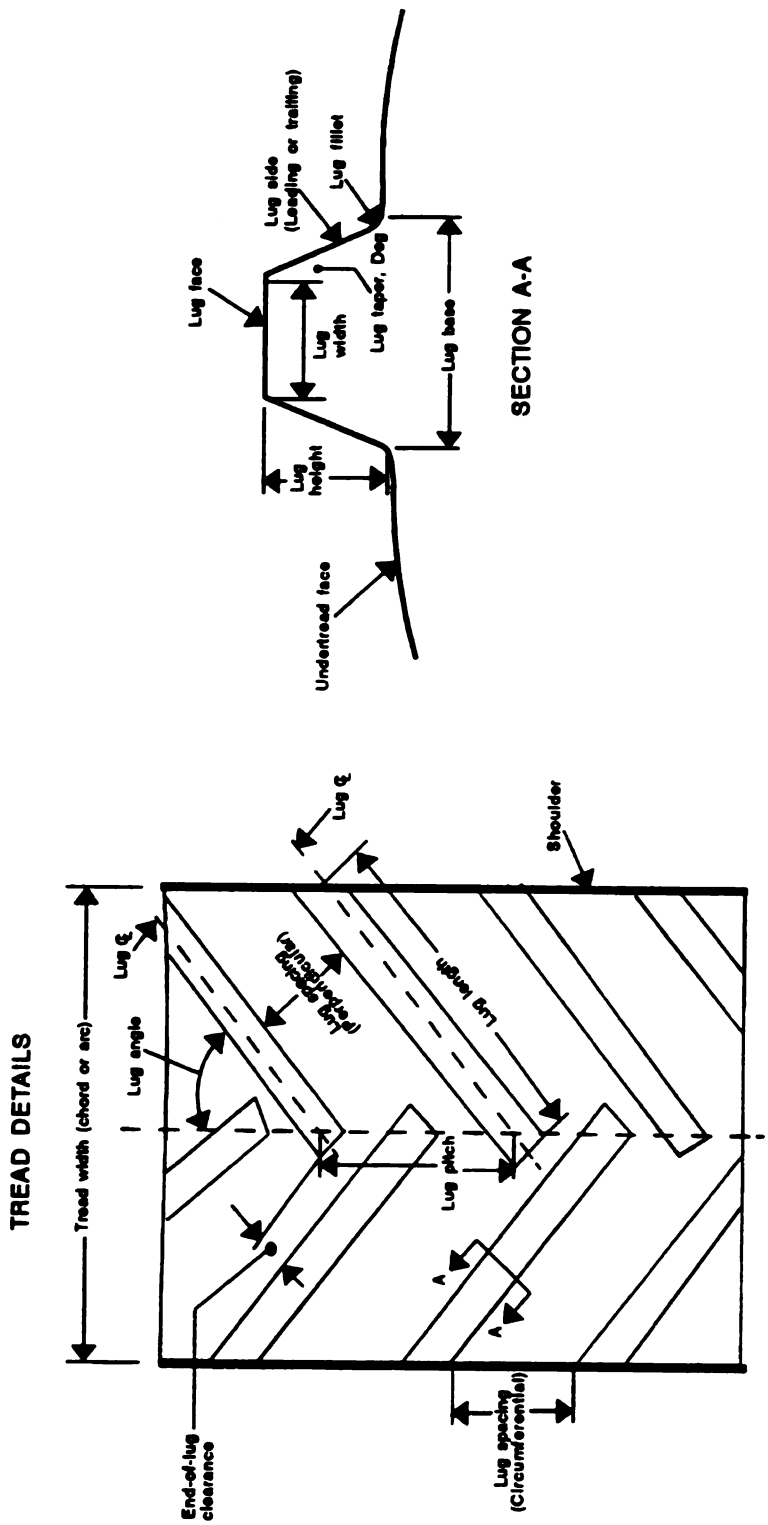

Figure 2.4 Tractor tire lug and tread diagram (ASAE Standard:ASAE S296.3, 1994)

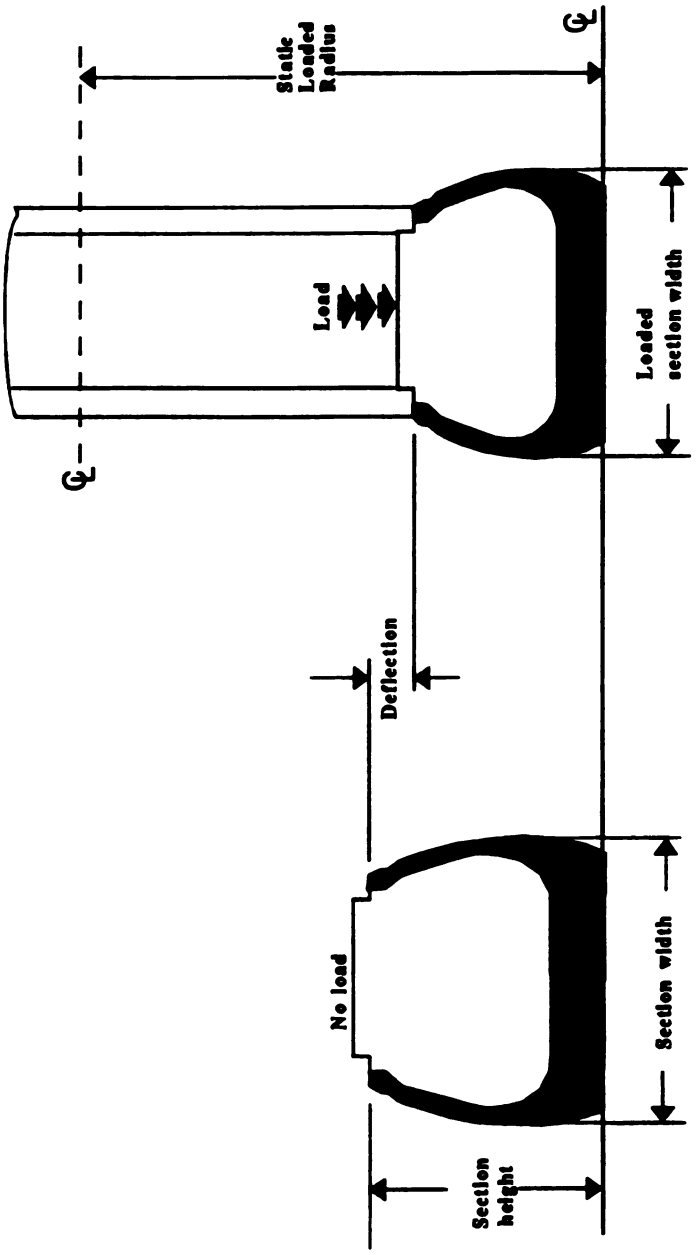

Figure 2.5 Tire and rim dimensions (Srivastava, et al, 1993)

Lug height: Distance measured from the undertread face to the lug face (Figure 2.4, section A-A).

Lug length: Distance measured from end to end along the centerline of the lug face (Figure 2.4).

Lug pitch: Center-to center spacing (circumferential) of lugs on one side at the centerline of the tire at the lug face (Figure 2.4).

Lug side: The lug surface between the undertread face and the lug face (Figure 2.4, section A-A).

Lug spacing, circumferential: The distance from the leading side of a lug to the trailing side of the lug ahead of it, measured parallel to the centerline of the tire at the lug face (Figure 2.4).

Lug spacing, perpendicular: The distance, measured perpendicularly, from the leading side of a lug to the trailing side of the lug ahead of it at the lug face (Figure 2.4, section A-A).

Lug width: Width of lug face measured perpendicularly to the centerline of the lug face (Figure 2.4, section A-A).

Overall width: The width of a new tire, including normal growth caused by inflation, and including protective side ribs, and decorations (Figure 2.6).

Ply rating: Identification of a given tire with its maximum recommended load when used in a specific type service. It is index of tire strength and does not necessarily represent the number of cord plies in the tire.

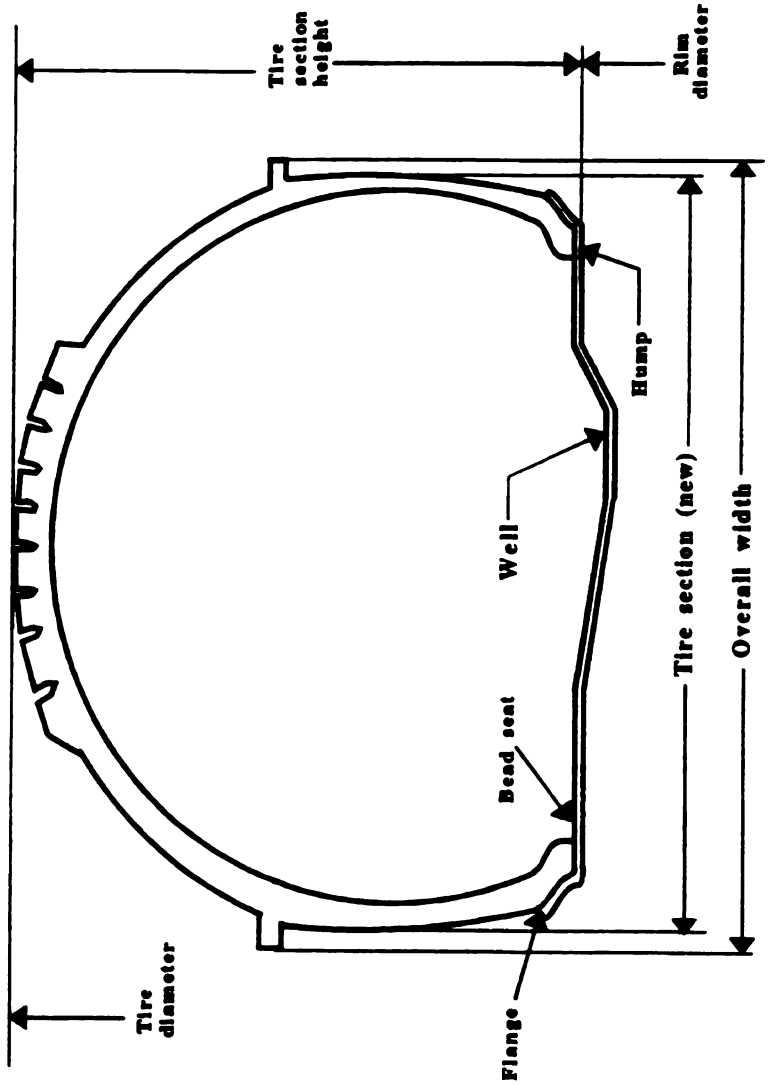

Figure 2.6 New tire and rim dimensions (ASAE Standard:ASAE S296.3, 1994)

Radial-ply tire: A tire which the cords of the body plies run radially from bead to bead (Figure 2.5).

Rim diameter: The nominal diameter at the intersection of the bead seat and the vertical portion of the rim flange (Figure 2.6).

Tire diameter: Tire circumference measured over the lugs in the center plane divided by π with the tire mounted on its recommended rim and inflated to recommended operating pressure in an unloaded condition (Figure 2.6).

Tire section width: The width of a new tire, including normal growth caused by inflation and including normal side walls but not including protective side ribs, bars or decorations (Figure 2.5 and 2.6).

Tire section height: The height of a new tire, including normal growth caused by inflation, measured from the rim diameter to the point of maximum radius, on the lug face (Figure 2.5 and 2.6).

Tread radius: The radius of curvature of the lug faces measured at right angles to the center plane of the tire width. the tire mounted on its recommended rim and inflated to recommended pressure (usually not constant).

Tread width: The distance from shoulder to shoulder (Figure 2.4)

Undertread face: The outer most surface of the rubber on the carcass where no lugs are located (Figure 2.4, section A-A).

2.1.3 Traction Models

Stress-strain behavior of soil under a tractor tire is important in traction modeling. Upadhyaya et. al. (1987) indicated that soil parameters such as cohesion, angle of internal friction and soil shear modulus may help in predicting traction. They also pointed out that soil cone index and moisture content are not sufficient predictors of soil condition for the purpose of predicting traction and that changes in soil condition significantly influence tire performance.

In reviewing the traction models, Upadhyaya and Wulfson (1990) suggested that analytical methods based on elasto-plasticity or critical state soil mechanics, yield criteria and associated plasticity flow are expected to be the key to a better understanding of this complex problem. They also indicated that the difficulty in prescribing proper boundary conditions at the soil-tire interface can be overcome by modeling the soil-tire system in a comprehensive model. Such a model involves geometric non-linearity of large strain and deformation along with gap-closure at the contact boundary. They also pointed out that this type of model requires knowing fundamental engineering properties of soil in order to relate stress-strain and define yield criterion.

The semi-empirical approach utilizes two analog devices to represent soil-traction device interaction. Vertical deformation of the soil under load is assumed analogous to soil deformation under a plate. The shear deformation of the soil under a traction device is assumed to be similar to the shear due to a torsional shear device or a rectangular grosser unit. The normal stress under a flat plate is assumed to be the form (Bekker, 1960);

$$p = \left(\frac{k_c}{b} + k_\Phi \right) z^n \qquad (2.1)$$

where,

p= Normal pressure under plate

b= minimum dimension of a rectangular plate (equal to the diameter for a circular plate)

z= sinkage

k_c, k_ϕ, n= soil parameters

The empirical method is based on evaluation of the soil physical properties in the field. Soil cone index has been used as a soil strength parameter. Dimensional analysis has been used to form a dimensionless term called wheel numeric. For cohesive-frictional soil, Wismer and Luth (1974) defined the wheel numeric as,

$$C_n = \frac{CIbd}{W} \qquad (2.2)$$

where,

CI= cone index

b= section witdh of tire

d= diameter of tire

W= axle load

Using the above term, Wismer and Luth (1974) developed the following widely accepted traction equations for soils that are not "highly compactible";

$$\frac{R}{W}=\left(\frac{1.2}{C_n}\right)+0.04 \tag{2.3}$$

$$\frac{P}{W}=0.75\left(1-\exp^{-0.3\,C_n S}\right)-\left(\frac{1.2}{C_n}+0.04\right) \tag{2.4}$$

where,

P= pull

R= rolling resistance

C_n= wheel numeric

S= slip (in decimals)

Karafiath and Nowatzki (1978) discussed the results of empirical approach. They indicated that the results of cone penetration tests in frictional-cohesive soils may leave doubt about whether performance curves for purely frictional or purely cohesive soils should be used. Even worse, the non-homogeneity of natural soil and moisture content variations with depth may cause cone penetration measurements to be erroneously interpreted as indicative of purely frictional or purely cohesive soils. The point is that the cone penetration resistance is not a reliable measure of soil strength and the results of cone penetrometer tests are highly dependent on subjective interpretation. Thus, over-simplification of the complex problem of tire-soil interaction by relating tire performance

to results of cone penetration tests may be attractive at the first glance but can not be considered as an absolute solution of the general problem.

The mechanical properties of the terrain are undoubtly among the most important factors that affect off-road mobility. The mechanics of soil must be included in the broader context of terrain-vehicle interaction that ultimately determines mobility.

The logical approach to the various problems of mobility must follow a sequence of development of theories and field techniques. The first step in such an approach is the definition of the mobility problem with respect to the basic parameters involved. Then, a concept describing interactions among the vehicle, tire and soil parameters has to be developed into a soil mechanics theory.

Clark (1984) studied the importance of each coefficient in the generalized form of the Wismer & Luth model;

$$\frac{NT}{W} = c_6\left(1-\exp^{c_7 C_n s}\right)-\left(\frac{c_4}{C_n}+c_5\right) \qquad \textbf{(2.5)}$$

where,

c_4 and c_5= constants depending on soil surface

c_6= constant representing the maximum (NT/W) ratio

c_7= constant depending on soil surface and tires.

For cone index changing between 0 and 5 MPa, Clark showed that the order of decreasing importance for the coefficients was c_6, c_7, c_5 and c_4. Clark then used test data

and statistical analysis to obtain optimum coefficients for a front-wheel assist tractor on three types of soil surfaces: short mowed grass on a soil that had not been disturbed for at least five years; tall, dense and approximately one foot high grass on a soil undisturbed for at least five years; and a bare soil surface disked one month before the test and having received some soaking rain.

VandenBerg and Reed (1962) studied the three carcass design factors; ply arrangement, flatness of tread base, and rim width effect on tractive performance. From their study they concluded that:

1) Radial-ply carcass construction does not affect maximum traction but does improve traction performance in the normal operating range of 0 to 30 percent travel reduction. For the five conditions tested, the average improvement due to radial ply was 15% for lugged tires. the performance was attained with a small gain in efficieny.
2) Narrow rims and a flattened tread base also improved tractive performance in the 0 to 30 percent travel-reduction range, but each had approximately one-half the effect of radial-ply construction.

McRae (1964) developed an equation to predict the towed force based on the sinkage of a wheel on soil. The model that was developed was in the form of (Figure 2.7);

$$P_t = W\left(\frac{z}{l}\right) \tag{2.6}$$

where,

Pt= towed force for towed wheel

W= vertical load on the wheel

Z= sinkage

l= horizontal projection of the center line of tire contact in the line of travel

McRae (1967) developed two new equations, one for towing resistance for a single wheel which appears to hold equally well for dry sand and wet clay, an one for maximum drawbar pull for a single wheel. The following semiempirical formula was developed for towing resistance for a single wheel;

$$P_t = 0.85\left(\frac{Z}{l}\right)^{0.77} \tag{2.7}$$

For maximum drawbar pull, the formula given below was also developed for a single wheel;

$$P_m = \left(\frac{CI}{12.5} \cdot A \cdot \cos\alpha\right) - 0.85\, W\left(\frac{z}{l}\right) \tag{2.8}$$

where,

Pt, Z, and l defined above and shown in Figure 2.7

A= Area of soil-tire interface

The major assumptions McRae (1964) made to develop the equations were;

1. The machine has sufficient horsepower to utilize the full shearing resistance of the soil and is utilizing the ultimate soil shear strength over the wheel contact area.

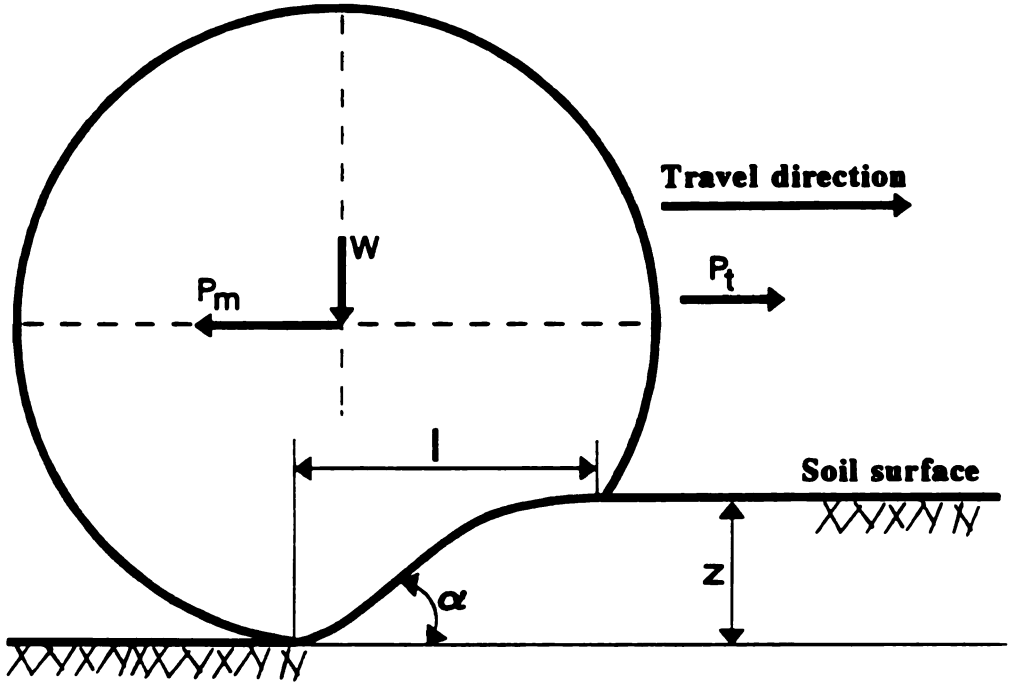

Figure 2.7 Tire and soil variables as used in equations 2.6, 2.7 and 2.8 (McRae, 1964)

2. The shearing resistance between tire and soil is equal to or greater than the ultimate shear strength of the soil.

3. The effective shear strength of the soil can be determined.

4. The towing resistance formula given above is applicable.

Domier and Persson (1968) studied the tire and soil variables and their effect on drawbar performance. They concluded that;

1) Increased tire diameter resulted in increased tire performance except for one case where an interaction between tire pattern and soil moisture was indicated.

2) On a firm soil surface differences in tire performance were due to a diameter effect, whereas on loose soil surfaces the increase in performance characteristics could be accounted for by the "load factor effect".

3) The drawbar horsepower of seven tractors was predicted from basic parameters obtained with a standard tractor. The agreement between predicted and measured output was reasonable taking into consideration natural soil variability and the testing procedure used.

Wittig and Alcock (1990) developed a single wheel tester using a small drive wheel mounted behind a tractor to measure topsoil traction conditions by measuring the maximum transferable torque for known loads. Drawbar pull tests were run simultaneously with a Ford 8000 tractor fitted with Goodyear 18.4-38 Dyna-Torque II rear tires inflated at 100 kPa. Cone index, soil moisture content and bulk density

recorded. Non-linear regression analysis was used to compare the measured tractor coefficient for net traction for the tractor values predicted by the Wismer-Luth model with respect to slip. A linear relationship was found between wheel torque and dynamic load measured with the single-wheel tester. Stepwise regression analysis was then used to obtain a model relating the tractor net traction coefficient to soil moisture content and bulk density, slope of the torque/dynamic load curve, and a dimensionless number computed for each soil surface. This number, called test wheel numeric, was similar in meaning to the wheel numeric C_n used in the Wismer-Luth model, but was computed, for each soil surface, as the average maximum torque observed with the wheel tester, divided by the product of wheel dynamic load and rolling radius, (Tmax/(W rR)) ave. Cone index, and therefore C_n, were rejected as traction indicators because of the large scatter in cone index values throughout a same soil.

Brixius (1987) developed equations to predict the tractive performance of bias-ply tires operating in cohesive-frictional soils. Prediction equations for the torque and motion resistance ratios were developed using curve-fitting techniques to analyze results from field tests of 121 soil-tire combinations. Data were obtained in separate experiments by USAE Waterways Experiment Station, National Institute of Agricultural Engineering, U.S. Army Tank Automotive Command and Deere & Company.

The equations developed for a wheel driven through soil were developed in the following form;

$$\frac{Q}{rW}, \frac{M}{W} = f\left(\frac{CIbd}{W}, S, \frac{b}{d}, \frac{\delta}{h}\right) \tag{2.9}$$

where,

Q/rW: Torque ratio

r: rolling radius of tire

W: Dynamic load

S: Slip

CI: Cone index

b: Wheel width

d: Wheel diameter

δ: deflection

h:Section height

M/W: Motion resistance ratio

Using dimensional analysis, Brixius introduced a new dimensionless term called mobility number that accounts for the deflection of tire and it is given in the following form;

$$B_n = \left(\frac{CIbd}{W}\right)\left(\frac{1+5\frac{\delta}{h}}{1+3\frac{b}{d}}\right) \tag{2.10}$$

where,

B_n: Mobility number

The mobility number is used in the equations to predict the combined effect of the soil-wheel parameters on tractive performance of a tire. Torque ratio is given in the following form;

$$\frac{Q}{rW}=0.88(1-\exp^{-0.1B_n})(1-\exp^{-7.5S})+0.04 \qquad (2.11)$$

Motion resistance ratio has the form;

$$\frac{M}{W}=\frac{1}{B_n}+0.04+\frac{0.5S}{\sqrt{B_n}} \qquad (2.12)$$

Brixius described the causes of motion resistance by several factors:

1. Tire flexing and scrubbing (hard surface)
2. Compaction of soil
3. Bulldozing of soil to the side
4. Lateral drag caused by soil adherence and viscosity

Combining the torque and motion resistance ratio Brixius introduced the new traction model as in the form of;

$$\frac{P}{W}=0.88(1-\exp^{-0.1B_n})(1-\exp^{-7.5S})-\left(\frac{1}{B_n}+\frac{0.5S}{\sqrt{B_n}}\right) \quad (2.13)$$

where,

P/W: Pull ratio

Brixius also introduced an equation to predict the performance of the rear wheels; The equation introduced was for the prediction of cone index that is altered due to passes of the front wheels on soil and compacting the soil and causing less motion resistance and so increasing the traction of rear wheels. The relationship between after traffic (ATCI) and before traffic cone index (BTCI) is given as;

$$\frac{ATCI}{BTCI}=1+1.8\exp^{-0.11B_n} \quad (2.14)$$

Zoerb et al. (1988) conducted a computer simulation based study using the traction equations developed by Gee-Clough et al.(1978). The conclusions drawn from the study are:

1. The range of traction coefficient for maximum tractive efficiency is from 0.3 to 0.4. The average traction coefficient value of 0.36, or the weight/pull ratio of 2.8, can be used for normal farm tractor design and operation.

2. For 4WD tractors, if implement draft is constant, the tractive efficiency becomes maximum when the traction coefficient of the front wheels equals to that of the rear wheels from the theory by Gee-Clough et al. (1978).

The field tests of a 4WD tractor and the laboratory tests of a 4WD model tractor proved to some extent the analytical result. The model tractor tests showed the tractive efficiency was dependent upon the dynamic wheel load ratio. The result indicated the tractive efficiency was higher when the dynamic wheel load ratio was greater than one. The tests showed a potential advantage to the practice of shifting ballast from front to rear or vise versa.

Evans et al. (1989) developed a traction and ballast selection model. A traction prediction equation and ballast selection model based on the traction prediction equations of Brixius (1987) was developed. Evans et al. from their study concluded that the model may predict the pull from a small front wheel assist tractor operating on a grass surface if the slip parameter is changed.

Wittig and Alcock (1990) developed a new method of predicting the drawbar pull developed by agricultural tractors. A single wheel tester was used to establish topsoil traction conditions by loading the tire with known loads and measuring the maximum transferable torque. As a conclusion from their study, Wittig and Alcock concluded that the soil cone penetrometer was shown to be an unsuitable device for characterizing the ability of the topsoil to support traction and the Wismer and Luth prediction equation, which uses only cone index as a soil parameter, gave predictions for coefficient of traction

that were consistently less than the measured values. They also indicated that the changes in topsoil conditions have a greater impact on traction than differences among tires.

Grisson et al. (1991) evaluated the tractive performance of 18.4R42 and 18.4R46 tractor tires mounted on 2WD and MFWD agricultural tractors on three different firm soil conditions. They concluded that when the 2WD tractor operated on a disked surface, the tractive efficiency of the 18.4R42 tires was slightly higher than the 18.4R46 tires. The MFWD tractor, operated with single rear tires, tended to pull more at a given slip than a MFWD equipped with duals. The results obtained showed no tractive advantage of 18.4R46 tires over 18.4R42 tires. The results were influenced by high tire inflation pressures and firm soil conditions. These factors reduced the advantage of radial tires.

Bashford, Al-Hamed and Jenane (1992) compared the dynamic traction ratio and tractive efficiency for a tractor equipped with three different size rear tires each operating at three different inflation pressures and two different soil surfaces were used. The followings were concluded from their study,

1. On a stubble field, tires with lower inflation pressures exhibited better tractive performance.
2. On a plowed surface, the 42-inch rim diameter tire exhibited better tractive performance at the lower inflation pressure.
3. On a plowed surface, the tractive performance of the 46-inch rim diameter tire was inconsistent with inflation pressure.

4. On a stubble surface, the larger diameter tires exhibited better tractive performance than the smaller diameter tires at 18-psi inflation pressure.
5. On a plowed surface, the 46-inch rim diameter tire performed better than the 54-inch tire which performed better than the 42-inch tire with the inflation pressure constant at 18-psi.

Gu and Kushwaha (1992) studied the effect of dynamic load distribution on the tractive efficiency, traction ratio and power distribution of a 1/4 scaled model tractor under two different soil conditions. The effects of the interactions of dynamic load distribution with slip, total dynamic load were investigated. They concluded that;

1. The similitude analysis and the tests of the model tractor indicated that the design of the model tractor had satisfied the essential model similarity requirements.
2. The statistical analysis of the data obtained in the soil bin showed that the dynamic load distribution significantly affected the tractive performance. The interactions of dynamic load distribution with slip and total dynamic load were also significant. The effect of dynamic load distribution on the tractive performance was larger on tilled soil than on packed soil.
3. A method to investigate the relationships of dynamic load ratio, slip and tractive performance of 4WD tractors was proposed.
4. The model tractor soil bin tests showed that the maximum tractive efficiency occurred at slip levels of 10 to 12% in 4WD mode. The corresponding pull/weight ratio for a 4WD tractor was found to be 0.32.

5. When slip was larger than 7%, the power distribution was affected only by the dynamic load distribution. The torque distribution was more sensitive to dynamic load distribution on tilled soil. The dynamic load distribution should be around 48% on tilled soil and 54% on packed soil to reduce the power train wear and maintain uniform power distribution between the axles.

Self and Summers (1988) investigated the effects of wheel speed ratio, dynamic load distribution, forward velocity, wheel slip and soil cone index on tractive performance. From the field experiment and regression equations developed, the following conclusions were made:

1. Motion resistance as measured by self-propelled torque ratio was significantly affected by wheel speed ratio, dynamic load ratio, and a three way interaction of dynamic load ratio, wheel speed ratio and slip. The effects of the three way interaction could not be quantified.
2. Self-propelled torque ratio for each axle was increased by a) increasing the wheel speed of the axle in relation to the other axle; b) shifting dynamic load from the axle to the other axle; c) and decreasing soil strength as measured by cone index.
3. Dynamic traction ratio for a four-wheel drive tractor was significantly affected by wheel speed ratio, dynamic load ratio,wheel slip and a three way interaction of these same parameters. The effects of the three way interaction could not be quantified.
4. To maintain maximum dynamic traction ratio as wheel speed ratio or undisturbed soil cone index increases, front dynamic load must be increased.

5. Tractive efficiency was significantly affected by dynamic load ratio, wheel slip, and two way interaction, dynamic load ratio by wheel speed ratio and dynamic load ratio by wheel speed ratio by slip.
6. As dynamic load on the front axle decreases, wheel speed ratio must increase to maintain maximum tractive efficiency.
7. Maintaining a dynamic load distribution of 35 to 45 % front dynamic load should result in adequate tractive performance for wheel speed ratios seen on most agricultural tractors and a wide range of soil conditions.

Turner (1993) developed a simple instrumentation and test procedure to measure power delivery parameters on a farm tractors during field operation. The system does not measure standard tractive efficiency, but instead measures an alternative or substitute called power delivery efficiency. results with this method show the same accuracies, trends and principles as classic traction efficiency measurement techniques. The developed system requires significantly less set-up and commitment than traditional approaches, and directly benefits farmers as they set up their tractors.

Godbole and Alcock (1992) presented a new approach to the traction prediction equation. They proposed an equation of the form;

$$\frac{P}{W}=\left(\frac{A}{W}C+\tan\phi\right)\left[1+\frac{K}{il}(\exp^{\frac{-il}{K}}-1)\right] \qquad (2.15)$$

where,

A: Contact area

l: Contact length

i: Slip

K: Soil deformation modulus

P: pull

W: Axle load

The values of the deformation modulus, K, were determined from shear-displacement curves for different levels of normal stress, . The value of K was interpreted as the ratio of maximum shear stress (max) and the slope of the tangent drawn at the origin of each curve.

$$K=\frac{\tau_{max}}{slope_{(0,0)}} \tag{2.16}$$

Thus, as a result of their study, Godbole and Alcock suggested that an exact definition of soil modulus, K, needs to be established but some other factors affecting K such as moisture content, bulk density have to be studied.

Taylor et al. (1976) compared a radial and a bias tire on soft and firm soil in terms of tractive efficiency. Their results showed that:

1. The coefficient of net traction for the radial tire exceeded that for the bias tire from 6 to 18 percent (at 15 percent travel reduction) in five of the seven soil conditions.

2. The tractive efficiency of the radial tire was slightly higher than that of the bias tire across the full range of travel reduction in five of the seven soil conditions.

It was concluded from their study that the radial ply tire had its great advantage on firm surfaces where most of the soil-tire deformation took place in the tire, and that this advantage was gradually lost as the soil became softer, causing more of the total soil-tire deformation to take place in the soil and less in the tire.

Burt et al. (1979) tested pneumatic tires for various soil conditions and determined that dynamic load, as well as, travel reduction (slip) plays an important role in tractive performance. The data indicated that in many field conditions tractive efficiency could be improved by selecting an appropriate dynamic load for a particular soil condition. From their study, Burt et al. (1979) concluded that;

1. The performance of pneumatic tires is a function of both dynamic load and travel reduction.
2. The reciprocal of the rolling radius for a given tire and soil condition is a linear function of dynamic load.
3. At constant travel reduction, tractive efficiency increases with dynamic load on compacted soil and decreases with increases in dynamic load on soils that have an uncompacted subsurface.
4. Input power is linear with respect to dynamic load and nonlinear with respect to travel reduction.
5. Output power is nonlinear with respect to both dynamic load and travel reduction.

Burt et al. (1982) studied the effects of ballast and inflation pressure on tractive efficiency of bias and radial-ply tractor tires operated under field conditions. The results indicated that at constant drawbar pull, the tractive efficiency of both radial-ply and bias-ply tires can be maximized by selecting appropriate levels of dynamic load and inflation pressure. Other results found by Burt et al. (1982) are summarized as follows;

1. The differences in tractive efficiency found between the least efficient condition tested and the most efficient condition tested is dependent on soil condition and tire construction.
2. Maximum tractive efficiency does not necessarily occur at the minimum travel reduction required to develop a given level of drawbar pull. Therefore, if a control system is designed to maximize tractive efficiency, the system will need to select dynamic load and inflation pressure values based on maximum tractive efficiency rather than values based on minimum travel reduction.

Taylor et al. (1982) focused on the multipass behavior of a pneumatic tire in tilled soils. A 13.6-38 tractor tire was operated at the recommended load of 16.3 kN and also at half load to simulate dualing. They ran the tire in three different soils. Each soil was freshly tilled and loose before the first pass. Results showed that both net traction and tractive efficiency significantly lower on the first pass than on subsequent passes. Sinkage and bulk density changes were noted after each of the four passes.

Gee-Clough et al. (1982) used empirical equations developed to obtain a curve giving the drive tire load per unit of available axle power which is required to ensure that a

drive tire can work at maximum tractive efficiency at any forward speed. Gee-Clough et al. (1982) from the study concluded that in order to obtain maximum power output from a wheeled tractor working a frictional cohesive soil, the following things must be done;

1. For a given axle power and working speed, the load on the drive tires must be adjusted to the value given in the following equation;

$$\frac{W}{P} = \frac{1.79}{V} \tag{2.17}$$

where,

W= Total tractor weight (kN)

P= Total axle power (kW)

V= Forward speed (m/s)

This load should be adjusted in the static condition and should include the static weight transfer from the implement.

2. The drive tires should be of sufficient size to carry this load at low inflation pressure (110 kPa or less is recommended).
3. The draft force from the implement should be adjusted so that a good average value is about 10%.

Using the individual wheel models, Macnab et al. (1977) developed a computer model. The model developed determined the expected drawbar pull by summing the results for each wheel, whether towed or driven.

Chesness, et al. (1970) attempted to predict field cone index by developing a regression equation with reconstituted laboratory soils. The regression prediction equation calculated cone index as a function of soil moisture, bulk density and depth. From their study , they concluded that, with the soil type used, remolded soil samples do not exhibit the same cone index, even though the field soil has similar bulk density and moisture content, at the same depth, as in-situ soils. Thus it is not possible to estimate field cone index by measuring soil moisture and bulk density.

Leviticus and Reyes (1983) used the generalized form of the Wismer and Luth model to obtain the traction characteristics of the tractors tested on the concrete track of the Nebraska tractor test. The model they created was of the form:

$$\frac{P}{W} = A\left(1 - \exp^{-k\frac{bd}{W}S}\right) \qquad (2.18)$$

where,

P= pull

W= dynamic weight on drive axle

b= tire section width

d= tire diameter

S= slip

A= constant, equivalent to the maximum P/W

k= constant related to the rubber hardness or tire resilience

They noted that the k-factor would be the cone index for a tire moving on a soil, but this is not correct, for the k-factor would be 0.3 times the cone index according to Wismer and Luth (1974). Leviticus and Reyes (1983) then used an iterative regression analysis along with data for a number of tractors over a five-year period from Nebreska tractor test to determine the best fit values of A and k.

Brixius and Wismer (1978) studied the role of slip in traction and concluded that relative motion between traction elements (tires and tracks) and soil, i.e., slip, is one of the most significant variables in traction. Its effect on tractive performance must be defined to adequately predict the traction process. The definition of slip must be based on some measurement of the effective zero condition. Measuring the zero slip condition at zero pull on a hard surface (self-propelled condition) provides a good estimate of relative moments over a broad range of surface conditions that include convenience, consistency of measurement and resulting meaningful values of wheel slip. Using an incorrect value of rolling radius for wheels is reflected in estimating how the energy is lost in the traction process. Total energy (power) lost due to slip and motion resistance is not affected by the choice of rolling radius but the distribution of loss between the two is affected.

Ali and McKyes (1978) studied the effect of angle and length of individual lugs and lugged tires on the traction force were studied in the laboratory and the field under different soil conditions. From the experiments the following conclusions were made:

1. The magnitude of soil thrust increased by increasing the lug angle and projected width for the same lug length. Moreover, for the same wheel width, increasing the lug angle

decreased the lug length which, in turn, decreased the wheel soil thrust. However, the optimal lug angle did not change by changing the lug length, soil moisture content or soil type.

2. The relationship between soil thrust and lug length was linear within the range of the lug length studied. Therefore, the effect of lug length on soil thrust per unit tire width was negligible within the range of angle, soil moisture content and the two soil types.

Upadhyaya, Wulfsohn, and Jubbal (1987 and 1989) developed equations to predict tractive performance of radial tires. These theoretical equations gave justification to the empirical equations commonly used at the University of California, Davis, in curve-fitting techniques (Upadhyaya, 1988; Wulfsohn, Upadhyaya, and Chancellor, 1988).

Evans, Clark and Manor (1989) tried to fit the generalized equation for gross pull ,

$$GT = W\left[c_a\left(1-\exp^{-c_b B_a}\right)\left(1-\exp^{-c_c S}\right)+0.04\right] \qquad (2.19)$$

where,

c_a, c_b and c_c were regression coefficients.

The equation for motion resistance was not generalized since the fitted data satisfactory. Also, motion resistance was relatively small compared to gross traction. The most significant coefficient was the slip coefficient c_c.

Grisso et al. (1991, 1992) compared the field tractive performance of 18.4R46 and 18.4R42 and they used non-linear regression. The regression equations they were;

$$\frac{P}{W} = c_d\left(1 - \exp^{c_e S}\right) + c_f \tag{2.20}$$

$$\frac{GT}{W} = c_g\left(1 - \exp^{c_h S}\right) + c_i \tag{2.21}$$

where c_d, c_e, c_f, c_g, c_h, and c_i were the regression coefficients.

No significant tractive advantage was found for any of the two tires, which were operated at high inflation pressure on firm soil.

Zoz (1987) introduced a computerized spreadsheet method to refine and chart developed previously (Zoz, 1972). The Lotus 1-2-3 template used equations developed by Brixius (1987) for field performance prediction, and equations proposed by Zoz and Brixius (1979) to predict performance on concrete of tractors mounted with bias-ply tires. Tire dimensions and PTO/axle efficiencies for both axles were required to be the inputs. Several options were given, such as calculations for a concrete surface or field soil, for two-wheel drive or four-wheel drive (or mechanical front-wheel drive (or mechanical front-wheel assist),with an emphasis either on performance (tractive efficiency and drawbar pull), or on dynamic weight distribution of the tractor.

Al-Hamed et al.(1990) modified the spreadsheet program according to recommendations made by Brixius (1987) to accommodate radial tires, and to include a ballast optimization scheme. Optimum weight distribution was computed either from the

maximum tractive efficiency case, or from the design tractive efficiency case (3 % slip above the slip value at maximum tractive efficiency).

Evans, Clark and Manor (1989) used another form of the model because they were interested in the effects of surface. Later, Evans, Clark and Manor (1991) added surface condition effects in a traction model they used to help farmers optimize ballast combinations by drawing tractive efficiency contour maps with front and rear axle ballast as entries.

Grisso et al. (1992a) used a modified version of the Zoz (1987) spreadsheet templates to show the effects of tire construction (bias vs.radial), tire number (single vs.duals), travel speed, tire size, ballast distribution, soil condition and drive mode (2WD vs 4WD or Front Wheel Assisted) as an educational tool for students in undergraduate classes and farmers. They used non conventional variables to better describe tractor tractive performance.

Ramp and Siemens (1990) proposed a program matching tractors with implements to obtain maximum productivity and best use of tractor available power. The program was based on Brixius traction prediction equation and permitted for incremental rather than continuous increases in implement sizes. The implement giving the highest draft without exceeding tractor maximum pull for a chosen gear ratio was retained as a possible match. Several gear ratios were tested, and the corresponding implement size, slip and productivity values computed. The combination giving the highest productivity could then be selected.

Gee-Clough et al. (1978) proposed a model combining traction equations to implement draft equations to predict field productivity of tractor-implement combinations and for plowing operations in particular.

Dwyer (1978), in his study, presented methods to maximize performance by matching tractor weight, tire sizes and travel speed to the available power. The Gee-Clough model was used for traction prediction in the identification of tractor-implement combinations suitable for a given field operation, and a particular soil type under specified climatic conditions. Other models were included in the expert system to estimate soil moisture content, cone index, and implement draft.

2.2 Tire-Rigid Surface Interactions and Tire-Soil Interface Pressures

Tire-rigid surface interaction has been a favorable point for the researchers in the field of soil mechanics. Most studies focused on finding the tire contact area as a function of inflation pressure and axle load on rigid surface as it was much more difficult to make this determination on soil. Based on rigid surface area approximations, studies were carried out to find the average stress distribution in soil. The latest study by Upadhyaya and Wulfsohn (1990) is one of those studies. Upadhyaya and Wulfsohn (1990) developed mathematical expressions for 2-D contact length, contact width and contact area of a pneumatic tire on a rigid surface based on the geometry and deflection characteristics of the tire. They then verified their mathematical expressions with experimental results. The tire geometry was defined by R_1 as the overall tire radius and R_2 as the tread radius, then

defining a point on the tread outer surface by a x,y, z co-ordinates system with z axis pointed vertically downward (Figure 2.8). They defined that ;

$$x=R_2 \sin\phi \tag{2.22}$$

$$y=[R_1-R_2(1-\cos\phi)]\sin\theta \tag{2.23}$$

$$z=[R_1-R_2(1-\cos\phi)]\cos\theta \tag{2.23}$$

They found that the contact length, contact width, and contact area of pneumatic tires on a hard surface are of the following form;

$$\frac{l_c}{d}=2\sqrt{\frac{\delta_z}{d}} \tag{2.24}$$

$$\frac{l_w}{2R_2}=2\xi\sqrt{\frac{\delta}{2R_2}} \tag{2.25}$$

If $l_w<w$, then otherwise $l_w=w$

$$A_c=\frac{l_c l_w}{4}[\pi-2\eta] \tag{2.26}$$

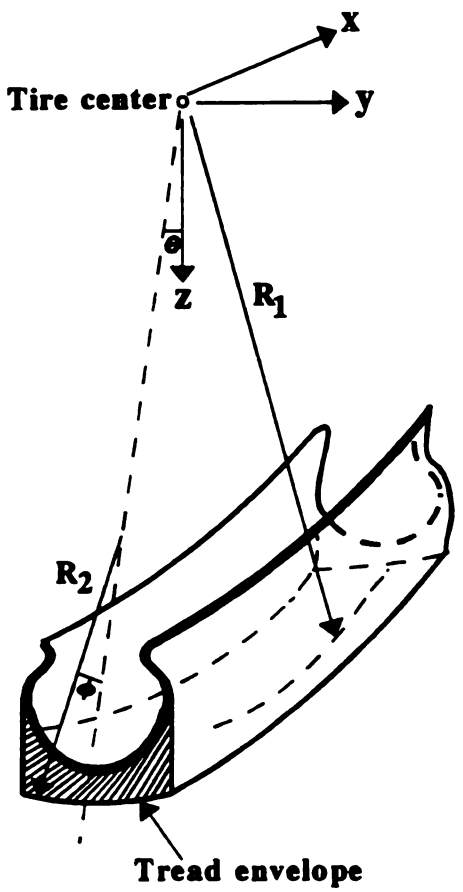

Figure 2.8 Tire geometry as defined by Upadhyaya & Wulfsohn, 1990.

where,

lc=Contact length

lw=Contact width

w= Width of the tire

ζ= Correction factor

Upadhyaya and Wulfsohn (1990) defined that;

$$\eta = \begin{bmatrix} 0 & if\ l_w < w \\ \left[2\left(1-\frac{2}{l_w}\right)\right]^{1/2} - \left(\frac{w}{l_w}\right)\left[1-\left(\frac{w}{l_w}\right)^2\right]^{1/2} & if\ \ l_w > w \end{bmatrix} \qquad (2.27)$$

The most recent study on soil-tire interface pressures by Way et al. (1993) has reported the effect of lug height on tire-soil interface pressures. The conclusion drawn from their experiment was that soil-tire interface pressures on 18.4R38 radial-ply R-1 tires with lug height of 31, 55 and 100% of the new tire lug height were generally greater near the edge of the tread on a lug face than on other locations on the lug face and undertread. Way et al. also found that the soil-tire interface pressures on the lug faces generally increased as the lug height increases and as firmness of the soil surface increases. Pressures on the undertread generally decreased as lug height increases.

Vandenberg and Gill (1962) measured pressures at the interface between a smooth tire and the surface on which the tire was operating. They embedded transducers in the

carcass of a smooth rubber tire in order to determine the stress pattern under a dynamically loaded wheel. The data they collected indicated that the pressure distribution pattern is influenced by the soil conditions as well as by the tire. Vandenberg and Gill also indicated that changes in inflation pressure alter the pressure distribution pattern considerably; also the influence of sidewall stiffness becomes evident at the lower inflation pressures. Due to the rigidity of the tire carcass, the stress applied by the tire is generally greater than the internal pressure. When a very flexible tire such as a low-inflation pressure tire is used, the pressure distribution is quite uniform. They also suggested that for some soil compaction research studies, this type of tire may be very useful because the inflation pressure is essentially the pressure applied to the soil.

The early studies on soil-tire interface studies was conducted by Trabbic et al. (1959). Trabbic et al. (1959) measured the soil-tire interface pressures on the undertread, lug face, and the leading and trailing lug sides on an R-1 bias-ply tire. As inflation pressures increased, interface pressures near the centerline of the tread on the lugs increased and pressures on the lugs at the edge of the tread generally decreased. Pressures on the undertread near the centerline of the tread increased as inflation pressure increased, but inflation pressure had only a minor effect on pressures applied to the undertread near the edge of the tread.

Normal stresses were measured at the soil-tire interface of a radial-ply tractor tire (18.4R38) by Burt et al. (1988). They used two different soils, sandy and clay loam. From their experiments they concluded that the effect of dynamic load on the normal stress at a

point on the soil-tire interface was dependent on the compacted condition of the soil and the position of the point on the tire at which the stress is measured. At the lug center and tire center positions on a lug on firm soil, an increase in dynamic load caused a decrease in normal stress level. At the outside edge of the tire on the lug and at all measured positions on the undertread, an increase in dynamic load on loose and firm soils, in general, caused an increase in normal stress level. They also found that in general, for a tire operating on loose soil at all measured locations at the soil-tire interface, an increase in dynamic load caused an increase in normal stress and dynamic load effects on normal stress were not affected by soil type.

Kaga et al. (1977) calculated the displacements and stresses and strains of a radial tire of 600-mm and 1707-mm diameter while the tire was in contact with a rigid surface. As a result of their study they found that the axisymetric finite element method under asymetric loading conditions was applicable to the tire stress-strain analysis because agreement between the calculated and measured results was satisfactory.

Rothert et al. (1985) studied the effect of different friction coefficients on the interaction of tire and the rigid surface. They divided the tire footprint area into smaller areas that either stick or slide at the interface between the tire and its supporting structure when frictional forces are applied.

Faria et al. (1989) studied on the steady state formulation of the rolling contact problem with friction that allows the analysis of free rolling, cornering, acceleration, and

braking. They developed a layered tire of shell elements with shear deformation that allows for large deflection and rotation used.

Yong, Fattah and Boonsinsuk (1978) analyzed and predicted tire-soil interaction and performance using the finite element method. By applying the finite element method and the Hertz theory of contact between two elastic bodies, tire-soil interaction was formulated by assuming that a tire is idealized as cylindrical body with an infinite width while the soil was modeled as another cylindrical body. As a conclusion Yong et al. found that the analysis for evaluation of the performance of wheel-soil interaction to the situation of flexible tires and their associated deformation energy losses was found to be satisfactory between the predicted results and those obtained from drawbar pull tests in the laboratory.

Abeels (1988) investigated the tire deformation, inflation pressure and effects on hard and soft supports. A mathematical model was developed for the deformation of the modulus of rigidity corresponding to each deflecting portion of the tire such as sidewall and the tread.

Another study by Hu and Abeels (1994) revealed information on the effect of load and inflation pressure on contact pressure. They concluded that the mechanical characteristics of the tire envelope and the interactions with a rigid surface can be investigated by the finite element method in 2-D. The main findings of their study was given as in the following;

1. The distribution of contact pressure along the cross-section can only be modified by tire load, and that the inflation pressure only makes differences in the magnitude of

contact pressure, not in its distribution shape.

2. Tire deflection increases with increasing tire load and increases with the reduction of inflation pressure.
3. Lateral displacement increases with increasing tire load and decreasing inflation pressure. Generally the value of tire deflection is higher than that of lateral displacement when tire load and inflation pressure are identical.
4. The tangential stress distributions obtained had a minimum value around the middle point of the half cross-section. The tangential stress decreases from the tread centerline plane to the middle plane of the half cross-section and then increases to the extremity of the tread end. The direction of tangential stress is pointed towards the tread centerline plane when its value is negative. On the other hand, for positive values, the direction is oriented towards the exterior from the symmetrical axis.
5. Their comparison of tire deflection with the measured data showed that the finite element analysis is suitable for predicting the tire properties and its interaction with the contact surface.

Ridha (1980) computed the stresses, strains and deformations of tires using the finite element method. He concluded that analysis of tire stresses and deformations due to footprint loadings requires further development. A "gap element" may be used to model a nonlinear foundation behavior with small stiffness before contact and high stiffness after the gap has been closed through contact with the roadway. A promising approach to tire

contact problems is the use of contact algorithms with stick-slip capabilities to model different friction conditions in the footprint. Application of such algorithms in conjunction with isoparametric elements would enable the calculation of forces and moments in the footprint and the use of this data to predict tire and vehicle handling characteristics.

One of the three-dimensional tire modeling studies is by Hu and Abeels (1994). Hu and Abeels predicted tire deformation and distribution of contact pressures between the tire and rigid surface and contact area under various axle load and inflation pressures. Based upon their finite element study, they concluded that the contact pressure and area studies can be investigated by the finite element method.

Chapter 3

ESSENTIAL THEORETICAL BACKGROUND

3.1 Theory of Slip Planes and Slip Lines (Zone Failure)

Failure in solids is usually described mathematically by substituting some failure criterion into a set of equilibrium equations to obtain expressions for the state of stress in the solid on the point of failure. For soils, failure has traditionally been defined by combining the Mohr-Coulomb criterion with the equations of static equilibrium. Since the Mohr-Coulomb criterion is stress-oriented criterion, large deformations may occur before "failure" is reached. This situation may be handled by using the theory of plasticity in combination with the Mohr-Coulomb yield criterion to obtain a set of equations called equations of plastic equilibrium. Plastic equilibrium deals with the stresses in soil masses at failure. The ideally plastic material at failure yields and undergoes deformation at a constant rate without change in stress. If a two dimensional element of soil is stressed to fail under principal stresses σ_1 and σ_3, failure occurs along a "slip plane" inclined at an angle α with the major principal plane (Figure 3.1). To determine α, use is made of the failure criterion,

$$s = c + \sigma \tan\phi \tag{3.1}$$

The normal and shear stresses (σ and τ) are shown in Figure 3.2 when $\theta=\alpha$ and are given below;

$$\sigma = \frac{\sigma_1+\sigma_3}{2} + \frac{\sigma_1-\sigma_3}{2}\cos 2\alpha \tag{3.2}$$

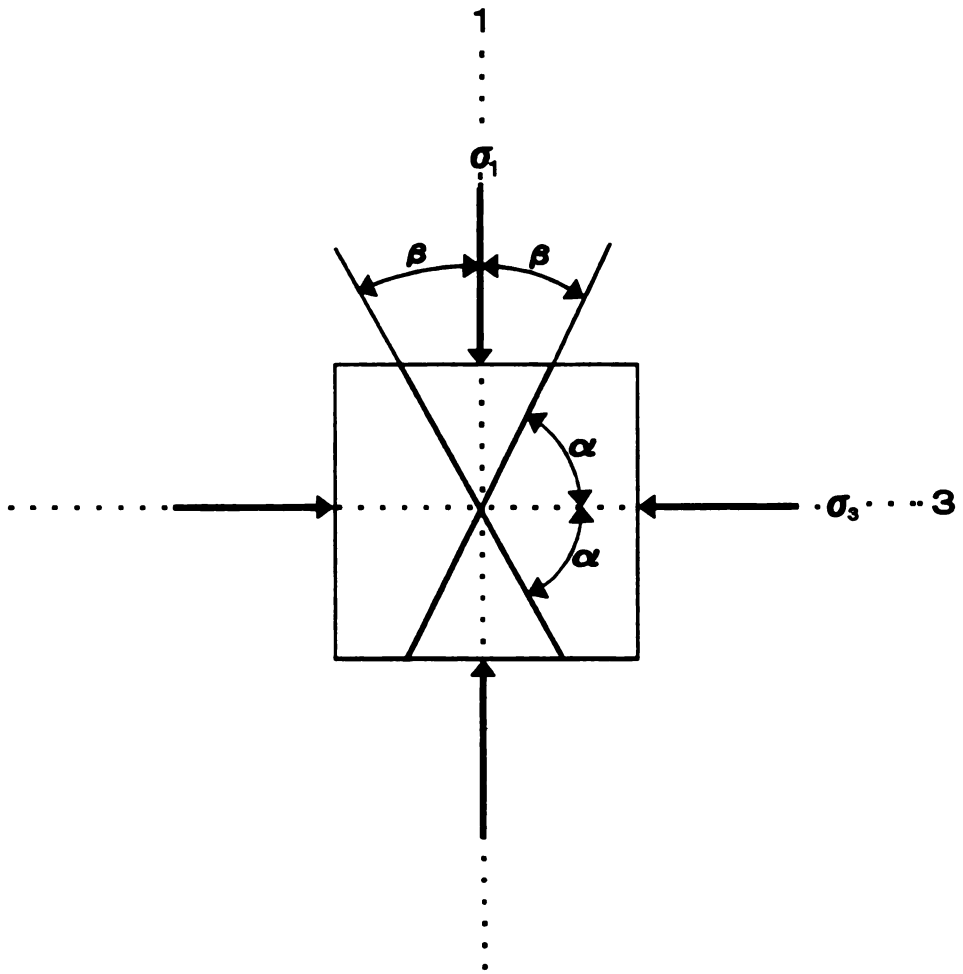

Figure 3.1 Failure planes (Wu, 1976)

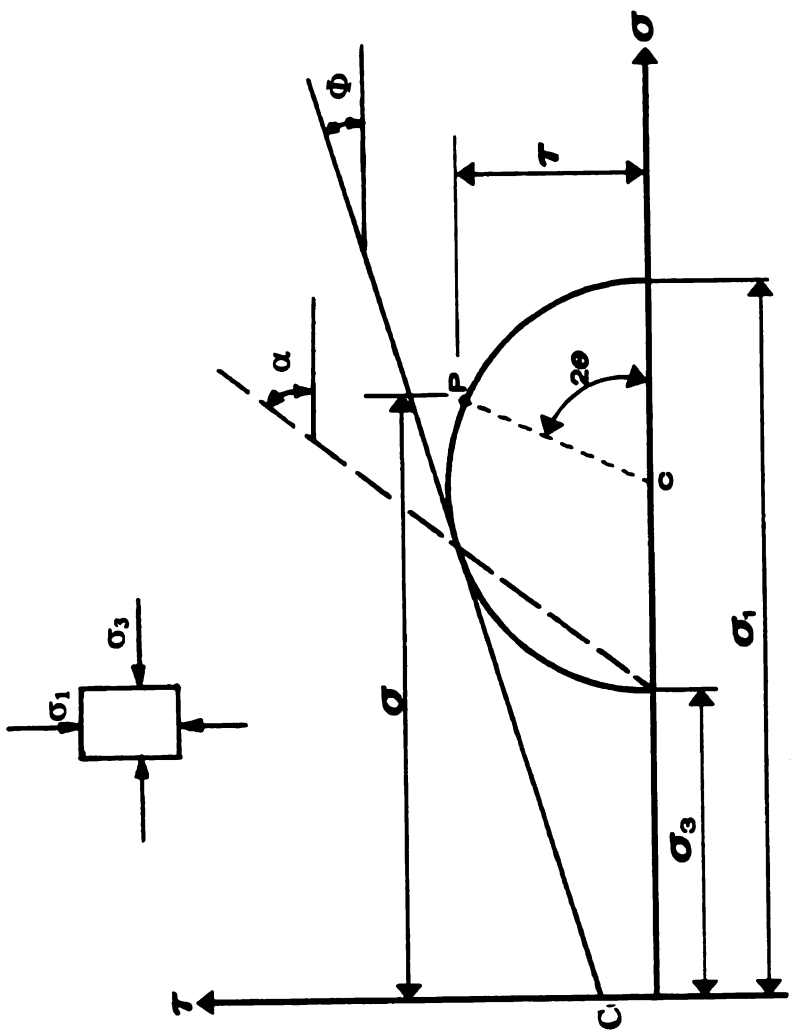

Figure 3.2 Mohr-Coulomb yield surface.

$$\tau = \frac{\sigma_1 - \sigma_3}{2} \sin 2\alpha \tag{3.3}$$

At failure the shear stress on the failure surface must be equal to the shear strength s. Substituting equation (3.3) in equation (3.1) and setting τ equal to s,

$$\frac{1}{2}(\sigma_1 - \sigma_3)\sin 2\alpha = c + \left(\frac{\sigma_1 + \sigma_3}{2} + \frac{\sigma_1 - \sigma_3}{2}\cos 2\alpha\right)\tan\phi \tag{3.4}$$

By application of the trigonometric relations,

$$\sin 2\alpha = 2\sin\alpha\cos\alpha\,; \quad \cos 2\alpha = 2\cos^2\alpha - 1 \tag{3.5}$$

this may be transformed into,

$$\sigma_1 \sin\alpha\cos\alpha - \sigma_3 \sin\alpha\cos\alpha = c + \tan\phi\left[\sigma_3 + (\sigma_1 - \sigma_3)\cos^2\alpha\right] \tag{3.6}$$

or it could be written as,

$$\sigma_1 = \sigma_3 + \frac{c + \sigma_3\tan\phi}{\sin\alpha\cos\alpha - \cos^2\alpha\tan\alpha} \tag{3.7}$$

The quantity of α is determined by the condition that the stresses on the failure plane are the critical ones and control the value of σ_1 for a given value of σ_3. Once failure develops along this plane, σ_1 can not be increased any further, even though failure has not taken place on all the other possible planes. In other words, the failure plane is the one with the angle that gives a minimum value of σ_1 for a given value of σ_3. Hence, the critical value of α may be determined by setting,

$$\frac{d}{d\alpha}(\sin\alpha\cos\alpha - \cos^2\alpha\tan\phi) = 0 \tag{3.8}$$

This leads to

$$\cos^2\alpha - \sin^2\alpha + 2\tan\phi\sin\alpha\cos\alpha = 0 \tag{3.9}$$

from which we obtain,

$$\alpha = 45° + \frac{\phi}{2} \tag{3.10}$$

Since the stresses are symmetrical with respect to the 1 and 3 axes, to sets of failure planes making angles of ± α with the major principal plane (Figure 3.1).

Although the single-failure surface analysis of the stability of slopes is applied in practice to all types of soils, a more realistic picture of the mode of failure for cohesionless and c- soils is given by the concept of zone failure. Unlike the concept of single-surface failure where only the soil along one surface is considered to fail, zone failure implies that the transition of a soil from a state of elastic equilibrium to a state of plastic equilibrium takes place when incipient shear failure occurs along two sets of surfaces of sliding within the entire earth mass or ***in another terminology, slip line fields, are those areas where shear stress is equal to shear strength of soil*** (τ=s). This problem was first studied and addressed by Rankine. Rankine's active and passive state of stresses can be exemplified by a mass of soil bounded by a frictionless wall a-a that extends to infinite depth (Figure 3.3). An element of soil at depth y is subjected to a vertical stress σ_y and a horizontal stress α_x. There exists no shear stresses on the vertical and horizontal planes, and these are the principal planes. Therefore, α_x and α_y are also the principal stresses. If the frictionless wall a-a is allowed to move away from the soil mass, the value of σ_x decreases. If this deformation continues, σ_x soon reaches to a value that failure of the soil occurs and

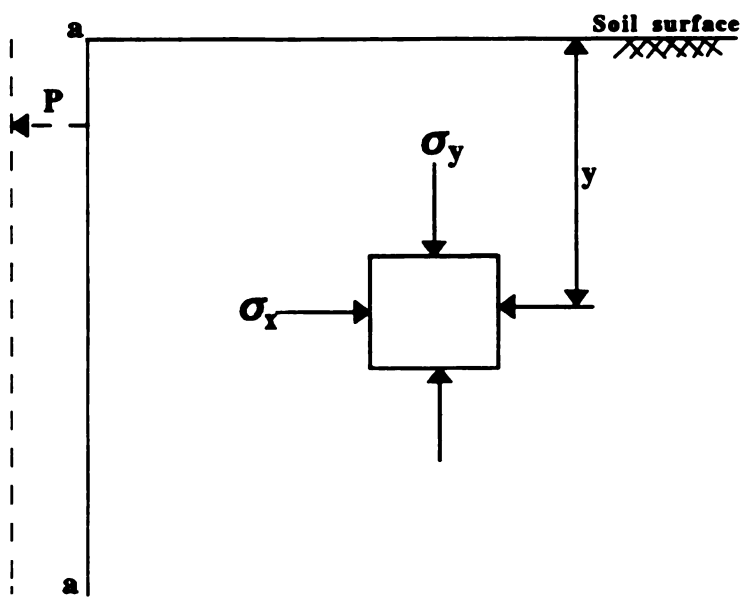

Figure 3.3 Stresses in a soil element behind a frictionless wall (Wu, 1976).

plastic equilibrium is attained in the soil. Since failure is obtained by reducing σ_X, it must be the minor principal stress σ_3, while σ_Y is the major principal stress σ_1. The relationship between σ_1 and σ_3 at failure is given by equation 3.7. Substituting equation 3.10 into equation 3.7 results in,

$$\sigma_3=\sigma_1 \tan^2\left(45°-\frac{\phi}{2}\right)-2c\tan\left(45°-\frac{\phi}{2}\right) \tag{3.11}$$

or

$$\sigma_x=\sigma_y \tan^2\left(45°-\frac{\phi}{2}\right)-2c\tan\left(45°-\frac{\phi}{2}\right) \tag{3.12}$$

If the wall is a-a is moved against the soil so that the soil is compressed laterally the horizontal pressure σ_Y is the minor principal stress σ_3. If these are substituted into equation (3.11), it is obtained,

$$\sigma_x=\sigma_y \tan^2\left(45°+\frac{\phi}{2}\right)+2c\tan\left(45°+\frac{\phi}{2}\right) \tag{3.13}$$

Since the vertical stress is equal to the weight of soil,

$$\sigma_y=\gamma y \tag{3.14}$$

so that the equations (3.12) and (3.13) become, respectively,

$$p_a=\sigma_x=\gamma y\tan^2\left(45°-\frac{\phi}{2}\right)-2c\tan\left(45°-\frac{\phi}{2}\right) \tag{3.15}$$

and

$$p_p=\sigma_x=\gamma y\tan^2\left(45°+\frac{\phi}{2}\right)+2c\tan\left(45°+\frac{\phi}{2}\right) \tag{3.16}$$

The two conditions of stress are often called Rankine's active and passive states of stress and the pressures P_a and P_b. They are, respectively, the minimum and maximum pressures that the soil can exert on a smooth wall extending to infinite depth. the ratio of σ_x/σ_y is called the coefficient of earth pressure and is denoted by K_a and K_p for the active and passive states, respectively.

In the development of mobility theories, the behavior of soil beneath rigid wheels has been a favored starting point since the simple geometry of the rigid wheel eases the mathematical problems as well as the performance of experiments. The earliest experiments in which soil deformation patterns were measured under the loading by a rigid wheel are those performed and reported by Bekker (1969). An extensive research was carried out by Wong and Reece (1966). In these experiments it was clearly established that the extent and form of the failure zones may vary with loading conditions and slip. ***The existence of failure zones is consistent with the view that the shear strength of soil is the controlling factor in mobility problems.*** The field itself is usually shown as consisting of a number of intersecting lines along which the failure conditions occur. Generally, two separate zones of failure or slip line fields develop beneath wheels (Figure 3.4), a forward field, where the soil tends to fail in the direction of travel and a backward, or rear field, where the soil tends to fail in the opposite direction. In each field there are mainly two zones corresponding to different states of stress (Rankine's active and passive states of stress). These zones are called active and passive zones. Figure 3.5 shows the slip line fields in rear and forward failure zones under a tire.

3.2 Theoretical Considerations to Traction

Predicting the performance of a traction device requires the distribution of normal and shear stresses at the soil-tire interface, and the geometry of the 3-D contact surface be

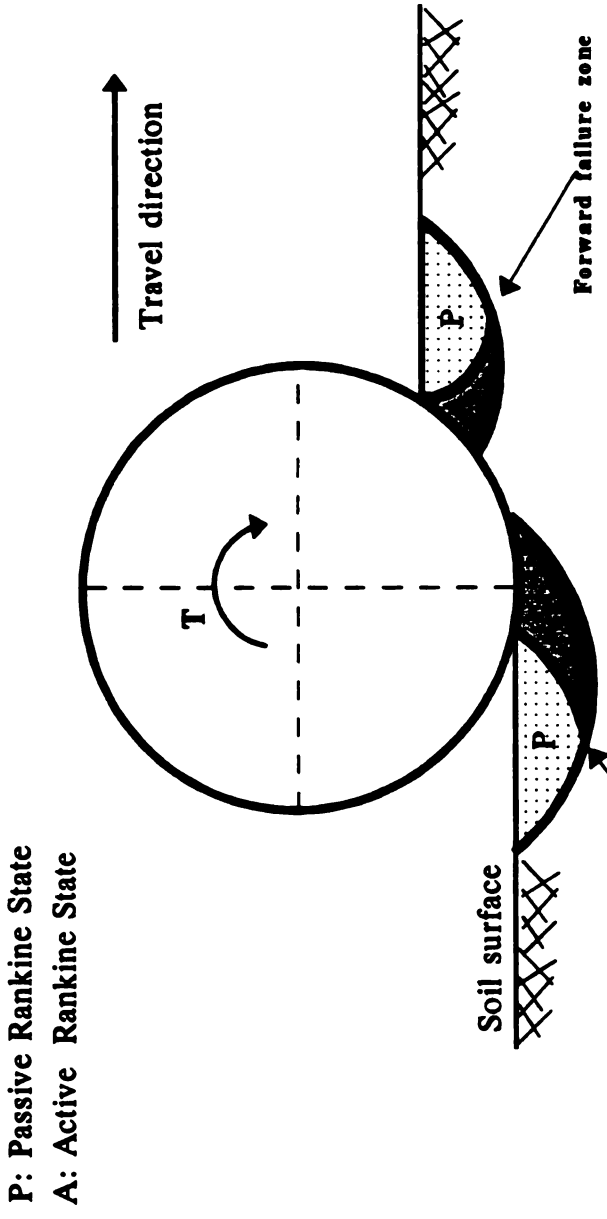

Figure 3.4 Active and passive zones in soil under a tire. (Karafiath and Nowatzki, 1978)

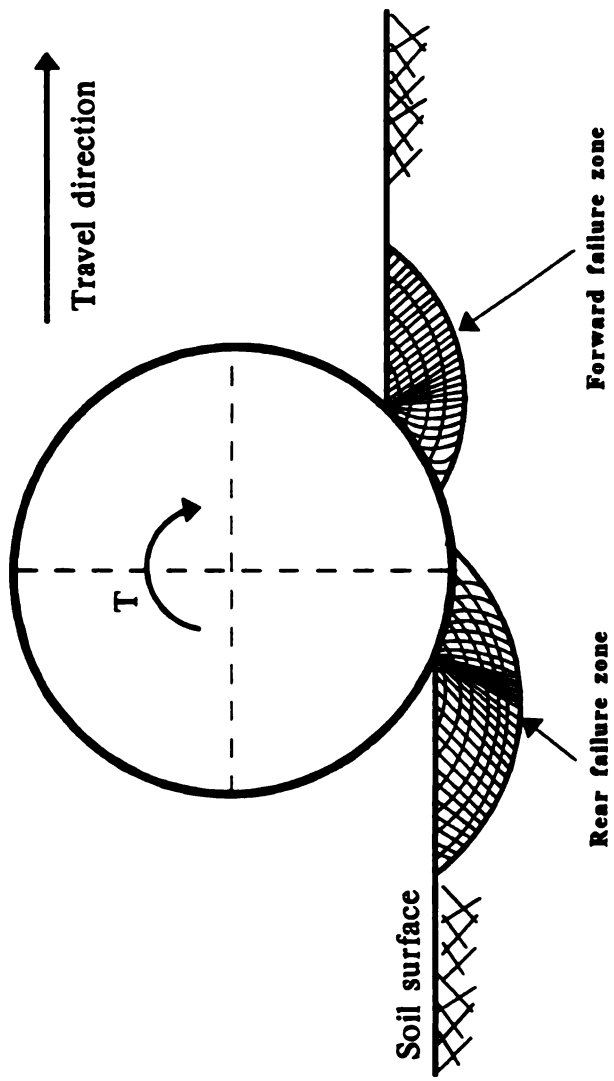

Figure 3.5 Slip line field in soil under a tire (Karafiath and Nowatzki, 1978).

known. Once the geometry and stresses are known, the traction parameters (Figure 3.6) can be determined as follows (Upadhyaya and Wulfsohn, 1990):

$$W = \int_{A_c} [\sigma \cos(\varphi) + \tau \sin(\varphi)] dA \tag{3.17}$$

$$D = \int_{A_c} [\tau \cos(\varphi) - \sigma \sin(\varphi)] dA \tag{3.18}$$

$$T = \int_{A_c} [\tau \cos(\theta - \varphi) - \sigma(\theta - \varphi)] r \, dA \tag{3.19}$$

where,

W= axle load

D= draft load

T= torque

σ = normal stress at the soil-tire interface

τ= shear stress at the soil-tire interface

r= rolling vector from axle to any point on the contact surface

A_C= contact area

θ = angle subtended by the radius vector r with the vertical

φ= angle subtended by the normal stress with the radius vector

In the case of rigid wheels, the relation between interface shear stresses and applied torque is straightforward: equilibrium requires that the integral of shear stresses over the contact area multiplied by the wheel radius be equal to the applied torque. In the case of pneumatic tires no such relation exist since the line of action of the interface normal stresses generally bypasses the axle because of the deflection of the tire.

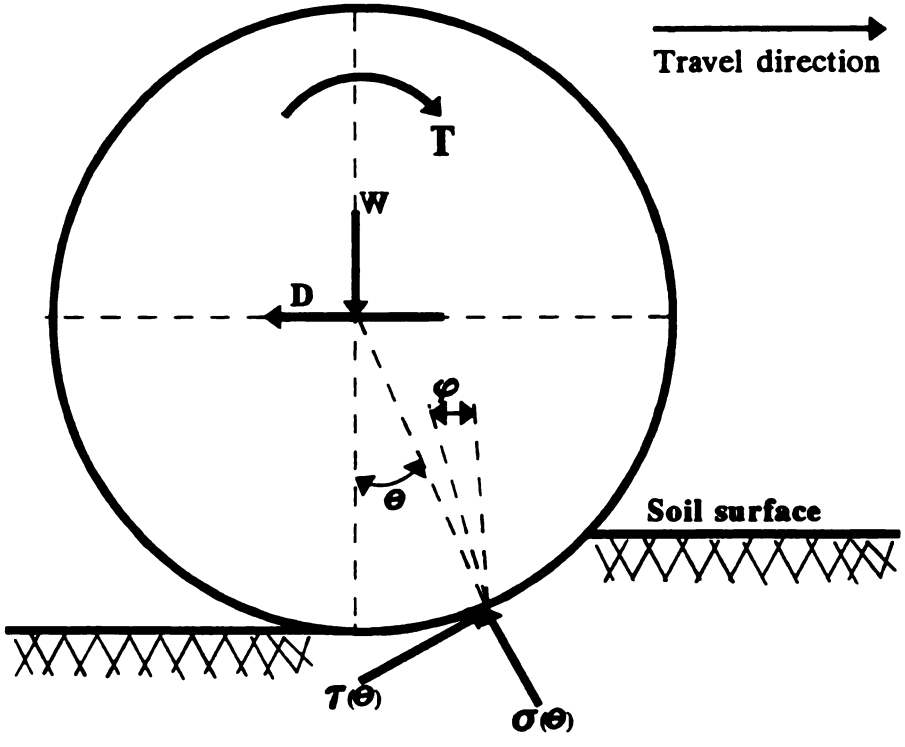

Figure 3.6 Schematic representation of soil-tire interaction (Upadhyaya & Wulfson, 1990)

Thus, the interface normal stresses enter into the equilibrium equations for the applied torque. Nevertheless, the major portion of the driving torque is transmitted to the soil in the form of interface stresses.

The lack of knowledge of the true 3-D soil-tire contact area and the distribution of normal stresses on this area makes the evaluation of equation 3.17, 3.18 and 3.19 impossible. Thus the development of shear stresses at the interface, associated with slip, and mathematical formulations for the relationship between the shear stress and slip have been proposed by various researchers. Of these, the most useful is the empirical one proposed by Janosi and Hanamoto (1961) on the basis of analogy with the direct shear test. This relationship, proposed for tracked vehicles, is as follows (Figure 3.7),

$$\tau_{mob}=\tau_{max}(1-\exp^{-s/k}) \tag{3.20}$$

where,

τ_{mob}= mobilized shear strength

τ_{max}= maximum shear strength

s= slip

k= shear deformation modulus

Slip (s) in the above equation is defined as,

$$s=\left(1-\frac{V_a}{V_t}\right) \tag{3.21}$$

where, V_a and V_t are the actual and theoretical travel speed, respectively.

For compressible soils that are of primary interest in off-road locomotion, this equation properly describes the relationship between shear stress and slip.

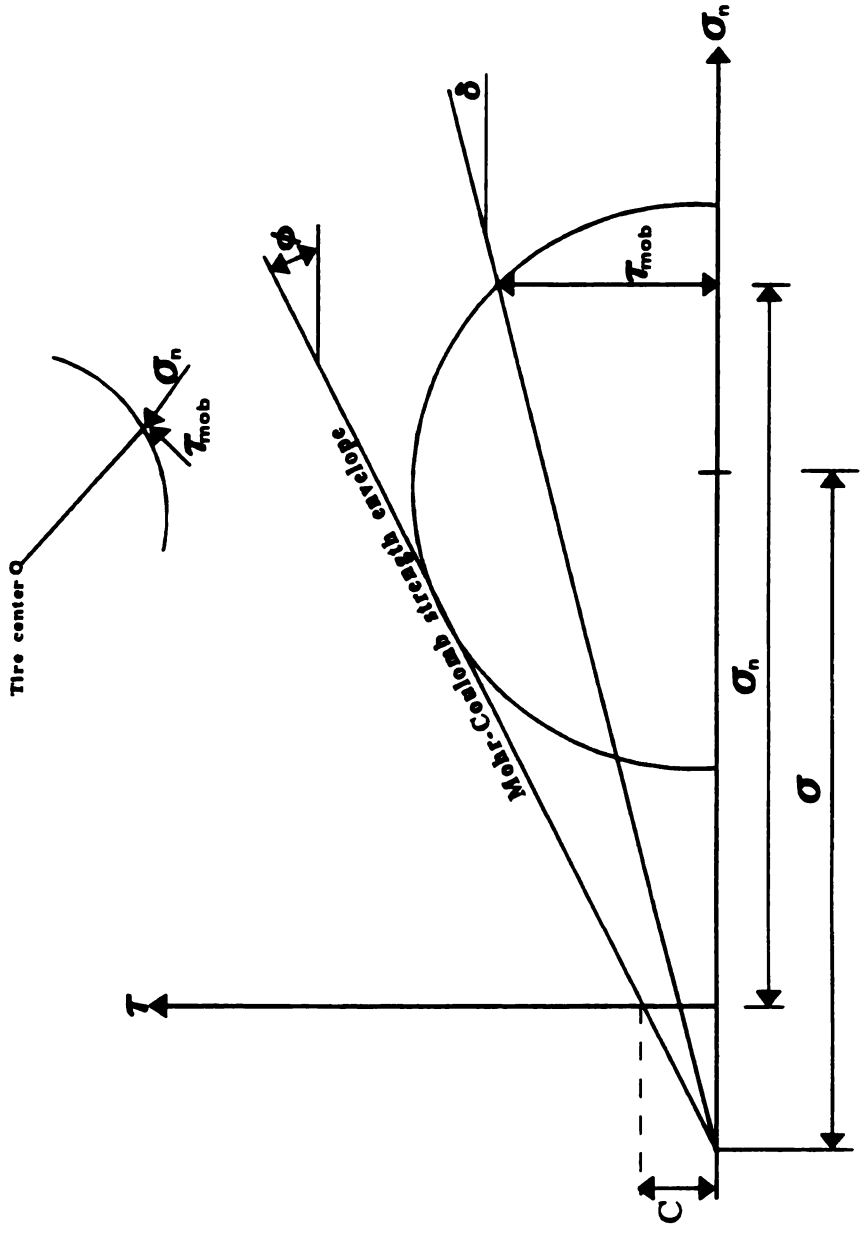

Figure 3.7 Mohr circle and mobilized shear strength. (Karafiath and Nowatzki, 1978)

When this relationship is applied to the rigid wheel or pneumatic tire, a constant, s_0, must be included in the slip term to account for the fact that a threshold perimeter shear exists, at which the movement of the wheel starts. Thus equation (3.20) is modified as follows;

$$\tau_{mob}=\tau_{max}\left(1-\exp^{\frac{s+s_o}{K}}\right) \tag{3.22}$$

Upadhyaya (1987) based on the approach developed by Janosi and Hanamoto (1961) developed mathematical expressions for traction equation coefficients for a simplified case which will be used as a guide to analyze these coefficients using a step-wise regression technique. Upadhyaya assumed that the contact surface lies in a horizontal plane and that it is rectangular in shape with width b, and length l. Soil deformation at a point y along this contact length can be represented by j. The corresponding tire deformation be η. Both the maximum soil and tire deformation be proportional to the contact length. Then

$$NT=K_t\eta_t \tag{3.23}$$

$$NT=\int_0^l \tau_{max}(1-e^{-j/k})b\,dy \tag{3.24}$$

where,

η_t = tire deformation in tangential direction

K_t = tangential tire stiffness

Assuming that normal stress to be constant over the footprint and approximately equal to inflation pressure,

$$\sigma \cong p \cong \frac{W}{bl} \tag{3.25}$$

Soil deformation is also assumed to be proportional to contact distance at any point under the tire,

$$j = i'y \tag{3.26}$$

where,

y= constant distance along the direction of travel from the beginning of soil contact with tire (Figure 3.8)

i'= proportionality constant

Using the equations (3.25) and (3.26) in equation 3.24 and carrying out the integration yields,

$$NT=\tau_{max} bl\left[1+\frac{k}{i'l}\left(e^{-i'lk}-1\right)\right] \tag{3.27}$$

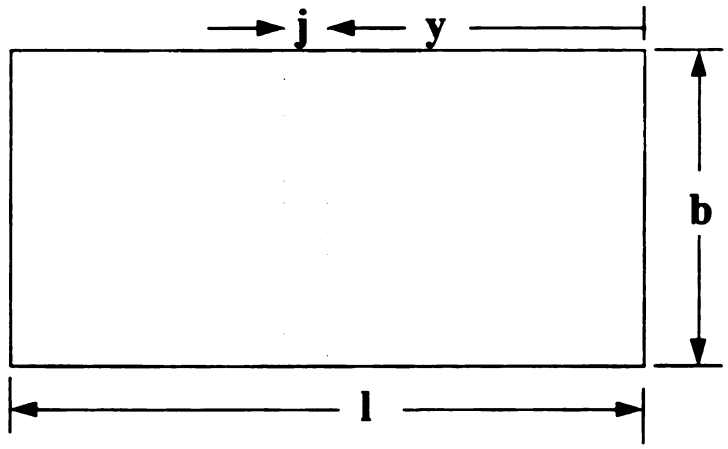

Figure 3.8 Contact geometry and soil deformation for the simplified case (Upadhyaya et al., 1987)

Chapter 4

MEASUREMENT OF SOIL-TIRE INTERFACE PRESSURES

Since the concept of soil compaction was recognized as being important by researchers, much research has been conducted to understand many aspects of this phenomena. The studies targeting compaction began in 1950's when agricultural operations were become more mechanized (Schafer et, al., 1992). As indicated by Schafer et al. (1992) knowledge of soil compaction and the relation of soil compaction to the cropping system are important inputs for effective management of soil physical condition to improve crop production. The desired degree of compaction depends on the intended purpose: for example, the requirements for traction and mobility are quite different from those for infiltration and root propogation.

There are two main aspects that must be investigated to understand the problem. The first aspect is the cause or causes of soil compaction and the second is the level of compaction that affects the results. When the causes of soil compaction are considered, tractor tires are accepted as the most important. The assessment of soil compaction is still a complex phenomena since the soil-tire interaction has not been fully understood because of the variables associated with tires (inflation pressure and axle load and their interaction) and soil. Also the cost of conducting experiments to better understand the effect of such variables, has limited the studies as well. Hence, a small experiment was planned and conducted to understand the effects of tire-related variables (dynamic load, inflation pressure and slip) on soil-tire interface pressures. The specific objectives are given below.

4.1 Objectives

The specific objectives of this sections were as follows;

1. To understand the distribution of pressures on a lug and undertread area of a tire at the interface of the tire on soil.
2. To investigate how interface pressures were affected by tire variables such as inflation pressure, load and slip.

4.2 Experimental Procedure

The soil-tire interface pressure measurements were made at the National Soil Dynamics Laboratory (NSDL), a facility of the USDA Agricultural Research Service in Auburn, Alabama, using the NSDL single-wheel traction research vehicle. The details of single -wheel traction vehicle as described by Burt et al. (1980) are given below.

4.2.1 Single-Wheel Agricultural Tire Tester

Structural systems: The single-wheel agricultural tire tester is a machine designed to operate on the NSDL soil bins. The two main structural components of the machine are a car structure and a superstructure. The car structure is a vehicle that is supported on the soil bin rails by pneumatic tires. The superstructure is carried by the car structure and is the support member for the test tire and the hydraulic power unit. This structure can be moved laterally to position the test tire in the soil bin.

The forces on the test tire are measured by load cells located at three points between the superstructure and the framework that supports the tire. A horizontal pivot shaft at one end of the framework connects the framework through the load cells to the superstructure at two points. The load cells at each of these points are arranged in a two-

dimensional dynamometer system that isolates and measures the net traction and torque reaction force generated by the operation of the test tire. The two-dimensional dynamometer system is connected to the superstructure through a subassembly that is movable in a vertical direction to permit the pivot shaft to be kept level with the center of the tire. The pivot shaft eliminates the transmission of moments by the wheel framework into the two-dimensional dynamometer system.

The third suspension point is directly over the center of the test tire. This point is connected to the superstructure by means of a vertical hydraulic cylinder-load cell link. Gimbals are used on each end of this link for flexibility.

A reaction type torque dynamometer measures the input torque to the test tire. This dynamometer is mounted internally to the test wheel framework.

Drive and control systems: Each major function (the angular velocity of the test tire, the forward velocity of the car and the vertical load on the tire) has its own control system that can operate in either a steady-state or continuously variable (ramp) mode. The steady-state mode is used when it is desirable to hold a particular variable at a constant value. The ramp mode is used when it is desirable to continuously increase or decrease the value of a variable. Each ramp function has a programmable time period between the zero level and the maximum level of the controlled variable.

Test Tire Drive: The test tire drive subsystem consists of a radial piston hydraulic motor, a chain drive for speed reduction and the closed loop servo control for the angular velocity of the test tire. Control of the angular velocity is available in two separate stages within the range of 0.3 and 4.2 rad/s (3 and40 rpm). The torque capability of the drive is 42,000

N m (31,000 ft-lb). Maximum torque can be attained only at angular velocities of less than 2.1 rad/s. The servo controls for this subsystem have one feature that is not available on the remaining subsystem. The ramp mode has a programmable minimum, as well as a maximum, level for angular velocity. This feature can be used to run variable traction tests in a sequence without stopping the machine between tests. When this feature is in use the minimum level is programmed at the angular velocity required for zero travel reduction , and the maximum level is programmed for the maximum desired level of travel reduction. By use of this feature, repeated travel reduction tests can be run in a minimum of soil bin space.

Car propulsion: The car propulsion subsystem consists of a radial piston hydraulic motor, a chain and shaft drive to connect the motor to the drive wheels on the car , and closed loop servo control for the forward velocity of the test car. It is designed to provide up to 44.5 kN (10,000 lb) force for either driving or braking the test tire. The velocity range of the car is 0 to 1.3 m/s (0 to 3 mph).

Vertical loading: The vertical loading subsystem consists of a hydraulic cylinder assembly and closed loop controls for the applied vertical load. A pneumatic-over-hydraulic system minimizes changes in vertical load with minute changes in test tire elevation. Capacity of the vertical loading system is 71.2 kN (16,000 lb). However, the configuration of the test wheel framework causes the torque reaction force to oppose the applied vertical load. The dynamic load is the difference between these two forces. The torque reaction force is measured by the two-dimensional dynamometer system at the supported end of the test wheel framework. Therefore, the maximum dynamic load on the

test tire is limited to about 44.0 kN (10,000 lb) when the input torque is at its maximum value.

Drawbar elevation: A separate automatic control system adjusts the height of the two-dimensional dynamometer system relative to the test tire. When the elevation of the test tire changes, such as when a change in sinkage occurs, the elevation of the dynamometer system automatically changes by a corresponding amount. This synchronization of elevation is accomplished by electro-hydraulic servo control of a hydraulic cylinder that supports the dynamometer system. Control of the elevation of the dynamometer system is necessary to maintain an orthogonal force system.

Subsystem control capabilities: The controls on each of the subsystems are capable of automatically controlling a steady-state value within +0.5 percent of the maximum (or full-scale) value. Limited traction of the car propulsion driving wheels that operate on the bin rails, together with the flexibility of the car structure , increases this tolerance slightly under extreme conditions. Recent tire tests with this tester show significant improvements in the precision and repeatability of tire test data.

4.2.2 Tire

The tire powered by the traction research vehicle was a 18.4R38 Armstrong Hi-Traction Lug Radial (1-Star) R-1 tire. The tire circumference had 30 long and 30 short lugs. The mean lug height of the long lugs at the circumferential centerlines was 43.3 mm.

Six pressure transducers were mounted on the tire, with three on a long lug and three on the portion of the undertread on the trailing side of the long lug. The lug pattern of the tire and the location of transducers on tire are shown in Figure 4.1.

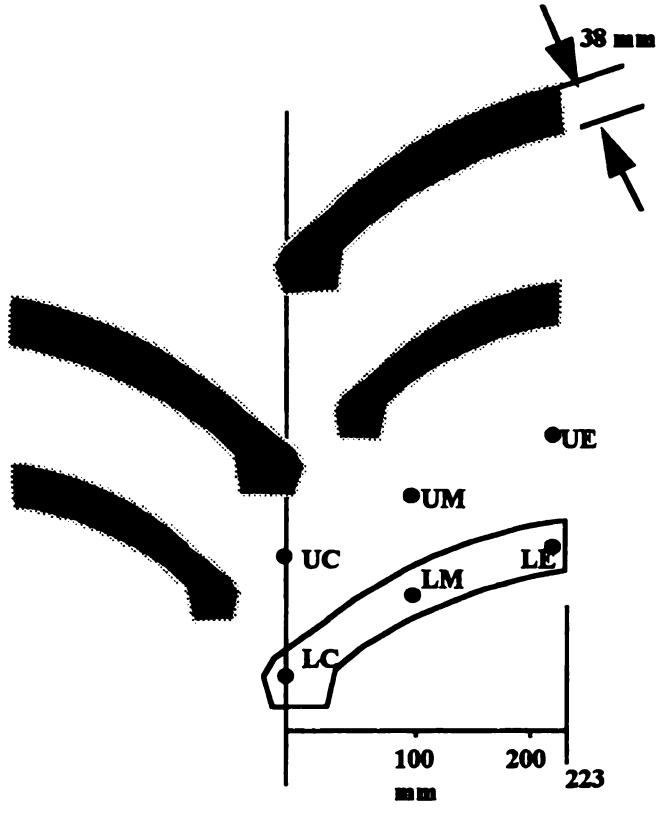

Figure 4.1 Lug pattern of 18.4R38 tire and location of transducers

The transducers used were Sensotec Model F Subminiature Transducers with diaphragm diameter of 9.7 mm. The nominal capacities of the sensors were 690 kPa for the transducers on the lug face and 350 kPa for the transducers on the undertread. The transducers on the lug were designated with letter L that indicates the lug sensor and a second letter was used to indicate the location of the sensor on the lug, so that LE, LM and LC indicate the transducer on the lug at the outside edge of the tread, the lug near the midpoint of the lug length and the lug near the circumferential centerline of the tread respectively. In a similar way the undertread sensors were designated UE for the undertread at the outside edge of the tread, UM for the undertread at the midpoint between the edge and the centerline, and UC for the undertread at the circumferential centerline of the tread.

4.2.3 Experiment Design

The experiments were conducted on NSDL's one of two indoor soil bins containing Norfolk sand loam soil (NSL) (Typic Paleudults) in March, 1995. The content of NSL as reported by Way et al. (1993) is 71.6% sand, 17.4% silt and 11.0% clay.

The soil was loosened with a rotary tiller and then compacted with a roller to obtain a specific compaction level for interface pressure measurements. Soil samples were taken to determine the moisture content and the bulk density at different locations within the soil bin before the tire traffic was applied. Cone index measurements were also made by using a cone that had base area of 323 mm^2 (0.5 in^2). The speed of pushing the cone was maintained at 30 mm/s, which is the ASAE standard. The mean initial soil conditions are given in Table 4.1 Four different tire variables (dynamic load, inflation pressure, slip

and location) were considered to be the variables that affect the interface pressures and the combination of these variables were assigned to the plots randomly. A completely randomized block type experiment design is shown in Figure 4.2.

Table 4.1 Mean initial soil conditions

Soil	: Sandy
Moisture content	: 6.37 % d.b.
Bulk density	: 1.408 Mg/cm^3
Cone index	: 0.412 MPa

Cone index is the average of 12 measurements (C.V.=3.05%)
Moisture content and bulk densities are the average of 6 measurements
CV for Moisture content is 21.6% and for bulk densities is 3.19%.

Two replications were carried out for each combination. All tire variables were kept constant during the tests and interface pressures were measured as the wheel rotates.

The pressures measured were the pressures normal to the diaphragms of the transducers on the tire. During the experiments the orientation of each soil-tire interface pressure transducer was not measured since the tire was not equipped with instrumentation to measure orientation of the transducers relative to the rim as the tread flexed. The measurement of transducer orientation is quite complex (personal communication, Dr. Thomas Way, USDA, NSDL, Alabama).

Two different levels of dynamic load, inflation pressure and slip were chosen. Dynamic load was 13.1 and 25.3 kN. Inflation pressure was chosen as 83 kPa and 110 kPa and slip was 7.5% and 10%. Interface pressures were measured at three different locations on tire lug and undertread area, totally at six locations. Combinations of the variables chosen are given in Table 4.2.

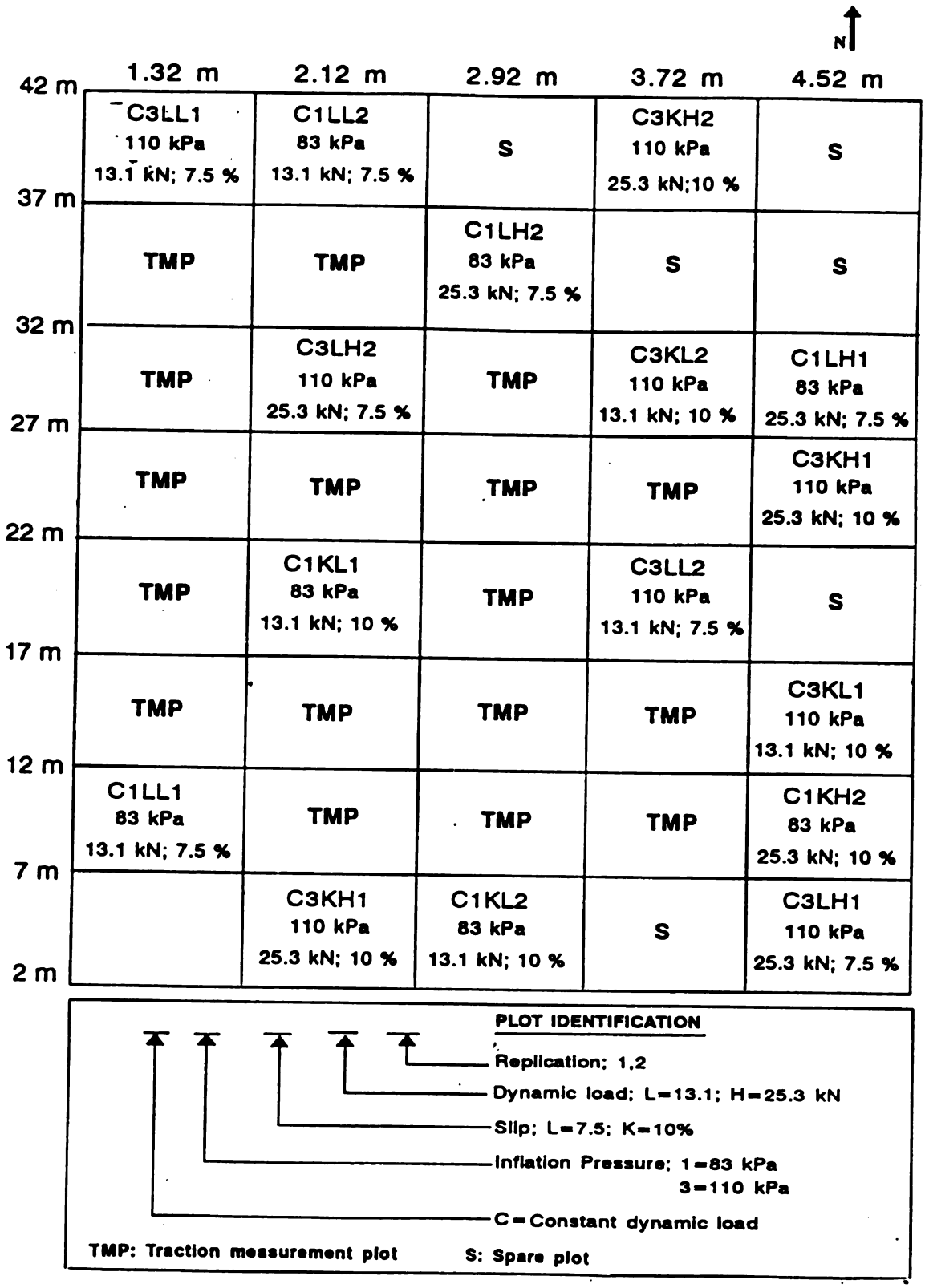

Figure 4.2 Completely randomized block design type of experiment design for soil-tire interface pressure measurements.

Table 4.2 Combinations of dynamic load, inflation pressure and slip chosen for the soil-tire interface pressure measurements.

Treatments*	Dynamic load (kN)	Inflation Pressure (kPa)	Slip (%)
C1LL	13.1	83	7.5
C1LH	25.3	83	7.5
C3LL	13.1	110	7.5
C3LH	25.3	110	7.5
C1KL	13.1	83	10
C1KH	25.3	83	10
C3KL	13.1	110	10
C3KH	25.3	110	10

***: Treatments as shown in figure 4.1**

All variables were controlled by computer throughout each test. The data acuasition system read each transducer once per 20 mm of distance travelled. Zero conditions for slip calculations consisted of zero net traction for the 18.4R38 tire operating on concrete. The wheel angle data were adjusted so the value of 0° on the wheel angle axis represents the bottom dead center (BDC) position for each of the pressure transducers. For each pressure transducer, pressures at negative wheel angles occurred when the pressure transducer was in front of its BDC position and pressures at positive wheel angles occurred when the pressure transducer was to the rear of its BDC position (Figure 4.3).

4.3 Results and Discussion

Using the single-wheel agricultural tester, the data collected with acquisition system were stored in different files for further analysis. An example from interface pressure data is given in Appendix A, Table A.1.

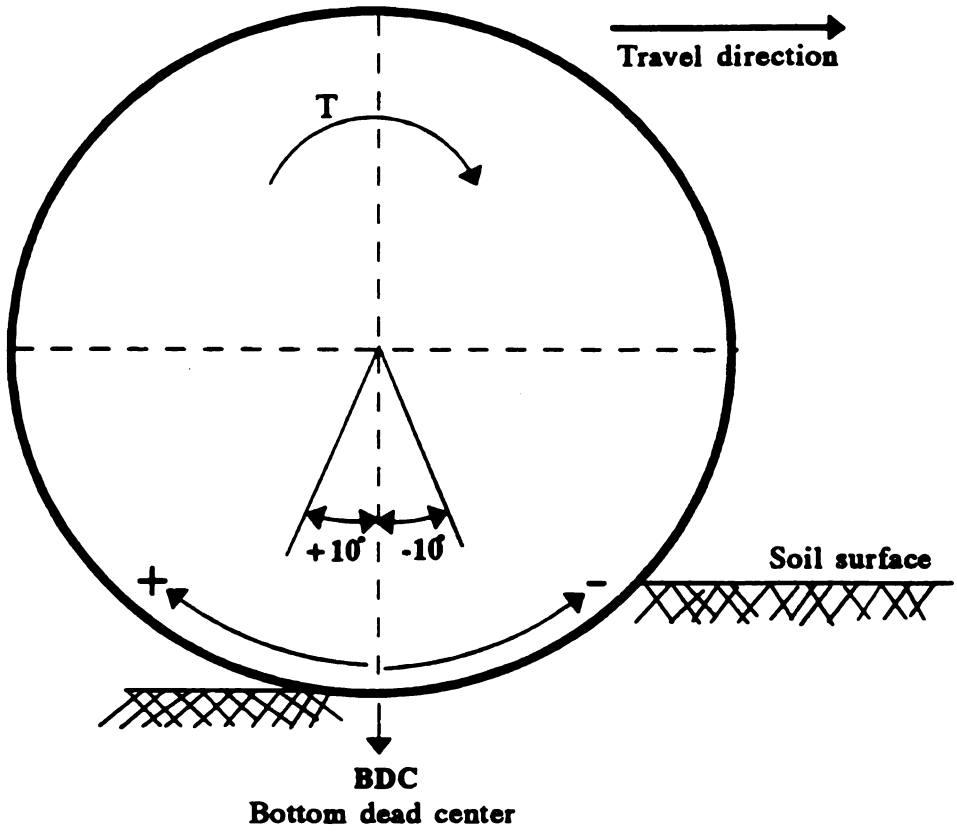

Figure 4.3 Bottom dead center and wheel angles used for statistical analysis.

Cone index measurements were also analyzed to understand whether or not the soil was uniformly prepared for the soil-tire interface pressure measurements. An example of cone index data is shown in Figure 4.4. Cone index results as the average of 12 measurements are given in Figure 4.5. As seen from the figure, it is possible to state that the soil was uniformly prepared with an acceptable level of variation.

Figures 4.6 thru 4.14 are drawn to indicate the soil-tire interface pressures obtained on the lug transducers only. Interface pressures obtained at the undertread area are not presented in the same figures since the pressures at the undertread area were low as compared to those obtained on the lug.

Figure 4.6 shows the effect of low inflation pressure (83 kPa) and the low dynamic load (13.1 kN) considered in this study. This is one of two exceptional cases that the interface pressure at the edge of the tire was lower than the other two locations on the lug. As seen from figure 4.6 the maximum interface pressure at the edge of the tire is obtained almost at BDC (0° angle).

The maximum interface pressures for the other two locations were obtained at different wheel angles. As seen from Figure 4.6, while interface pressures at the edge shows a normal distribution shape, the shape of the distrubition for other two locations is different. The interface pressure range for the middle and center were obtained in the range of -25° and +8° while the range for the edge one was -15° and +6°.

The interesting point in interface pressure-wheel angle relations as shown in figure 4.6 and in the following figures is that the contact length could be calculated from a range of the wheel angles where zero interface pressures were sensed by the transducers.

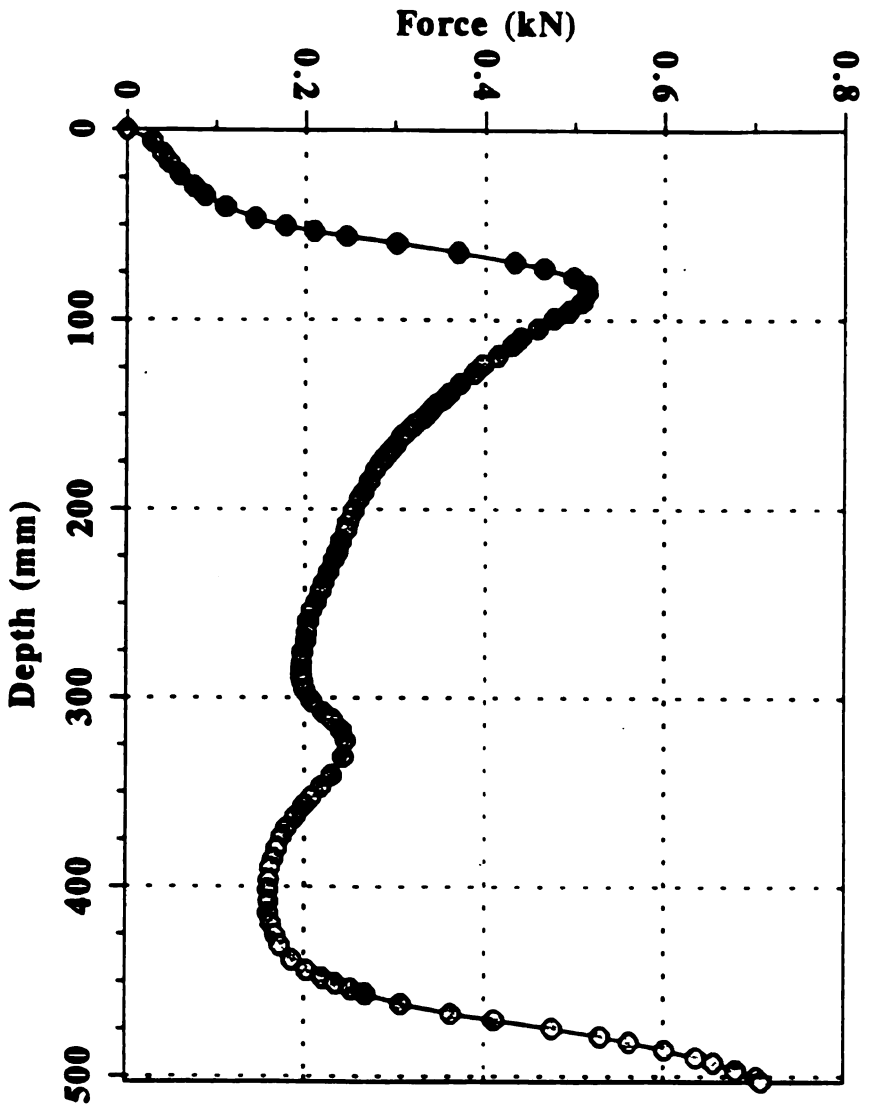

Figure 4.4 A sample cone index measurement result obtained from non-traffic area.

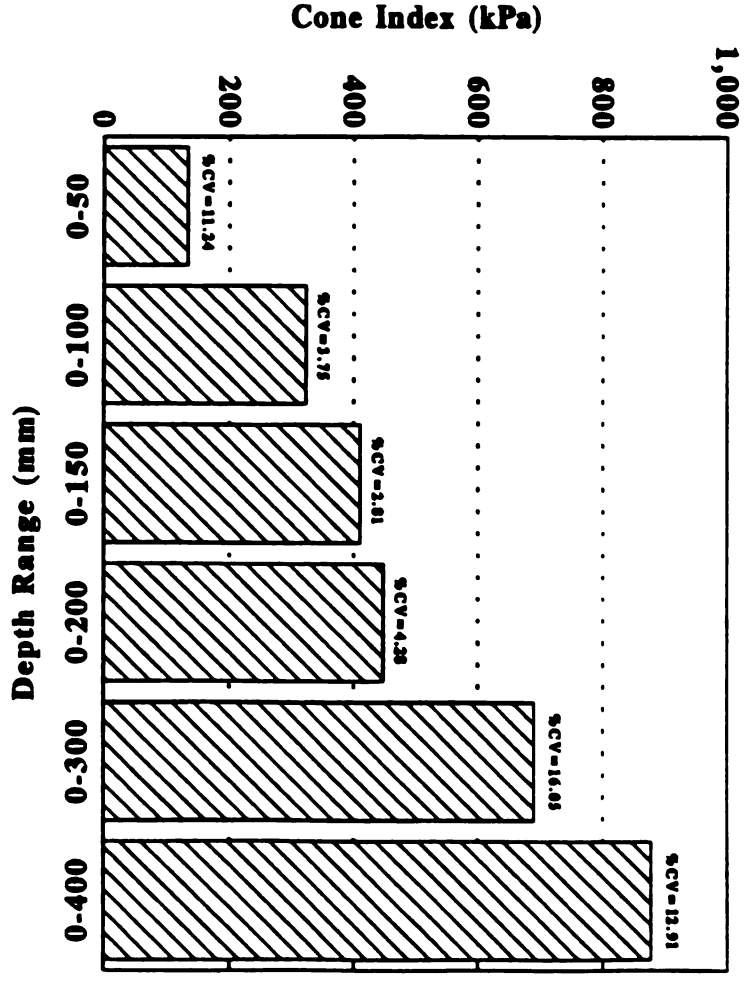

Figure 4.5 Cone index results from non-traffic area as a function of depth Coefficient of variations are the average of 12 measurements.

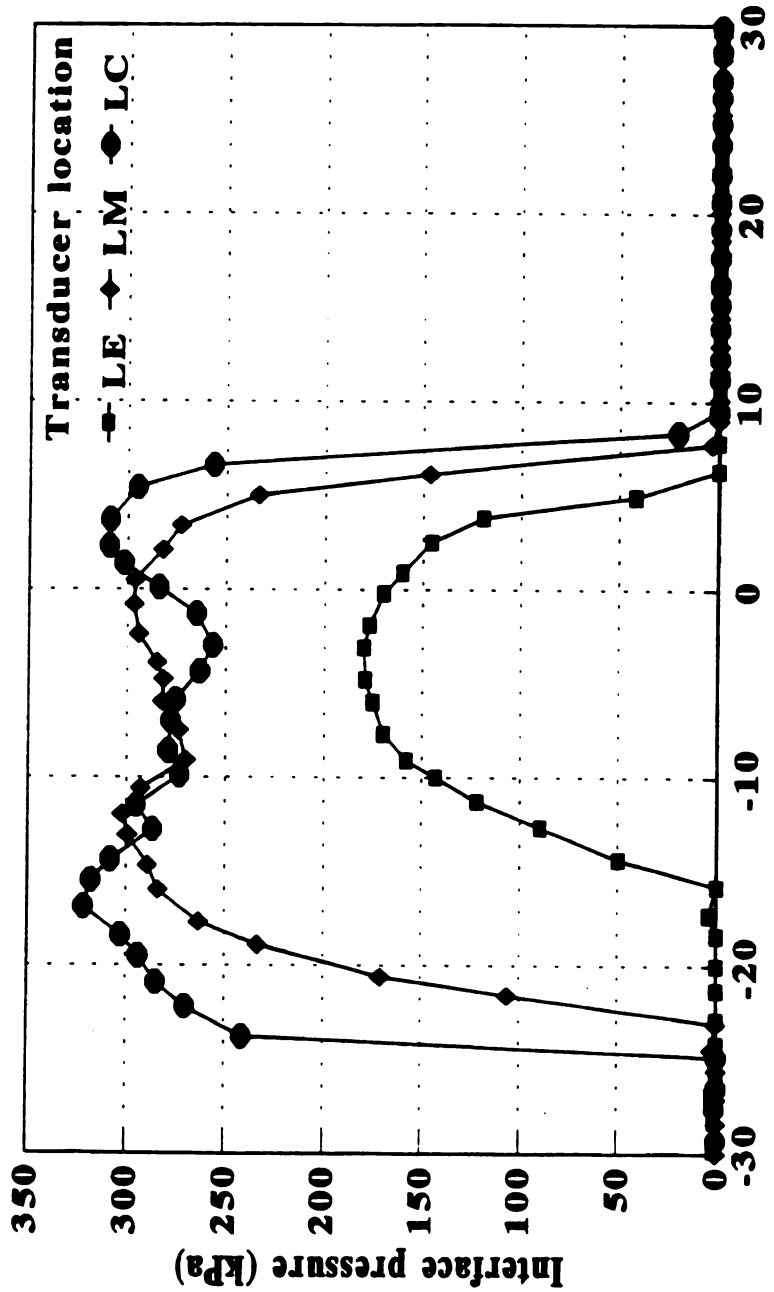

Figure 4.6 Soil-tire interface pressures at 83 kPa inflation pressure and 13.1 kN dynamic load (7.5 % slip)

Figure 4.7 shows the effect of dynamic load increase on interface pressures. While the interface pressure at the edge reaches a maximum at 0° of angle and keeps this at +10° and -10° interval, the interface pressures in the middle and at the center of the tire lug are minimum at -10° of wheel angle and they showed an increasing trend while they were away from the center and they became zero at -30° and +20°. A normal distribution shape at the edge was also obtained in this measurement. The increased range for the edge, middle and center location indicates the effect of increased contact width as a result of loading the tire with a higher dynamic load (25.3 kN). The center transducer read the interface pressures in the -30° and +18° range which was less than the other two locations.

When slip increased, some important changes took place on interface pressures. Figure 4.8 indicates the effect of low dynamic load, inflation pressure (83 kPA) and slip (10%) on interface pressures. When compared to figure 4.6, the location of maximum interface pressures changed the trend and the magnitude. The maximum stress was obtained at the edge and the stresses at two other locations were lower. When the slip was 7.5%, the maximum interface pressure for the edge was 180 kPa but it became 350 kPa at 10% slip. An increased slip changed the location and the magnitude of the soil-tire interface pressures for the edge transducer.

When the dynamic load increased to 25.3 kN, the trend in terms of the location of maximum interface pressures at 0° of wheel angle did not change, as shown in figure 4.9. indicates this. Figure 4.8 and 4.9 are the typical examples of increased contact length of the tire. While the range for zero interface pressures was -20° and +10° for low dynamic load (13.1 kN; Figure 4.8) the range was -30° and +20° for the high dynamic load (25.3

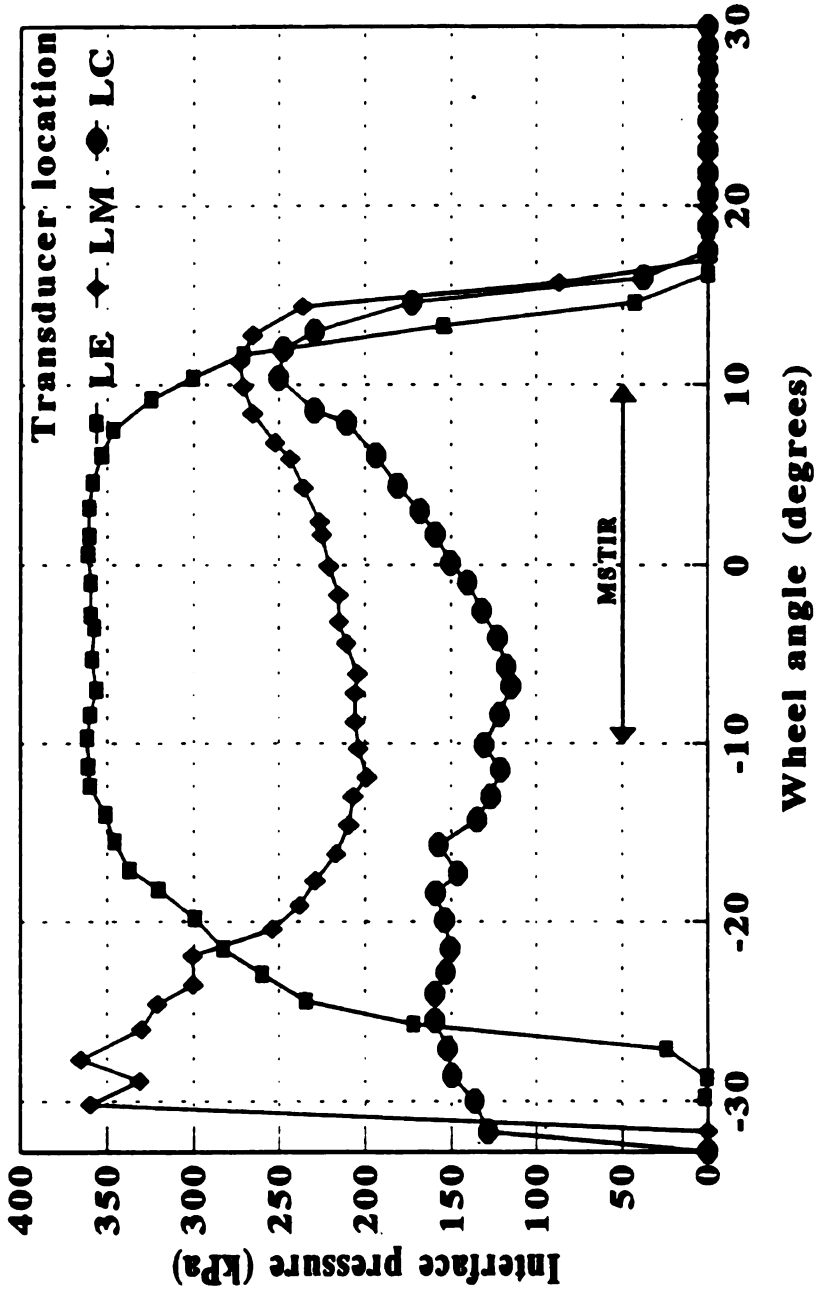

Figure 4.7 Soil-tire interface pressures at 83 kPa inflation pressure and 25.3 kN dynamic load (7.5 % slip)

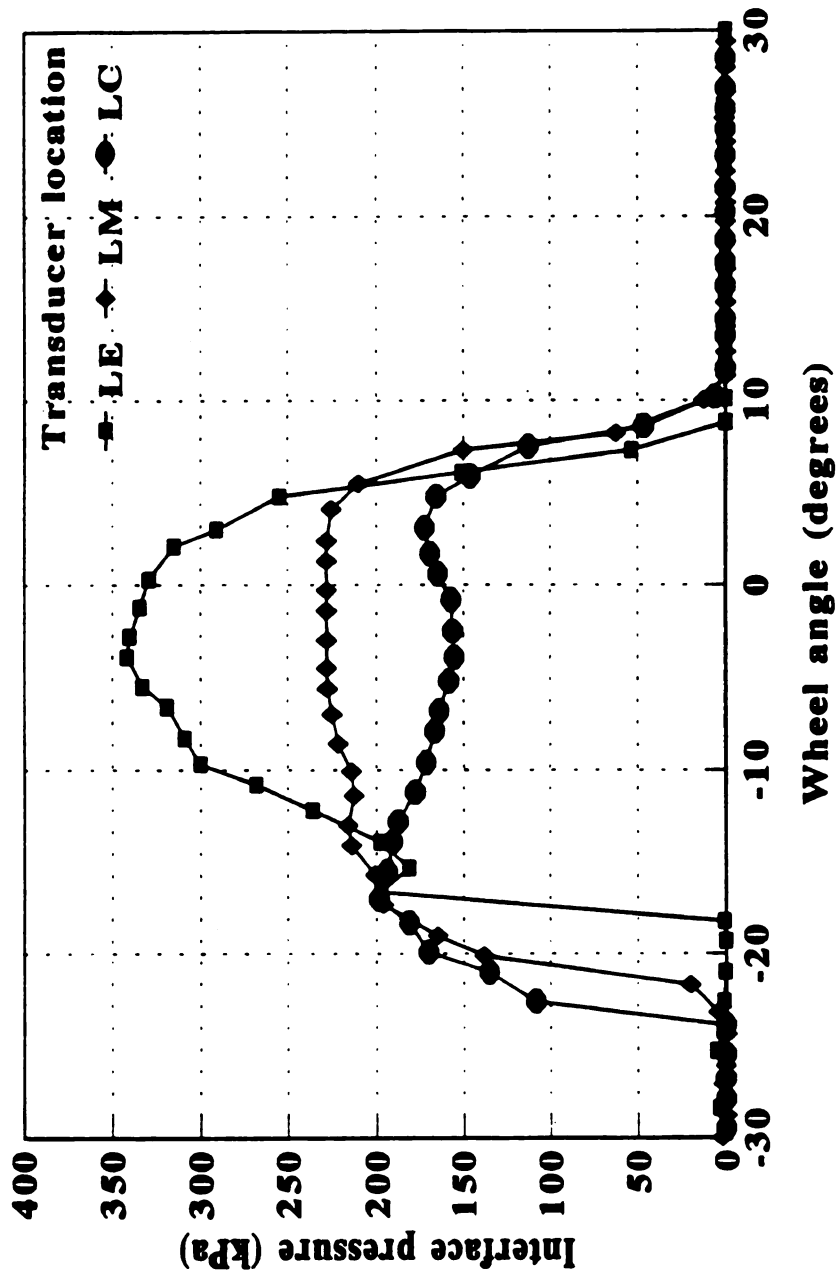

Figure 4.8 Soil-tire interface pressures at 83 kPa inflation pressure, 13.1 kN dynamic load (10 % slip)

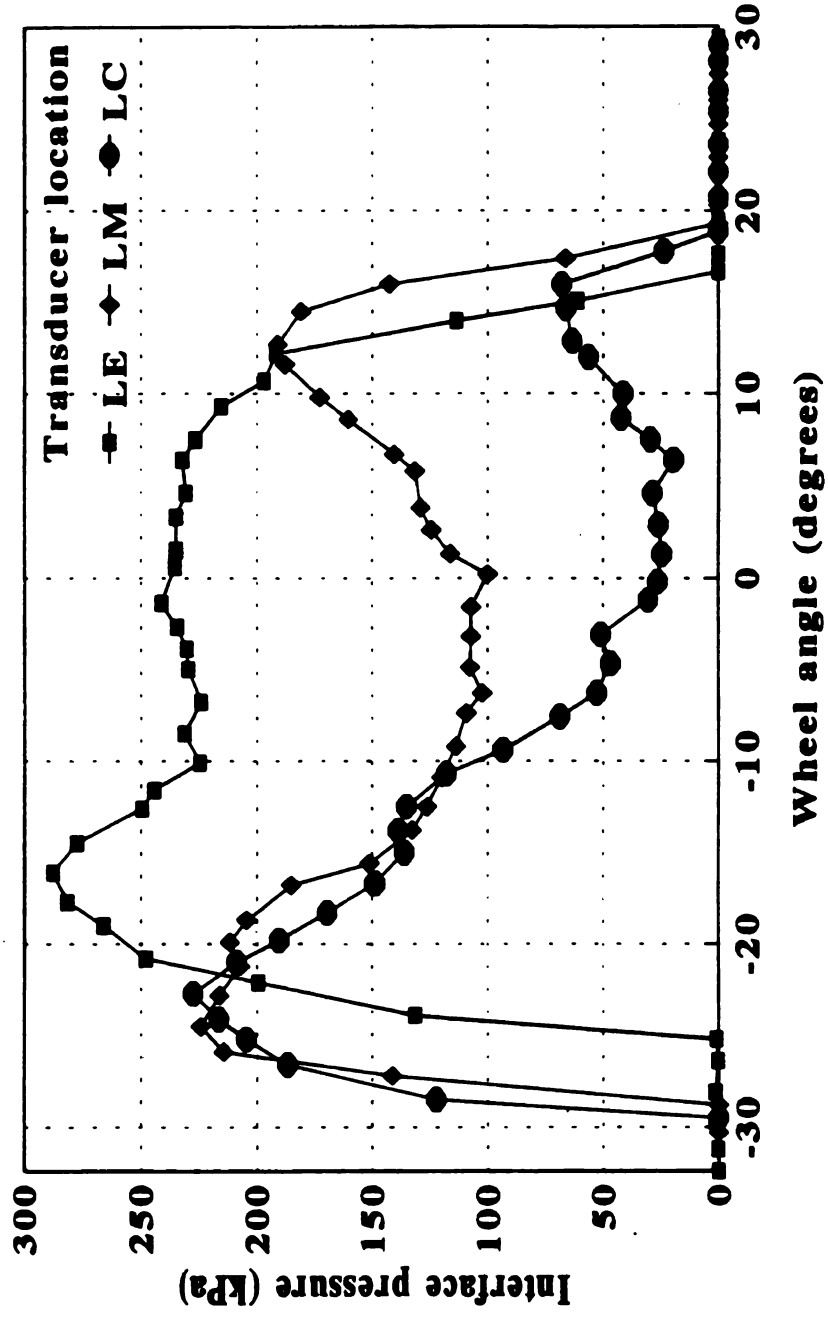

Figure 4.9 Soil-tire interface pressures at 83 kPa inflation pressure and 25.3 kN dynamic load (10% slip)

kN; Figure 4.9).

The the trend in terms of the location of the maximum interface pressure in the range as shown in Figure 4.9 did not change but the magnitude for all locations did change considerably. This could only be explained by the change in slip. It is also interesting to observe that the shape of interface pressures as a function of wheel angle for all locations is the same.

When inflation pressure increased from 83 to 110 kPa, there were also some corresponding changes observed as there was when slip was changed.

Figure 4.10 and 4.11 shows the interface pressures at 13.1 and 25.3 kN dynamic load, 110 kPa inflation pressure and 7.5% slip, respectively. As seen from figure 4.10 the maximum stress at 0° of wheel angle was obtained in the middle of lug. The same trend was also observed when the inflation pressure was 83 kPa (Figure 4.6).

When the dynamic load increased to 25.3 kN, the results of the two replications were different. In one experiment the maximum interface pressure at 0° was obtained in the middle (Figure 4.11) while the maximum interface pressure was measured at the edge of the tire with the same magnitude (Figure 4.12). This kind of discrepancy was only obtained in this case and this can be explained by the variations in soil conditions.

High inflation pressure (110 kPa) as seen from figure 4.10 thru 4.12 as compared to the ones at 83 kPa inflation pressure did not cause a change in the interval of interface pressures measured.

Figure 4.13 and 4.14 are the examples of high slip considered in this study. The dynamic load effect can be easily seen when the figures are examined. The location of

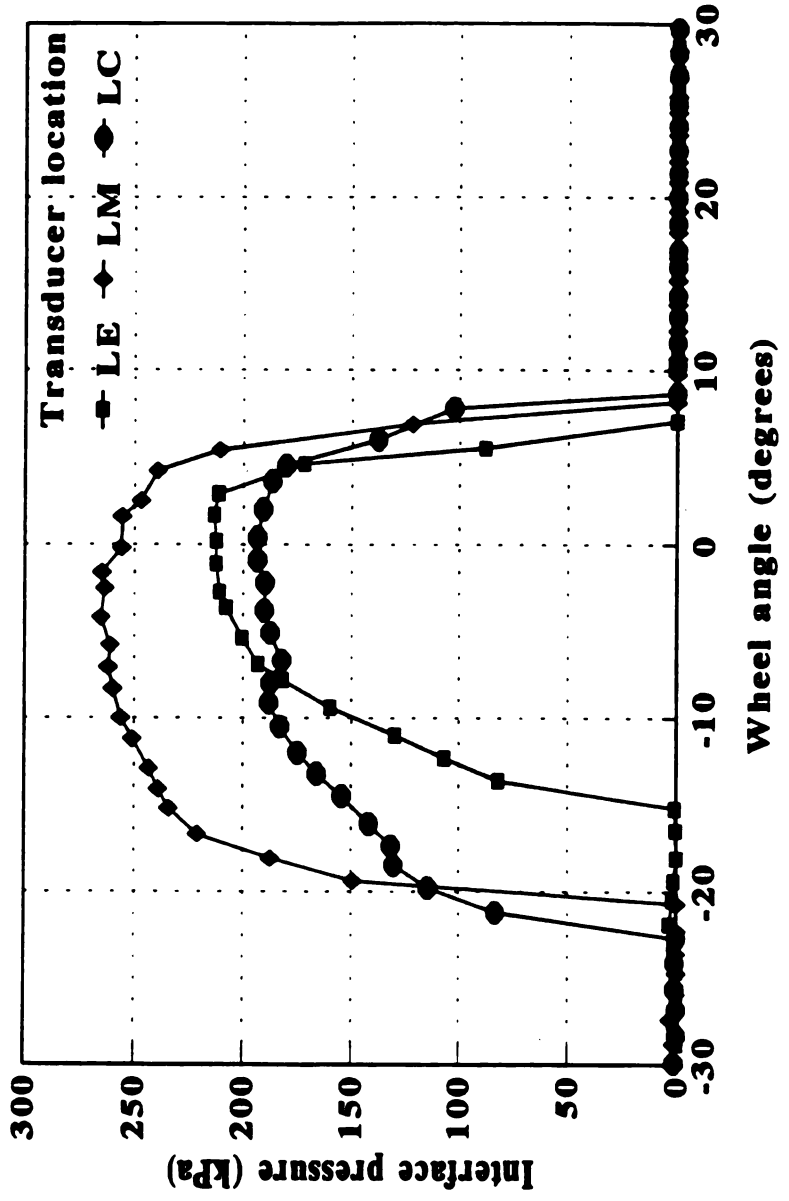

Figure 4.10 Soil-tire interface pressures at 110 kPa inflation pressure and 13.1 kN dynamic load (7.5 % slip)

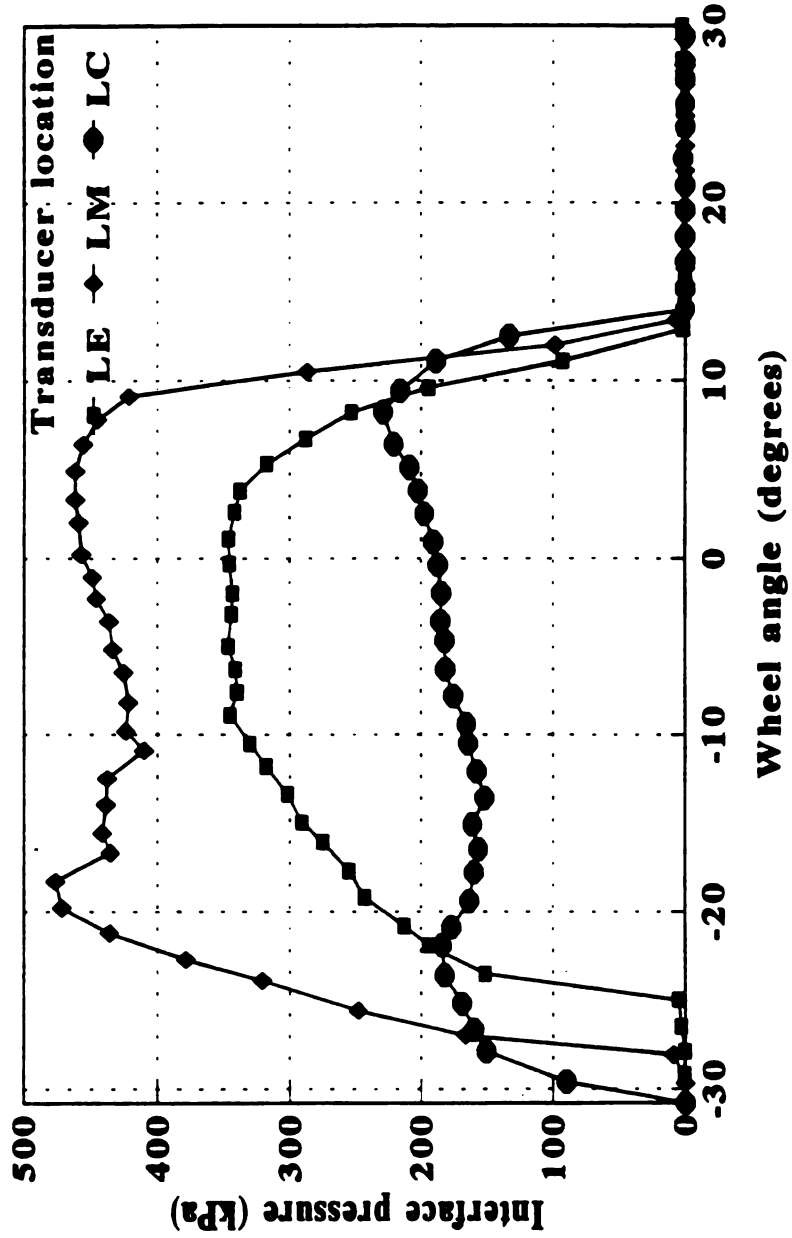

Figure 4.11 Soil-tire interface pressures at 110 kPa inflation pressure and 25.3 kN dynamic load (7.5% slip)

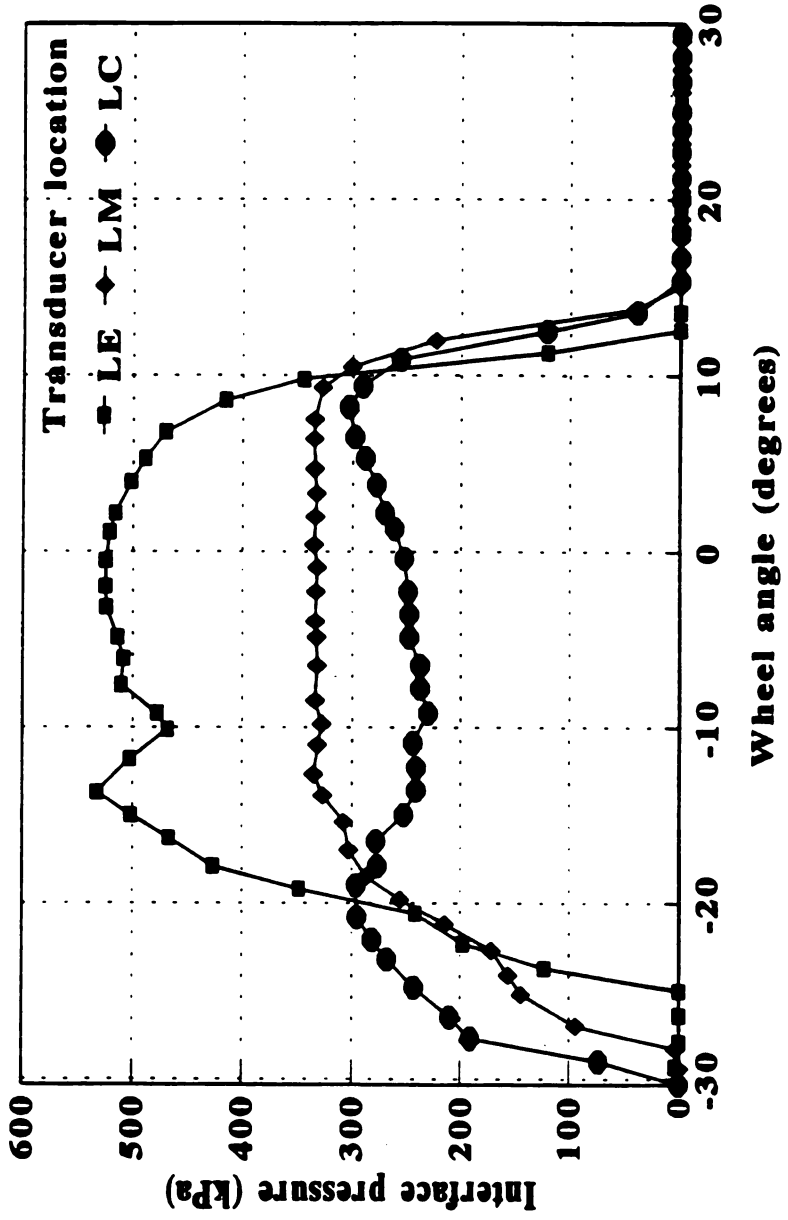

Figure 4.12 Soil-tire interface pressures at 110 kPa inflation pressure and 25.3 kN dynamic load (7.5 % slip)

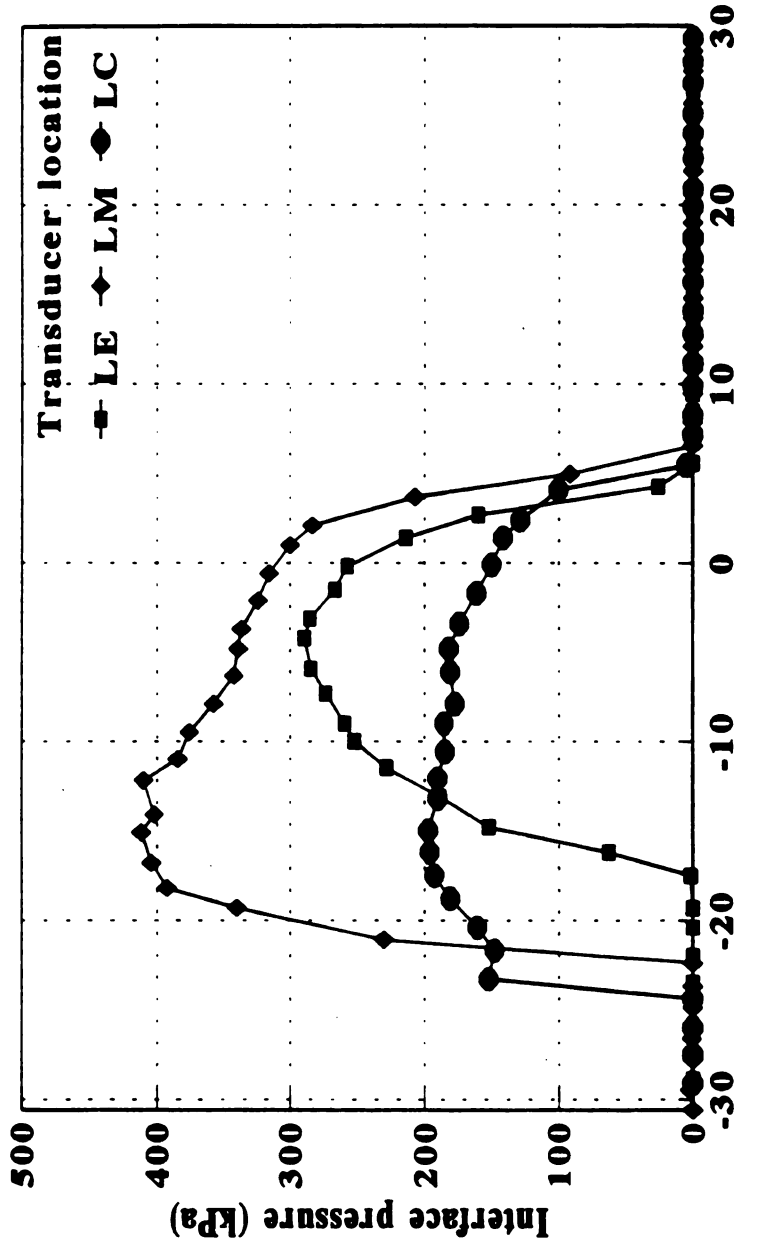

Figure 4.13 Soil-tire interface pressures at 110 kPa inflation pressure and 13.1 kN dynamic load (10 % slip)

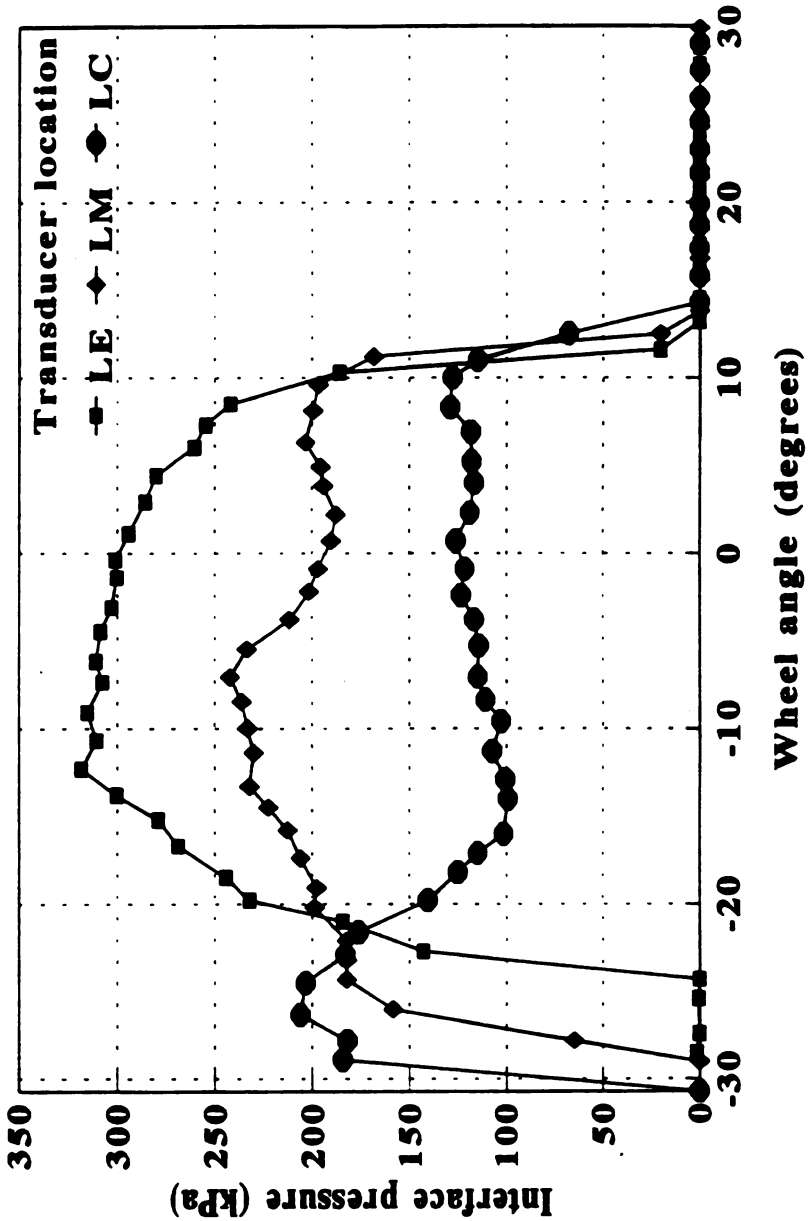

Figure 4.14 Soil-tire interface pressures at 110 kPa inflation pressure and 25.3 kN dynamic load (10% slip)

maximum interface pressure changes from the middle to the edge when the dynamic load increases to 25.3 kN at 0° of wheel angle.

The transducers located at undertread part of the tire were not shown along with interface pressures measured on the lug ones since the undertread transducers read quite low interface pressures as shown in Figure 4.15 and 4.16. These were the maximum undertread pressures obtained out of 16 experiments as a combination of two dynamic load, inflation pressure and slip with two replications. The low interface pressures sensed by the transducers at the undertread area can be explained by the soil condition such that only lugs were in contact with the soil and the axle load was carried by the contact area of the lugs.

The general results of mean soil-tire interface pressures as calculated in -10° and +10 ° of wheel angle are given in Table 4.3.

The interface pressure data as a function of tire operating variables (dynamic load, inflation pressure and slip) were statistically analysed only for those obtained on the lug transducers. A statistical package program, MSTAT, was used for the analyses. For the analyses, the -10° and +10° wheel angle was chosen as suggested by Way et al. (1993) since the maximum soil-tire interface pressures occur in this range. The wheel angle data were adjusted so the value of zero on the wheel angle axis represents the bottom dead center (BDC) position for each of the pressure transducers. For each pressure transducer, pressures at negative wheel angles occurred when the pressure transducer was in front of its BDC position and pressures at positive wheel angles occurred when the pressure transducer was to the rear of its BDC position (Figure 4.1).

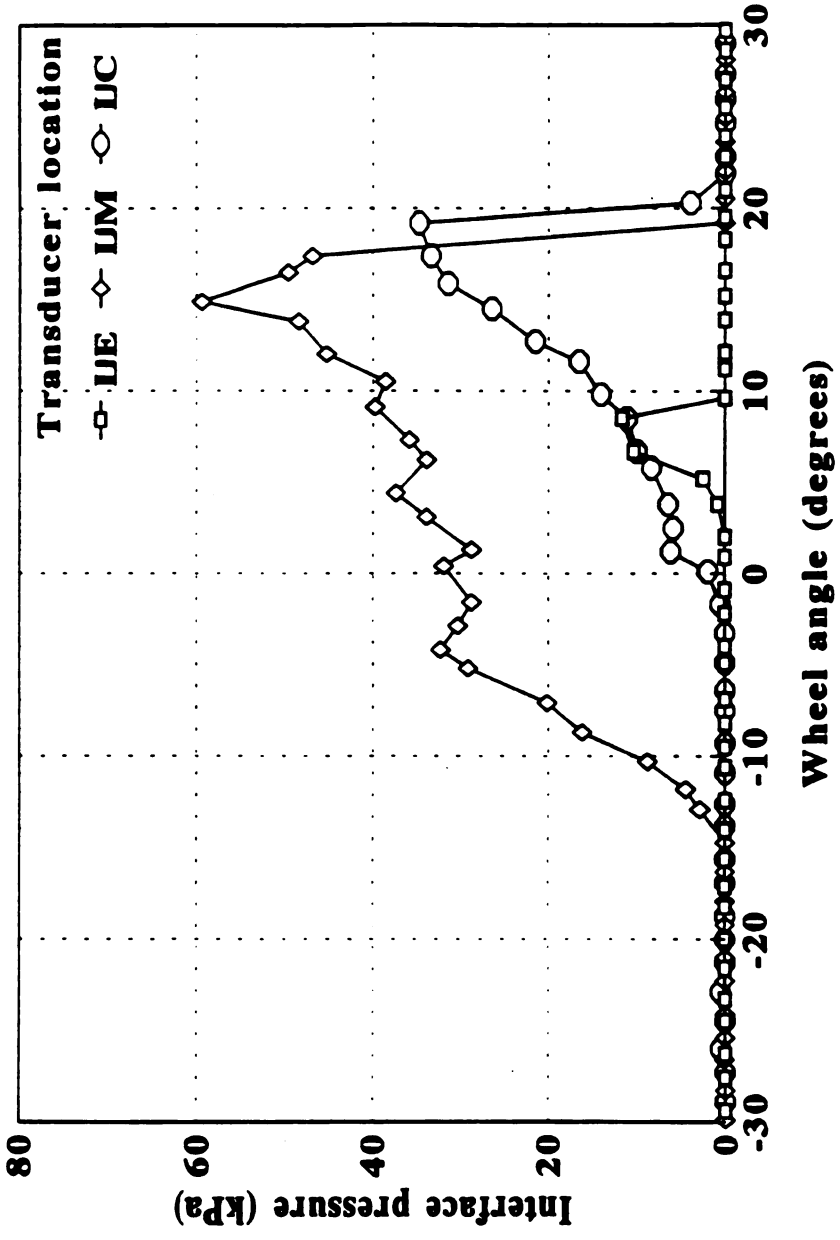

Figure 4.15 Soil-tire interface pressures at 83 kPa inflation pressure and 25.3 kN dynamic load (Undertread transducers; 10% slip)

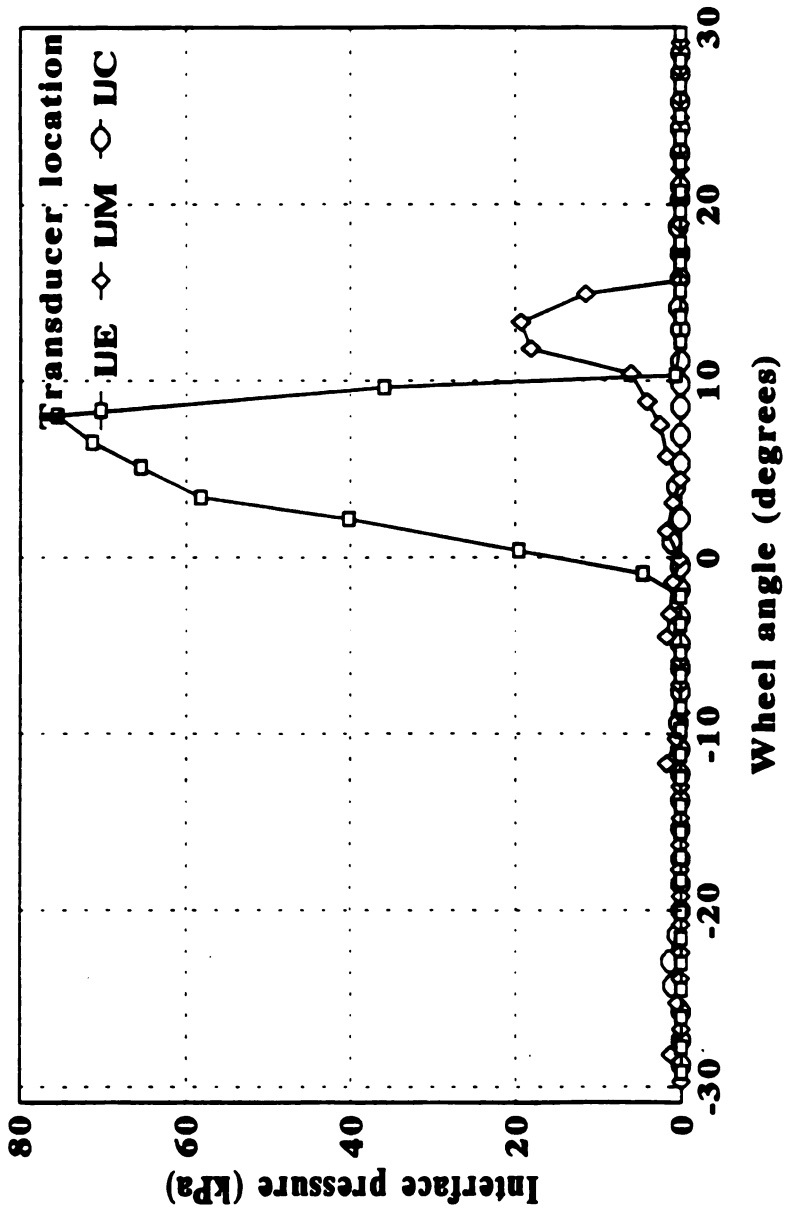

Figure 4.16 Soil-tire interface pressures at 110 kPa inflation pressure and 25.3 kN dynamic load (undertread transducers; 10% slip)

Table 4.3 Results of soil-tire interface pressures measurements.

Inflation pressure (kPa)	Slip (%)	Dynamic load (kN)	Location	Mean Interface pressure* (kPa)
83	7.5	13.1	LE	**116.4**
		13.1	LM	**228.0**
		13.1	LC	**235.5**
		25.3	LE	**320.6**
		25.3	LM	**242.6**
		25.3	LC	**170.6**
	10	13.1	LE	**238.5**
		13.1	LM	**182.4**
		13.1	LC	**135.7**
		25.3	LE	**241.9**
		25.3	LM	**171.6**
		25.3	LC	**57.9**
110	7.5	13.1	LE	**179.4**
		13.1	LM	**292.0**
		13.1	LC	**189.2**
		25.3	LE	**394.1**
		25.3	LM	**384.3**
		25.3	LC	**228.1**
	10	13.1	LE	**191.8**
		13.1	LM	**239.0**
		13.1	LC	**141.2**
		25.3	LE	**293.2**
		25.3	LM	**211.7**
		25.3	LC	**185.0**

*Mean interface pressures are the average of two measurements. LE: Lug edge; LM: Lug middle; LC: Lug edge

The results of mean soil-tire interface pressures from the statistical analysis are given in Table 4.4. The details of the analysis are also presented in Appendix A, Table A.2.

Using the results of mean interface pressures least square difference (LSD) tests for the multiple comparisons were achieved and interpreted at α=0.05 and from the analyses, the effect of each independent variable was found to be significant (Table 4.4).

Table 4.4 Results from the variance analysis

Source	DOF	MS	F Value	Prob.
Factor I	1	28698	11.3	0.0025
Factor S	1	39757	15.7	0.0006
Inter. I*S	1	1185	0.46	
Factor D	1	23624	9.3	0.0054
Inter. I*D	1	13023	5.1	0.0324
Inter. S*D	1	18190	7.2	0.0130
Inter. I*S*D	1	10	.004	
Factor L	2	32122	12.7	0.0002
Inter. I*L	2	2135	.84	
Inter. S*L	2	6522	2.58	0.0964
Inter. I*S*L	2	4900	1.94	0.1655
Inter. D*L	2	23516	9.3	0.001
Inter. I*D*L	2	1783	.70	
Inter. S*D*L	2	5886	2.33	0.118
Inter. I*S*D*L	2	2096	0.83	
Error	24	2525		

I: Inflation Pressure S: Slip
D: Dynamic Load L: Location
DOF: Degrees of freedom
MS: Mean square

Inflation pressure has become an important variable for many researchers in recent years and the limits for inflation pressures for certain type of tires used in agricultural

operations have been lowered by tire manufacturers. In this study, the importance of inflation pressure was also studied and showed a significant effecton interface pressures ($p=0.0025$, mean interface pressure at 83 and 110 kPa inflation pressure is 195.2 and 244.1 kPa, respectively). This means that the higher the inflation pressure the higher the mean interface pressures were.

Dynamic load acted in the same way that inflation pressure did on interface pressures. Increasing dynamic load ($p=0.0054$, mean interface pressure at 13.1 and 25.3 kN dynamic load is 197.4 and 241.8 kPa, respectively) resulted in increased interface pressures on the lug transducers. An increased dynamic load effect was also confirmed by Burt et al. (1988).

Interface pressures on the lug were also found to be location dependent ($p=0.0002$). An average of 16 measurements of interface pressure measurements on the lug edge, middle and center (found from the variance analysis) were 247.0, 244.0 and 167.9 kPa, respectively. But LSD test for the comparison of statistical difference did not indicate any significant difference between the edge and the middle interface pressures but the difference was found to be significant when lug edge and the middle were compared to the center one. From the above findings it can be stated that dynamic load and inflation pressure are the important variables that must be considered for a better understanding of traction and soil compaction.

The interesting finding in this study was the slip effect on interface pressures. Slip affected the interface pressures adversely. Just the opposite of dynamic load and inflation pressure. An increase in slip caused a decrease in interface pressures, even though a close

range was used for the slip due to a technical problem for the experiments. A significant difference ($p=0.0006$) was found between 7.5 and 10% slip. This finding can be explain by examining a figure (Figure 4.17) given by Karafiath and Nowatzki (1978). Karafiath and Nowatzki (1978) also supported this finding and concluded that "***the effect of slip is primarily on the application of shear stresses at the soil-tire interface by reducing the normal stresses, necessitates an increase in the contact area in order to balance the wheel load. Hence, tangential stress components act in the direction of soil failure and tend to facilitate this failure. In effect they reduce the normal stresses that would otherwise be necessary to cause failure***".

Three out of six interactions were found to be significant at $\alpha=0.05$ level. One of these was the inflation pressure-dynamic load interaction ($p=0.0324$). The Slip-dynamic load interaction ($p=0.013$) also affected soil-tire interface pressures and it was statistically significant.

The dynamic load-location interaction was the interaction that affects soil-tire interface pressures ($p=0.001$).

From the above interactions it can be said that dynamic load appears to be the most important variable since its effect as an independent variable and also in combination with other independent variables was found to be significant.

The effect of independent variables (dynamic load, inflation pressure and slip) and their interactions are discussed below along with the interactions.

Figure 4.18 shows the effect of dynamic load at 83 kPa inflation pressure and 7.5% slip. As seen from the figure increased dynamic load changes the location of highest

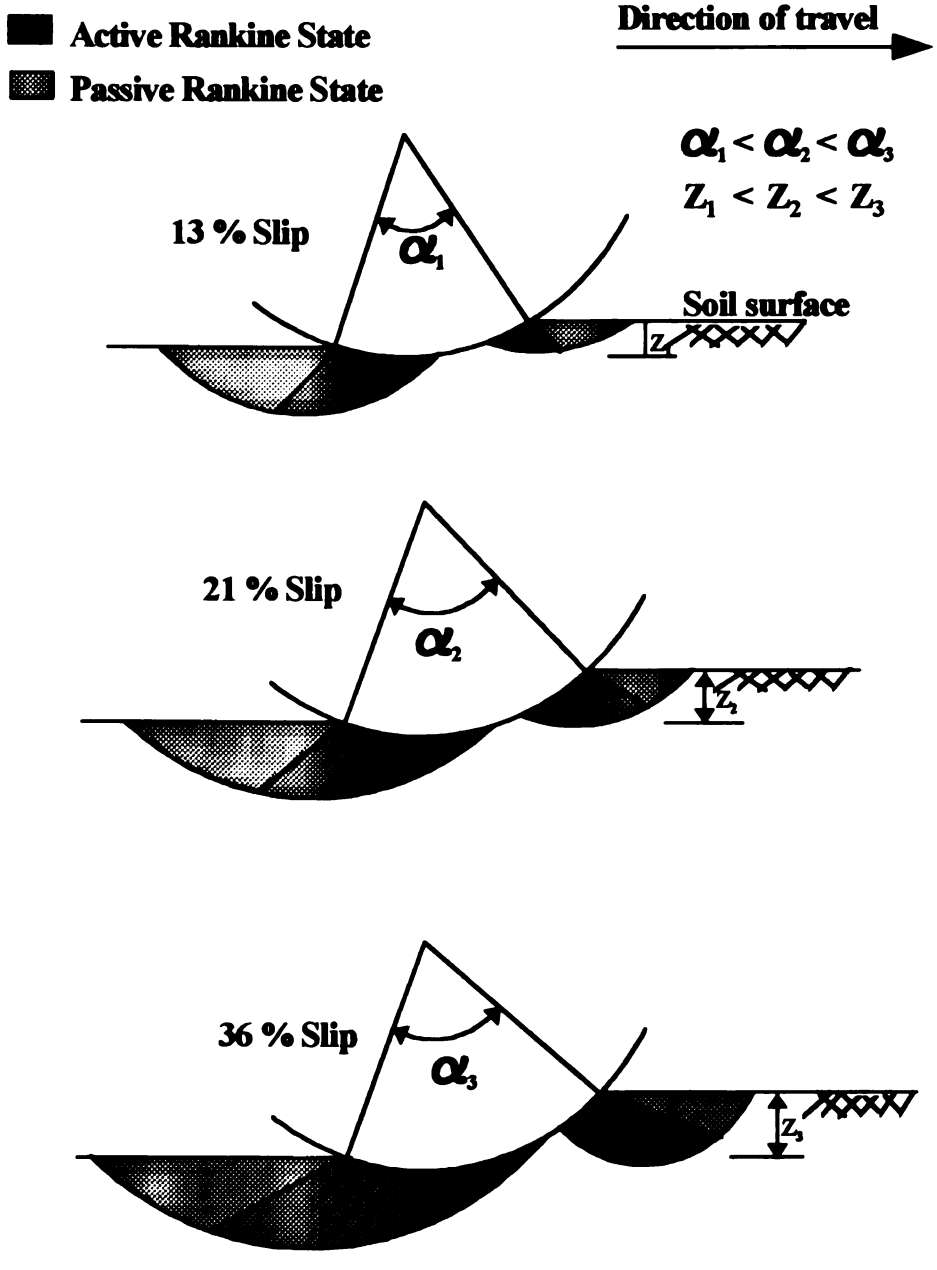

Figure 4.17 Tire centerline and outlines of slipline fields at various slip. (Karafiath and Nowatzki, 1978). *: Not shown in original figure

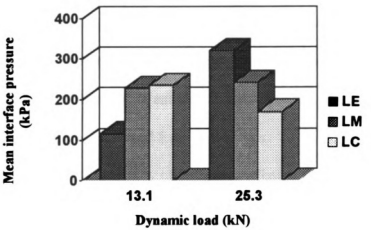

Figure 4.18 Mean interface pressures at different locations on the lug of 18.4R38 tire at different dynamic loads (Inflation pressure 83 kPa and slip: 7.5%)

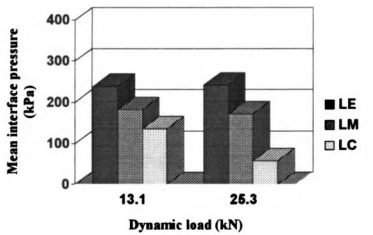

Figure 4.19 Mean interface pressures at different locations on the lug of 18.4R38 tire at different dynamic loads (Inflation pressure: 83 kPa and slip: 10%)

interface pressure on the tire lug. Maximum interface pressure was attained at the outer edge of the tire lug for high load while maximum pressure was located at the center for low dynamic load No change in the middle was indicated from the statistical analysis.

Examining the same phenomena at 10% slip as discussed above from figure 4.19 indicates that at 10% slip, the effect of dynamic load did not affect the location but affected the magnitude in the middle and the center of the lug. This clearly indicates the dynamic load-slip interaction obtained from the analysis.

Figure 4.20 shows the effects of increased inflation pressure as compared to the one given in figure 4.18. Especially at high load (25.3 kN), the magnitude of interface pressure changed

At high slip (10%), the effect of inflation pressure can seen in Figure 4.21.

4.4 CONCLUSIONS

The following conclusions have resulted from this study.

1. Inflation pressure effect on interface pressures was found to be significant at 95% probability level. This study suggests that a low inflation pressure causes less interface pressures on soil that it may help avoid excessive soil compaction.
2. Soil-tire interface pressures on the lug of 18.4R38 tire was found to be affected by dynamic load. An increase in dynamic load increased interface pressures.
3. Slip was also found to be an important variable on soil-tire interface pressures. This needs to be studied further and extensive research on slip effect is highly recommended. If the effect of slip as obtained in this study is repeated, the results will help in

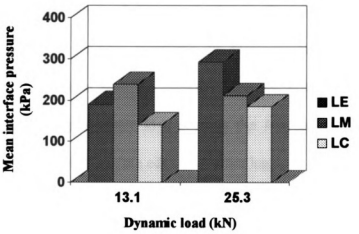

Figure 4.20 Mean interface pressures at different locations on the lug of 18.4R38 tire at different dynamic loads (Inflation pressure: 110 kPa and slip: 7.5%)

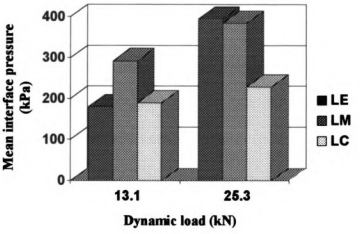

Figure 4.21 Mean interface pressures at different locations on the lug of 18.4R38 tire at different dynamic loads (Inflation pressure: 110 kPa and slip: 10%)

optimising traction and soil compaction, since slip is the most important variable to obtain a desirable level of traction efficiency.

4. Interaction between slip and dynamic load was also statistically significant. While dynamic load is kept constant, increasing slip decreases the soil-tire interface pressures.
5. The location of highest interface pressures was found to be load dependent. That means an increase in dynamic load changes the location of the maximum interface pressures from the middle to the edge on the tire lug.

Chapter 5

SIMULATION OF SOIL-TIRE INTERFACE PRESSURES

Tires are one of the most important components of agricultural tractors today. Along with the changes in construction , the size of tractor tires are becoming larger to handle bigger tasks. The performance of tires are now more important than they have been in the past due to economics and fuel prices. Since tractor tire performance and soil compaction are interrelated problems, understanding tire behavior under different loading conditions along with the changes in soil conditions will enable one to design or modify the tire variables to reduce soil compaction that affects yield in the field.

While the studies following Trabbic's work (1950) were mostly experimental, some recent simulation based studies have focused on the interaction of agricultural tire and rigid surface and interface pressures (Hu and Abeels, 1994a, 1994b). In the first case the interaction of tire-soil was mostly experimental and the tire behavior on soil was interpreted by using the measured data. Now with tires varying in size and construction being used in agriculture and forestry and also tire variables such as load, and inflation pressure, the simulation of such conditions using computers becomes a very powerful research method. An insight into soil-tire interaction has great importance in the study of soil compaction and it is important in the selection of an optimum range in terms of traction and soil compaction. The complex nature of the tire is such that analytical methods are not well-suited to study the soil and tire interaction. However, the Finite

Element Method as a simulation tool has been successfully applied to such structural problems in the past, the interaction of a tire on a rigid surface. But the simulation of tire-soil interaction has always been a challenging problem for researchers since modeling soil behavior under load itself is a complex phenomena. Soils exhibit elasto-plastic behavior under load and there is still no unique soil constitutive model in the literature. Obtaining soil properties requires some laboratory experiments and modeling studies from the literature. Sampling of the soils, especially cohesionless soils such as sandy soil is another problem since obtaining undisturbed samples of such soils is quite difficult.

Due to the reasons given above, up to the present, soil-tire interaction has always been studied experimentally. Any changes in geometrical shape and loading conditions can change the stresses applied to the soil. As a result of these changes, interface pressures may show variations depending upon the loading conditions. However, obtaining soil-tire interface pressures and stress distribution in soil is of interest to researchers for traction modeling and understanding traction and it appears that simulation based studies are the best approach to investigate this phenomena. Once a methodology is developed to study the tire-soil interactions, studying the effect of tire variables such as inflation pressure and dynamic load is possible for other researchers and the tire-soil interaction and tire performance on soil can be explored and studied in depth. One example of such phenomena was the tire lug height effect on interface pressures as investigated by Way et al. (1993). Considering the above points, a simulation study using the Finite Element

Method was carried out, **with the main objective of this study being, to develop a methodology to study soil-tire interactions.**

5.1 Objectives

The specific objectives of this section were given as follows;

1. To investigate the tire behavior on various surfaces such as rigid and deformable.
2. To determine the effects of tire variables such as load, inflation pressure, size and construction (radial or bias) on interface pressures.
3. To study the effects of initial soil conditions (firm or soft) on soil-tire interface pressures.
4. To develop a methodology to study soil-tire interaction

5.2 Materials and Methodology

5.2.1 Materials

5.2.1.1 Tires and their material properties

Four tires, as a combination of two different sizes (14.9-30 and 18.4-38) and two different constructions (radial and bias) for each size were considered in this study. Agricultural tractor tires have not yet been converted to metric sizes. Thus, the tire sizes given above are in inches. As an example of 14.9-30 tire, the first number is the section width (14.9) and the second number is the rim diameter (30). Hyphen between the two numbers is designated to indicate a bias tire whereas R indicates the radial tire. Significant dimensional differences between radial and bias tires used in this study are compared in Table 5.1.

Hu and Abeels (1994a), indicated that tire materials showed high anisotropic properties and in order to overcome difficulties such as convergence problems in Finite Element Modeling, the material properties of tire components were assumed to be isotropic. The material properties used in the finite element simulations are given in Table 5.2.

Table 5.1 Dimensional comparison of tires used in simulations.

Dimension	Tire size and Construction			
	14.9-30	**14.9R30**	**18.4-38**	**18.4R38**
Section height (mm)	**327.9**	**338.0**	**394.9**	**407.6**
Section width (mm)	**367.0**	**368.3**	**457.2**	**456.4**
Full arc width (mm)	**360.6**	**361.9**	**447.0**	**447.0**
Diameter (mm)	**1417.8**	**1438.1**	**1755.1**	**1780.5**
Lug height (mm)	**38.6**	**41.14**	**140.8**	**43.68**

Table 5.2 Material poperties of tire components.

Tire component	Modulus of Elasticity		Poisson's ratio
	Mpa	(psi)	
Carcass	1000	145000	0.3
Belt	2000	290000	0.3
Beadwire	500	72500	0.3
Sidewall	6.21	900.6	0.49
Lug	6.21	900.6	0.49
Tread	4.14	600.4	0.49

5.2.1.2 Soils and Determination of Their Mechanical Properties

Since tire-soil interaction and traction is a surface related phenomena, the soil samples were taken at various depths before the tire traffic was applied and bulk density and moisture content determinations were made. The traction and soil-tire interface pressure measurements were conducted in the soil bin at the National Soil Dynamics

Laboratory, Auburn, Alabama). Table 5.3 shows the mean initial soil conditions. The samples taken at a depth up to 15 cm were assumed to be the representative of the soil used for the experiments.

Table 5.3 Soil conditions used for triaxial tests

	Soft soil*	Dense soil
Soil type	Sandy	Sandy
Cone index	0.412 MPa	0.862 MPa
Moisture content	6.37 % (d.b)	5.97% (d.b.)
Bulk density	1.408 Mg/cm3	1.639 Mg/cm3

* Coefficient of variations (C.V.) are given in Table 4.1
For dense sloil: Moisture content and bulk density values are the average of 19 measurements. CV for moisture content and bulk density was 3.9 and 2.89% , respectively.
Cv for cone index is %9.

Some air dried soil was brought to the Michigan State University from The National Soil Dynamics Laboratory (NSDL) for the triaxial test purposes. For each triaxial test, some soil was first sieved with a sieve (#10 sieve) of 2 mm mesh and then molded in a special apparatus at the moisture content and bulk density obtained before the traction (March 1994 and 1995) and interface pressure measurements (March,1995). The Consolidated-Undrained tests at three different confining pressure at 69 (10 psi), 138 (20 psi) and 345 kPa (50 psi) with two replications were conducted. The details of how the soil samples were molded and triaxial tests were conducted are given in Appendix B. From the normalized stress-strain graphs, the initial Youngs Modulus determination using earth pressure at rest was made. Poissons ratio of 0.3 was assumed for soils to use in the Finite Element simulations. Based on their initial Youngs Modulus and initial bulk densities, soils in this study were classified as soft and dense soil.

5.2.2 Methodology

5.2.2.1 Finite Element Formulation of the Problem

The Finite Element Method is a general method of structural analysis in which a continuous structure is replaced by a number of elements interconnected at a finite number of nodal points. This study uses the finite element method to simulate soil-rigid surface and soil-tire interaction as affected by soil and tire variables.

The finite element method analysis consists of the following basic operations;

1. Development of stiffness matrix of an arbitrary element with respect to local co-ordinate system.
2. Transformation of the element stiffness from the local co-ordinate system to a global co-ordinate system of the complete structural assemblage.
3. Superposition of individual element stiffness to obtain the total stiffness matrix of the total system.
4. Formulation of equilibrium equations relating the applied nodal forces and resulting nodal displacements and their solution.
5. Computation of element stresses resulting from the computed nodal displacements making use of the element stiffness matrices.

A commercial finite element program called MARC was used to simulate tire and soil behavior as separate deformable bodies and then as an integrated one deformable body under various soil and tire conditions. The tire and soil behavior was studied as a plane-

strain problem that assumes the applied loads lie in the x-y plane, then the displacement in the z direction is zero.

5.2.2.2 Tire Geometry and Tire Boundary Conditions (TBC)

Four different tires and their geometries were modeled and simulated. The tires used for simulations were 18.4R38, 18.4-38, 14.9R30 and 14.9-30. Modeling tires were made with the assumption that the gaps between the lugs were filled with the same material as the tire lugs since the tire geometry was symmetrical in the tread centerline plane with the exception of the lugs. The blue prints of the tire cross-sections were obtained from Pirelli-Armstrong Tire Corp. Even though an entity can be meshed using automesh option in the program, due to the geometries of tires and the identification of the materials at the cross-section, the meshing procedure achieved automatically in the program was limited. As a result, the meshing procedure used a transparency divided in inches that was made by hand. During the process of meshing and creating nodes, special attention was given to create equally spaced and sized elements. The tires were meshed by using quadratic elements and few triangular elements. The mesh was made as suggested by Hu and Abeels by keeping the size of the elements about 10 mm. This was necessary for accurate results. The two co-ordinates (x and y) of each node then was defined in the program to create a whole tire cross-section for simulation purposes. A total of four tire cross-sections were created in the same way and the materials were identified. Figure 5.1 shows the components of a bias and a radial tire at cross-section.

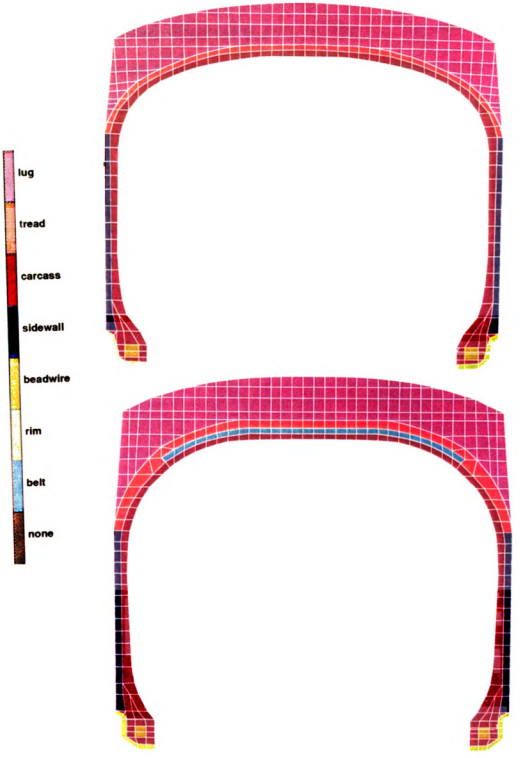

Figure 5.1 Cross-section and components of tires (A: 14.9-30;B:14.9R30)

In addition to the dimensional differences as given in Table 5.1, the main difference between a radial and bias tire at their cross-section as seen from these two figures is the presence of a belt in radial tires. The number of elements used in the program is given in Table 5.4.

Table 5.4 Number of elements used at the half of the cross-section of each tire in Finite Element Modeling.

Tire component	Tire size and Construction			
	14.9-30	14.9R30	18.4-38	18.4R38
Carcass	94	93	107	105
Belt	-	14	-	17
Beadwire	13	15	16	14
Sidewall	47	53	84	81
Tread	2	2	2	2
Lug	20	20	24	34
Σ number of elements	176	200	233	253

Due to the symmetry around the y-axis, only half of the tire cross-section was used for simulation purposes. Three boundary conditions were applied to the tires to investigate the effect of inflation, while four boundary conditions were applied for the tire-rigid surface and tire-soil simulations.

Inflation pressure effects on tire deformation were studied with three boundary conditions. These boundary conditions are shown in Figure 5.2. The first tire boundary conditions (TBCI1) was that the nodes that makes the tire symmetrical around the y-axis have no displacement in x-direction. The second boundary condition (Figure 5.2; TBCI2) was that the nodes at the rim have no displacement in x and y direction since the tire was considered to have no contact with any surface, being inflated only.

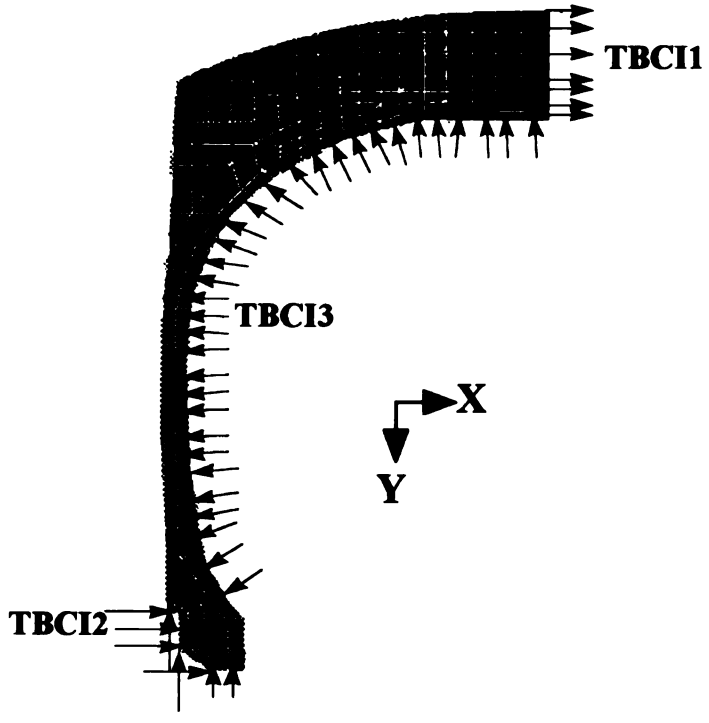

Figure 5.2 Tire boundary conditions applied to study inflation pressure effect on soil deformations (nodes not shown).

A third boundary condition, inflation pressure (Figure 5.2; TBCI3) was uniformly distributed on the internal surface of the cross-section of the tire. The application of the inflation pressure on the inside walls of the tire was achieved in an incremental fashion and generally the predetermined inflation pressure was applied at 20 increments. Some special simulations using the whole cross-section were also made and for these simulations, the first boundary condition (Figure 5.2; TBCI1) given above was not defined.

For tire-rigid surface and tire-soil simulations, three boundary conditions were applied. The first boundary condition (Figure 5.3; TBCR1) was that the nodes that make the tire symmetrical around the y-axis and the nodes of rim have no displacement in x direction. The second tire boundary condition (Figure 5.3; TBCR2) was the application of inflation pressure to the inside walls of the tire and this was achieved in an incremental fashion along with the vertical displacement (calculated from the stiffness values of the tire at a certain inflation pressure) to the rim nodes (Figure 5.3; TBCR3). The application of inflation pressure and displacement was carried out at various increments depending upon the load ranging from 2 to 20 kN. The stiffness values were obtained from another study by Brassart (1994). Brassart tested the tires used in this study and obtained the stiffness values as a function of inflation pressure. These values are given in Table 5.5. Some modifications were made in order to be consistent in terms of tire construction and their deformational behavior under load at a certain inflation pressure. Modifications were made only for 18.4-38 tire and new stiffness values were chosen based on that tire's

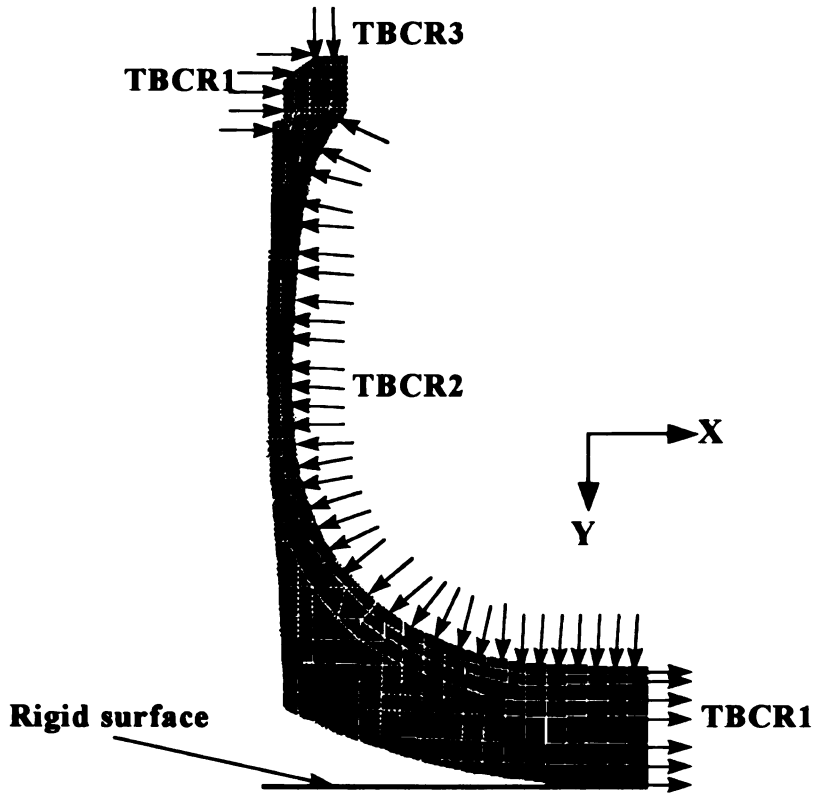

Figure 5.3 Tire boundary conditions applied to study axle load + inflation pressure on rigid surface (nodes not shown).

dynamic stiffness values by comparing it to the same size but different construction tire (18.4R38).

Table 5.5 Static stiffness (kN/m) of tires as a function of inflation pressure.

Inflation Pressure (kPa)	Tire size and Construction			
	14.9-30	14.9R30	18.4-38	18.4R38
41	161.8♦	135.0♦	164.7❖	137.8♦
83	224.8♦	202.8♦	248.8❖	224.1♦
97	245.8❖	225.3❖	276.8❖	252.8❖
110	265.3❖	246.3❖	302.9❖	279.5❖
124	286.3❖	268.8❖	330.9❖	308.4♦
138	307.3❖	291.4❖	358.7❖	337.1❖
207	431.8♦	402.8♦	496.9❖	478.9❖

♦: **Measured stiffness (kN/m) by Brassart,1994.**
❖: **Predicted stiffness (kN/m)**

The details of how the stiffness modifications were made is given in Appendix C. Comparison of tire stiffness vs inflation pressure relationship for tires is given in Figure 5.4. Figure 5.5 shows the vertical deflection of tires as a function of load used in simulations at 83 kPa inflation pressure.

5.2.2.3 Soil Constitutive Model

Other stress-strain models (Constitutive models) are available in the program but due to studying the tire-rigid surface and tire-soil interaction as a plane strain problem, the study was limited to the use of only the Drucker-Prager model defined especially for plane strain problems. The other models such as non-linear eleastic model by Duncan and Chang (1970) and Cam-Clay model by Schofield and Wroth (1968) requires eight-nodded element use and these models are used to simulate soils as an axisymmetric problem.

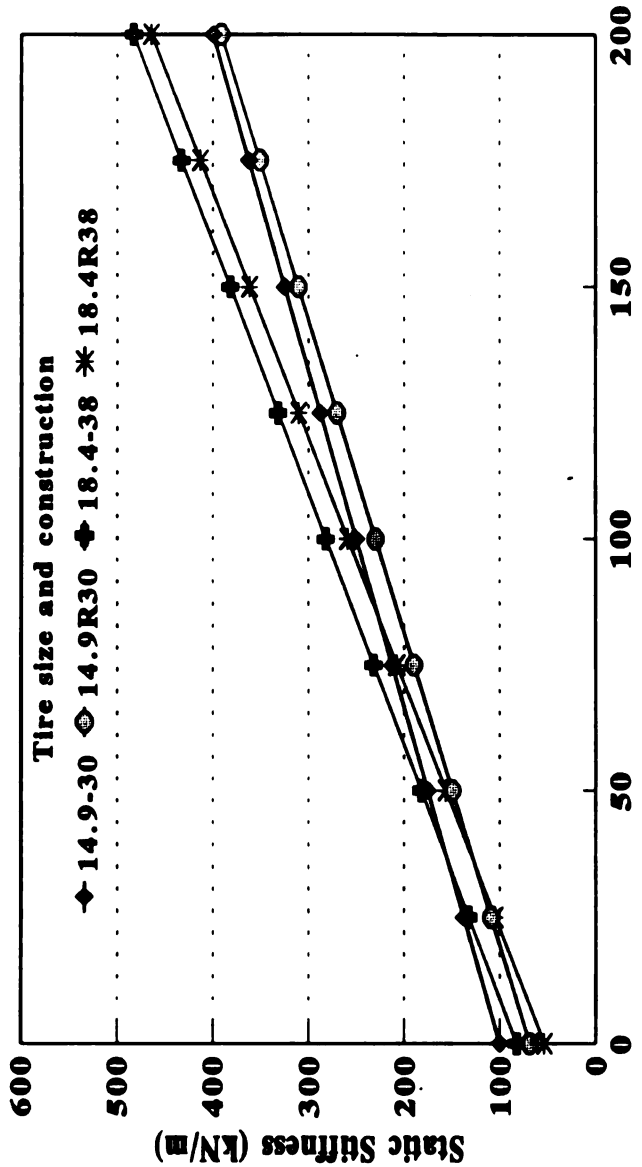

Figure 5.4 Static stiffness of tires at various inflation pressures.

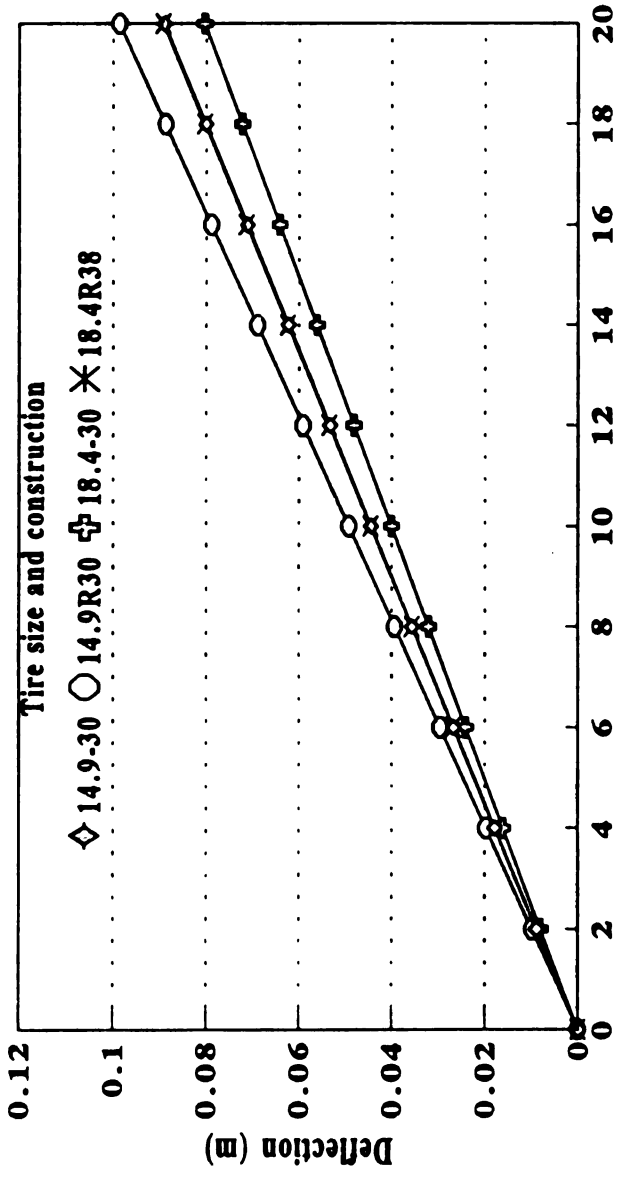

Figure 5.5 Vertical displacements as a function of load at 83 kPa inflation pressure.

The Drucker-Prager surface can be considered as a three dimensional approximation to the Mohr-Coulomb failure criterion with a simple smooth surface. This criterion is expressed as a linear combination of the first invariant of stress tensor I_1 and the square root of the second deviatoric stress tensor together with two material constants and k. The Drucker-Prager yield surfaces in different spaces are given in Figure 5.6. The simplified Drucker-Prager failure criterion as fixed yield function is in the following form;

$$f=\sqrt{J_2}-\alpha I_1-k \tag{5.1}$$

When f function is less than zero, the soil undergoes elastic strain only. Otherwise elastic and plastic strains occur in the soil.

The constants and k are related to cohesion c and the angle of internal friction and they are defined for the plain strain case as;

$$\alpha=\frac{\tan\phi}{\sqrt{9+12\tan^2\phi)}} \tag{5.2}$$

$$k=\frac{3c}{\sqrt{9+12\tan^2\phi)}} \tag{5.3}$$

Using equation 5.2 and 5.3, the constants α and k for soft and dense soil was determined to be 0.176 and 0.18 respectively. These constants were used in finite element simulations along with the soil initial Youngs Modulus and Poisson's ratio (Table 5.6).

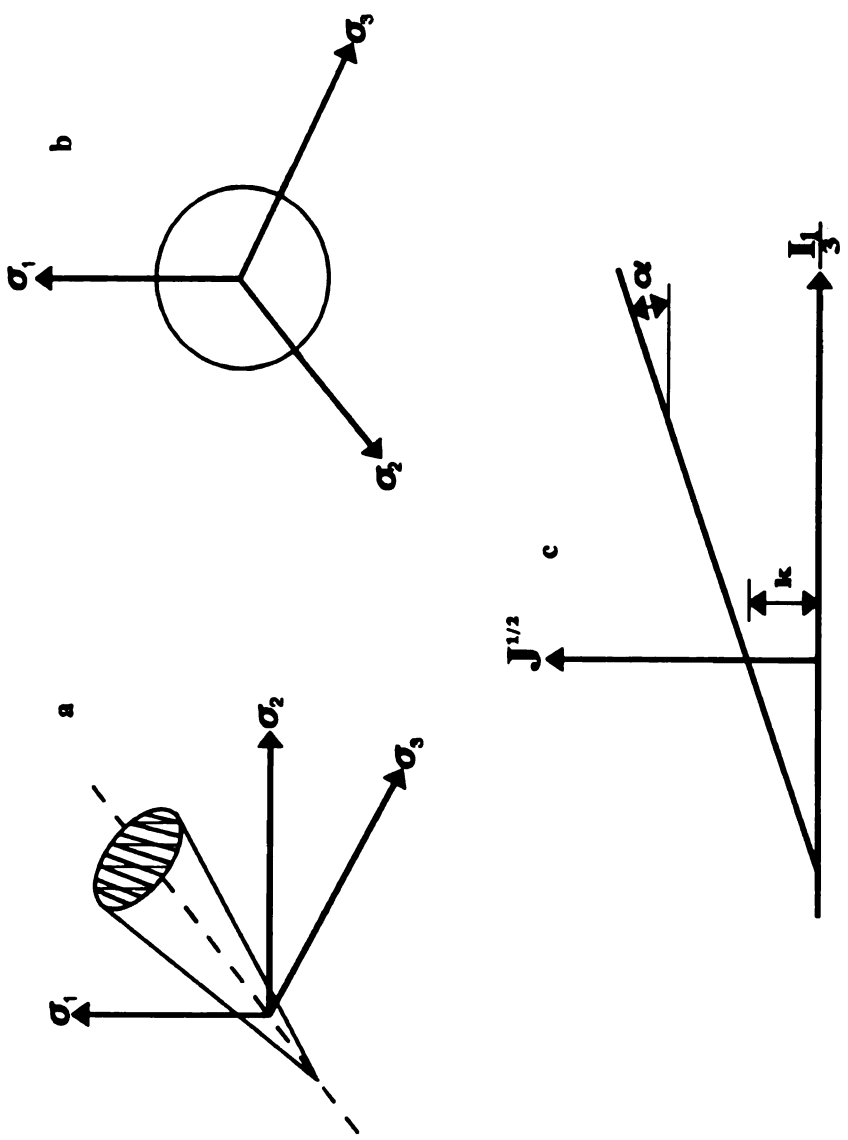

Figure 5.6 a. Drucker-Prager yield surface in principal space b. in the π plane c. Drucker-Prager yield surface in the $J^{1/2}$- I/3 space

Table 5.6 Mechanical properties of soft and dense soil

Soil condition	Modulus of Elasticity (MPa)	Poisson's ratio	Angle of internal friction	Cohesion (kPa)
Soft	1.804	0.3	35.64°	15.7
Dense	9.18	0.3	35.64°	15.7

5.2.2.4 Soil Boundary Conditions (SBC)

Soil boundaries were determined as suggested by Pollock et al. (1986). The soil mass under tires (18.4R38 and 18.4-38) had radius and depth equal to six times the radii of the contact area. The contact area determination as a function of tire size, load and inflation pressure for the axle loads was made using a multiple linear regression model that was developed by using the data from Goodyear, 1994 (Appendix D; Table D.1). The multiple linear regression model developed is also given in Appendix D; Table D.2.

Contact area calculations for each tire for a normal load range from 2 to 20 kN were made and the average contact radius assuming a circular contact area was calculated for a tire at predetermined loads ranging from 2 to 20 kN. The idealized soil mass included 502 and 462 elements for 18.4R38 and 18.4-38 tire, respectively. The radius and depth was determined to be 1.06 m (42 inches).

For small tires used in this study, the idealized soil mass had 310 elements for both 14.R30 and 14.9-30 tire. The radius and the depth of the soil was 0.81 m (32 inches).

Two soil boundary conditions were applied to the soil body in the program. The first boundary condition (Figure 5.7; SBC1) was that the nodes on the y-axis have no

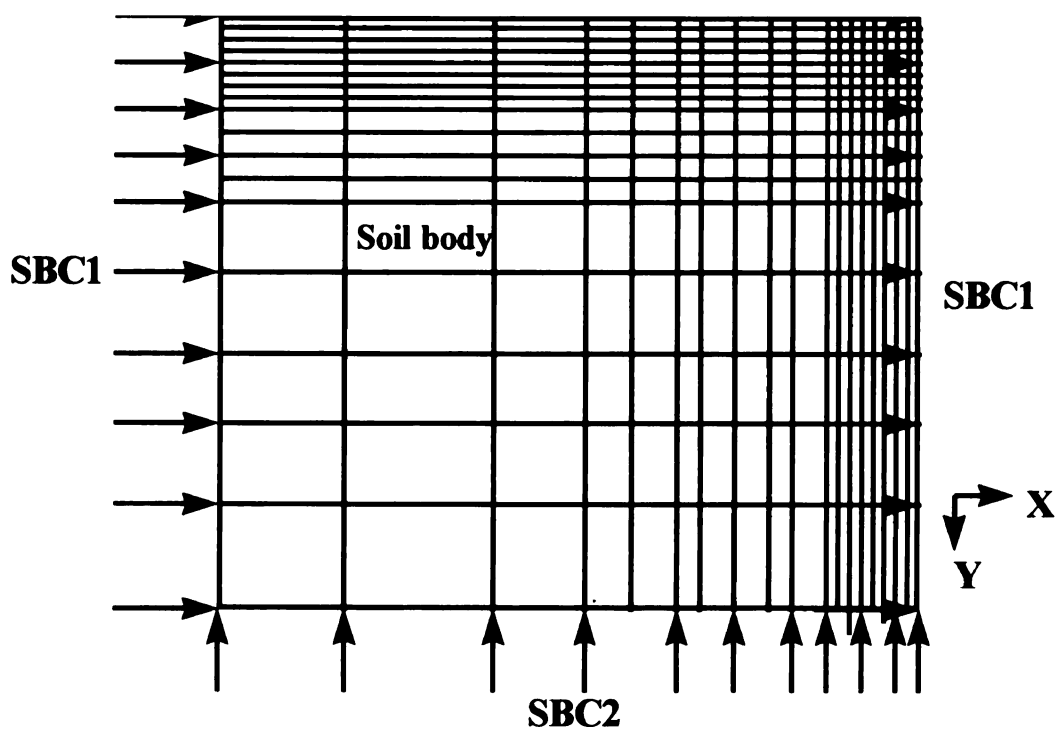

Figure 5.7 Soil boundary conditions (nodes not shown).

displacement in x direction and the nodes on the bottom of the soil body as shown in Figure 5.7 (SBC2) the x-axis have no displacement in y direction.

The soil mesh was made finer at the tire-soil interface and below so that the values could be obtained with an acceptable level of accuracy. The number of elements used for soil mesh given above was for the case where the tires are in full contact, and used the whole width as in the application of higher loads on tires. In other cases the number of soil elements was less than the full contact case.

5.2.2.5 Special Features Used in the Program (MARC)

Follower Force Option

Ridha (1980) indicated the importance of **"Follower Force"** loading option for tire modeling studies using the Finite Element Method especially when high inflation pressures were used. Follower force option makes the applied loads normal to the surface when any deformation occurs. The follower force option available in Marc was used to make the inflation pressure type of loading act perpendicular to the inside walls of the tire.

Large Deformations

Large deformations may occur in soils before failure is reached. This situation was handled in the program by using the large deformations option.

Contact option

The contact option for the simulation of soil-rigid surface and soil-tire was used so that the non-penetration constraint between tire and rigid surface and tire-soil elements were imposed. A friction coefficient of 0.5 was used for the tire-rigid surface simulations

in this study while no friction coefficient was assigned for tire-soil simulations since tire and soil was considered and studied as an integrated body. The contact option and its implementation in the program is given below (Marc user's manual, 1992).

The basic concept in the contact features of Marc was the definition of bodies. The boundary surfaces of these bodies contained all the geometrical information necessary to impose non-penetration. In most circumstances, the bodies corresponded to the physical model being analyzed with finite elements. In some cases, however, a body was present for the sole purpose of constraining other bodies, with no analysis required. This lead to the concept of defining both deformable and rigid bodies. Deformable bodies are a simple collection of finite elements. Rigid bodies are pure geometrical entities. A requirement that at least one deformable body must be present for any finite element analysis to be performed. The non-penetration constraint, as exemplified in Figure 5.8 is expressed as;

$$U_A.n \leq D \qquad (5.4)$$

where U_A is the displacement vector, n is the normal vector, and D is the distance between the body and the rigid surface.

In the finite element framework this constraint can be imposed by several means: Lagrange multipliers, penalty functions, or solver constraints. The contact feature used the latter approach.

Whenever contact between a deformable-body and a rigid body was detected, imposed displacements were automatically created. Whenever contact between two

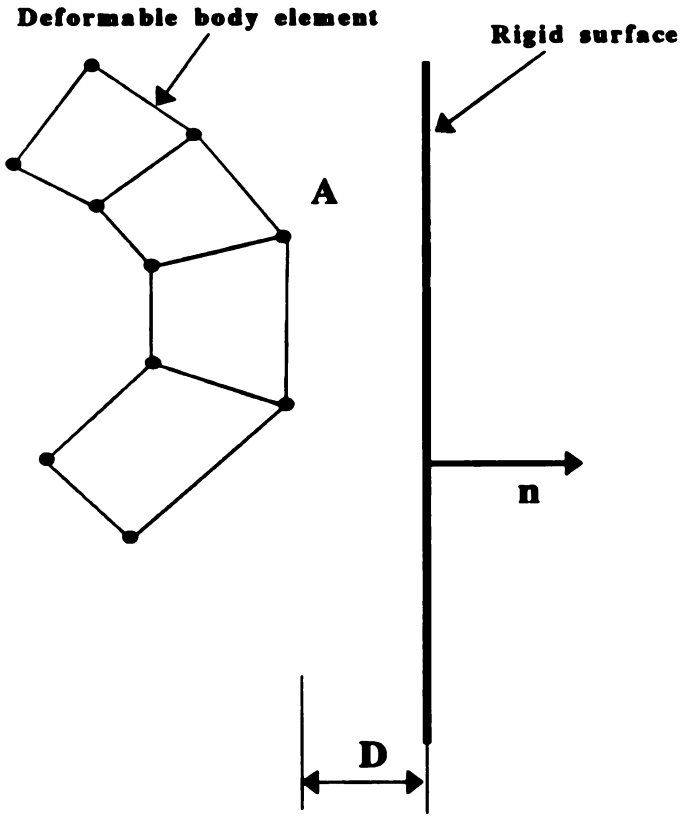

Figure 5.8 Non-penetration constrain in Finite Element Modeling.

deformable bodies was detected, multipoint constraints (called Ties) were automatically created. No contact between rigid bodies was ever considered.

As stated above, a deformable-body was defined by the user as a set of elements. Marc determined all of the nodes on the boundary, which became the set of candidate nodes for contact. That is, the contact algorithm attempted to prevent penetration of any these nodes into any defined body.

A rigid-body was defined by means of a set of geometrical entities which define the boundary surface. It was not necessary to completely define a full body envelope. Only the regions of potential contact must be defined, provided they are all connected. Several geometrical primitives were accepted as building blocks to construct surfaces such as straight lines, circles and splines in two dimensions and patches, ruled surfaces, surfaces of revolution and bezier surfaces in three dimensions.

The implementation of the contact algorithms requires that the following steps were performed at every increment of an analysis.

1. Find all the nodes that were in contact. This was determined by the distance between the nodes and surfaces. Since the distance was a calculated number, there were always roundoff errors involved. Thereof, a contact tolerance was provided such that if the distance calculated was below this tolerance, a node was considered in contact. This tolerance was provided either by the user, or calculated by Marc as 1/15 of the smallest element size for solid elements or 1/2 of the thickness for shell elements. In general,

the contact tolerance should be a small number compared to the geometrical features of the configuration being analyzed.

2. For all the nodes that were in contact, determine either the typing constraints or the imposed displacement increments along the normal to the contacted surface, as well as a local transformation that defines such a normal. This step was repeated for each cycle of a nonlinear problem in order to permit a node to find its equilibrium position along the contact surface.
3. Once a convergent solution was found, contact forces were analyzed. If a contacting node had a tensile contact force greater than the separation tolerance, the node was released and another solution was found. The program automatically calculated the separation tolerance force based upon the residual forces or the user could enter it directly. A large separation tolerance ensures that there would not be any separation. If the user wanted to move two contacting bodies apart, a solution requiring substantial artificial stretching might be required before the decision to separate is made.

5.2.2.6 Development of a Methodology to Study Soil-Tire Interaction

The necessary steps to study soil-tire interaction followed and as a result of this, the methodology developed in this study is given in Figure 5.9 as a flow chart and the details are described below. Once a tire comes in contact with any surface that could be rigid or deformable, the new section height may not be obtained in Finite Element Analysis. For this reason, the deformations that take place in tires were investigated under inflation pressure as a first step in this study. Since deformations are directly related to

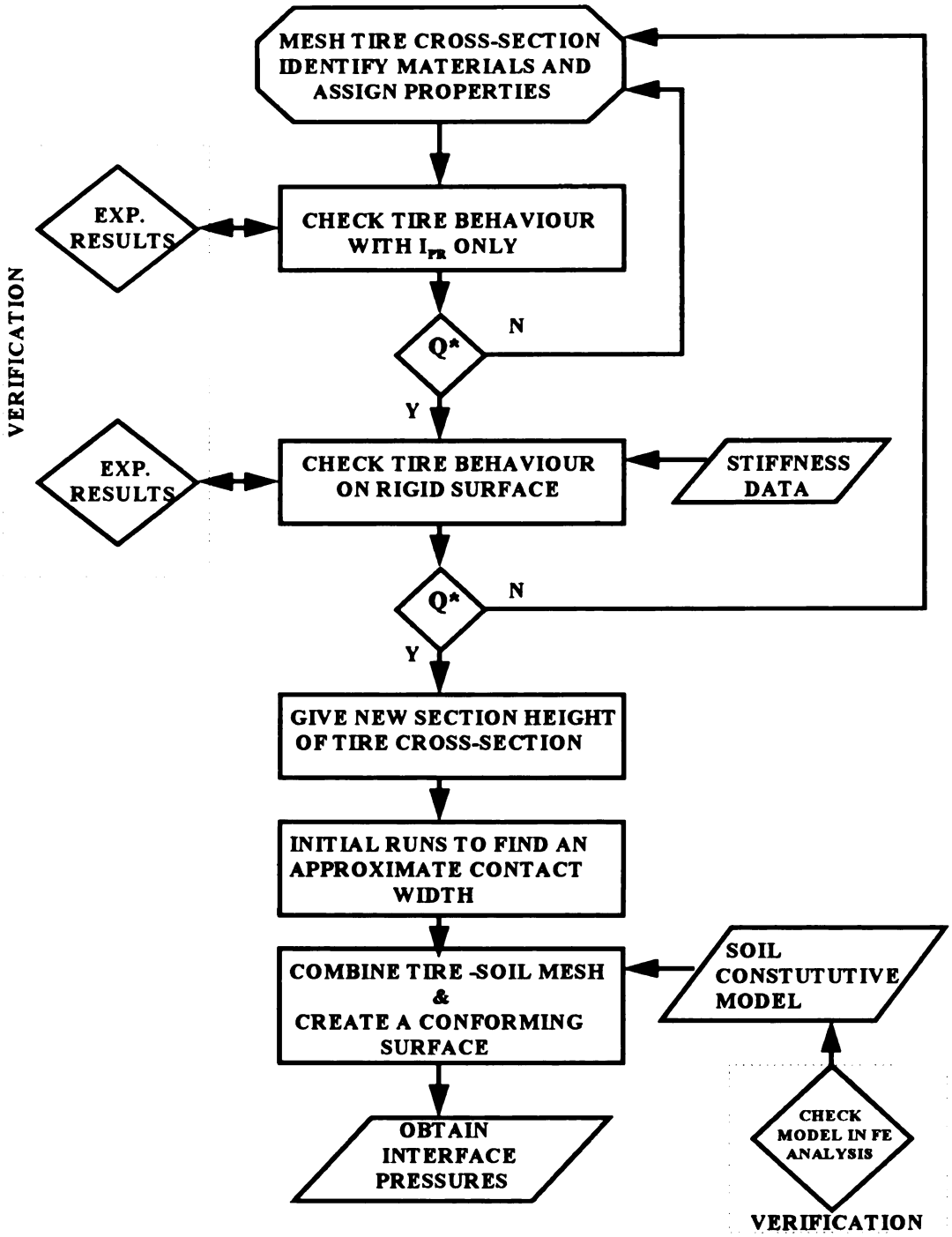

Figure 5.9 Methodology developed to study soil-tire interactions (Ipr: Inflation pressure and Q is the question "Does the tire model verify the experimental results?.

tire size and construction, behaviour of tires under inflation pressure was studied seperately for each tire. The results of such runs were also used for comparison purposes to verify that the tire geometries were well defined and the material properties were properly chosen. The vertical displacements obtained from those runs were then assigned to the related nodes and the new section height of the tire was formed and as a result, a new tire geometry was created.

The tires were then examined under load and inflation pressure on a rigid surface. Inflated profile was used for these runs and the contact option was activated and the candidate elements whose nodes will come contact with rigid surface were identified. The results obtained from the rigid surface simulations were compared with some literature findings. After verification of material properties and the tire geometry, the last step to simulate soil-tire interaction was initiated. In this step, the soil properties obtained from the triaxial tests were used and the soil model was checked in the program. Then the soil and inflated tire cross-section was combined to create a deformable integrated body. With the common nodes of both deformable bodies (soil and tire) at interface, some runs were made. The purpose of those runs was to obtain the approximate contact width which was thought to be different than the one on rigid surface. This was the last step of creating an idealized soil-tire mesh as shown in Figure 5.10. Based on an approximate contact width, initially matching nodes were created before any loading was applied to the tire. Soil-tire interface pressures were then studied by creating a special conforming soil surface for each loading case and filling the soil-tire gap with the soil elements.

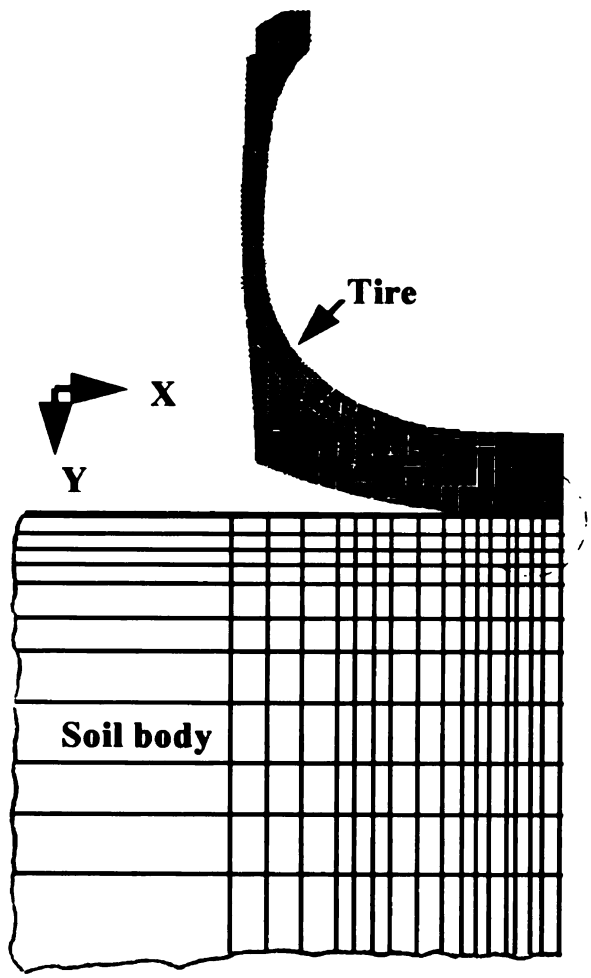

Figure 5.10 Idealized soil-tire mesh

5.3 RESULTS AND DISCUSSION

The effect of inflation pressure on tire deformations was investigated at different inflation pressures. One of the tires, 18.4-38 was used for verification of simulation results. At certain inflation pressures, the section height of the tire was measured at the crown as shown in Figure 5.11 in the laboratory at Michigan State University. Using the same inflation pressures, finite element simulations were carried out. The results of the Finite Element Method and experimental findings are given in Table 5.7. As seen from the table above, the measured and simulation results are in good agreement and the difference is less than 1% in all cases considered.

Upon finding a close agreement, the cross-section of other tires were then simulated under various inflation pressures to obtain deformations. Figure 5.12 and 5.13 shows the vertical displacements that take place in tires,14.9-30 and 14.9R30, at 110 kPa inflation pressure, respectively.

Table 5.7 Comparison of section height (mm) for 18.4-38 tire under various inflation pressures.

Inflation Pressure (kPa)	FEM	Experimental
80.1	404.8	405.1
93.7	408.4	408.1
161.4	409.4	410.2
175.0	409.9	411.2
195.3	411.7	412.2

The maximum point of vertical displacement under inflation pressure was obtained at the crown for both bias and radial tires as seen from Figure 5.12 and Figure 5.13. On

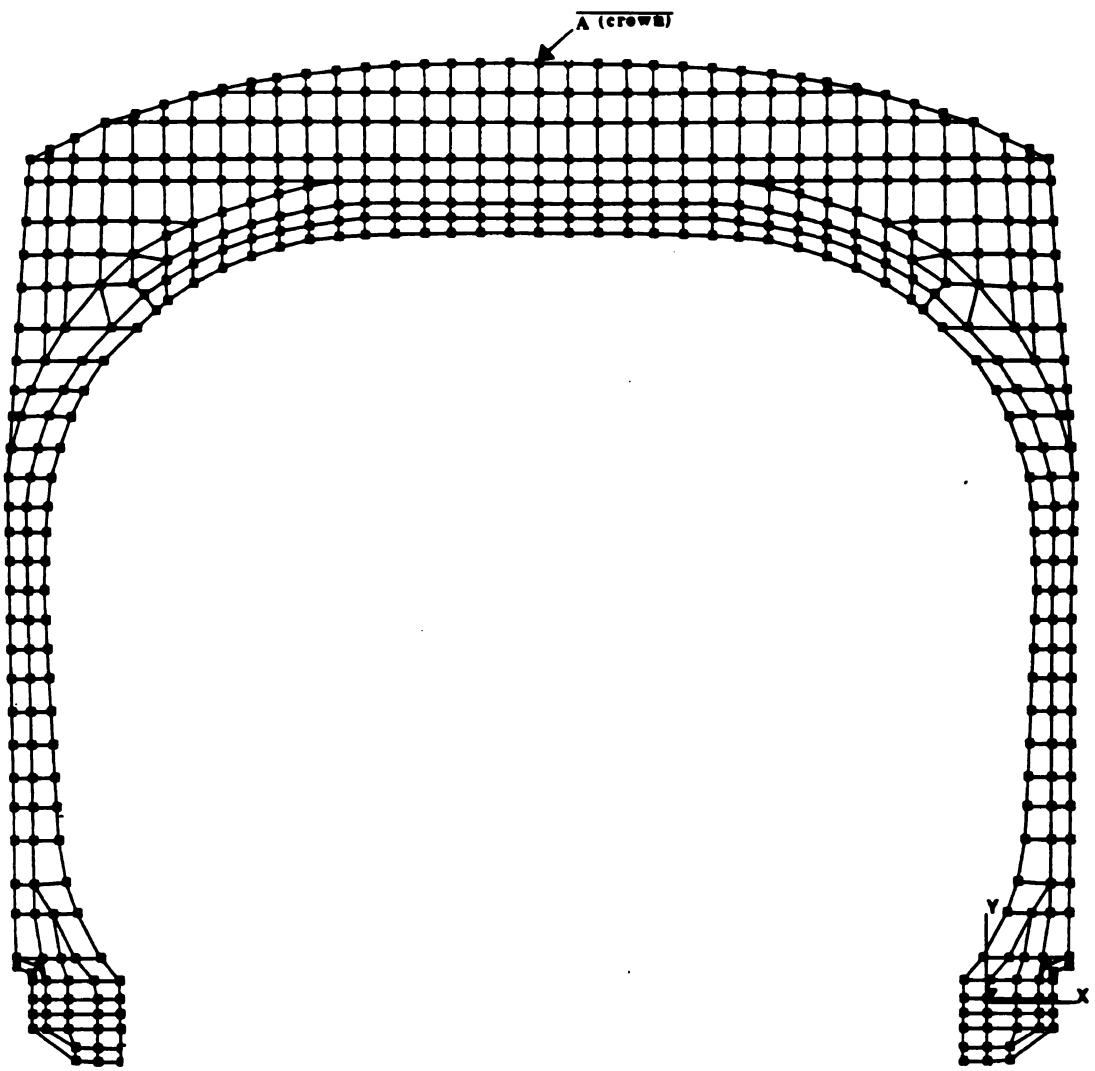

Figure 5.11 Meshed cross-section of 14.9-30 tire and point of max displacement (crown) under inflation pressure.

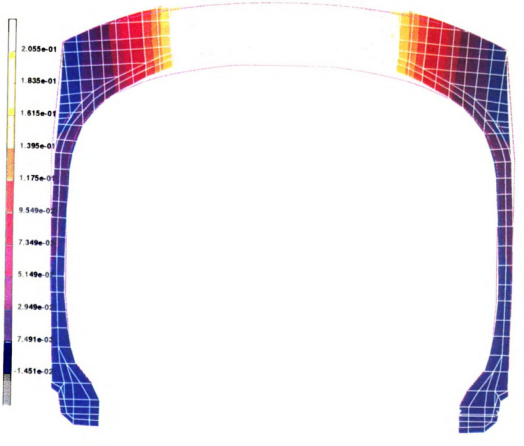

Figure 5.12 Undeformed and deformed cross-section of 14.9-30 tire (Inflation pressure applied: 110 kPa; scale on the left shows vertical displacements in inches)

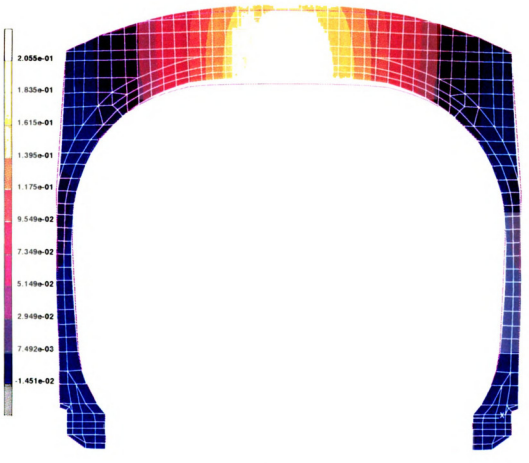

Figure 5.13 Undeformed and deformed cross-section of 14.9R30 tire (Inflation pressure applied: 110 kPa; the scale on the left shows vertical displacements in inches).

the other hand, the magnitude of lateral and vertical displacements were found to be not only depended upon the tire construction but also tire size. The vertical displacement of bias tires is much more than that of radial tires under the same inflation pressure. This trend changed when lateral displacements were considered. Figure 5.14 shows the lateral displacements that take place in the 14.9-30 tire inflated to 110 kPa inflation pressure. Studying the same conditions with the 14.9R30 tire resulted in a different lateral diplacment profile as shown in Figure 5.15. This constructional dependent behaviour was also observed by Forrest (1962) and it was attributed to the existence of a belt in radial tires. Since in the belted tire, the radial direction of the body plies provides a very flexible sidewall while the circumferentially placed braker layers provide a very stiff hoop or belt, resistant to circumferential compression or extension (Figure 5.15) shows the lateral displacements that take place in belted tires at 110 kPa inflation pressure. Figure 5.16 and 5.17 are drawen to show the differences between tire sizes. As seen from the figures the lateral displacements in magnitude are also size dependent and they are higher as bigger tires are used. The numerical values obtained from the finite element simulations to generate Figure 5.16 and 5.17 are given in Appendix E, Table E.1. An example Finite Element simulation showing the detailed results (displacements at the nodes of a tire) are given in Appendix F.

Studying the inflation pressure effect and comparing the behavior of one of the tires used for the simulations indicated that the tire material properties were properly chosen and the tire geometries were well-defined.

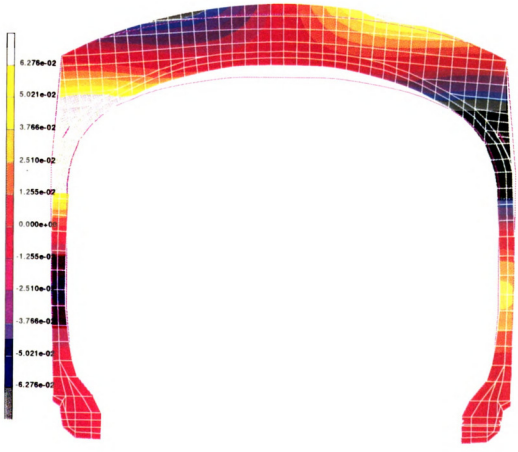

Figure 5.14 Undeformed and deformed cross-section of 14.9-30 tire (Inflation pressure applied: 110 kPa; the scale on the left shows lateral displacements in inches).

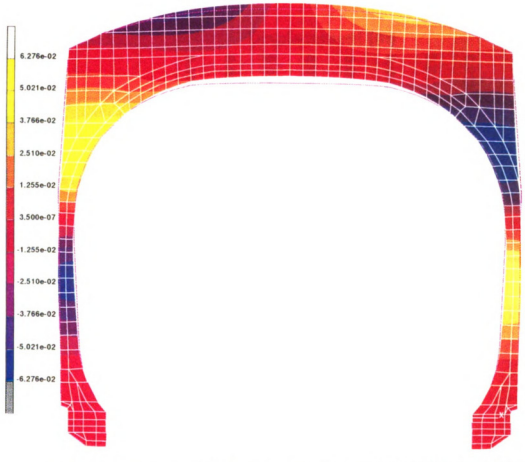

Figure 5.15 Undeformed and deformed cross-section of 14.9R30 tire (Inflation pressure applied: 110 kPa; the scale on the left shows lateral displacements in inches).

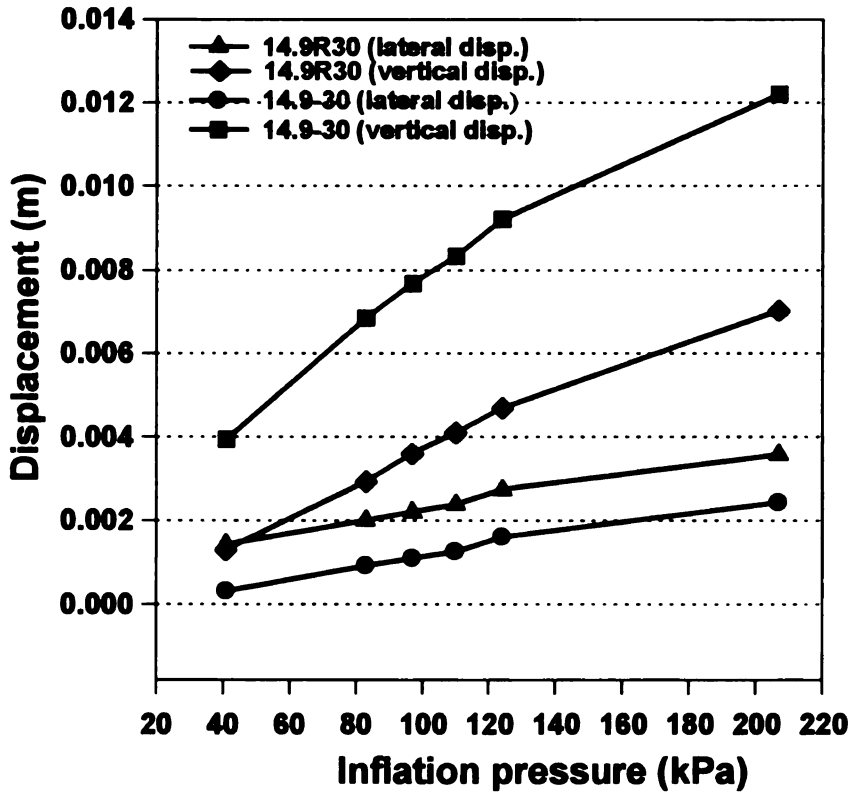

Figure 5.16 Finite Element simulation results of lateral and vertical displacements for 14.9-30 and 14.9R30 tires at various inflation pressures.

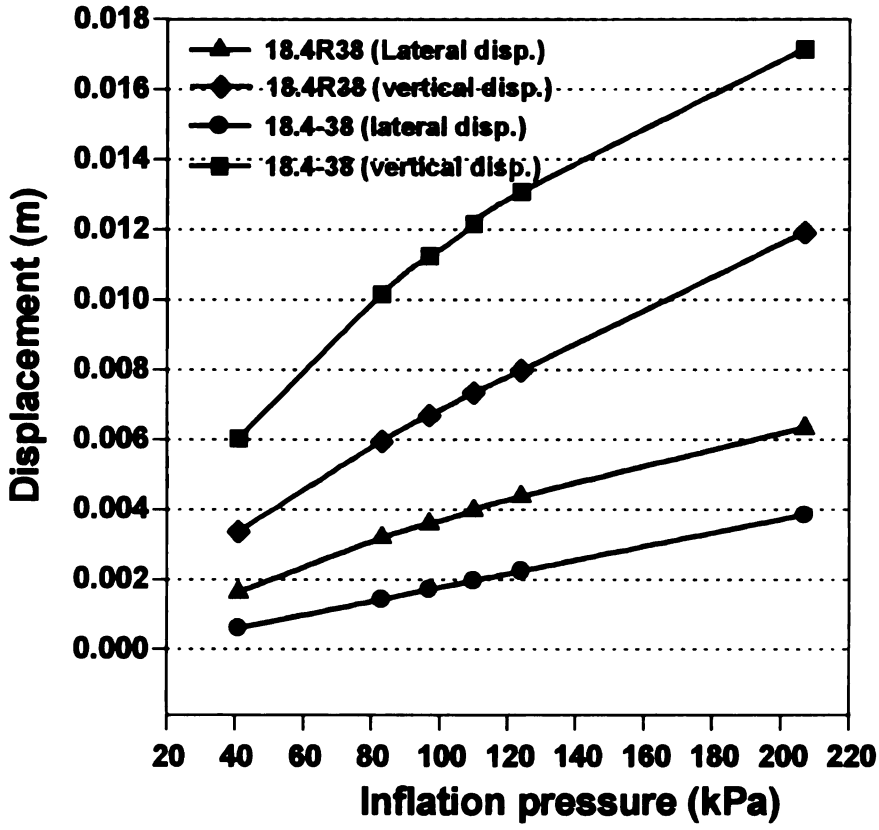

Figure 5.17 Finite Element simulation results of lateral and vertical displacements for 18.4-38 and 18.4R38 tires at various inflation pressures.

The second step was the simulations that considered both inflation pressure and axle load effect on a rigid surface. A comparison was also made using the data available in the literature to chech the tire behaviour on a rigid surface. Upadhayaya (1990) used one of the tires (18.4R38) whose behavior on a rigid surface was simulated in this study. The results are given in Table 5.8. The simulation and experimental results were found to be in good agreement.

Table 5.8 Comparison of contact width simulations with Upahyaya's study (1990)

Axle load (kN)	Inflation pressure (kPa)			
	83		124	
	FEM	Upadhyaya	FEM	Upadhyaya
12	0.18	0.29	*	*
17	0.31	0.34	*	*
22	0.41	0.43	*	*
27	0.43	0.43	0.43	0.43

*: no data available; resultant contact width of the tire from Finite Element simulations was doubled since half of the cross section was used.

The general results obtained from the Finite Element simulations considering all the tires used in this study are given in Table 5.9. Radial tires on a rigid surface under the same load and inflation pressure deflected much more than the bias tires in the radial direction and this resulted in a wider contact width for radial tires. This could be the verification of the well-known information that radial tires usually have larger contact area than bias tires under the same loading conditions even though the simulations were achieved in 2D and the deformations in the third dimension were neglected. For a better visualization and comparison of load and construction effect on tires on a rigid surface, Figure 5.18 thru 5.21 are presented.

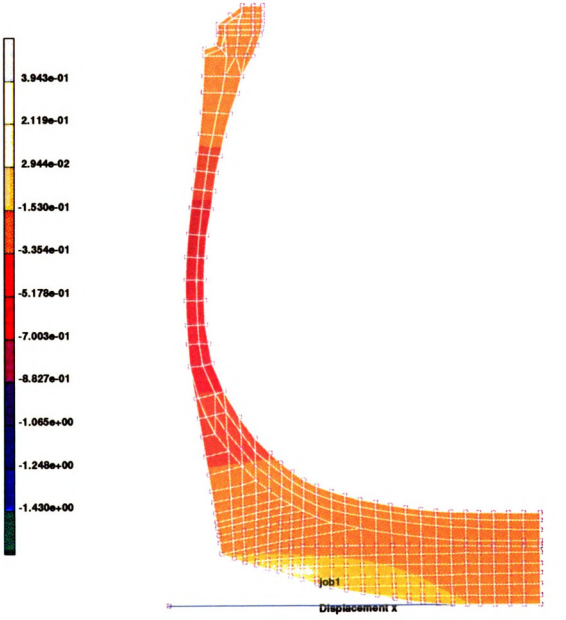

Figure 5.18 Lateral displacements at 110 kPa inflation pressure at 2 kN load (Tire: 18.4R38).

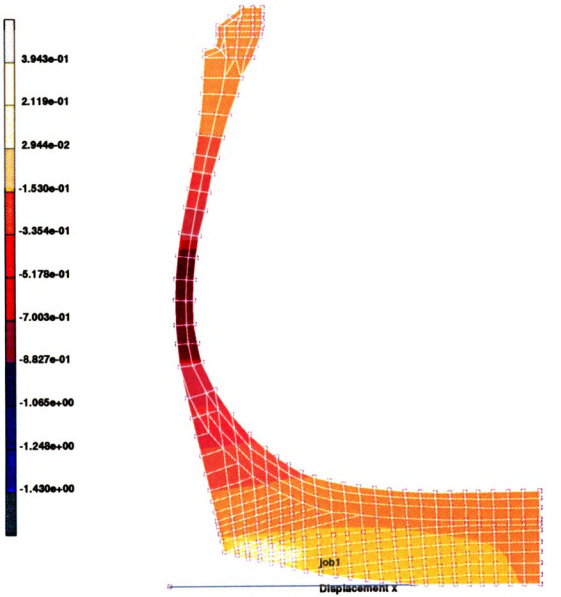

Figure 5.19 Lateral displacements at 110 kPa inflation pressure at 4 kN load (Tire: 18.4R38).

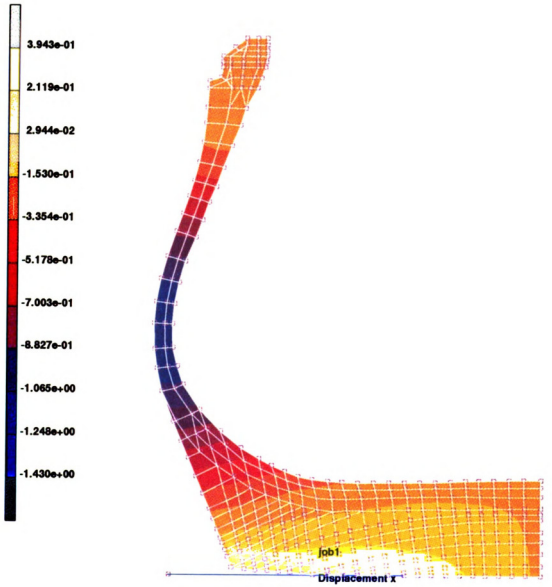

Figure 5.20 Lateral displacements at 110 kPa inflation pressure at 8 kN load (Tire: 18.4R38).

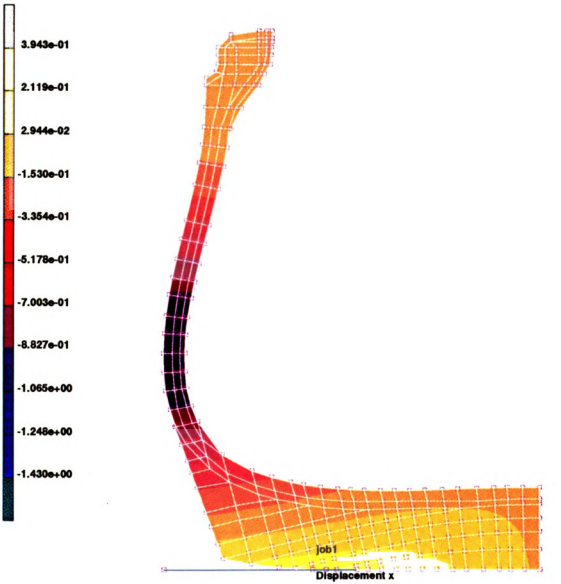

Figure 5.21 Lateral displacements at 110 kPa inflation pressure at 2 kN load (Tire: 18.4-38).

Table 5.9 Vertical and maximum lateral displacements under different axle loads and inflation pressures (Finite element simulation results).

Tire size and const.	Inflation Pressure (kPa)	Max.lateral disp. (mm)	Vertical disp. (mm) and equivalent load (kN)	
			mm	kN
18.4R38	83	8.53	8.91	2
		13.99	17.83	4
		23.57	35.68	8
		45.69	71.39	16
		56.46	89.23	20
18.4R38	110	9.62	7.13	2
		13.20	14.30	4
		20.65	28.60	8
		36.47	57.22	16
		45.44	71.52	20
18.4-38	83	6.73	8.02	2
		9.93	16.05	4
		16.45	32.13	8
		33.78	63.83	16
		44.04	80.36	20
18.4-38	110	7.08	6.55	2
		9.62	13.18	4
		14.80	26.39	8
		26.33	52.81	16
		34.54	66.01	20
14.9R30	83	7.06	9.85	2
		12.24	19.71	4
		23.59	39.44	8
		46.3	78.89	16
		53.72	98.62	20
14.9R30	110	6.65	8.10	2
		10.82	16.23	4
		19.83	32.46	8
		39.52	64.94	16
		45.92	81.17	20
14.9-30	83	5.51	8.80	2
		8.99	17.78	4
		16.58	35.58	8
		37.71	71.17	16
		44.95	88.95	20
14.9-30	110	5.56	7.51	2
		8.43	15.06	4
		14.32	30.14	8
		31.19	60.29	16
		39.54	75.36	20

As seen from Figures 5.18 and 5.20, increasing the axle load and keeping the inflation pressure constant (110 kPa) resulted in increased displacements and sidewall-bulging phenomenon. The construction effect can be attained when Figure 5.20 and 5.21 are compared. Under the same loading condition, the behavior of radial and bias tires were different and the displacements on the sidewall of radial tire was greater than the bias tire. This behavior can be explained by the construction and differences in the stiffness of the tires.

Following the steps described in Figure 5.9, the soil-tire interaction was studied considering tire construction (bias or radial tire) and operational variables (axle load and inflation pressure) and the initial soil conditions.

The dense soil condition was only used to compare the results of simulations from the point of interface pressure in this study and no measurement results are avaliable for the dense soil case.

Due to the cost of conducting soil-tire interface pressure measurement type of experiments, results of a limited number of cases on which the tire was operated were used for comparison purposes and the results of those conditions at three lug locations are given along with the simulation results in Table 5.10 and 5.11. Slip was not a variable for the simulations since the static case was simulated. For the static case simulations, static load was found from the dynamic and static load relationship using the measurements made. The simulation results are in good agreement with the experimental measurements

Table 5.10 Results of soil-tire interface pressures at different locations on the lug of 18.4R38 tire as a function of inflation pressure, dynamic load and slip.

Inflation pressure (kPa)	Load (kN)	Slip %	Lug edge	Lug middle	Lug center
83	13.1	7.5	170	296	284
83	25.3	7.5	359	215	140
83	13.1	10	329	228	164
83	25.3	10	235	99	26
110	13.1	7.5	212	255	193
110	25.3	7.5	345	448	187
110	13.1	10	521	333	261
110	25.3	10	257	315	145

Table 5.11 Results of soil-tire interface pressures from the FE analysis at different locations of 18.4R38 tire as a function of load and inflation pressure.

Inflation pressure (kPa)	Load (kN)	Slip %	Lug edge	Lug middle	Lug center
83	13.1	-	375	300	132
110	13.1	-	378	211	111
83	25.3	-	*	*	*
110	25.3	-	432	240	179

*: No result is available

especially at 10% slip. In one case, no result was obtained from the simulations as indicated in Table 5.11 due to the excessive deformations that took place in 18.4R38 tire. The program generated figures 5.22 and 5.23 show the stress distribution in both soil and tire. These figures represent the two different tire loading conditions as given in Table 5.11. As seen from the figures (Figure 5.22 and 5.23), the point of maximum stress is the edge of the tire. This agrees with the result concluded from the statistical analysis in the previous chapter of this study. Similar findings were also obtained by Way et al (1993). An example Finite Element output that shows the normal stresses in soil and at the interface is given in Appendix G.

Figures 5.24 thru 5.30 are computer generated graphs that give a better visualization of the stress distribution and displacements that take place in the tire and soil. The result of an increased axle load on soil stresses can be seen as by comparing Figure 5.24 and 5.25 . As a result of an increased load, there is a noticable changes in contact width and stresses. The comparison of Figure 5.25 and 5.28 reveals the effect of initial soil condition on soil-tire interface pressures. As the scale on the left is the same for both figures, it allows a good comparison of the two conditions. The shear stresses used to obtain the sliplines(the shear strength of the soil equals the shear stress) were also obtained from the simulations using the Von-Mises stresses. Figure 5.27 is the typical example of the Von-Mises stress distribution in soil and tire. Figure 5.29 and 5.30 are presented to visually show the initial soil condition effect on tire deformations. As the soil gets firmer the tire conforms to the surface and most of the deformations take place in the

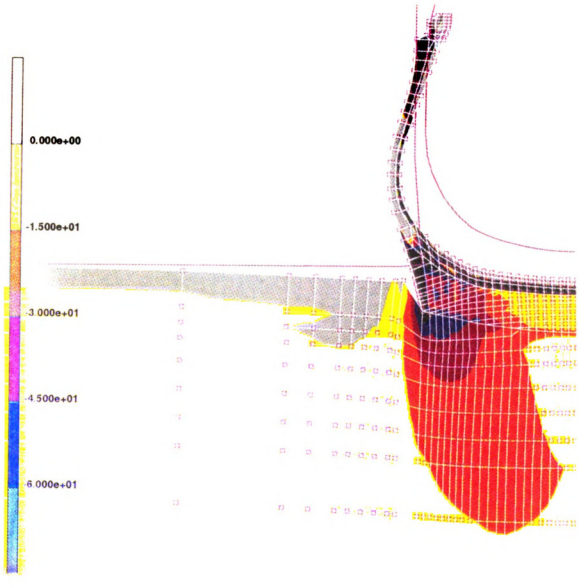

Figure 5.22 Stresses (σ_3) in soil and tire (Tire: 18.4R38; Inflation pressure: 83 kPa; 16 kN static load (equivalent of 13.1 kN dynamic load; Soil condition: soft).

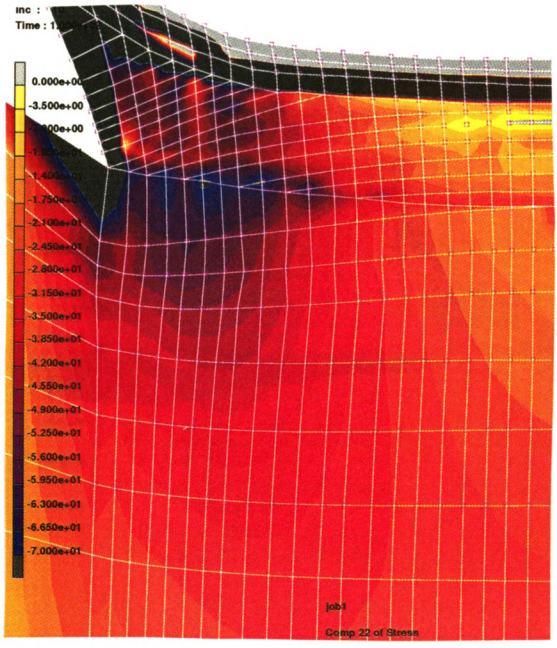

Figure 5.23 Stresses (σ_z) in soil and tire (Tire: 18.4R38; Inflation pressure: 110 kPa; 30 kN static load (equivalent of 25.3 kN dynamic load; Soil condition: soft).

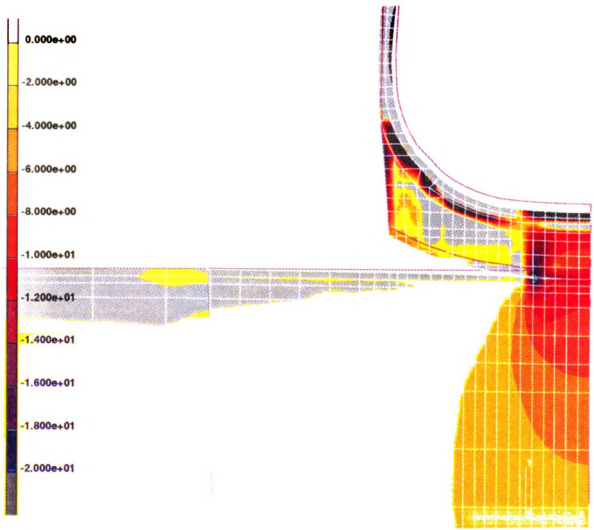

Figure 5.24 Stresses (σ_2) in soil and tire (Tire: 14.9R30; Inflation pressure: 110 kPa; 2 kN load ; Soil condition: soft). Stresses are in psi

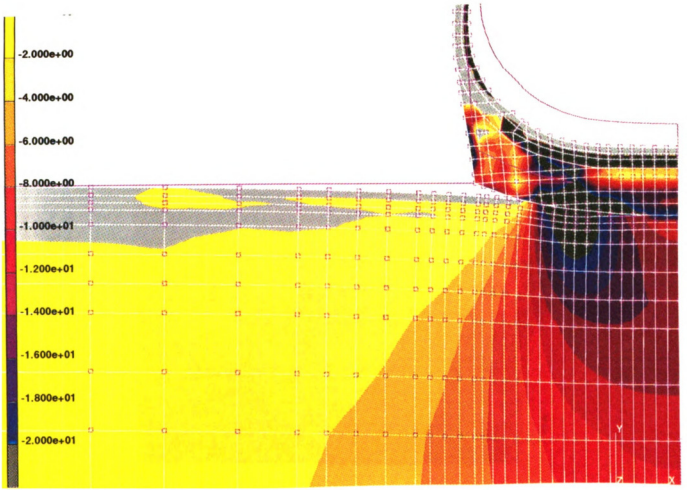

Figure 5.25 Stresses (σ_2) in soil and tire (Tire: 14.9R30; Inflation pressure: 110 kPa; 8 kN load ; Soil condition: soft).

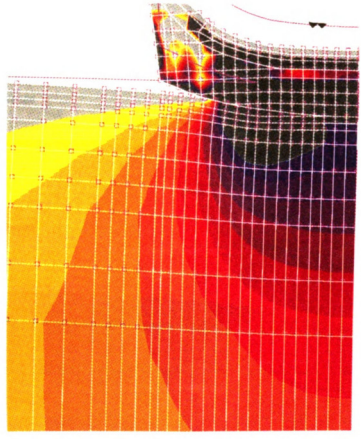

Figure 5.26 Mean normal stresses in soil and tire (Tire: 14.9R30; Inflation pressure: 110 kPa; 8 kN load ; Soil condition: soft).

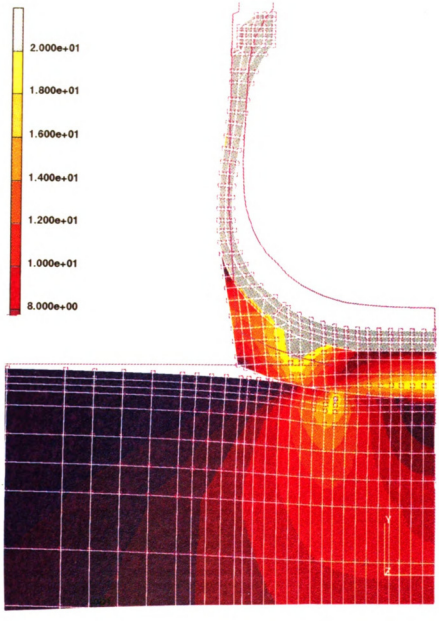

Figure 5.27 Von-Mises stresses in soil and tire (Tire: 14.9R30; Inflation pressure: 110 kPa; 8 kN load ; Soil condition: soft). Stresses are in psi

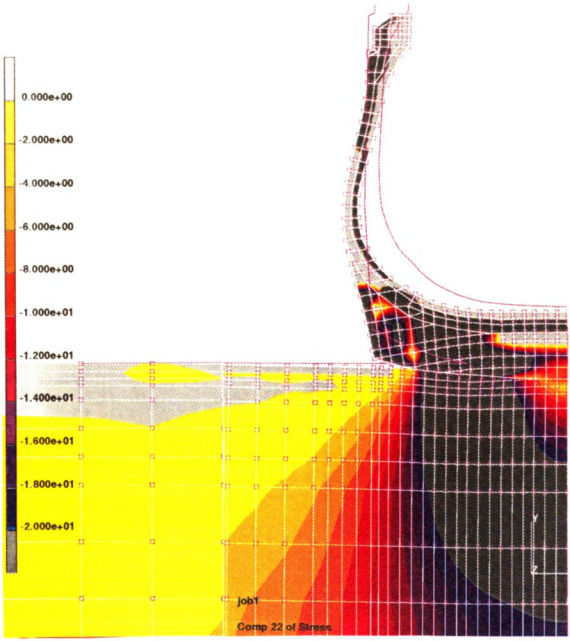

Figure 5.28 Stresses (σ_z) in soil and tire (Tire: 14.9R30; Inflation pressure: 110 kPa; 8 kN load ; Soil condition: dense). Stresses are in psi

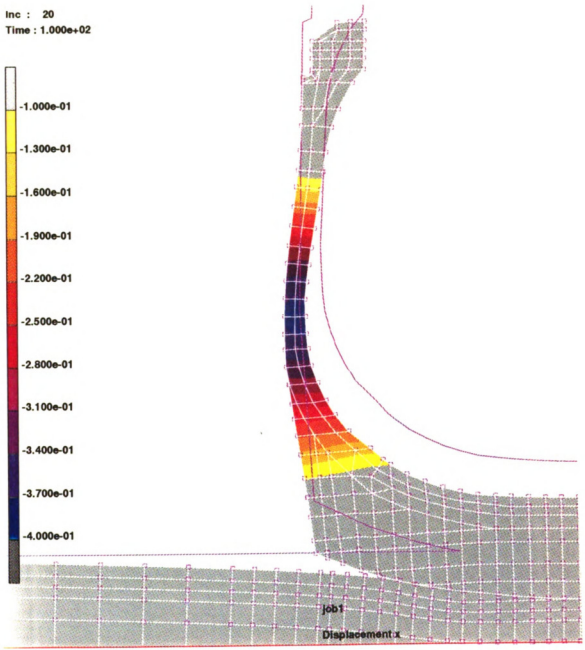

Figure 5.29 Lateral displacements in soil and tire (Tire: 14.9R30; Inflation pressure: 110 kPa; 2 kN load ; Soil condition: soft).

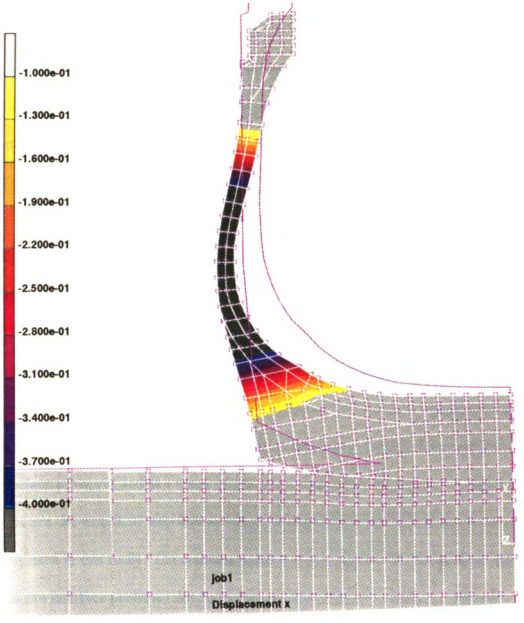

Figure 5.30 Lateral displacements in soil and tire (Tire: 14.9R30; Inflation pressure: 110 kPa; 8 kN load ; Soil condition: dense).

tire rather than the surface. As seen from Figure 5.29, when the soil initially is soft the deformations are shared by tire and soil but when it is initially dense the deformations take place in the tires (Figure 5.30). This behavior also depends upon the tire size, construction, tire loading variables.

The effects of the tire loading variables (inflation pressure and axle load) and the initial soil conditions on soil-tire interface pressures are discussed below. The data used to generate the Figures (Figure 5.31 thru 5.43) for the discussion are given in Appendix H (Table H1 thru H8).

In general, the results of the Finite Element analysis were verified by the literature findings such as inflation pressure and axle load effect on soil-tire interface pressures as discussed in the previous chaper.

Increasing inflation pressure and axle load resulted in increased interface pressures. Figure 5.31 indicates both inflation pressure and axle load effect on interface pressures when the soil was soft. Comparing figure 5.31 and 5.32 clearly shows the effect of initial soil conditions on soil-tire interface pressures. Initially dense soil causes higher interface pressures and as a result of this more compacted soil structure. Figures 5.31 thru 5.38 are the results of interface pressures averaged over the half of the contact width of tires used in this study. The common point in these graphs is the effect of increased mean soil-tire interface pressures due to an increased inflation pressure and axle load.

Figure 5.39 is drawn to indicate the initial soil condition effect on soil-tire interface pressures. Comparison of tire size and construction effect on soil-tire interface pressures

Figure 5.31

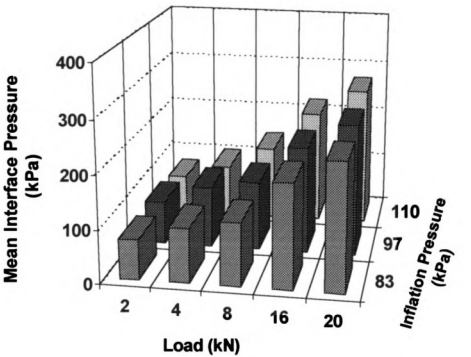

Figure 5.31 Mean interface pressure averaged over the half of the contact width of 18.4R38 tire at various inflation pressure and axle load (Soil: sofft).

Figure 5.

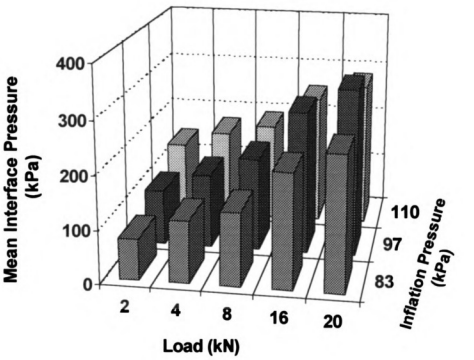

Figure 5.32 Mean interface pressure averaged over the half of the contact width of 18.4R38 tire at various inflation pressure and axle load (Soil: Dense).

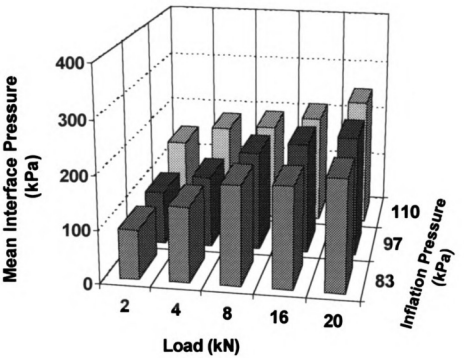

Figure 5.33 Mean interface pressure averaged over the half of the contact width of 18.4-38 tire at various inflation pressure and axle load (Soil: Soft).

Mean Interface Pressure (kPa)

Figure 5.34

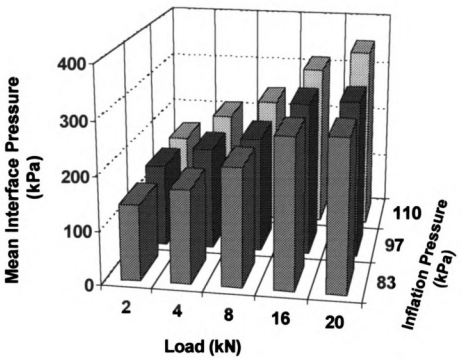

Figure 5.34 Mean interface pressure averaged over the half of the contact width of 18.4-38 tire at various inflation pressure and axle load (Soil: Dense).

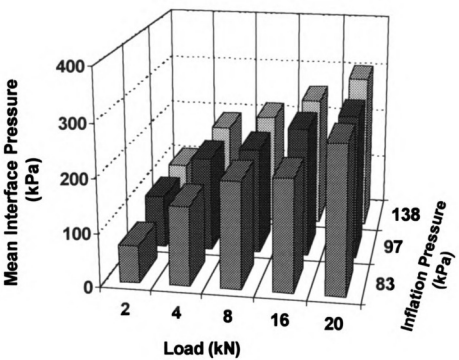

Figure 5.35 Mean interface pressure averaged over the half of the contact width of 14.9R30 tire at various inflation pressure and axle load (Soil: Soft).

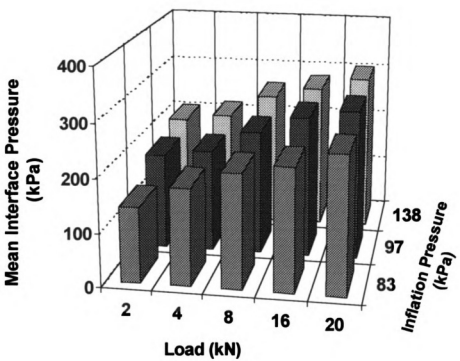

Figure 5.36 Mean interface pressure averaged over the half of the contact width of 14.9R30 tire at various inflation pressure and axle load (Soil: Dense).

Figur

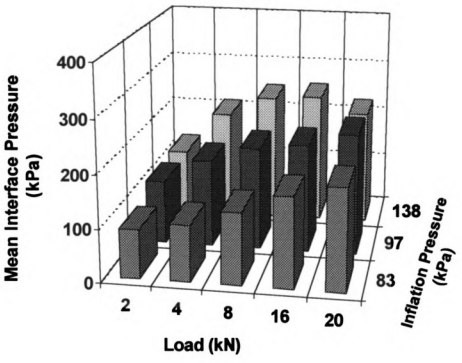

Figure 5.37 Mean interface pressure averaged over the half of the contact width of 14.9-30 tire at various inflation pressure and axle load (Soil: Soft).

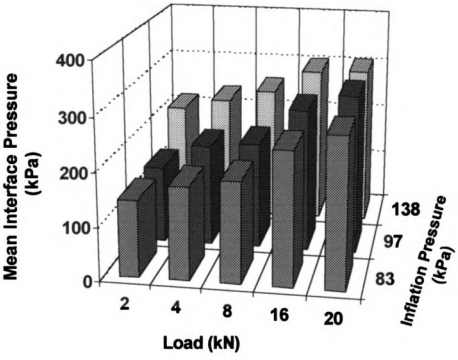

Figure 5.38 Mean interface pressure averaged over the half of the contact width of 14.9-30 tire at various inflation pressure and axle load (Soil: Dense).

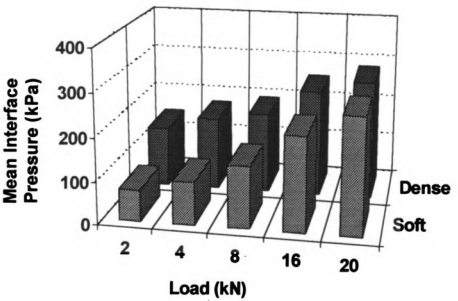

Figure 5.39 Effect of initial soil condition on mean interface pressures over the half of the contact width of 18.4R38 at 110 kPa inflation pressure.

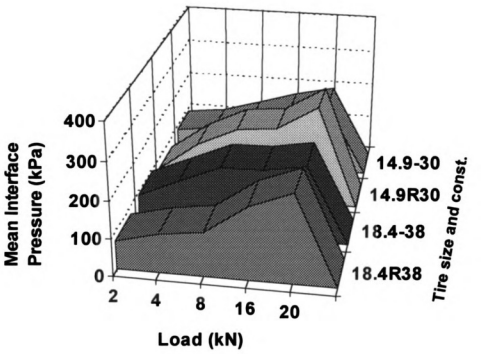

Figure 5.40 Effect of tire size and construction on mean interface pressures averaged over the half of the contact width of tires (Inflation pressure: 83 kPa; Soft Soil).

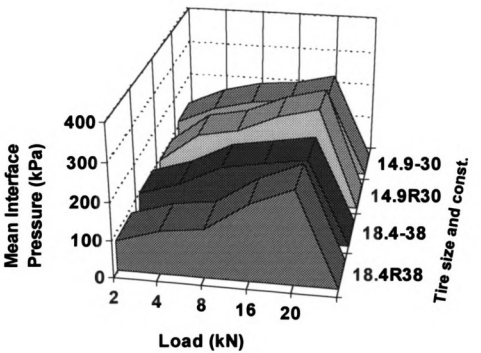

Figure 5.41 Effect of tire size and construction on mean interface pressures averaged over the half of the contact width of tires (Inflation pressure: 97 kPa; Soft Soil).

Fig

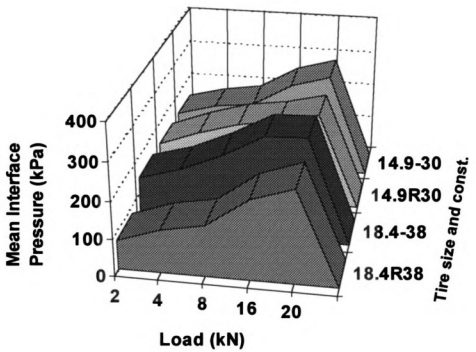

Figure 5.42 Effect of tire size and construction on mean interface pressures averaged over the half of the contact width of tires (Inflation pressure: 83 kPa; Dense Soil).

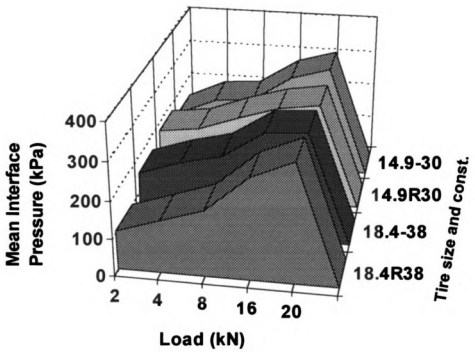

Figure 5.43 **Effect of tire size and construction on mean interface pressures averaged over the half of the contact width of tires (Inflation pressure: 97 kPa; Dense Soil).**

is also an important outcome of this study. As seen from Figure 5.40, there is a noticable changes in the magnitude of soil-tire interface pressures especially at higher loads (16 and 20 kN). An interesting observation is the higher interface pressures in these graphs due to radial tire use. A similar trend was also obtained at 97 kPa inflation pressure. On dense soil, the advantage of using radial tires is clear when figures 5.42 and 5.43 are compared the ones on soft soil, especially at 83 kPa inflation pressure. It can be concluded that the soil-tire interface pressures are dependent upon tire size, construction, loading conditions and the initial soil condition.

5.4 CONCLUSIONS

The followings were concluded from the study;

1. Tires respond to inflation pressure and axle load and inflation pressure in a way that their size and construction play an important role on their deformational behaviour.
2. Bias tires under the same inflation pressure deflect more than radial tires vertically but this trend is reversed when the lateral deformations are considered and the tires are not in contact with any surface loading.
3. Load affects the soil-tire interface pressures and inreasing the axle load on a tire results in increased interface pressures.
4. Inflation pressure is an important variable on interface pressures and soil-tire interface pressures go up if inflation pressure increases. So the pressures recommended by tire manufacturers should be considered along with the load.

5. Initial soil conditions play a vital role in terms of interface pressures, the stiffer the soil is, the higher the interface pressures will be.
6. Tire construction effect on interface pressures was only found when the soil was dense. On soft soil the interface pressures were higher beyond 16 kN load when radial tires were operated.
7. The Finite Element Method is a tool that can be used to study the complex behaviour of tires and their interaction with a rigid surface and soil.

A STUDY OF SOIL-TIRE INTERACTIONS USING FINITE ELEMENT METHOD

VOLUME II

By

ADNAN DEGIRMENCIOGLU

A DISSERTATION

Submitted to
Michigan State University
in partial fulfillment of the requirements
for the degree of

DOCTOR OF PHILOSOPHY

Department of Agricultural Engineering

1997

As

resources

vehicles s

S

(19~4), t

modifica

research

help to i

.

problem

interact

mechan

formula

tractabl

method

the theo

very ge

Chapter 6

TRACTION MODEL

As energy from petroleum becomes expensive, the efficient utilization of energy resources becomes a main concern. Optimizing the performance of energy-dependent vehicles such as tractors is one of the goals that many researchers have addressed.

Since the cone index based traction model was proposed by Wismer and Luth (1974), there have been many studies to improve the prediction of that model with some modifications. Brixius's model and others could be given as examples. However; researchers often make assumptions on things such as mechanical properties of soils that help to improve the prediction of their models.

The first step to approach the problem considered here was to define the mobility problem with respect to the basic parameters involved. Then, a concept describing interactions among the vehicle, tire and soil parameters was developed and a soil mechanics theory that applies to the determination of soil behavior in this context was formulated within the framework of reasonable assumptions that made the solution tractable. The soil properties associated with the soil mechanics theory were defined and methods for their determination in the laboratory established. At this stage, validation of the theoretical concepts under controlled laboratory conditions was accomplished. *In a very general sense, even without clearly formulated theoretical concepts, researchers*

in the field of off-road mobility have recognized that the shear strength of soil is the most important property that governs mobility. In exteremly adverse conditions the mobility of cross-country vehicles is limited by the shear strength of the soil. In "no-go" situations soil prevents the development of traction necessary to overcome whatever motion resistance has been created by the sinkage caused by soil failure. Obviously, the shear strength of the soil is the controlling factor in these critical cases of immobility. While this "no go" situation is of great importance in the trafficability evaluation of the terrain, equally important is the evaluation of vehicle performance under "go" conditions. The role of shear strength of soil in "go" conditions depends on the nature of the interaction between the wheels or tracks of the vehicle and the soil. Experimental observations as well as theoretical considerations indicate that the performance of rigid wheels is always controlled by shear strength of the soil since soil failure develops in practically all loading conditions of interest. Pneumatic tires are fundamentally different from rigid wheels in that their contact area in soils is at least as large as that on a rigid surface under the same load. Thus, the soil is not necessarily in the plastic state of failure beneath pneumatic tires. Nevertheless, in most cases of interest, soil failure conditions govern the performance of pneumatic tires (Karafiath and Nowatzki, 1978).

In this study, interface pressures as a function of tire variables such as load, inflation pressure, size and construction were investigated using the finite element method and the results given in a previous chapter. Thus, using the failure conditions in soil under various tire and soil conditions, a new approach for traction modeling was proposed. The

proposed model was created by pooling measurements and simulation results in a new dimensionless term called "Rigidity Index".

6.1 Objectives

The specific objectives of this study were as follows:

1. To develop and test a theoretical traction model.
2. To incorporate soil's dynamic behavior into a model that is based on soil slip lines theory.

6.2 Materials and Methods

6.2.1 Measurement of Traction

Traction measurements were carried out in 1994 and 1995. During the measurements made in 1994, a total of four tire; two different sizes (14.8-30 and 18.4-38) and two different constructions, radial and bias for each size were used. Only one tire (18.4R38) was operated using the single-wheel tire tester whose details are given in Chaper 4 of this study. All tests were performed in the indoor soil bin containing Norfolk sandy loam. The single wheel tire tester is a soil-bin vehicle with the capability of measuring the variables; travel reduction, dynamic load, inflation pressure, and tractive efficiency (Burt and Bailey, 1982).

The soil bin was prepared twice for the experiments since only two tires could be tested in one soil bin preparation during the measurements in 1994. So the smaller tires (14.-30 and 14.9R30) were tested in the first soil preparation while the other tires (18.4-38 and 18.4R38) were tested in the second soil preparation. The experiment plans for those experiments are given in Figure 6.1 and 6.2. Some plots were reserved for any error

that might have occured during the experiments. Dynamic load, slip and inflation pressure were chosen as the variables and 3 inflation pressures and slip levels were chosen. For the smaller tires inflation pressures were chosen to be 83, 138 and 207 kPa and slip was 7.5%, 15% and 25%. For the 18.4-38 size tires, inflation pressures were chosen to be 83,97,100 kPa. Slip was the same as used for the smaller tires. Dynamic load was ramped up over the duration of the test in each plot.

The rolling radius of the tire was determined on a rigid surface at net traction equals zero. To determine the rolling radius, the tire was run on concrete at zero net traction over a range of dynamic loads and inflation pressures. The data obtained were used to define rolling radius as a function of dynamic load and inflation pressure. Later, when the tire was operated on soil, this rolling radius function was used in travel reduction calculations. Slip during the tests on concrete was considered to be irrelevant. The variables mentioned above (dynamic load, inflation pressure and slip) was randomly distributed over the plots as shown in Figures 6.1, 6.2 and 6.3. During the tests made in 1995, some soil-tire interface pressure measurements were also carried out and for this purpose, plots randomly distributed over the soil bin were used. Soil conditions for all soil conditions are given in Chapter 5, Table 5.3 in this study. there was no difference between the two soil preparations made in 1994, so the dense soil condition given in Table 5.3 represents the two soil conditions on which four tires were operated.

6.2.2 Concept of Soil Rigidity Index

The consideration of the geometry changes in pneumatic tire-soil interaction is one of the most difficult problems of the mathematical simulation of this interaction due to the

42 n

35 n

28 n

21

14

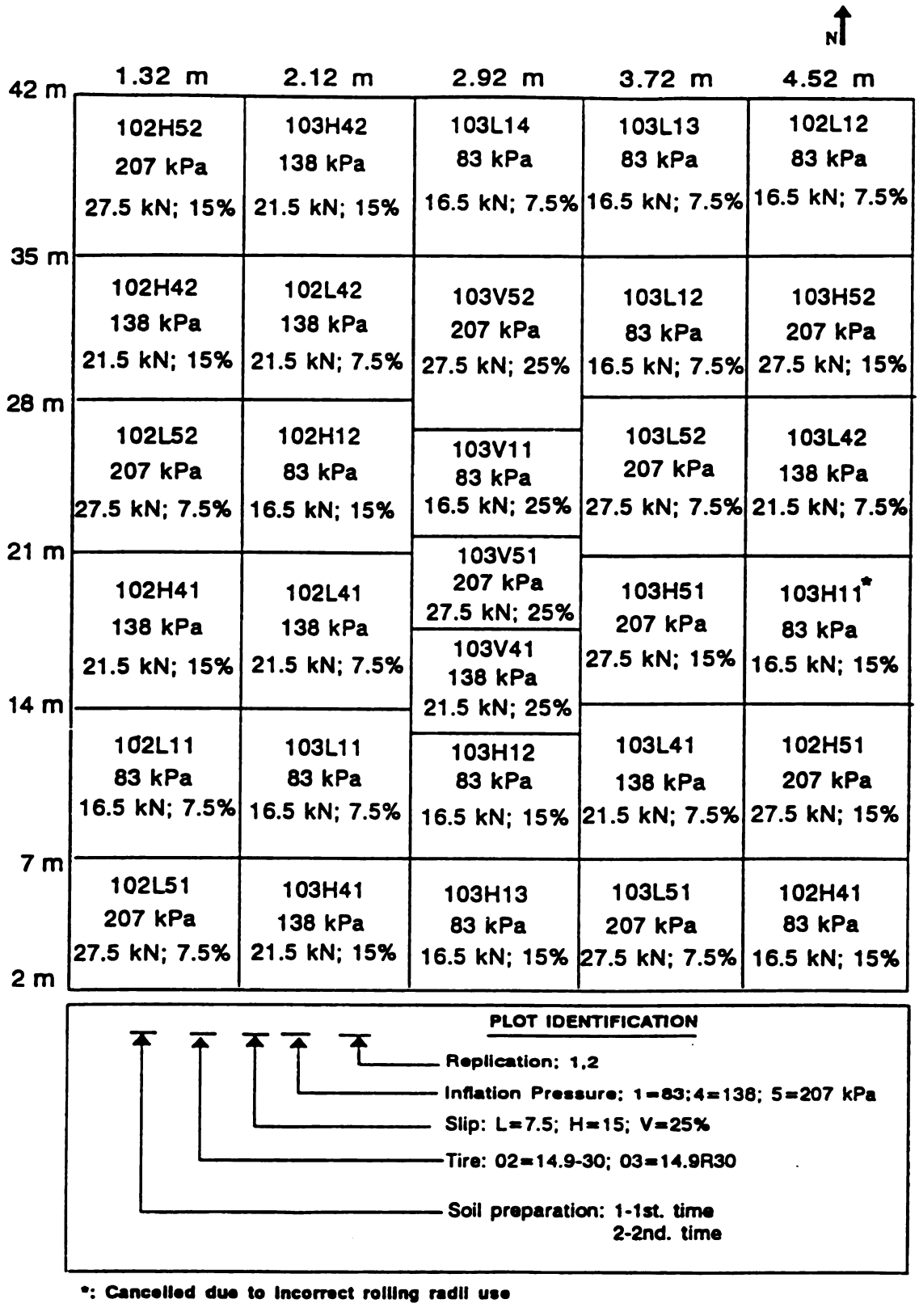

Figure 6.1 Experiment desing for testing 14.9-30 and 14.9R30 tire (March, 1994)

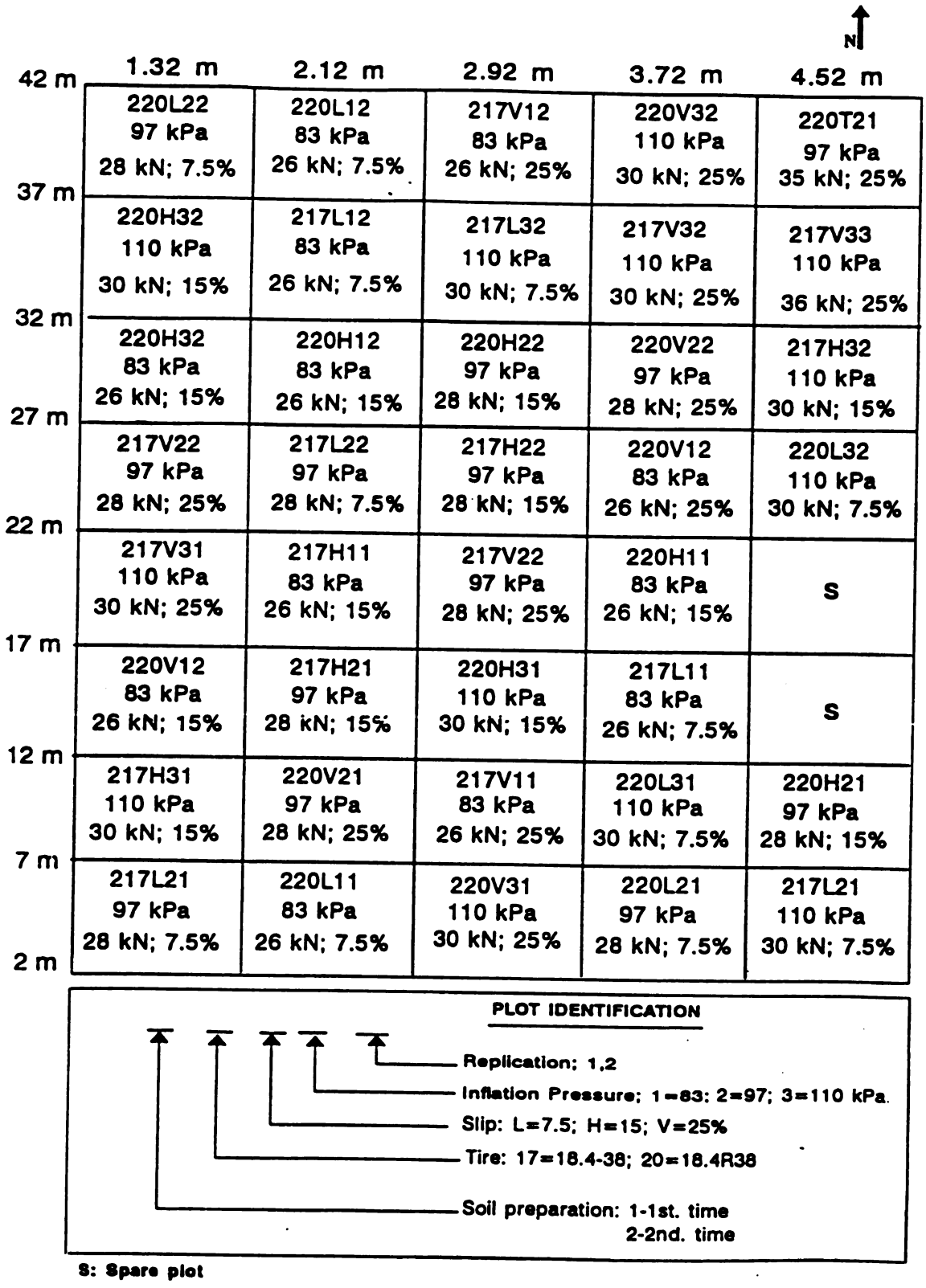

Figure 6.2 Experiment design for testing 18.4-38 and 18.4R38 tire (March, 1994)

42 m

37 m

32 m

27 m

22 m

17 m

12 m

7 m

2

F

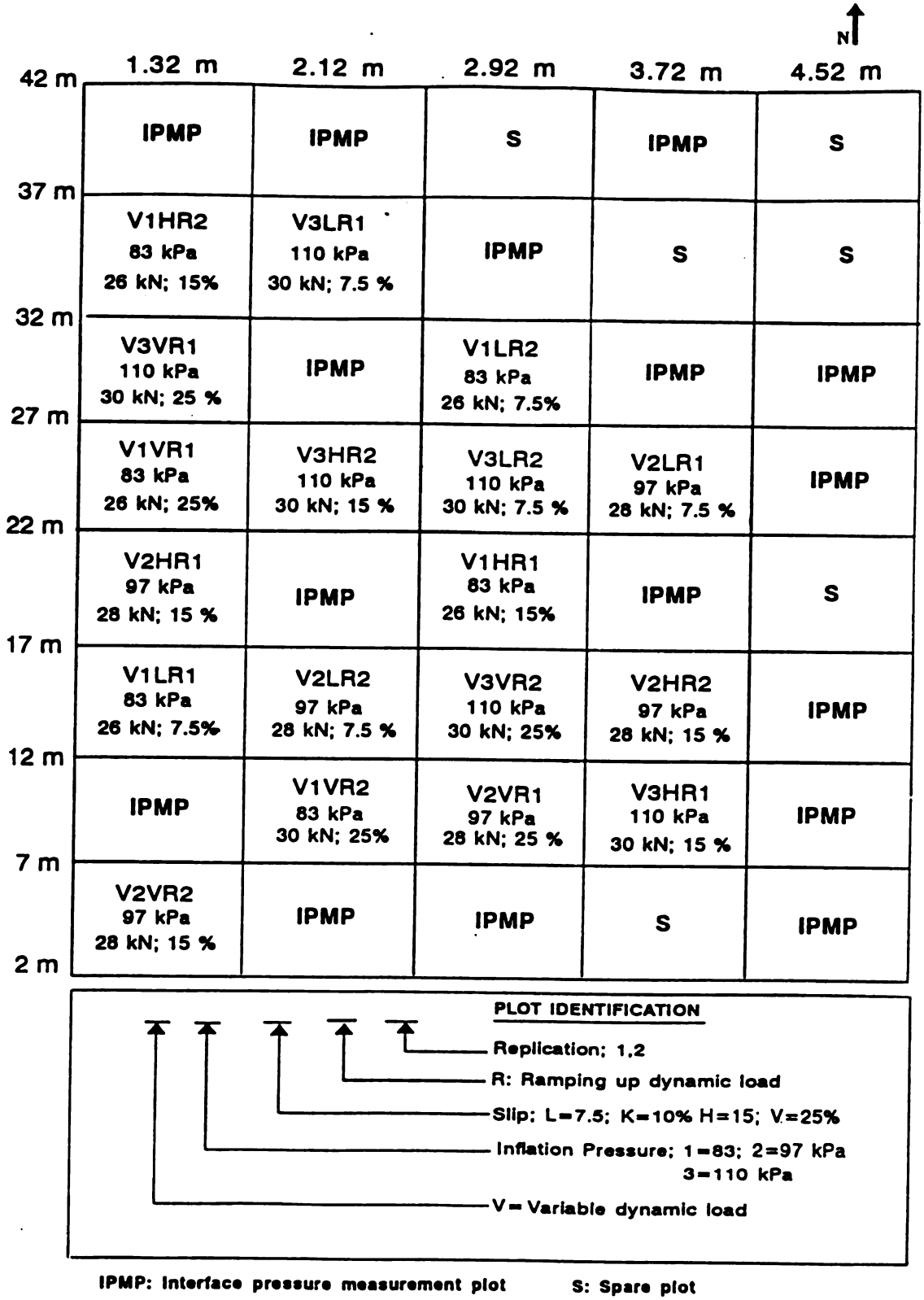

Figure 6.3 Experiment design for testing 18.4-38 and 18.4R38 tire (March, 1995)

tire deflection under various loading conditions. But the rigid wheel-soil interaction can be used as a model of the pneumatic tire and the pneumatic tire behaves as a rigid wheel.

Depending upon the soil, tire and loading conditions, there are three principal modes of failure of soils under loads. These are general shear, local shear and punching shear failure (Vesic, 1975). Each of these modes depend upon the relative compressibility of the soil in the particular geometrical and loading conditions. If the soil is practically incompressible and has a finite shearing strength, it will fail in general shear. On the other hand, if a soil of a given strength is very compressible, it will fail in punching shear. Even though these modes are defined, there is no general numerical criteria that can be used for prediction of mode of shear failure of soils under load. A parameter for evaluation of the relative compressibility of soil masses under load is the rigidity index. The **Rigidity Index** (I_r) merges the two theories and it is defined by Vesic (1975) as;

$$I_r = \frac{G}{c + \sigma \tan\phi} \tag{6.1}$$

where,

G: shear modulus

c: cohesion

Φ : angle of internal friction

σ : normal stress

and sh

where

E: Mo

v: Po

Writin

rigidi

assoc

indet

relat

6.2.1

inde

how

The

part

slip

and shear modulus (G) is defined as;

$$G = \frac{E}{1+\nu} \tag{6.2}$$

where,

E: Modulus of deformation

ν: Poisson's ratio

Writing the shear modulus in terms of the modulus of deformation and poisson's ratio, the rigidity index becomes;

$$I_r = \frac{E}{(1+\nu)\ (c+\sigma\tan\phi)} \tag{6.3}$$

This index, appearing in solutions of expansion of cavities in an infinite solid, is associated with the assumed ideal elastic-plastic behavior of soil. A high value of rigidity index is an indicator of incompressible soil, whereas a low value of rigidity index shows a relatively compressible soil as defined by Vesic (1975).

6.2.3 Development of A Traction Model Based on Soil Rigidity Index

The idea behind the proposed rigidity index based model was to replace the cone index used to predict traction. The cone index has been widely used by many researchers, however, it does not account for the dynamic behavior of the soil under load.

The proposed model was presented by dividing the traction model into two parts. One part of the model was gross tractive force. It is the function of rigidity index of soil and slip and it was given as follows;

$$\mu_g = \frac{F}{W} = f\ (I_r\ , s) \tag{6.4}$$

where,

μ_g = gross traction coefficient.

The second part was the towed force or motion resistance of a pneumatic tire. This depends on the rigidity index of the soil and it was written as;

$$\rho = \frac{TF}{W} = f\ (I_r\ ) \tag{6.5}$$

where,

ρ = motion resistance ratio.

The net pull that can be developed by a tire was then written as;

$$\mu = \frac{P}{W} = f\ (I_r\ , s\ ) - f\ (I_r\ ) \tag{6.6}$$

where,

μ = net traction ratio.

The ratio of gross tractive force and dynamic load and its relationship with slip is well known from the studies available in the literature (VandenBerg and Reed, 1962; Wismer and Luth, 1974; Taylor et al., 1976; Brixius, 1978; Self, 1988; Grisso et al., 1991; Gu and Kuswaha, 1992). This relationship can be written in the following form;

$$\frac{F}{W} = c_1(1 - e^{-c_2 s}) \tag{6.7}$$

where,

$c_1..c_2$ are model constants.

The relationship needed to be determined was the ratio of the gross tractive force and the dynamic load with the rigidity index.

The soil stress-strain model developed by Bailey and Johnson (1994) enabled us to determine the relationship between the gross traction ratio and the rigidity index since the Bailey and Johnson's model can be considered as a traction model. This model is given as,

$$\frac{\tau_{max}}{\sigma_1} = K'(1 - \beta \exp^{-h\gamma/\epsilon_v}) \tag{6.8}$$

where,

τ_{max} = maximum shearing stress

σ_1 = major principal stress

γ = maximum natural shearing strain

ε_v = natural volumetric strain occurring after initiation of shear stress

K', β, and h are coefficients.

Since the pull that was developed by a tire was due to the shear stress, then in the above equation, shear stress can be replaced by P (pull) in the traction and dynamic load models.

Combining the two parts of the traction model, gross tractive force (T/W) and towed force (TF/W), to find net traction or pull, the model proposed in this study was written as follows,

$$\frac{P}{W} = c_1(1-e^{-c_2 I_r})(1-e^{-c_3 s}) - f(I_r) \qquad (6.9)$$

Unlike the stresses, a zero strain condition can be assumed for a soil at any condition. Whenever any external load is applied on soil, the soil parameters are subject to change as in the case of traction. This means that the traction phenomena under tires requires defining the soil firmness or rigidity at different loading and geometrical conditions. This dynamic behavior was modeled by having the dimensionless term, rigidity index, in the traction model proposed in this study.

6.3 Results and Discussion

From the results of Finite Element simulations, the points where the soil shear strength equals the shear stress were determined and for this purpose Equivalent Von-Mises stresses were used. The most important part of developing the model was the determination of the point where the rigidity index was calculated. From the observations made from the Finite Element simulations it was found that the critical point where soil shears was near the surface. At this point an assumption was made such that the rigidity index evaluation was to be at the point where the mean interface pressures were calculated for half of the contact width. So, using the modulus of elasticity for the soils used for traction measurements given in Table 5.6 and assuming a constant poisson's ratio, the rigidity index value was developed. This index was used to develop the traction model. An

example traction data file is given in Appendix I. As seen from the data file, dynamic load was changed from zero to 27.5 kN for smaller tires and 30 kN for bigger (18.4-38) size tires. Using the static load values given in the previous chapter in this study (Tables H1..H8), some linear functions were developed. The functions developed were used to calculate the mean interface pressures at intermediate loads (normal loads) and the rigidity index was calculated. Since slip was not considered in Finite Element simulations, the functions develeloped were the functions of load and inflation pressure only and they were used for all slip levels (7.5, 15 and 25%).

In the process of developing the model, the next step compiled the all data files into one so that the relationships between the variables could be seen. The initial investigations in the filed showed a big variation and the effect of dynamic load was not found to be effective on net traction-pull ratio. For this reason the initial functions between the dynamic load and net traction were developed (one example is given in Appendix J). Using 7976 data points and developing an exponential function for the slip and net traction-dynamic load ratio, the rigidity index based model given below was developed with an r^2 of 94.6%.

$$\frac{P}{W}=0.527\,(1-\exp^{-9.8s})\,(I_r)^{0.031} \qquad \textbf{(6.10)}$$

The coefficient of variations of slip and rigidity index term was 0.66 and 9.93%, respectively. The exponential model given in the traction model was capable of explaning 91% of the variation in the data collected. Thus the effect of rigidity index term was 3%.

It seems that the slip becomes dominant as the soil gets firmer. One of the soil

conditions presented was the soft soil condition. But it was found in the second chapter of this study that in the soft soil conditions the undertread transducers did not come in contact with the soil and did not develop significant interface pressures as compared to the pressures at the lugs. That means the soil identified as `soft` was actually quite a dense soil. Figure 6.4 was drawn from almost 900 data points to demonstrate the effect of slip on net traction-dynamic load ratio. As seen from the figure data points, there are three distinguisable lines. These lines are the ones where 7.5, 15 and 25 % slip was applied. The rigidity index as seen from the figure changes between 30 and 90. Considering all data points, the range for the rigidity index was between 20 and 95.

The comparison of measured and predicted net traction using all data points can be seen from figure 6.5. As seen from the figure the rigidity index based model prediction is in agreement up to 8 kN range and then underpredicts the traction as tractor load increases.

6.4 Conclusion

The rigidity index term is a dimensionless term that can represent the dynamic behavior of the soil under load. Due to the soil conditions, the effect of slip on traction became dominant and the effect of rigidity index was reduced. As a result of this the contribution of rigidity index to the model was less than expected. But it is believed that testing the rigidity index in a variety of soil conditions will result in a better contribution of the rigidity index to the traction model.

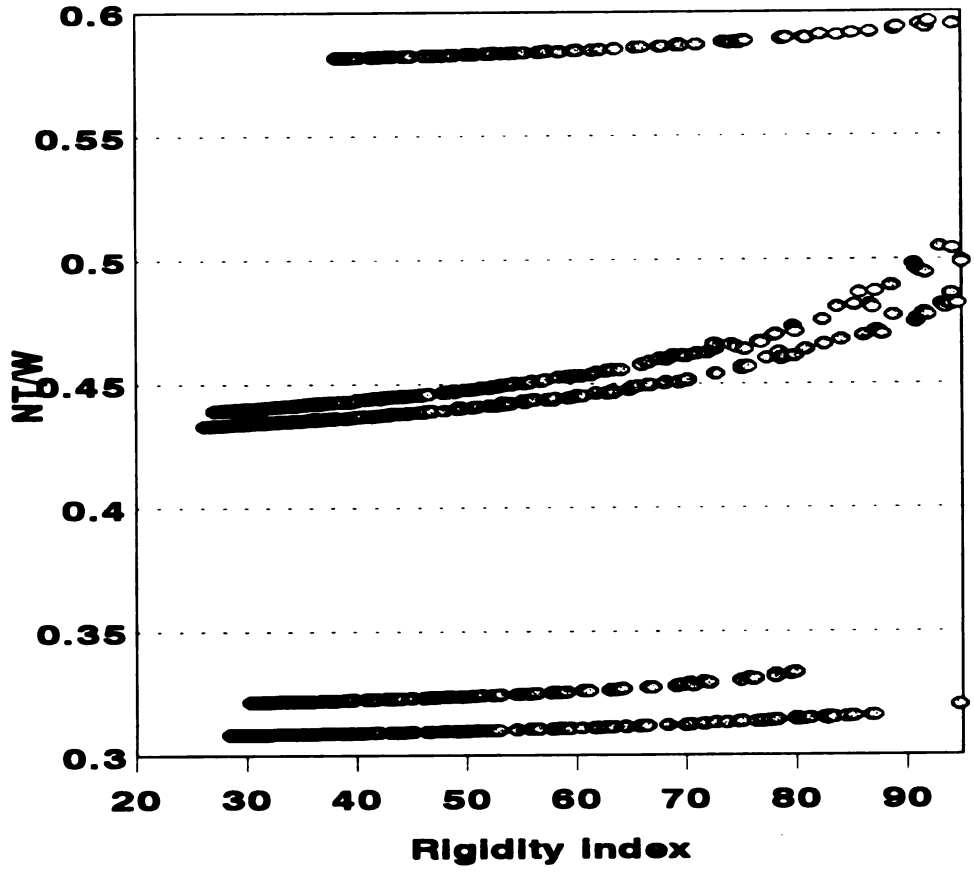

Figure 6.4 Rigidity Index and Net traction/pull relationship


Predicted net traction (kN)

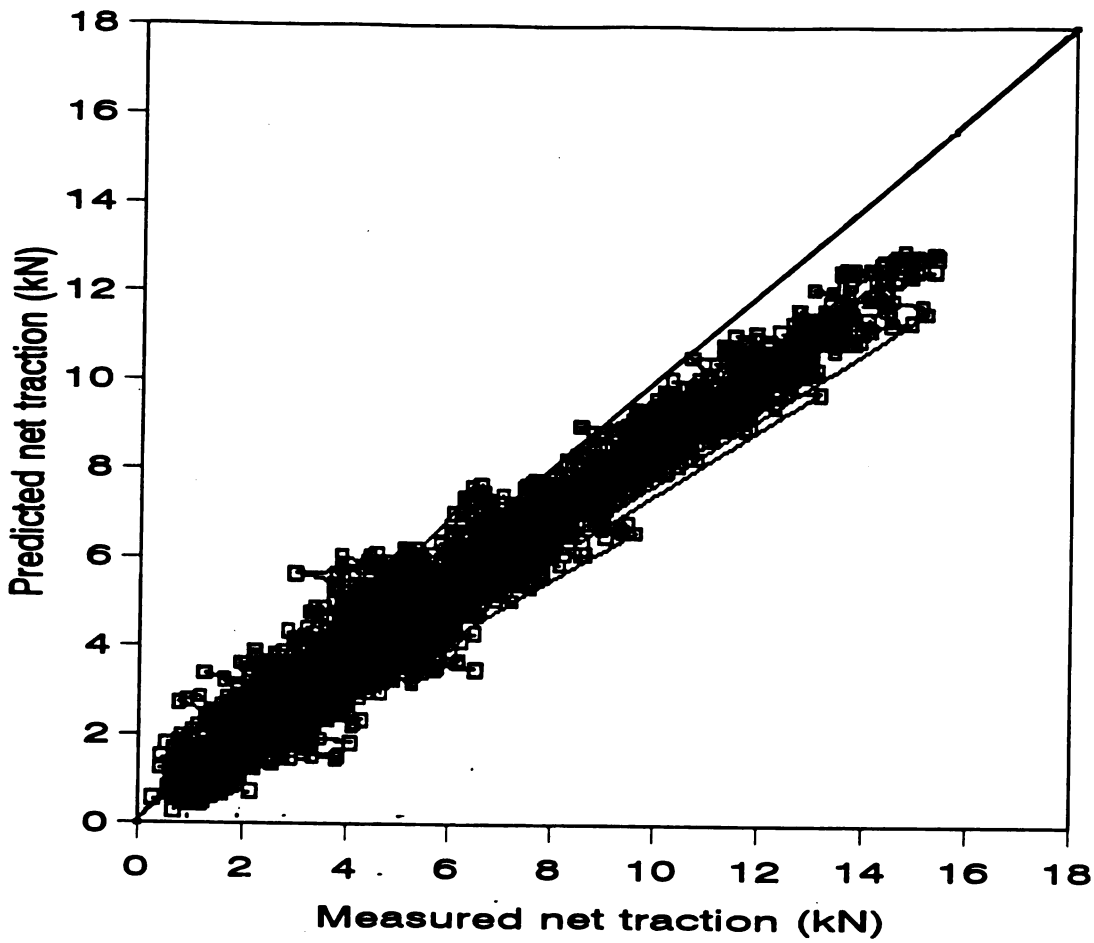

Figure 6.5 Comparison of measured and predicted net traction

7.1 Summ

Th

agricultur

conducte

phenome

establish

conducte

the resu

must be

compac

conside

underst

with th

Labora

interfac

interfac

indoor

Chapter 7

SUMMARY AND CONCLUSIONS

7.1 Summary

The study of soil compaction began to increase significantly in the 1950s as agriculture became more mechanized. Considerable compaction research has been conducted in the last 40 years, but due to the complex and difficult nature of the phenomenon, today there are probably still more opinions about compaction than there are established facts (Schafer et al., 1992). Even though many research studies have been conducted there are still many difficulties that researchers experience when trying to assess the result of soil compaction. The propagation and distribution of the stresses in the soil must be known in order to predict the stress state which in turn can be used to predict compaction. When the causes of soil compaction are considered, tractor tires are considered to be the most important. Hence, experimental studies are quite important to understand the effect of tires on soil compaction. Understanding soil compaction begins with the knowledge of interface pressures applied by tires.

One experiment in this research was conducted at the National Soil Dynamics Laboratory (NSDL), Auburn, Alabama to study the effect of tire-related variables on interface pressures. The single-wheel traction research vehicle was used for soil-tire interface pressure measurements. The experiment was conducted at one of two NSDL's indoor soil bins containing Norfolk sandy loam soil (Typic Paleudults). The soil was

loosen

compa

resear

tire ci

on th

trailin

slip w

83 an

throug

the tir

distan

18.4R

on the

pressu

occurr

positiv

positio

statisti

pressur

chosen

for the

loosened with a rotary tiller and then compacted with a roller to obtain a specific compaction level for interface pressure measurements. The tire powered by the traction research vehicle was a 18.4R38 Armstrong Hi-Traction lug Radial (1-Star) R-1 tire. The tire circumference had 30 long and 30 short lugs. Six pressure transducers were mounted on the tire, with three on a long lug and three on the portion of the undertread on the trailing side of the long lug. Two different levels of dynamic load, inflation pressure and slip were chosen. Dynamic load was 13.1 and 25.3 kN. Inflation pressure was chosen as 83 and 110 kPa. Slip was 7.5 and 10%. All variables were controlled by a computer throughout each test and interface pressures were obtained as a function of wheel angle as the tire rotated. The data acquisition system read each transducer once per 20 mm of distance traveled. Zero conditions of slip calculations consisted of zero net traction for 18.4R38 tire operating on concrete. The wheel angle data were adjusted so the value of 0° on the wheel angle axis represents the bottom dead center (BDC) position for each of the pressure transducers. For each pressure transducer, pressures at negative wheel angles occurred when the pressure transducer was in front of its BDC position and pressures at positive wheel angles occurred when the pressure transducer was to the rear of its BDC position. The interface pressures data obtained as a function of tire variables were statistically analyzed for the interface pressures obtained on the lug transducers since the pressures obtained at the undertread area were low . The -10° and +10° wheel angle was chosen as suggested by Way et al. (1993).

Using the results of mean interface pressures, least square difference (LSD) tests for the multiple comparisons were achieved and interpreted at α=0.05 and from the

analyse

the loca

years a

operati

found t

that in

also fo

increas

1988.

LSD t

than t

affect

reduc

Nowa

shear

neces

tange

failur

analyses, the effect of each independent variable (dynamic load, inflation pressure, slip and the location of measurement) was found to be significant.

Inflation pressure has become an important variable for many researchers in recent years and the limits for inflation pressures for certain type of tires used in agricultural operations have been lowered. Confirming this knowledge, from the analyses, it was found that interface pressures were significantly affected by the inflation pressure in a way that increasing inflation pressure increased interface pressures. Dynamic load effect was also found to be significant and increasing dynamic load increased interface pressures. An increased inflation pressure and dynamic load effect were also confirmed by Burt et al., 1988.

Interface pressures on the lug were also found to be location dependent. From the LSD test it was found that the edge and middle transducers read higher interface pressures than the center one.

The interesting finding in this study was the slip effect on interface pressures. Slip affected the interface pressures adversely. This means that increasing slip results in reduced interface pressures. This interesting finding was also confirmed by Karafiath and Nowatzki (1978). They indicated that the effect of slip is primarily on the application of shear stresses at the soil-tire interface pressures. Reducing the normal stresses, necessitates an increase in the contact area in order to balance the wheel load. Hence, tangential stress components act in the direction of soil failure and tend to facilitate this failure. Three out of six interactions were found to be significant at 95% probability level.

These v

interact

present

interac

and th

Due t

study

interfa

differ

const

tires.

const

blue

proc

mesh

elem

keep

node

secti

be is

These were dynamic load-location, dynamic load-inflation pressure and slip-dynamic load interaction.

While the studies following Trabbic's work were mostly experimental up to present. Simulation based studies have been increased to simulate tire-rigid surface interaction which is less complex than soil-tire interaction. The complex nature of tires and the difficulties to model soil behavior under load limited the simulation based studies. Due to the cost of conducting experimental studies, a study to develop a methodology to study soil-tire interaction was conducted. Finite element method was used to obtain the interface pressures in this study. With the developed methodology one may now study the different aspects of soil-tire interaction especially soil compaction under various tire sizes, construction, tire operating variables (load, inflation pressure) and initial soil conditions.

A methodology based study using finite element method was carried out with four tires, as a combination of two different sizes (14.9-30 and 18.4-38) and two different construction (radial and bias-ply). Half of the cross section of the tires were used and the blue prints of those tires were obtained from Pirelli-Armstrong Tire Corp. The meshing procedure of the tires using a transparency was made by hand. During the process of meshing procedure, special attention was given to create equally distanced and sized elements. The mesh of each tire was made as suggested by Hu and Abeels (1994) by keeping the size of the elements about 10 mm. The two co-ordinates (x and y) of each node then was defined in the finite element program called Marc. Then whole cross-section of each tire was created and materials identified. Tire materials were assumed to be isotropic to overcome the difficulties such as convergence problems in finite element

modeli

from th

the tir

inflatio

step t

geome

condit

follow

deform

of loa

the la

before

for tir

the rig

applie

and c

inflati

with

and

pressu

modeling. Material properties (Modulus of elasticity and Poisson's ratios) were obtained from the study by Hu and Abeels (1994). Due to the symmetry around the y-axis, half of the tire-cross section was used for simulations except the ones used to investigate the inflation pressures effect on tire deformations. According to the methodology the first step to study soil-tire interaction was to assure that the material properties and tire geometries are properly chosen and defined. Along with the necessary boundary conditions, some special features available in Marc were used for simulations. Those were follower force option that makes the applied loads normal to the surface when any deformation occurs. Follower force option was used to make the inflation pressure type of loading act perpendicular to the inside walls of the tire. The second special feature was the large deformation option, since large deformations may occur especially in soils before failure is reached. The last special option was the contact option and it was used for tire-rigid surface simulations to identify the elements that would come in contact with the rigid surface. The simulations were studied as a plane-strain problem that assumes the applied loads lie in the x-y plane, and the displacement in the z-direction was zero.

Using the experimental measurements made in the laboratory with the same size and construction tire used for simulations, some comparisons were made. Different inflation pressures were used for the comparisons and experimental results were compared with the finite element simulations. An 18.4-8 tire was inflated at 80.13, 93.67, 161.39 and 175 kPa inflation pressure in the laboratory and section height at each inflation pressure was measured. The results obtained from the simulations was found to be in

good agre

mentioned

O

further a

From the

play an i

deflect n

variable

simulati

literatu

the rigi

depend

differe

known

structu

expec

press

this

beha

simu

good agreement with the measurements and the difference was less than 1% in all cases mentioned above.

Obtaining a good agreement between the simulation and experimental studies further analysis was conducted to study the inflation pressure effect on tire deformation. From the simulations using all four tires, it was found that the tire size and construction play an important role on tire deformations. Bias tires under the same inflation pressure deflect more vertically than radial tires.

The behavior on a rigid surface was investigated considering two tire operating variables, axle load and inflation pressure. Inflated profiles of the tires were used for these simulations. The results obtained from the rigid surface simulations were compared with literature findings in order to verify the behavior of tire models on a rigid surface. From the rigid surface simulations it was found that the behavior of tires on a rigid surface depended upon size and construction. The simulations on a rigid surface pointed out the differences of sidewall displacements called sidewall bulging phenomenon. Radial tires are known to have a larger contact area than the same size bias tires due to their belted structure. This behavior was observed in the study and differences found were as expected.

After verification of tire models under inflation pressure and under both inflation pressure and axle load on a rigid surface, a soil-tire interaction study was conducted. In this step, the soil properties obtained from the triaxial tests were used to model soil behavior under load. The Drucker-Prager model was used as a stress-strain model for the simulations and two boundary conditions were applied to the soil body in the program.

The inflated t
integrated body
tire on soil whi
runs tire and so
and inflation pr
soil conditions
pressures. Th
measurements.
an acceptable le
were in especiall

In gener
findings such a
Increasing inflat
was the same a
always attained
and the inteface

As a res
conducted by th

Another
eliminates the
considered not
model was devel

The inflated tire profile and soil mesh was then combined to create a deformable integrated body. Some initial runs on soil were made initially to find the contact width of tire on soil which was thought to be different than on rigid surface. Based on those initial runs tire and soil interface pressures were obtained. Four different tires at different loads and inflation pressures were studied to obtain the interface pressures. Two different initial soil conditions were used to also find the soil compaction level effect on soil-tire interface pressures. The results obtained from the simulations were compared with the measurements. It was found that the soil-tire interface pressures could be obtained with an acceptable level of accuracy. The results obtained from the finite element simulations were in especially good agreement with the measurements made at 10% slip.

In general, the results of the finite element analysis were verified by the literature findings such as inflation pressure and axle load effect on soil-tire interface pressures. Increasing inflation pressure resulted in increased interface pressures. Axle load effect was the same as the effect of inflation pressure. The maximum interface pressure was always attained at the edge of the tire cross-section in all cases considered in this study and the inteface pressures increased from moving from the center of the tire to the edge.

As a result of this study, a methodology was developed for further studies to be conducted by the researchers in the field of soil mechanics.

Another objective of this study was to create a traction prediction model that eliminates the use of cone index, since the cone index based traction models were considered not to have any theory. Using the theory of sliplines, a theoretical traction model was developed using the principal of dimensional analysis. The rigidity index as

defined by Ve

model, the trac

were tested un

first pair was a

tire as they w

containing sand

research vehicl

Rolling radii me

soil surface for

inflation pressu

manufacturers.

while 18.4-38 si

from the soil bin

index calculation

were made whe

assumed to be re

values and tract

model. But the

the separate inve

found to be not

load and pull we

result of this proc

defined by Vesic was used to develop the traction model and to test it. To obtain the model, the traction data were obtained at the NSDL, Auburn, Alabama. Two pairs of tires were tested under two different soil conditions during the first year measurements. The first pair was a 14.9-30 and a 14.9R30 tire. The second pair was a 18.4-38 and 18.4R38 tire as they were used for the finite element simulations. Only the indoor soil bin containing sandy load was used for traction measurements. Tires were powered by the research vehicle and tested under different inflation pressure, dynamic load and slip. Rolling radii measurements were achieved on concrete first and then tires were brought to soil surface for the measurements. Three slip values, 7.5, 15 and 25% were used and inflation pressure was also changed depending upon the recommendations by the tire manufacturers. 14.9-30 size tires were tested at 83, 138 and 207 kPa inflation pressures while 18.4-38 size tires were tested at 83, 97 an 110 kPa inflation pressure. Data collected from the soil bins were used to develop the traction model. For this purpose, the rigidity index calculations were made using the simulation results. The rigidity index calculations were made where the soil shear strength equals the shear stress and those points were assumed to be representative of soil and tire interaction phenomenon. The rigidity index values and traction measurements were then pooled to obtain the rigidity index based model. But the collected data had a huge variation and the effect of dynamic load from the separate investigations in the files for each measurement from the NSDL's soil bin was found to be not effective on traction. For this reason, initial functions between dynamic load and pull were developed and these functions were used to obtain the model. As a result of this process, the soil rigidity index model was created with a r^2 of 94.6%. The

rigidity

of variat

load eff

conditio

7.2 Con

1. Expe

this s

2. Soil-t

press

3. Incre

press

4. Low

exces

5. The s

reduc

10%)

6. Finite

pressu

of ini

Furth

proble

rigidity index term explained the 3% of the variation in the data obtain and the coefficient of variation for this dimensionless term was 10%. As was mentioned above, the dynamic load effect was not clear in the data collected and the slip became dominant on soil conditions obtained in the soil bins as it was for the case on a rigid surface.

7.2 Conclusions

1. Experimental studies are of importance to researchers to verify simulated results as in this study.
2. Soil-tire interface pressure measurements indicated the effect of dynamic load, inflation pressure and slip on soil-tire interface pressures.
3. Increasing both, dynamic load and inflation pressure increased soil-tire interface pressures.
4. Low inflation pressure caused less interface pressures on soil and it may help avoid excessive soil compaction.
5. The slip affected the soil-tire interface pressures adversely. Increasing slip resulted in reduced interface pressures. Even though slip was changed in a narrow range (7.5 and 10%), a significant difference between the two was found from the statistical analysis.
6. Finite element method as a simulation tool can be used to obtain the soil-tire interface pressures. The capability of finite element method helped in understanding the effects of initial soil conditions and tire-related variables on soil-tire interface pressures. Furthermore, the finite element method can be used to study the soil compaction problem with the methodology developed in this study.

7. The maximu

all simulatio

8. Tire behavio

was size and

9. Finite eleme

but the result

As the soil g

10. The rigidity

But due to th

Hence a stud

of rigidity ind

7. The maximum soil-tire interface pressures were always attained at the edge of the tire in all simulations.
8. Tire behavior under inflation pressure and under both inflation pressure and axle load was size and construction dependent.
9. Finite element based traction model was created with an acceptable level of accuracy but the results indicated that slip becomes dominant depending upon the soil conditions. As the soil gets firmer the slip gets more dominant.
10. The rigidity index is a dimensionless term that indicates the soil behavior under load. But due to the soil conditions, the effect of rigidity index was not clear in this study. Hence a study that considers different level of initial soil conditions and a wider range of rigidity index, is highly remommended.

The foll

1. Studying th
recommende
efficiency. I
the optimizat
2. Using the Fi
simulation re
between the
But it is bel
achieved wit
3. The methodo
improved wi
4. Traction is a
conditions a
considers th
Finite Eleme
of slip was f
further impr
experiments.

SUGGESTIONS FOR FUTURE STUDIES

The followings are suggested for future studies:

1. Studying the slip effect on soil-tire interface pressures in a wider range is highly recommended since it is the most important variable to obtain a desirable traction efficiency. If the findings obtained in this study are repeated and verified it will help in the optimization of traction and soil compaction modeling.
2. Using the Finite Element Method a close agreement between the experimental and simulation results was obtained in this study in 2D with the assumption that the areas between the lugs are of the same material as the lugs and that the tire surface is smooth. But it is believed that in the future with faster computers, the simulation can be achieved without any assumption. Effect of slip can also be investigated in 3D.
3. The methodology developed in this study is for the 2D simulation case and it could be improved with the enhancement of the computer technology.
4. Traction is a phenomenon that is the result of soil-tire interaction. It varies when soil conditions and tire related variables changes. In this research, a new concept that considers the soil behavior under load was used to develop a traction model using both Finite Element simulation and experimental results. Due to the soil condition, the effect of slip was found to be dominant on traction. But the rigidity index term needs to be further improved and tested under different soil conditions with some additional experiments.

APPENDICES

APPENDIX A

Plot

Treatmer

Inflation
Slip
Dynamic

Explanat

ALE :
LE :
ALM :
LM :
ALC :
LC :
AUE :
UE :
AUM :
UM :
AUC :
UC :

APPENDIX A

Sample interface pressure data

Plot : **C1KH1**

Treatments

Inflation Pressure : 83 kPa
Slip : 10%
Dynamic Load : 25.3 kN

Explanation for the abbriviations

ALE : Angle of lug edge transducer (Degrees)
LE : Interface pressure of lug edge (kPa)
ALM : Angle of lug middle transducer (Degrees)
LM : Interface pressure of lug middle (kPa)
ALC : Angle of lug center (Degrees)
LC : Interface pressure of lug center (kPa)
AUE : Angle of undertread edge transducer (Degrees)
UE : Interface pressure of undertread edge transducer (kPa)
AUM : Angle of undertread middle transducer (Degrees)
UM : Interface pressure of undertread middle transducer (kPa)
AUC : Angle of undertread center transducer (Degrees)
UC : Interface pressure of undertread center transducer (kPa)

APPENDIX A

Table A.1 Sample Interface Pressure Data (Plot Identification: C1KH1)

ALE	LE	ALM	LM
deg	kPa	deg	kPa
133.3	1.732	138.5	1.629
134.8	0.181	140	0
135.8	1.215	141.1	0
137.5	1.215	142.7	0
138.7	0.181	144	0
140.4	0	145.6	0
142	0	147.3	0
143.8	0	149.1	1.283
144.7	0.181	150	1.976
146.5	0.181	151.8	1.629
147.8	0.698	153.1	0.5893
149.3	0	154.5	0.5893
151.1	0	156.3	1.976
152.4	0	157.6	0
154	0.698	159.2	0.2427
155.4	0.698	160.7	0
156.7	0.181	161.9	1.976
158.2	0	163.4	0
159.8	0.181	165	3.016
161.4	2.766	166.7	0
162.7	0	167.9	0
164.3	0.181	169.6	0

Table A.1 (Cont'd)

165.6	0	170.8	0
167.6	0	172.8	0
168.7	0.698	173.9	0.2427
170.1	0	175.4	0.2427
171.6	0	176.8	0.2427
173.4	0.698	178.6	0
175	1.732	180.3	0.2427
176.1	0	181.4	0
177.7	0	183	0.2427
179.4	0.181	184.6	0
180.6	0.698	185.9	0
182.5	0	187.7	0.2427
183.7	0.698	189	1.629
185.4	0.181	190.6	0
187.2	0.181	192.4	0.936
188.6	4.835	193.9	0
189.9	0	195.1	0
191.7	0	197	0
193.2	0	198.4	0
194.8	1.732	200	0.2427
196.1	0	201.3	2.669
197.5	0.181	202.8	0
199.1	0.181	204.4	0
200.4	0.698	205.7	0.2427
202.2	4.318	207.5	0.5893
203.5	0	208.7	0
205.1	0	210.4	0

Table A.1 (Cont'd)

206.6	0	211.8	0
208.4	0	213.6	0.2427
209.7	1.215	214.9	1.629
211.1	0	216.4	1.283
212.8	0	218	0
214	0	219.3	0.5893
215.7	0.698	220.9	0
216.9	0	222.2	0
218.6	0.698	223.8	0
220.4	0.181	225.6	0
221.6	0.698	226.9	0.936
223.1	0	228.3	0
224.9	0	230.1	0
226.2	0	231.4	0
227.6	0.698	232.9	0
229.1	0.698	234.3	0
230.7	0	235.9	0
232.2	0	237.4	0
233.8	0	239	10.64
235.4	0.698	240.7	163.5
236.7	0.181	241.9	226.3
238.3	0.181	243.6	253.7
239.2	0	244.5	246.7
241	0	246.3	253
242.5	0	247.7	224.9
244.3	137.2	249.6	207.2
245.6	197.7	250.8	195.1

Table A.1 (Cont'd)

246.9	207	252.1	190.2
248.7	210.6	253.9	197.2
250.1	214.8	255.4	196.8
251.9	229.8	257.2	212.4
253.2	257.2	258.4	184.7
254.7	275.8	259.9	201.7
256.3	280.9	261.5	197.5
258.1	309.9	263.3	210
259.4	308.9	264.6	224.5
260.8	314	266.1	223.2
262.1	315.6	267.3	214.1
263.7	295.4	269	216.2
265.4	282	270.6	202.4
267.2	276.8	272.4	204.4
268.1	270.6	273.3	214.1
269.7	271.1	274.9	219.3
271.2	268.5	276.4	230.8
272.4	262.9	277.7	250.2
274.2	251	279.5	236.7
275.5	225.1	280.8	217.6
277.1	194.6	282.4	111.5
278.6	142.9	283.8	43.92
280.4	135.7	285.6	0
281.7	70.5	286.9	0
283.1	0	288.4	0
284.9	0	290.2	0
286.8	0	292	0

Table A.1 (Cont'd)

287.8	0	293.1	0
289.1	0	294.4	0
290.9	0	296.2	0
292.4	0	297.6	0
293.6	0	298.9	0
295.3	0	300.5	0
296.9	0	302.2	0
298	0	303.2	0
299.8	0	305.1	0
301.4	0	306.7	0
303.1	0	308.3	0
304.5	0	309.8	0
305.6	0	310.9	0
307.4	0	312.7	0
309.1	0	314.3	0
310.7	0	315.9	0
312.3	0	317.6	0
313.4	0	318.7	0
315.2	0	320.5	0
316.7	0	321.9	0
318	0	323.2	0
319.8	0	325	0
321	0	326.3	0
322.7	0	327.9	0
323.9	0	329.2	0
325.6	0	330.8	0
327	0	332.3	0

Table A.1 (Cont'd)

328.5	0	333.7	0
330.3	0	335.5	0
331.7	0	337	0
333	0	338.2	0
334.6	0	339.9	0
336.1	0	341.3	0
337.9	0	343.1	0
339	0	344.2	0
340.4	0	345.7	0
342.1	0	347.3	0
343.7	0	348.9	0
344.8	0	350	0
346.6	0	351.9	0
-11.25	0	-6.015	0
-9.622	0	-4.382	0
-8.171	0	-2.931	0
-6.902	0	-1.662	0
-5.451	0	-0.2107	0
-3.818	0	1.422	0
-2.186	0	3.054	0
-0.5533	0	4.687	0
0.5349	0	5.775	0
1.986	0	7.226	0
3.256	0	8.496	0
4.888	0	10.13	0
6.339	0	11.58	0
7.972	0	13.21	0

Table A.1 (Cont'd)

9.423	0	14.66	0

Table A.1 (Cont'd)

ALC	LC	AUE	UE
deg	kPa	deg	kPa
144.7	1.573	127.8	0.2618
146.2	0	129.2	0.5891
147.2	0.6741	130.3	0
148.9	0	131.9	0
150.1	0	133.2	0
151.8	0	134.9	0
153.4	0.6741	136.5	0
155.2	0	138.3	0.5891
156.1	3.37	139.2	0.9164
157.9	2.472	141	0.5891
159.2	0	142.3	0
160.7	0	143.7	0.9164
162.5	0	145.6	0.5891
163.8	0	146.8	0
165.4	0	148.5	0
166.8	0	149.9	0.2618
168.1	1.123	151.2	0.2618
169.6	0.2247	152.6	0.2618
171.2	0.2247	154.3	1.244
172.8	1.573	155.9	0.5891
174.1	0	157.2	0
175.7	0	158.8	0
177	0	160.1	0
179	0.2247	162.1	0.2618
180.1	0	163.1	0.5891

Table A.1 (Cont'd)

181.5	0	164.6	0.5891
183	0	166	0
184.8	1.573	167.9	1.244
186.4	1.123	169.5	1.244
187.5	0	170.6	0
189.1	0	172.2	0.5891
190.8	0	173.8	0
192	0.6741	175.1	0.2618
193.9	0	176.9	0.9164
195.1	0	178.2	0.5891
196.8	2.022	179.8	2.226
198.6	0	181.6	2.226
200	0.6741	183.1	1.244
201.3	0	184.4	0
203.1	0	186.2	0.5891
204.6	0	187.6	0.5891
206.2	0	189.3	1.244
207.5	0.6741	190.5	1.571
208.9	0	192	0.5891
210.5	0.2247	193.6	0.9164
211.8	0.6741	194.9	0.9164
213.6	0.6741	196.7	0.5891
214.9	0	198	0
216.5	0	199.6	1.898
218	0	201.1	0.5891
219.8	1.123	202.9	0
221.1	0	204.1	1.571

Table A.1 (Cont'd)

222.5	0	205.6	0.2618
224.2	0	207.2	0.9164
225.4	0	208.5	0
227.1	0	210.1	1.571
228.3	0	211.4	0.5891
230	0	213	0.5891
231.8	0	214.8	1.244
233	0	216.1	3.207
234.5	0	217.6	0
236.3	0	219.4	1.898
237.6	0	220.6	0
239	178.2	222.1	0
240.5	207.4	223.5	0.2618
242.1	227.6	225.2	0.5891
243.6	211	226.6	0
245.2	181.3	228.3	0.5891
246.8	128.7	229.9	0.2618
248.1	114.8	231.2	1.244
249.7	104.9	232.8	0
250.6	104	233.7	0
252.4	107.6	235.5	0
253.9	108.1	237	0
255.7	103.1	238.8	0
257	109.4	240.1	2.226
258.3	104	241.3	0
260.1	84.26	243.1	0
261.5	73.47	244.6	0
263.3	70.33	246.4	0
264.6	64.49	247.7	0
266.1	66.73	249.1	0

Table A.1 (Cont'd)

267.7	59.09	250.8	0
269.5	31.23	252.6	0
270.8	47.41	253.8	0
272.2	46.06	255.3	0
273.5	61.79	256.6	0
275.1	71.68	258.2	0
276.8	81.56	259.8	0
278.6	96.39	261.6	0
279.5	109	262.5	0
281.1	114.4	264.2	0
282.6	116.6	265.6	0
283.8	69.88	266.9	0
285.6	6.067	268.7	1.898
286.9	0	270	9.099
288.5	0	271.6	22.19
290	0	273.1	18.26
291.8	0	274.9	14.01
293.1	0	276.1	17.28
294.5	0	277.6	21.54
296.3	0	279.4	19.57
298.2	0	281.2	0
299.2	0	282.3	0
300.5	0	283.6	0
302.3	0	285.4	0
303.8	0	286.8	0
305	0	288.1	0
306.7	0	289.8	0
308.3	0	291.4	0
309.4	0	292.5	0
311.2	0	294.3	0

Table A.1 (Cont'd)

312.8	0	295.9	0
314.5	0	297.6	0
315.9	0	299	0
317	0	300.1	0
318.8	0	301.9	0
320.5	0	303.5	0
322.1	0	305.2	0
323.7	0	306.8	0
324.8	0	307.9	0
326.6	0	309.7	0
328.1	0	311.2	0
329.4	0	312.4	0
331.2	0	314.2	0
332.4	0	315.5	0
334.1	0	317.1	0
335.3	0	318.4	0
337	0	320	0
338.4	0	321.5	0
339.9	0	322.9	0
341.7	0	324.8	0
343.1	0	326.2	0
344.4	0	327.5	0
346	0	329.1	0
347.5	0	330.6	0
349.3	0	332.4	0
350.4	0	333.5	0
351.8	0	334.9	0
353.5	0	336.5	0
355.1	0	338.2	0
356.2	0	339.3	0

Table A.1 (Cont'd)

358	0	341.1	0
0.1451	0	-16.78	0
1.778	0	-15.15	0
3.229	0	-13.7	0
4.498	0	-12.43	0
5.949	0	-10.98	0
7.582	0	-9.348	0
9.214	0	-7.716	0
10.85	0	-6.083	0
11.93	0	-4.995	0
13.39	0	-3.544	0
14.66	0	-2.274	0
16.29	0	-0.6419	0
17.74	0	0.8092	0
19.37	0	2.442	0
20.82	0	3.893	0

Table A.1 (Cont'd)

AUM	UM	AUC	UC
deg	kPa	deg	kPa
133.1	0.03928	138.5	0
134.5	1.218	139.9	0
135.6	0.03928	141	0
137.3	0.03928	142.6	0
138.5	0	143.9	0
140.2	0.03928	145.6	0
141.8	0.03928	147.2	0.2618
143.6	0.03928	149	0.2618
144.5	0.4321	149.9	0.2618
146.3	0.4321	151.7	0.5374
147.6	0.4321	153	0.5374
149.1	0	154.4	0
150.9	0	156.3	0
152.1	0.03928	157.5	0
153.8	0.4321	159.2	1.364
155.2	0	160.6	1.089
156.5	0.8249	161.9	0
157.9	0	163.3	0.2618
159.6	0.03928	165	0.2618
161.2	0.03928	166.6	0.2618
162.5	0	167.9	0
164.1	0.03928	169.5	0.2618
165.4	1.611	170.8	0
167.4	0	172.8	0
168.5	0.4321	173.8	1.089
169.9	0.4321	175.3	0.2618
171.4	0.03928	176.7	0
173.2	0.03928	178.6	0

Table A.1 (Cont'd)

174.8	0.8249	180.2	0.2618
175.9	0.4321	181.3	0
177.5	0.03928	182.9	0
179.2	0.8249	184.5	0
180.4	0.03928	185.8	0
182.3	0.4321	187.6	0
183.5	0.8249	188.9	0
185.2	2.003	190.5	0.2618
187	0.03928	192.3	0
188.4	0.8249	193.8	0
189.7	0.03928	195.1	0
191.5	0.03928	196.9	0
193	0.03928	198.3	0
194.6	0.8249	200	0.2618
195.9	1.611	201.2	0
197.3	0	202.7	0
198.9	0.03928	204.3	0
200.2	0.8249	205.6	0
202	0.03928	207.4	0
203.3	0	208.7	0
204.9	0	210.3	0
206.4	0.8249	211.8	0
208.2	2.003	213.6	0.5374
209.5	0	214.8	0
210.9	0.4321	216.3	0.2618
212.5	0	217.9	0.2618
213.8	0	219.2	0
215.4	0.8249	220.8	0
216.7	0.03928	222.1	0
218.3	0	223.7	0

Table A.1 (Cont'd)

220.2	0.03928	225.5	0
221.4	0.8249	226.8	0
222.9	0.4321	228.3	0
224.7	0.8249	230.1	0.813
226	0	231.3	0
227.4	0.03928	232.8	0
228.9	0	234.2	0
230.5	0.03928	235.9	0
231.9	0	237.3	0
233.6	0	239	0.2618
235.2	0.03928	240.6	0.2618
236.5	0	241.9	0
238.1	0	243.5	0.813
239	0	244.4	0
240.8	0	246.2	0
242.3	0	247.7	0
244.1	0	249.5	0
245.4	0	250.8	0
246.6	0	252	1.64
248.5	0	253.8	0
249.9	0.03928	255.3	0
251.7	0.03928	257.1	0
253	0	258.4	0
254.4	0	259.8	0
256.1	0	261.5	0
257.9	0	263.3	0
259.2	0	264.5	0
260.6	0.03928	266	0
261.9	0	267.3	0
263.5	0.03928	268.9	0

Table A.1 (Cont'd)

265.1	0.03928	270.5	0
267	0.03928	272.3	0
267.9	0	273.2	0
269.5	0.4321	274.9	0
270.9	0	276.3	0
272.2	0	277.6	0
274	0.8249	279.4	0
275.3	0	280.7	0.813
276.9	0	282.3	4.671
278.4	0	283.8	5.774
280.2	0	285.6	6.325
281.5	33.04	286.8	5.222
282.9	70.75	288.3	3.844
284.7	69.57	290.1	0
286.5	0	291.9	0
287.6	0	293	0
288.9	0	294.3	0
290.7	0	296.1	0
292.2	0	297.5	0
293.4	0	298.8	0
295.1	0	300.5	0
296.7	0	302.1	0
297.8	0	303.2	0
299.6	0	305	0
301.2	0	306.6	0
302.9	0	308.3	0
304.3	0	309.7	0
305.4	0	310.8	0
307.2	0	312.6	0
308.9	0	314.2	0

Table A.1 (Cont'd)

310.5	0	315.9	0
312.1	0	317.5	0
313.2	0	318.6	0
315	0	320.4	0
316.5	0	321.9	0
317.7	0	323.1	0
319.6	0	324.9	0
320.8	0	326.2	0
322.5	0	327.8	0
323.7	0	329.1	0
325.4	0	330.7	0
326.8	0	332.2	0
328.3	0	333.6	0
330.1	0	335.5	0
331.5	0	336.9	0
332.8	0	338.2	0
334.4	0	339.8	0
335.9	0	341.3	0
337.7	0	343.1	0
338.8	0	344.2	0
340.2	0	345.6	0
341.9	0	347.2	0
343.5	0	348.9	0
344.6	0	350	0
346.4	0	351.8	0
-11.46	0	-6.085	0
-9.832	0	-4.452	0
-8.381	0	-3.001	0
-7.112	0	-1.732	0
-5.661	0	-0.2807	0

Table A.1 (Cont'd)

-4.028	0	1.352	0
-2.396	0	2.984	0
-0.7633	0	4.617	0
0.3249	0	5.705	0
1.776	0	7.156	0
3.046	0	8.426	0
4.678	0	10.06	0
6.129	0	11.51	0
7.762	0	13.14	0
9.213	0	14.59	0

Mean soil-tire interface pressures obtained from statistical analysis

Factors and their levels used for factorial analysis

Factor A: Inflation pressure
Level 1 : 83 kPa
Level 2 : 110 kPa

Factor B: Slip
Level 1 : 7.5%
Level 2 : 10%

Factor C: Dynamic load
Level 1 : 13.1 kN
Level 2 : 25.3 kN

Factor D: Location of the transducer
Location 1 : Lug edge
Location 2 : Lug middle
Location 3 : Lug center

Table A.2 Table of mean soil-tire interface pressures obtained from the factorial analysis.

Factorial ANOVA for the factors:
Replication (Var 1: REPLICATION) with values from 1 to 2
Factor A (Var 2: INFLATION PRESSURE) with values from 1 to 2
Factor B (Var 7: SLIP) with values from 1 to 2
Factor C (Var 8: DYNAMIC LOAD) with values from 1 to 2
Factor D (Var 9: LOCATION) with values from 1 to 3

Variable 6: INTERFACE PRESSURES

Grand Mean = 219.657 Grand Sum = 10543.559 Total Count = 48

TABLE OF MEANS

1	2	7	8	9	6	Total
*	1	*	*	*	195.206	4684.940
*	2	*	*	*	244.109	5858.619
*	*	1	*	*	248.437	5962.494
*	*	2	*	*	190.878	4581.065
*	1	1	*	*	219.015	2628.184
*	1	2	*	*	171.396	2056.756
*	2	1	*	*	277.859	3334.310
*	2	2	*	*	210.359	2524.309
*	*	*	1	*	197.472	4739.336
*	*	*	2	*	241.843	5804.223
*	1	*	1	*	189.493	2273.914
*	1	*	2	*	200.919	2411.026
*	2	*	1	*	205.452	2465.422
*	2	*	2	*	282.766	3393.197
*	*	1	1	*	206.785	2481.420
*	*	1	2	*	290.089	3481.074
*	*	2	1	*	188.160	2257.916
*	*	2	2	*	193.596	2323.149

Table A.2 (Cont'd).

*	1	1	1	*	193.373	1160.240
*	1	1	2	*	244.657	1467.944
*	1	2	1	*	185.612	1113.674
*	1	2	2	*	157.180	943.082
*	2	1	1	*	220.197	1321.180
*	2	1	2	*	335.522	2013.130
*	2	2	1	*	190.707	1144.242
*	2	2	2	*	230.011	1380.067
*	*	*	*	1	247.015	3952.245
*	*	*	*	2	244.009	3904.144
*	*	*	*	3	167.948	2687.170
*	1	*	*	1	229.413	1835.303
*	1	*	*	2	206.218	1649.745
*	1	*	*	3	149.986	1199.892
*	2	*	*	1	264.618	2116.942
*	2	*	*	2	281.800	2254.399
*	2	*	*	3	185.910	1487.278
*	*	1	*	1	252.648	2021.184
*	*	1	*	2	286.773	2294.186
*	*	1	*	3	205.890	1647.124
*	*	2	*	1	241.383	1931.061
*	*	2	*	2	201.245	1609.958
*	*	2	*	3	130.006	1040.046
*	1	1	*	1	218.576	874.302
*	1	1	*	2	235.371	941.486
*	1	1	*	3	203.099	812.396
*	1	2	*	1	240.250	961.001
*	1	2	*	2	177.065	708.259
*	1	2	*	3	96.874	387.496
*	2	1	*	1	286.720	1146.882
*	2	1	*	2	338.175	1352.700
*	2	1	*	3	208.682	834.728
*	2	2	*	1	242.515	970.060
*	2	2	*	2	225.425	901.699
*	2	2	*	3	163.137	652.550

Table A.2 (Cont'd).

*	*	*	1	1	181.550	1452.402
*	*	*	1	2	235.406	1883.249
*	*	*	1	3	175.461	1403.685
*	*	*	2	1	312.480	2499.843
*	*	*	2	2	252.612	2020.895
*	*	*	2	3	160.436	1283.485
*	1	*	1	1	177.540	710.162
*	1	*	1	2	205.269	821.077
*	1	*	1	3	185.669	742.675
*	1	*	2	1	281.285	1125.141
*	1	*	2	2	207.167	828.668
*	1	*	2	3	114.304	457.217
*	2	*	1	1	185.560	742.240
*	2	*	1	2	265.543	1062.172
*	2	*	1	3	165.252	661.010
*	2	*	2	1	343.675	1374.702
*	2	*	2	2	298.057	1192.227
*	2	*	2	3	206.567	826.268
*	*	1	1	1	147.900	591.600
*	*	1	1	2	260.042	1040.170
*	*	1	1	3	212.412	849.650
*	*	1	2	1	357.396	1429.584
*	*	1	2	2	313.504	1254.016
*	*	1	2	3	199.368	797.474
*	*	2	1	1	215.201	860.802
*	*	2	1	2	210.770	843.079
*	*	2	1	3	138.509	554.035
*	*	2	2	1	267.565	1070.259
*	*	2	2	2	191.720	766.879
*	*	2	2	3	121.503	486.011
*	1	1	1	1	116.495	232.990
*	1	1	1	2	228.060	456.120
*	1	1	1	3	235.565	471.130
*	1	1	2	1	320.656	641.312
*	1	1	2	2	242.683	485.366
*	1	1	2	3	170.633	341.266
*	1	2	1	1	238.586	477.172

Table A.2 (Cont'd).

*	1	2	1	2	182.479	364.957
*	1	2	1	3	135.772	271.545
*	1	2	2	1	241.915	483.829
*	1	2	2	2	171.651	343.302
*	1	2	2	3	57.976	115.951
*	2	1	1	1	179.305	358.610
*	2	1	1	2	292.025	584.050
*	2	1	1	3	189.260	378.520
*	2	1	2	1	394.136	788.272
*	2	1	2	2	384.325	768.650
*	2	1	2	3	228.104	456.208
*	2	2	1	1	191.815	383.630
*	2	2	1	2	239.061	478.122
*	2	2	1	3	141.245	282.490
*	2	2	2	1	293.215	586.430
*	2	2	2	2	211.788	423.577
*	2	2	2	3	185.030	370.060

Coefficient of Variation: 22.88%

Table A.2 (Cont'd).

*	1	2	1	2	182.479	364.957
*	1	2	1	3	135.772	271.545
*	1	2	2	1	241.915	483.829
*	1	2	2	2	171.651	343.302
*	1	2	2	3	57.976	115.951
*	2	1	1	1	179.305	358.610
*	2	1	1	2	292.025	584.050
*	2	1	1	3	189.260	378.520
*	2	1	2	1	394.136	788.272
*	2	1	2	2	384.325	768.650
*	2	1	2	3	228.104	456.208
*	2	2	1	1	191.815	383.630
*	2	2	1	2	239.061	478.122
*	2	2	1	3	141.245	282.490
*	2	2	2	1	293.215	586.430
*	2	2	2	2	211.788	423.577
*	2	2	2	3	185.030	370.060

Coefficient of Variation: 22.88%

APPENDIX B

APPENDIX B

Molding Soil Samples

The purpose of the triaxial tests was to determine the mechanical properties of the soil samples obtained at the National Soil Dynamics Laboratory (NSDL) in Auburn, Alabama.

Due to difficulties to obtain undisturbed samples from sandy soils, the soil samples at bulk density and moisture content were prepared in the laboratory by molding the soil in a special apparatus called forming jacket. Triaxial samples wre formed from the same sand as those for which bulk density samples had previously been determined during the experiments of March 1994 and 1995 for interface pressure and traction measurements were formed. The procedure for molding a soil sample consisted of the following steps;

1. Soil was air dried in an oven at 105 ^{o}C for 24 hours.
2. Air-dried soil was then sieved by using a sieve # 10 (2.0 mm).
3. Soil passing # 10 sieve was then placed in a pot. Based on the moisture content obtained in the Laboratory at NSDL, the amount of water was calculated using the total weight of the soil sample. Water was pulverized on soil and soil was let to reach equilibrium for 16 hours to obtain homogenized soil and the pot was covered with a aluminum to avoid moisture loss.
4. Using the bulk density information obtained from the untraffic area in the laboratory in Auburn, Alabama, the amount of soil to form a 1" thick soil to obtain the necessary bulk density in the forming jacket was calculated.
5. Membrane was put inside the forming jacket.
6. The air between the membrane and the inside face of the forming jacket was evacuated by applying vacuum.

7. Soil was placed in the forming jacket while the vacuum is applied.
8. After placing soil in the forming jacket, the desired soil density was obtained by tamping the soil to the known volume..
9. Tamping process was completed when the whole sample reached 6".
10. At each soil sample addition the number of tams was increased so that the layers on the top can reach the bulk density needed.
11. The molded soil sample was then removed from the forming jacket with the membrane and used for the triaxial tests.

Triaxial Testing of the Molded Soil Samples

Molded soil samples were tested at different confining pressures. The triaxial compression test is used to measure the shear strength of a soil under controlled drainage conditions. In the basic triaxial test, a cylindrical specimen of soil encased in rubber membrane is placed in a triaxial compression chamber (Figure B.3 and B.4), subjected to a confining fluid or air pressure, and then loaded axially to failure. There are three types of basic compression tests. They are unconsolidated-undrained, consolidated-undrained, and consolidated-drained, subsequently referred to as the Q, R, and S tests. The type of test is selected to closely simulate, or to bracket, the conditions anticipated in the field. To simulate the conditions obtained in the laboratory for traction and interface pressure measurements made in March of 1994 and March of 1995 respectively, consolidated-undrained tests were conducted at the anticipated bulk density and moisture content in Auburn, Alabama. The bulk density, moisture content and some other soil related initial conditions are given in Table...

The traxial tests were achieved at 69.03 (10 psi), 138.06 (20 psi) and 345.15 kPa (50 psi) confining pressures. Air was used for confining purposes. Two replications at each

confining pressures were carried out and a total of 6 tests were made for the simulation of laboratory conditions anticipated at the National Soil Dynamics Laboratory in Auburn, Alabama.

The procedure followed for the triaxial tests is as in the following;

1. The discs were placed on top and bottom of the soil sample and some lubricant was used to prevent friction between disc and membrane and then "O" rings were placed on the mebrane.
2. The triaxial chamber was then placed and secured.
3. The chamber was then closed and then air was filled in the chamber up to the predetermined confining pressure.
4. The loading platform was raised until the steel ball on top of the piston touches the bottom of the load cell or the loading gear.
5. All valves were closed except the vacuum's and the cell was filled with air to the desired confining pressure.
6. The soil specimen was then loaded and the sheared at a constant strain rate of 5% per minute.
7. During the measurements, the vertical displacement and axial stress were recorded.
8. Throughout the test, the confining pressure was checked.

Throughout the testing procedure, volume change was not measured due to lack of proper equipment and the above procedure was followed in all tests at different confining pressures and bulk densities.

Prior to shear, the three principal stresses are equal to the confining pressure. During the shear the major prioncipal stress, σ_1 , is equal to the applied axial stress (P/A) plus the chamber pressure, σ_3. The applied axial stress, σ_1-σ_3, is termed the "deviatoric stress".

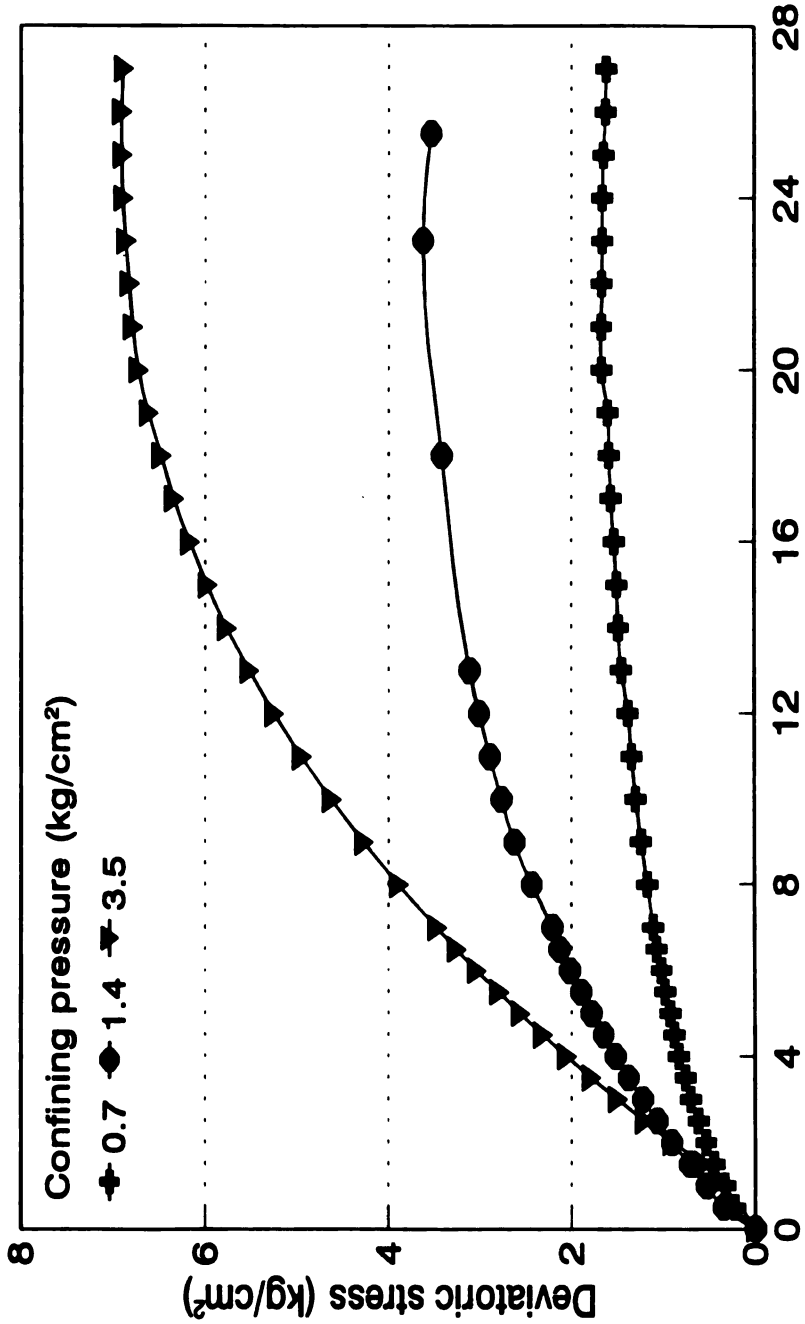

Figure B.1 Stress-strain relationship for soft soil at different confining pressures.

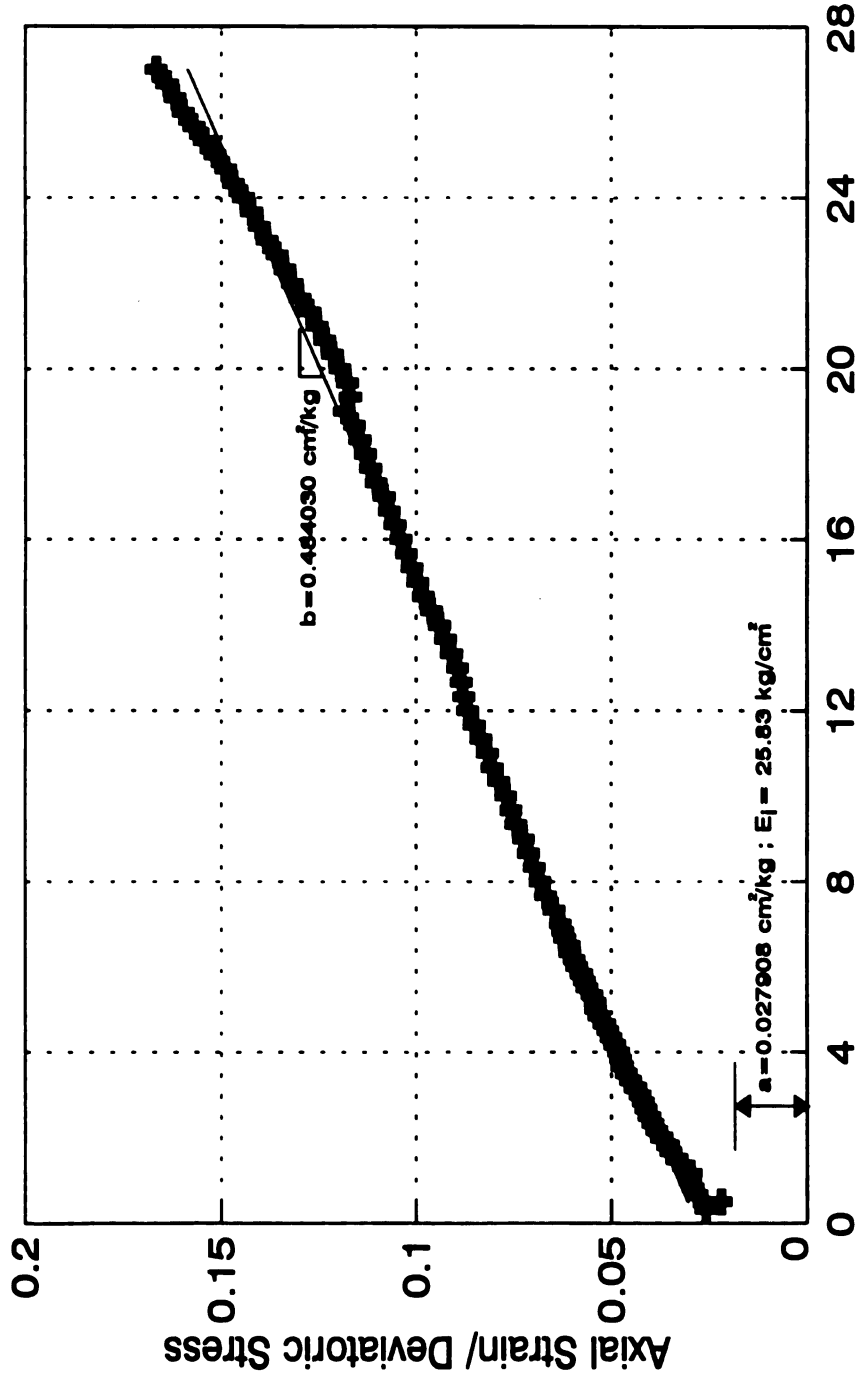

Figure B.2 Normalized stress-strain relationship for soft soil (Confining pressure 0.7 kg/cm²)

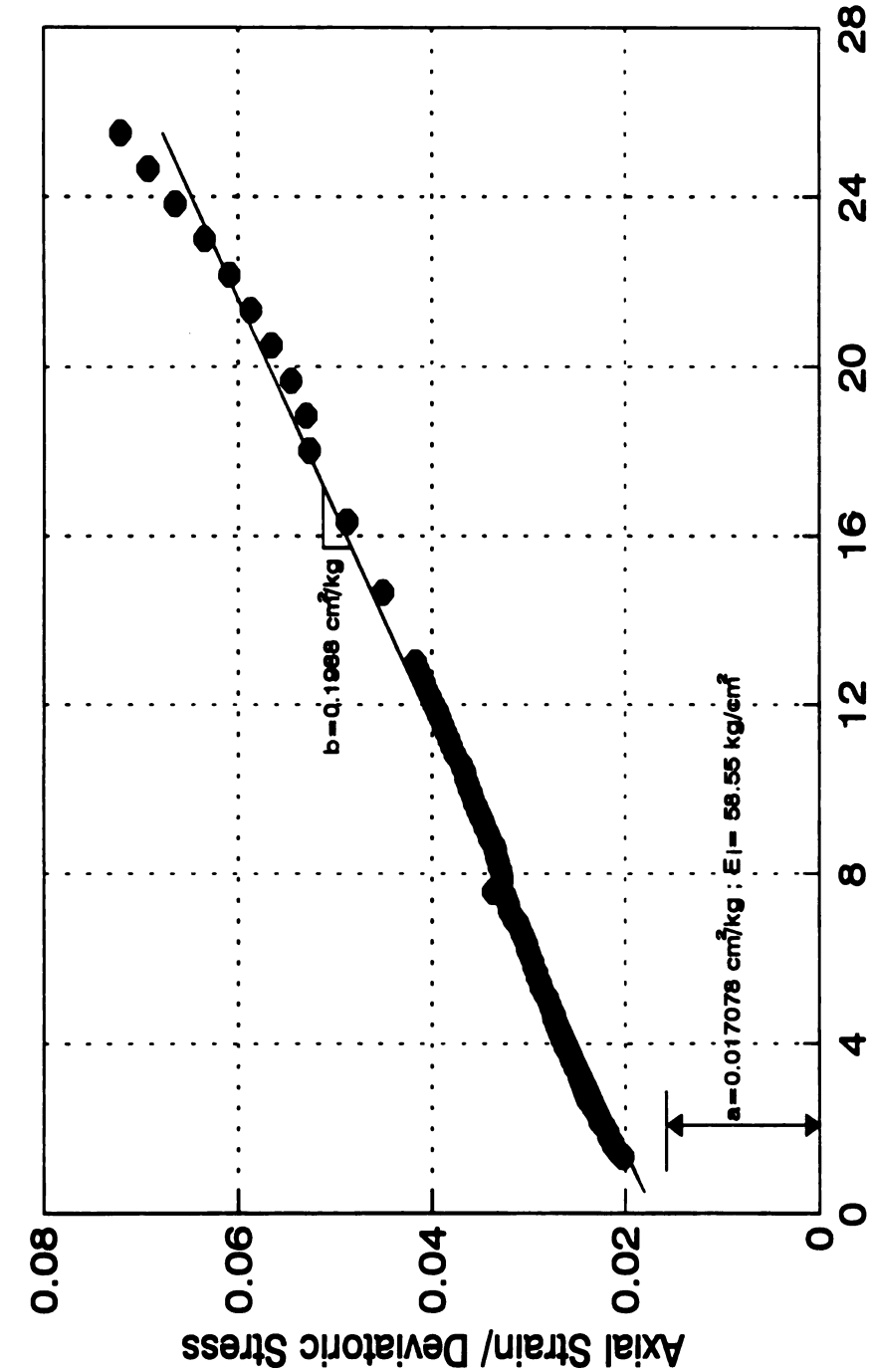

Figure B.3 Normalized stress-strain relationship for soft soil.
(Confining pressure 1.4 kg/cm²)

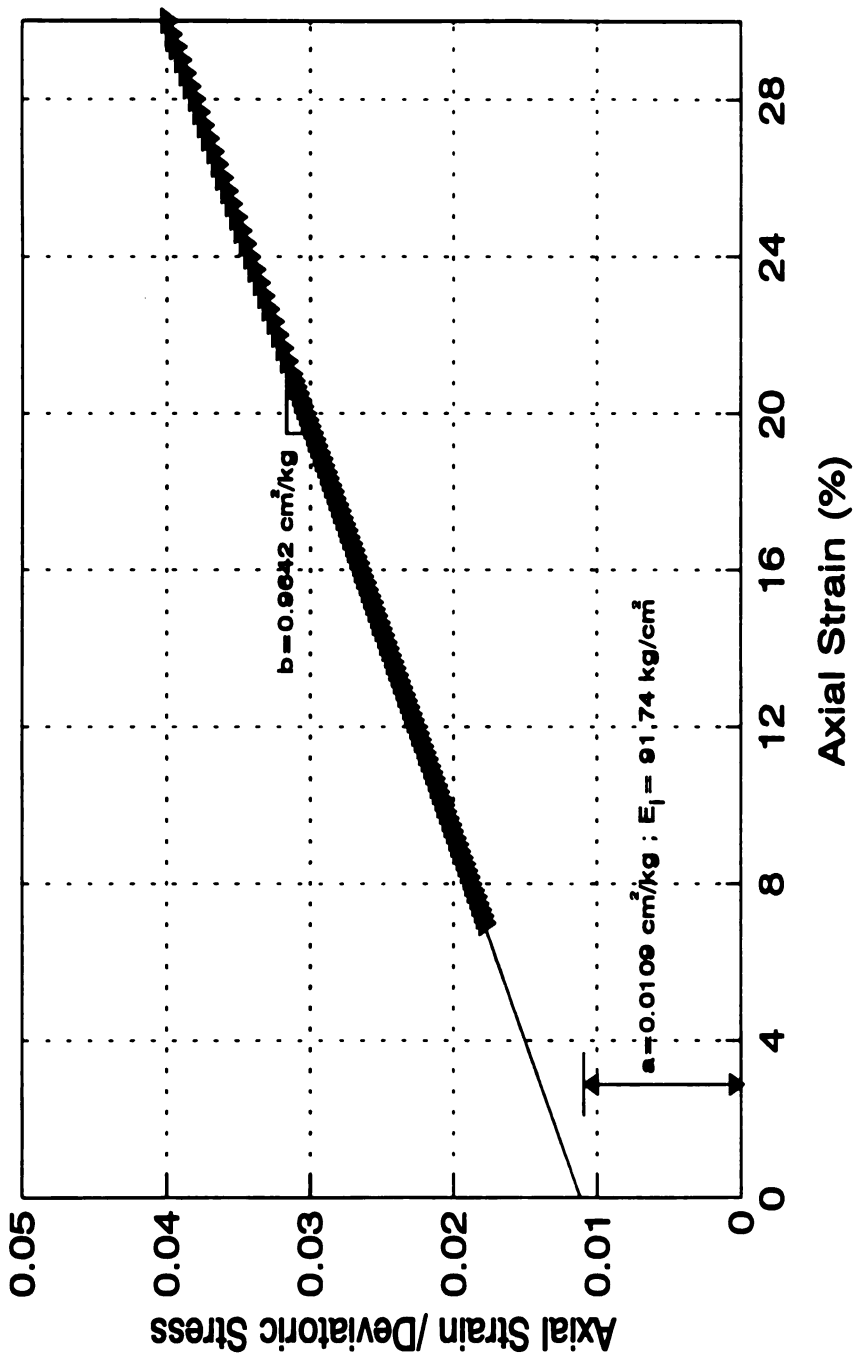

Figure B.4 Normalized stress-strain relationship for soft soil.
(Confining pressure 3.5 kg/cm²)

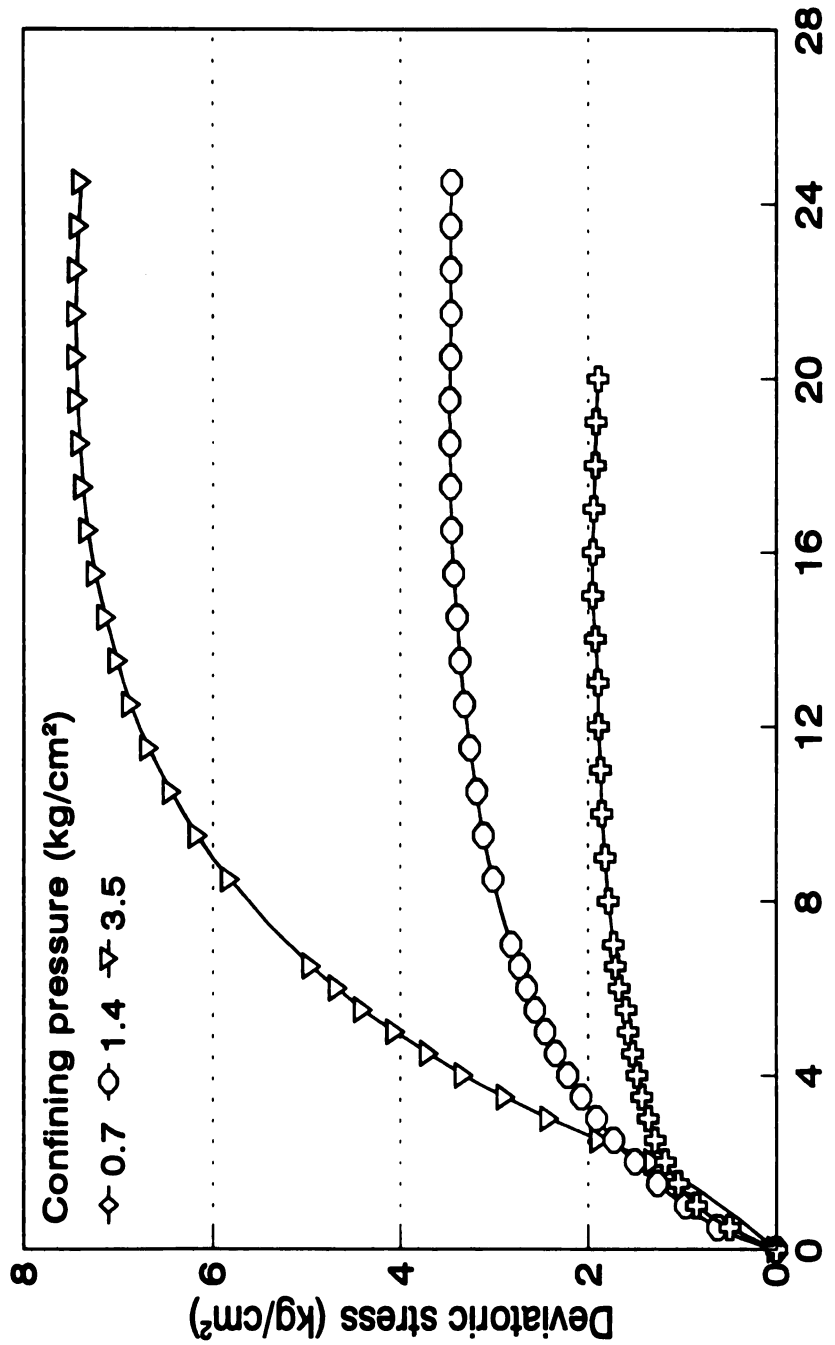

Figure B.5 Stress-strain relationship for dense soil at different confining pressures.

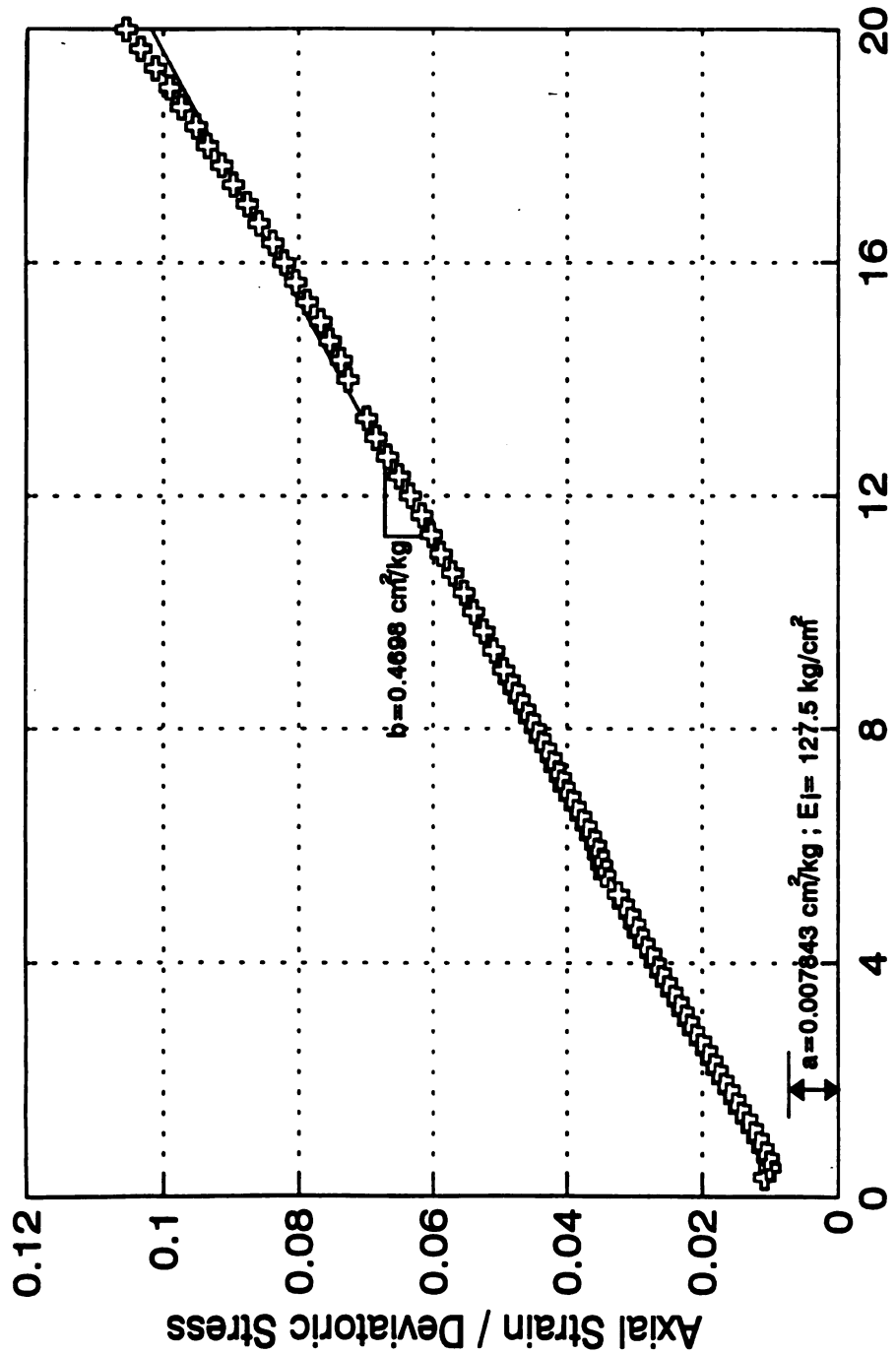

Figure B.6 Normalized stress-strain relationship for dense soil. (Confining pressure 0.7 kg/cm²)

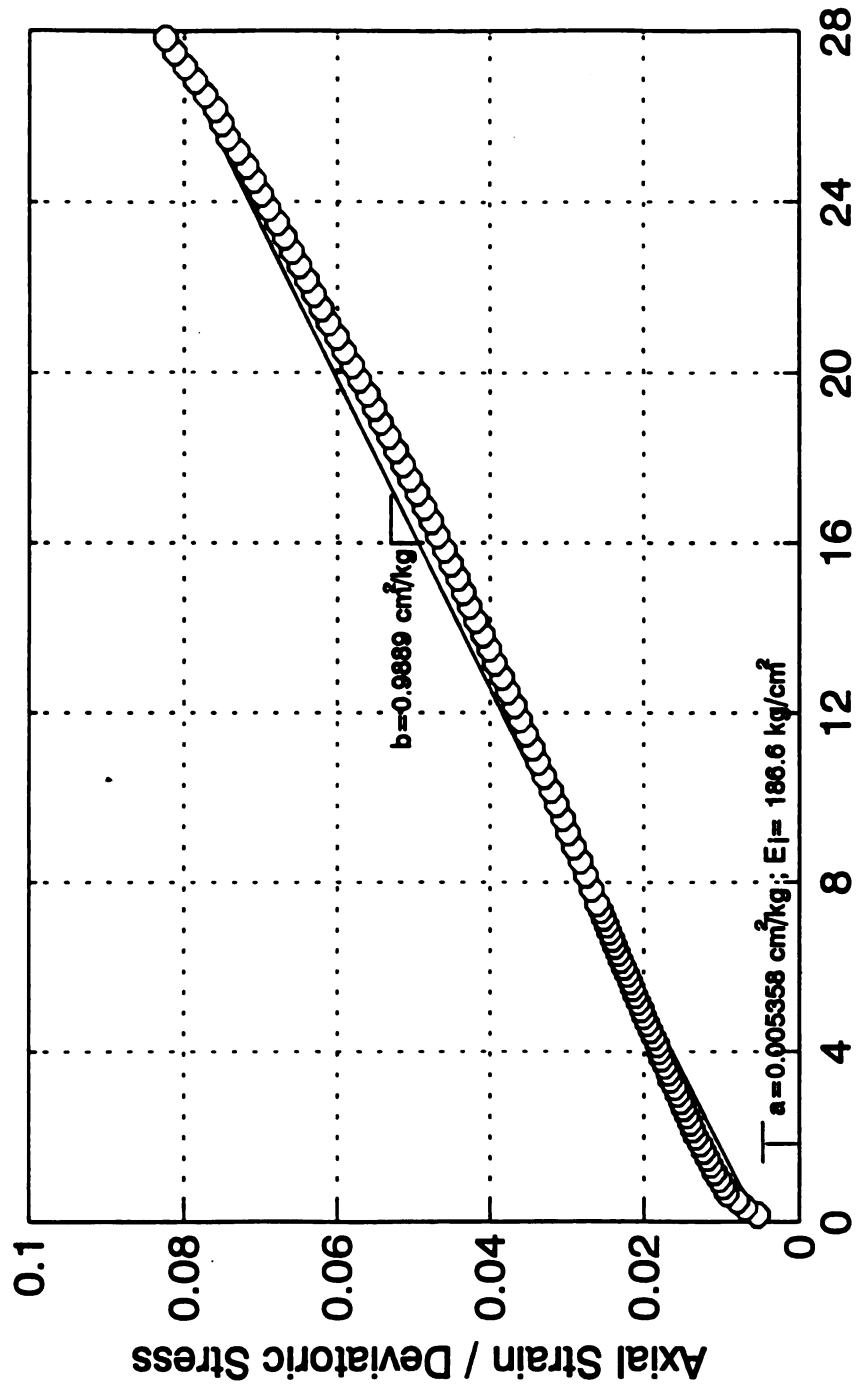

Figure B.7 Normalized stress-strain relationship for dense soil. (Confining pressure 1.4 kg/cm²)

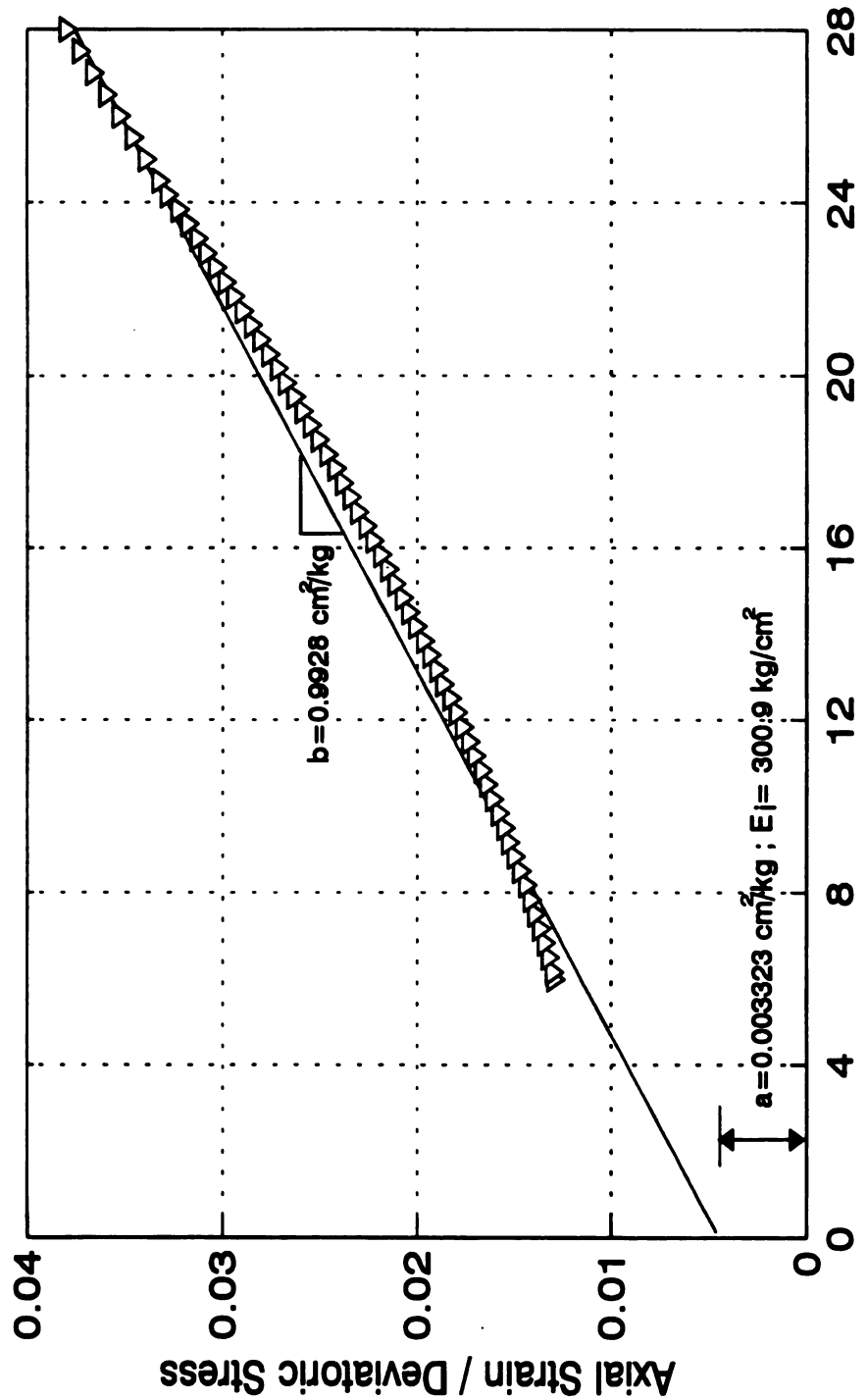

Figure B.8 Normalized stress-strain relationship for dense soil. (Confining pressure 3.5 kg/cm²)

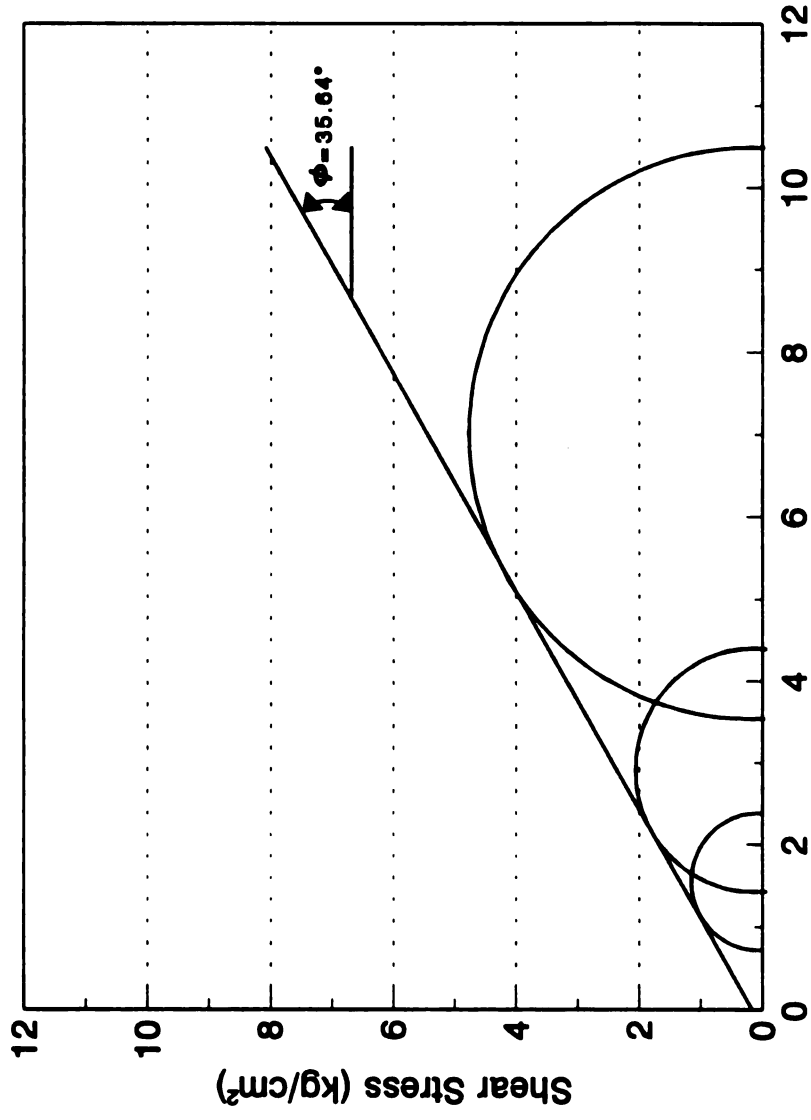

Figure B.9 Mohr circles and angle of internal friction

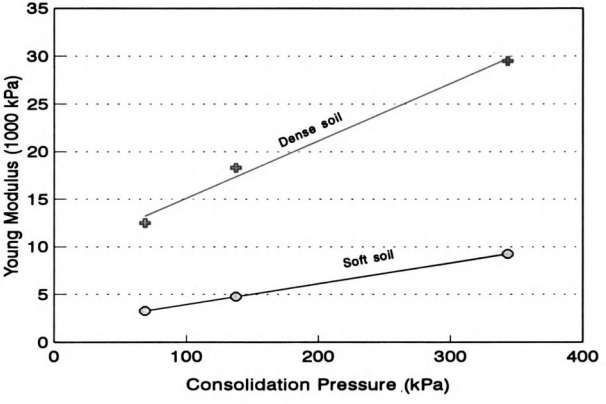

Figure B.10 Youngs Modulus for soft and dense soil as a function of consolidation pressure.

APPENDIX C

APPENDIX C

Table C.1 Measured static stifness values and linear model for 18.4 size tires

Inflation pressure (kPa)	18.4R38	18.4-38
41	137.8	164.8
83	224.1	248.8
110	*	302.9
124	308.4	*
Regration model	Y=53.51+(2.055Ip) r2=99.9	Y=53.51+(2.055Ip) r2=99.9

*:No value obtained by Brassart (1994)

Table C.2 Measured dynamic stifness valuess of 18.4 size tires

Inflation pressure (kPa)	18.4R38	18.4-38
41	216.7	245.4
83	327.0	370.6
110	*	451.2
124	434.6	*

*:No value obtained by Brassart (1994)

Table C.3 Measured static stifness values and linear model for 14.9 size tires

Inflation pressure (kPa)	14.9R30	14.9-30
41	135.0	161.8
83	202.8	224.8
207	402.8	*
221	*	431.8
Regration model	Y=68.87+(1.613Ip) r2=99.9	Y=100.3+(1.5Ip) r2=99.9

*:No value obtained by Brassart (1994)
Y:Stiffness
Ip:Inflation pressure

Dynamic and static stiffness values of 18.4 size tires are not consistent. So that the ratio of approximately 1.15 was used to increase the static stiffness of 18.4-38 tire.

APPENDIX D

APPENDIX D

Table D.1. Goodyear data used to create contact area function.

Overall width (Inc.)	Overall diameter (Inc.)	Maximum load (lbs)	Inflation pressure (psi)	Contact Area ($in.^2$)	Tire type
12.3	43.4	2400	17	134	Radial
14.3	51.6	2830	18	158	Radial
14.3	51.6	3740	30	158	Radial
15.7	49.8	3080	18	172	Radial
15.7	49.8	4180	30	172	Radial
15.7	53.8	3300	18	184	Radial
15.7	53.8	4540	30	184	Radial
15.7	55.8	4680	30	191	Radial
16	61.4	3640	18	205	Radial
18.1	56.5	4080	18	228	Radial
18.1	56.5	4940	24	228	Radial
18.1	58.5	4180	18	233	Radial
18.1	58.5	5080	24	233	Radial
18.1	66.5	4680	18	262	Radial
19.4	61.2	4940	18	276	Radial
19.4	65.2	5360	18	300	Radial
19.4	69.2	5680	18	318	Radial
19.4	69.2	6600	24	318	Radial
19.2	72.1	6950	24	335	Radial
21.4	72.4	6800	18	380	Radial
21.4	72.4	8050	24	380	Radial
21.4	76.4	8550	24	399	Radial
11.5	39.4	2400	24	116	Radial
12.6	44.9	3000	24	142	Radial
13.8	47	3200	24	149	Radial

Table D.1 (Cont'd)

13.8	51	3420	24	158	Radial
13.8	61.3	3960	24	197	Radial
15.4	48.7	3740	24	175	Radial
15.2	52.9	3960	24	184	Radial
15.2	54.9	4080	24	191	Radial
17.6	53.9	4800	24	221	Radial
17.6	56.1	4940	24	228	Radial
17.6	57.9	5080	24	233	Radial
17.6	62	5360	24	261	Radial
17.6	66	5680	24	262	Radial
19.2	56.8	5520	24	262	Radial
19.2	60.8	5840	24	272	Radial
19.2	64.8	6150	24	300	Radial
19.2	68.7	6600	24	318	Radial
21.6	72.2	8050	24	380	Radial
21.6	76.2	8550	24	399	Radial
28.3	63.3	9100	24	423	Radial
28.3	63.3	11400	35	423	Radial
30.1	71.5	12000	24	539	Radial
16.9	52.9	4540	23	229	Radial
19.1	56.1	5520	23	257	Radial
18.9	58.4	7850	35	264	Radial
19.2	62.2	6000	23	308	Radial
23.1	72.2	8550	23	437	Radial
23.3	58.7	7400	23	325	Radial
23.8	62.8	11700	46	374	Radial
24.2	71.4	9650	24	461	Radial
24.2	71.4	12000	35	461	Radial
26.8	72.6	10500	23	494	Radial
28	76	11700	23	490	Radial

Table D.1 (Cont'd)

30.1	64.4	9350	23	476	Radial
30.1	64.4	11700	35	476	Radial
32.2	73.1	12000	23	620	Radial
14.8	52	4400	30	179	Radial
15.2	59.8	4940	30	203	Radial
15.2	71.8	5840	30	240	Radial
17.5	52.7	4680	24	209	Radial
17	54.6	4800	24	221	Radial
19	69.1	5680	18	318	Radial
18.7	73.3	6950	24	335	Radial
19	77.1	8550	30	344	Radial
21.1	68.2	6400	18	358	Radial
21.2	72.2	6800	18	380	Radial
21.2	72.2	8050	24	380	Radial
21.2	76.2	8550	24	399	Radial
24.9	70.9	8250	18	461	Radial
29.8	71.5	9650	18	539	Radial
9.4	29.5	910	26	32	Bias
10.6	31.4	1030	22	42	Bias
10.6	31.4	1330	34	42	Bias
10.6	39.1	1780	34	56	Bias
11.9	33.3	1560	30	55	Bias
11.9	41.3	2070	30	73	Bias
11.9	58.7	2700	30	96	Bias
13.8	35.5	1410	18	71	Bias
13.8	43.4	1860	18	93	Bias
13.8	43.4	2310	26	93	Bias
13.8	41.5	1860	18	93	Bias
13.8	47.4	1990	18	99	Bias
13.8	55.5	2300	18	115	Bias

Table D.1 (Cont'd)

13.8	56.7	2300	18	115	Bias
15.1	45.8	2080	16	117	Bias
15.1	45.8	2640	24	117	Bias
15.1	45.8	3120	32	117	Bias
15.1	49.8	2220	16	125	Bias
12.4	56.9	2500	16	140	Bias
12.4	59.6	3260	24	145	Bias
11.6	63.4	3440	24	152	Bias
11.6	63.4	4640	40	152	Bias
13.9	47.9	2270	14	146	Bias
13.9	47.9	3400	28	146	Bias
13.8	51.9	2420	14	156	Bias
13.8	51.9	3150	22	156	Bias
13.8	51.9	4210	36	156	Bias
13.6	61.6	3660	22	181	Bias
13.9	57.6	2740	14	176	Bias
14.9	49.8	3330	20	150	Bias
14.9	49.8	3330	20	150	Bias
14.9	49.8	3880	26	150	Bias
14.7	48.5	2470	12	150	Bias
14.8	52.5	4520	32	155	Bias
14.9	54.3	2630	12	160	Bias
14.9	54.3	3550	20	160	Bias
14.9	54.3	4670	32	160	Bias
15	52.3	3550	20	160	Bias
14.5	62.7	4120	20	185	Bias
15.6	62.2	3890	20	175	Bias
17.5	52.7	3800	18	190	Bias
17.4	54.8	5080	28	196	Bias
17.3	56.4	4050	18	202	Bias

Table D.1 (Cont'd)

17.4	56.8	5250	28	202	Bias
16.9	58.5	4180	18	209	Bias
16.9	58.5	5420	28	209	Bias
16.5	57.4	4180	18	209	Bias
16.9	62.5	4440	18	222	Bias
16.9	62.5	5750	28	222	Bias
17.1	66.6	4700	18	235	Bias
18.5	44.6	2810	16	158	Bias
19	57.1	4380	16	246	Bias
19	57.1	4380	16	246	Bias
19	57.1	5830	26	246	Bias
18.8	59.1	4530	16	255	Bias
18.9	61.7	4670	16	263	Bias
19.2	60.5	4670	16	263	Bias
18.8	65.4	4960	16	279	Bias
18.8	65.4	5650	20	279	Bias
18.8	65.4	7440	32	279	Bias
19.2	64.5	5650	20	279	Bias

Table D.2 Contact area prediction model and standard error of independent terms.

Model: $A = -0.0446 + (0.139b) + (0.044d) + (0.004F) - (0.00028I_p)$

where: A = Contact area (m^2)
b = Tire width (m)
d = Tire diameter (m)
F = Maximum load (kN)
I_p = Inflation pressure (kN/m^2)

Independent term	Standard error
Tire width	0.035
Tire diameter	0.0085
Maximum load	0.00048
Inflation pressure	0.000046
r^2	97.7

APPENDIX E

APPENDIX E

Table E.1 Lateral and vertical displacements due to various inflation pressures (FE results)

Tire size and cons.	Inflation Pressure (kPa)	Lateral Deflection (mm)	Vertical Deflection (mm)
18.4R38	41	1.62	3.35
	83	3.17	5.94
	97	3.58	6.68
	110	3.96	7.34
	124	4.36	7.97
	207	6.32	11.09
18.4-38	41	0.60	6.01
	83	1.42	10.15
	97	1.70	11.23
	110	1.95	12.15
	124	2.23	13.06
	207	3.83	17.14
14.9R30	41	1.42	1.29
	83	2.00	2.94
	97	2.20	3.42
	110	2.38	3.85
	138	2.74	4.69
	207	3.58	7.03
14.9-30	41	0.30	3.93
	83	0.91	6.85
	97	1.09	7.67
	110	1.24	8.33
	138	1.60	9.65
	207	2.43	12.16

APPENDIX F

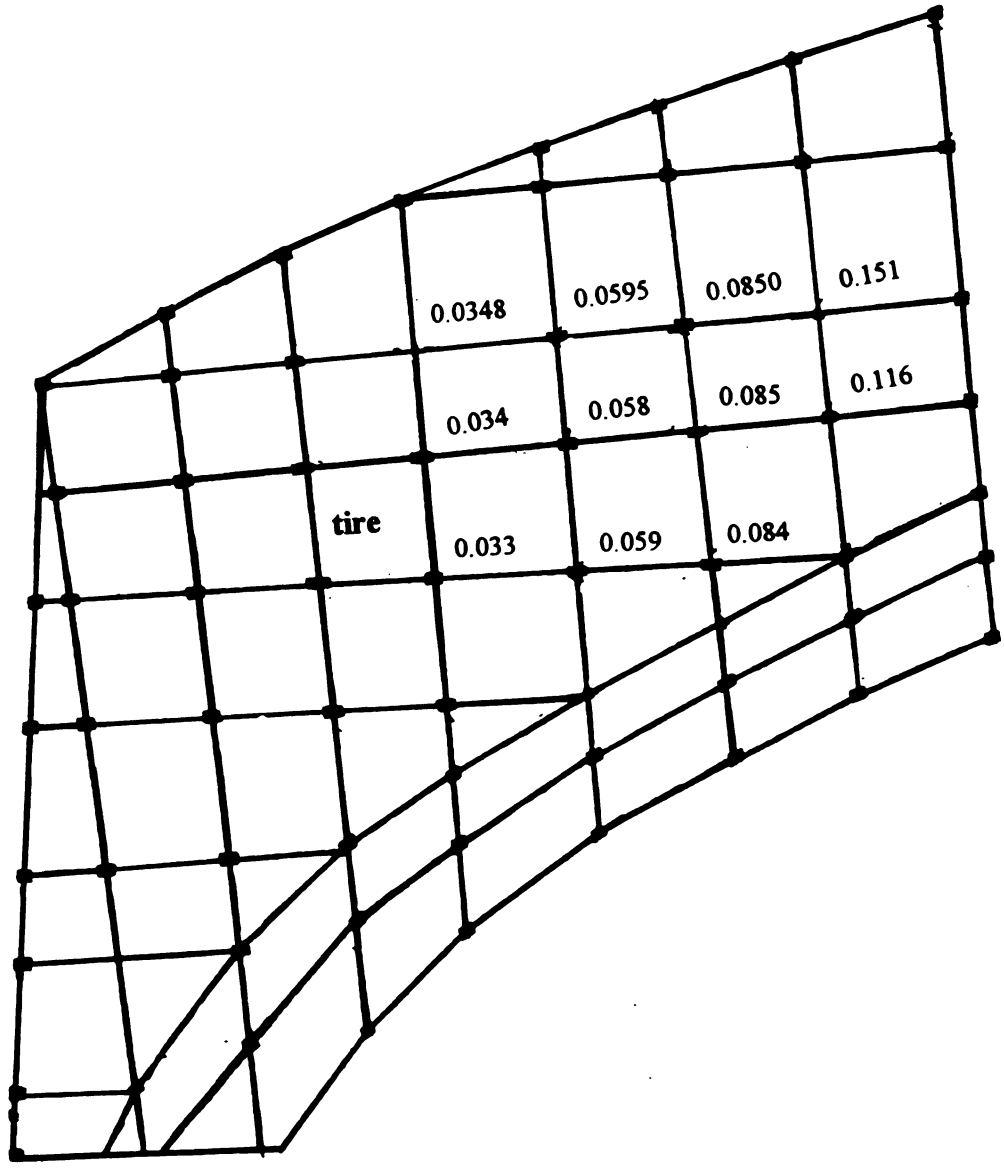

Figure F.1 Example finite element simulation output # 1 from the effect of inflation pressure on vertical tire deformations (Tire:14.9R30, Inflation pressure:83 kPa, deformations are in inches)

A part of tire only, some nodes and data points not shown

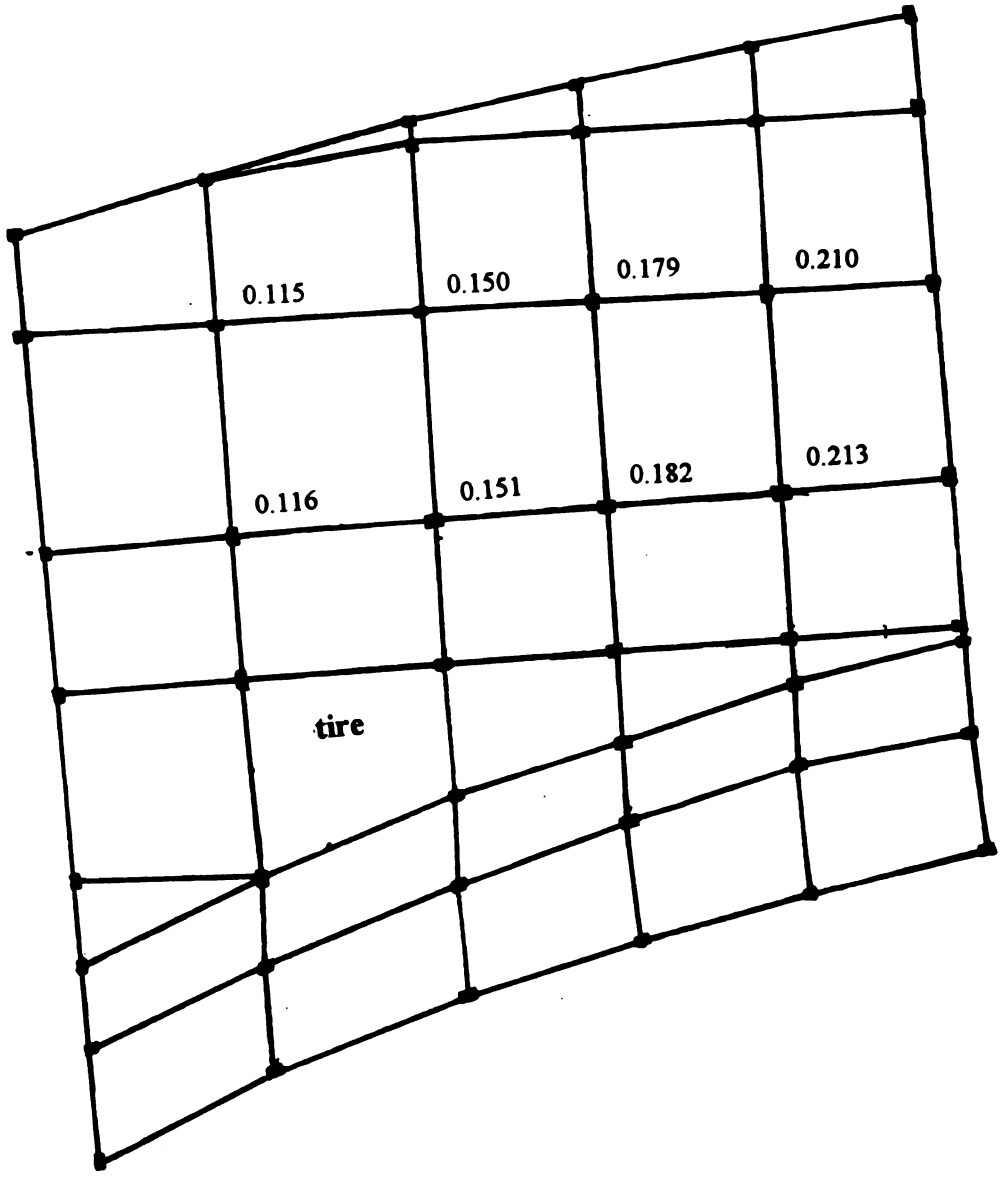

Figure F.2 Example finite element simulation output # 2 from the effect of inflation pressure on vertical tire deformations (Tire: 14.9R30, Inflation pressure: 83 kPa, deformations are in inches)
A part of tire only, some nodes and data points not shown

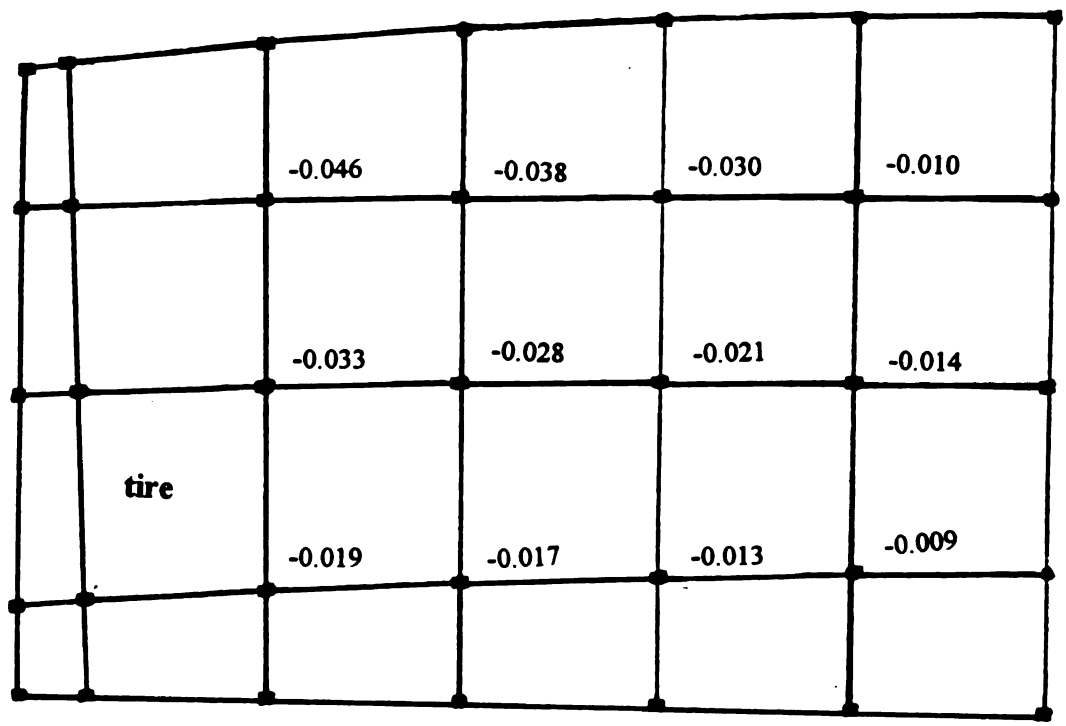

Figure F.3 Example finite element simulation output # 3 from the effect of inflation pressure on vertical tire deformations (Tire: 14.9R30, Inflation pressure: 83 kPa, deformations are in inches)
A part of tire only, some nodes and data points not shown

APPENDIX G

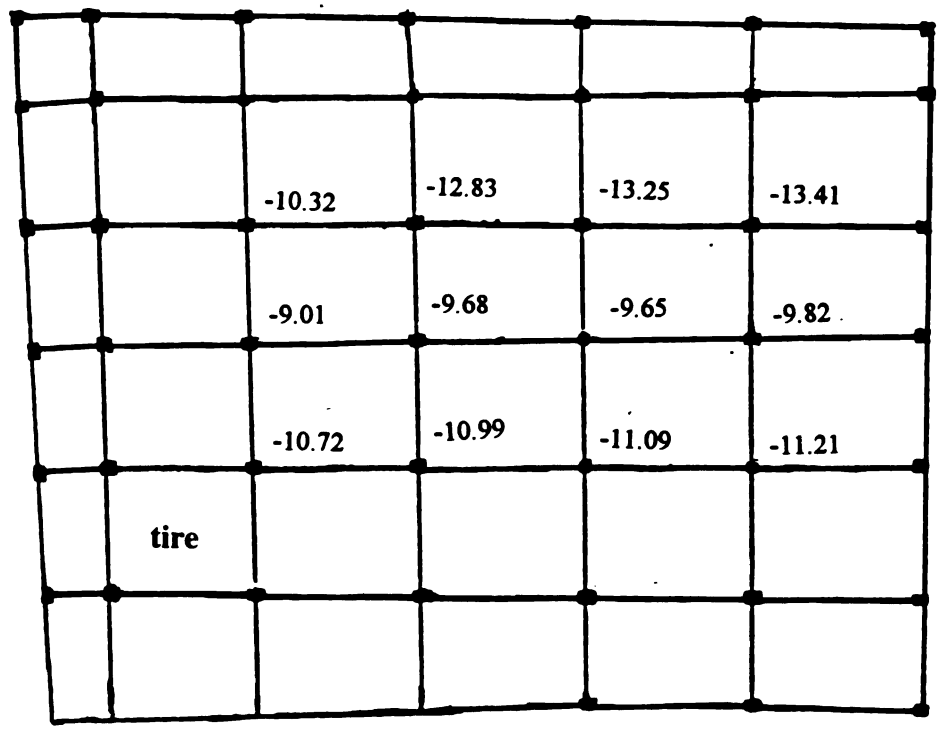

Figure G.1 Example finite element simulation output # 1 of interface pressures from the soil-tire interaction study (Tire: 18.4R38, Load 30 kN, Inflation pressure: 110 kPa; stresses are in psi)
A part of soil and tire only, some nodes and data points not shown

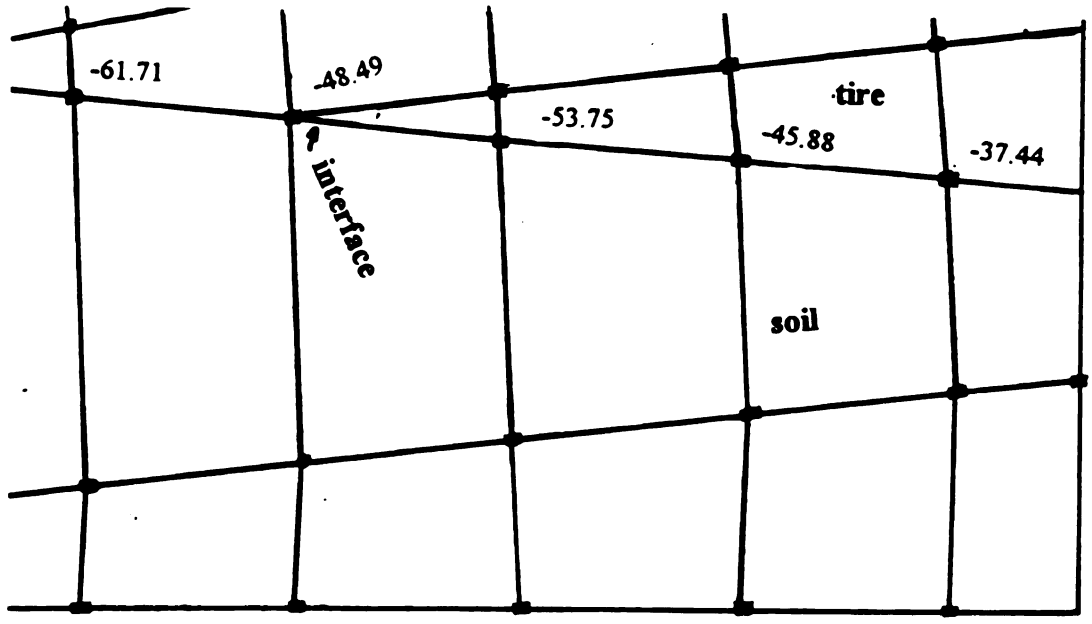

Figure G.2 Example finite element simulation output # 2 of interface pressures from the soil-tire interaction study (Tire: 18.4R38, Load 30 kN, Inflation pressure: 110 kPa; stresses are in psi)

A part of soil and tire only, some nodes and data points not shown

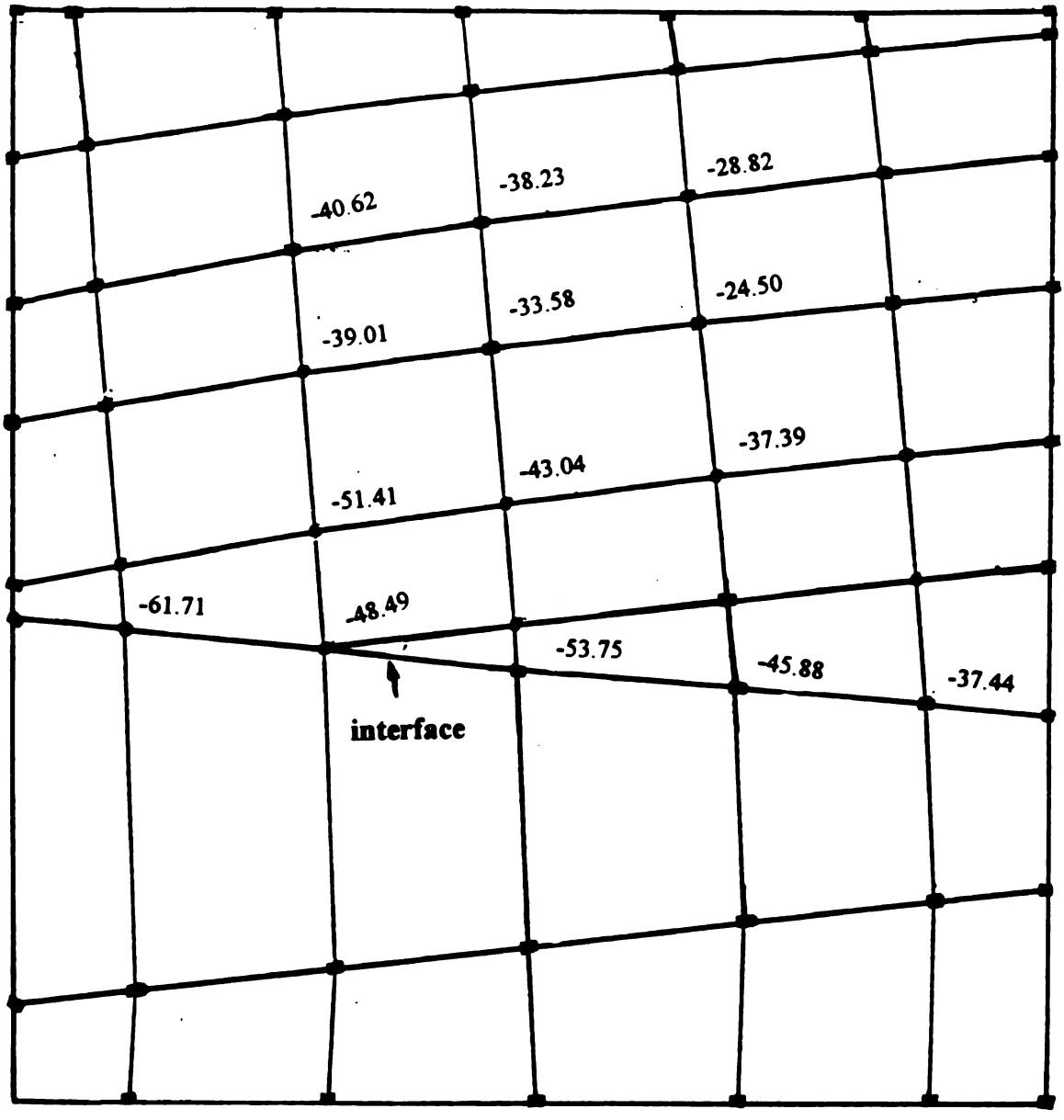

Figure G.3 Example finite element simulation output # 3 of interface pressures from soil-tire interaction study (Tire: 18.4R38, Load 30 kN, Inflation pressure: 110 kPa; stresses are in psi)
A part of soil and tire only, some nodes and data points not shown

APPENDIX H

Table H.1 Int

tire

Load (k
2
4
8
16
20

Table H.2 I

tir

Load
2
4
8
1
2

APPENDIX H

Table H.1 Interface pressures (kPa) averaged over the half of the contact width of 18.4R38 tire on soft soil as a function of inflation pressure and load.

Load (kN)	Inflation Pressure (kPa)		
	83	**97**	**110**
2	75.17	81.52	73.86
4	102.30	116.45	100.3
8	118.70	131.43	143.58
16	196.73	204.32	219.86
20	239.87	251.13	269.70

Table H.2 Interface pressures (kPa) averaged over the half of the contact width of 18.4R38 tire on dense soil as a function of inflation pressure and load.

Load (kN)	Inflation Pressure (kPa)		
	83	**97**	**110**
2	77.24	104.23	142.40
4	116.45	139.51	172.57
8	137.23	176.57	189.28
16	215.78	271.97	250.64
20	252.99	318.64	279.84

Table H.3 Interface pressures (kPa) averaged over the half of the contact width of 18.4-38 tire on soft soil as a function of inflation pressure and load.

Load (kN)	Inflation Pressure (kPa)		
	83	97	110
2	93.60	101.95	146.61
4	141.23	136.05	181.34
8	187.75	190.52	188.45
16	190.52	210.08	209.36
20	209.36	228.28	246.16

Table H.4 Interface pressures (kPa) averaged over the half of the contact width of 18.4-38 tire on dense soil as a function of inflation pressure and load.

Load (kN)	Inflation Pressure (kPa)		
	83	97	110
2	142.20	155.17	158.49
4	175.47	193.49	208.26
8	221.37	219.44	243.39
16	281.71	290.27	312.84
20	284.88	297.51	349.70

Table H.5 Interface pressures (kPa) averaged over the half of the contact width of 14.9R3 tire on soft soil as a function of inflation pressure and load.

Load (kN)	Inflation Pressure (kPa)		
	83	**97**	**138**
2	69.65	98.50	105.96
4	148.55	179.82	189.34
8	199.28	200.73	214.20
16	209.36	245.81	253.82
20	276.94	273.84	300.48

Table H.6 Interface pressures (kPa) averaged over the half of the contact width of 14.9R3 tire on dense soil as a function of inflation pressure and load.

Load (kN)	Inflation Pressure (kPa)		
	83	**97**	**138**
2	142.27	181.75	203.15
4	182.44	193.90	214.13
8	214.20	234.84	258.24
16	230.97	266.66	277.36
20	257.55	283.85	291.99

Table H.7 Interface pressures (kPa) averaged over the half of the contact width of 14.9-30 tire on soft soil as a function of inflation pressure and load.

Load (kN)	Inflation Pressure (kPa)		
	83	97	138
2	92.43	121.97	127.91
4	106.16	168.98	209.92
8	135.29	196.32	246.57
16	170.57	207.91	252.02
20	193.35	232.21	222.00

Table H.8 Interface pressures (kPa) averaged over the half of the contact width of 14.9-30 tire on dense soil as a function of inflation pressure and load.

Load (kN)	Inflation Pressure (kPa)		
	83	97	138
2	143.78	145.99	214.95
4	173.47	191.07	235.80
8	188.65	201.08	256.65
16	249.33	270.32	301.73
20	280.95	301.17	304.90

APPENDIX I

APPENDIX I

Explanation for the sample traction data

Plot ID: 217H11
Slip: 15%
Inflation pressure: 83 kPa
Tire: 18.4-38

APPENDIX I

Table I.1 Sample traction data

Case #	NL	TOR	IPR	VEL
	(kN)	(kN-m)	(kPa)	(m/s)
1	2.132	0.8876	82.45	0.1502
2	2.969	0.8876	83.27	0.1484
3	2.969	1.004	82.65	0.15
4	2.272	0.7416	83.47	0.154
5	2.585	1.345	82.65	0.1508
6	2.725	0.9946	83.06	0.1552
7	3.038	1.248	83.68	0.1554
8	3.282	1.17	83.27	0.156
9	3.561	1.218	82.86	0.1538
10	3.666	1.257	83.88	0.1514
11	3.875	1.053	83.88	0.151
12	3.91	1.52	82.65	0.1514
13	4.084	1.52	83.47	0.1492
14	4.397	1.316	82.24	0.1516
15	4.746	0.8973	83.47	0.1522
16	4.955	1.588	84.3	0.153
17	4.99	1.472	82.86	0.1514
18	4.816	1.695	83.88	0.1486
19	4.781	1.656	84.09	0.1532
20	4.85	1.588	83.68	0.1508
21	5.582	1.958	83.47	0.1508
22	5.443	2.124	83.47	0.1516
23	5.617	2.104	83.47	0.1516
24	5.756	1.715	83.06	0.1516
25	6.035	2.163	83.06	0.1462

Table L1 (Cont'd)

26	5.059	2.163	83.27	0.1446
27	5.896	2.201	83.88	0.1442
28	6.558	2.172	83.47	0.143
29	6.732	2.279	83.68	0.1448
30	6.767	2.221	83.27	0.1464
31	7.429	2.104	83.47	0.1516
32	7.464	2.075	83.88	0.1532
33	7.255	2.396	82.86	0.1464
34	7.394	2.406	83.06	0.15
35	7.429	2.406	82.65	0.15
36	7.812	2.435	82.86	0.1492
37	8.544	2.883	83.47	0.1502
38	8.509	3.077	83.47	0.1472
39	8.544	2.892	83.47	0.1494
40	8.927	2.98	83.47	0.1492
41	9.101	2.737	83.88	0.147
42	8.823	2.854	83.47	0.1464
43	8.753	3.272	83.47	0.1486
44	9.171	3.301	82.86	0.1478
45	9.589	3.515	83.06	0.1492
46	10.01	3.301	83.88	0.1508
47	10.7	3.486	83.68	0.1532
48	11.05	3.661	84.09	0.151
49	10.95	3.759	83.68	0.1492
50	10.56	3.515	83.06	0.151
51	11.12	2.941	83.68	0.1478
52	10.74	3.895	83.47	0.1478
53	10.98	4.177	83.27	0.1462
54	11.47	3.311	82.86	0.153

Table L1 (Cont'd)

55	11.75	3.953	83.68	0.1524
56	12.13	4.216	83.47	0.1502
57	12.17	4.469	83.27	0.1472
58	12.17	4.45	83.47	0.15
59	11.82	4.586	83.47	0.1472
60	11.47	4.43	83.47	0.1456
61	12.38	4.294	83.27	0.1454
62	12.73	4.654	83.27	0.1484
63	12.62	4.858	83.47	0.1484
64	12.83	4.965	83.88	0.1478
65	13	4.148	83.88	0.1512
66	13.21	4.693	83.68	0.1524
67	12.79	5.034	83.68	0.1522
68	12.86	4.927	83.88	0.1502
69	13.74	4.956	83.68	0.1502
70	14.08	5.092	83.68	0.1532
71	13.98	5.18	83.88	0.1514
72	14.36	5.452	82.86	0.1508
73	14.78	5.472	83.68	0.1538
74	14.64	5.403	83.27	0.1558
75	14.61	5.52	83.47	0.1538
76	14.85	5.656	83.27	0.1548
77	14.75	5.15	83.27	0.1516
78	15.06	5.666	83.27	0.1522
79	15.44	5.374	83.47	0.1508
80	15.76	5.929	83.27	0.1486
81	15.51	5.695	83.06	0.1492
82	16.49	5.588	83.27	0.15
83	16.04	5.705	83.27	0.1462

Table L1 (Cont'd)

84	15.65	5.929	82.86	0.1484
85	16.77	6.133	83.47	0.148
86	16.98	6.055	83.27	0.1472
87	17.39	6.562	83.27	0.1488
88	16.63	6.474	83.47	0.1484
89	17.32	6.416	83.68	0.1508
90	17.32	6.201	83.27	0.1462
91	17.01	6.406	83.68	0.1462
92	17.53	6.523	83.88	0.1446
93	18.16	6.883	83.06	0.147
94	18.51	6.678	83.88	0.1478
95	18.75	6.922	82.65	0.1516
96	18.79	7.165	83.27	0.1532
97	18.72	6.805	82.86	0.1486
98	18.75	6.795	83.27	0.147
99	19.17	6.824	83.27	0.1456
100	19.31	7.136	82.86	0.1448
101	18.72	7.087	83.47	0.1502
102	19.62	7.564	83.68	0.15
103	20.08	7.184	83.27	0.15
104	19.97	7.418	84.3	0.1478
105	20.18	7.408	83.47	0.1464
106	20.29	7.613	83.88	0.1442
107	19.8	7.535	83.47	0.142
108	20.04	7.768	83.27	0.1446
109	20.95	7.846	83.06	0.1464
110	21.19	7.681	83.06	0.147
111	20.95	7.7	84.09	0.1508
112	21.47	7.992	83.27	0.153

Table L1 (Cont'd)

113	21.65	7.593	83.06	0.1546
114	21.37	7.788	83.68	0.151
115	21.44	7.856	83.88	0.151
116	21.99	8.401	83.88	0.1526
117	22.1	7.778	83.06	0.1522
118	22.31	7.759	84.3	0.151
119	22.55	7.613	84.3	0.1508
120	22.76	7.905	84.3	0.1514
121	22.59	8.381	83.27	0.153
122	22.52	8.177	83.47	0.153
123	23.11	8.469	82.86	0.1516
124	23.21	8.245	83.68	0.1516
125	23.14	8.547	83.27	0.1522
126	23.74	8.576	83.68	0.1502
127	23.88	8.907	83.68	0.1494
128	23.63	7.973	84.91	0.1522
129	23.95	9.131	84.3	0.153
130	23.74	8.596	83.06	0.1508
131	24.05	9.014	83.68	0.1502
132	24.01	8.888	83.27	0.1528
133	24.99	8.051	83.47	0.15
134	24.99	9.15	83.68	0.1462
135	24.78	8.956	83.88	0.1472
136	25.65	9.52	83.06	0.1464
137	25.69	9.209	83.47	0.147
138	25.41	8.547	84.5	0.1448
139	25.23	9.423	83.88	0.147
140	25.62	9.812	83.27	0.1486
141	26.31	9.948	83.68	0.1478

Table L1 (Cont'd)

142	26.38	9.715	84.09	0.147
143	26.38	9.656	82.65	0.15
144	26.66	10.02	83.27	0.1478
145	26.73	10.12	83.88	0.1464
146	26.52	10.03	83.47	0.148
147	27.15	10.06	83.68	0.151
148	27.36	10.76	82.86	0.1486
149	28.02	10.28	83.88	0.145
150	27.81	10.34	83.88	0.1478
151	27.95	10.7	83.47	0.1508
152	27.92	10.35	83.27	0.151
153	28.54	10.61	83.47	0.1492
154	28.68	10.65	83.47	0.1532
155	29.03	10.77	83.88	0.1518
156	29.1	10.68	83.88	0.153
157	29.1	10.62	83.88	0.154
158	29.38	11.13	83.27	0.1508
159	29.69	10.84	82.86	0.1508
160	29.1	10.83	83.68	0.1486
161	29.52	10.87	83.68	0.1454
162	29.66	10.71	83.68	0.1464
163	29.76	10.96	84.5	0.1486
164	30.57	11.53	84.5	0.1486
165	30.77	11.18	83.88	0.15
166	30.36	11.23	83.68	0.1508
167	30.01	11.41	83.47	0.1508
168	30.64	11.11	83.27	0.147
169	31.09	11.68	83.27	0.1446

Table L1 (Cont'd)

Case #	DL (kN)	NT (kN)	TE
1	1.741	0.7917	0.6833
2	2.432	0.6869	0.5781
3	2.529	1.035	0.7218
4	1.74	1.682	1.795
5	2.16	1.248	0.6795
6	2.43	1.151	0.9379
7	2.62	1.334	0.7937
8	2.6	0.8054	0.5305
9	2.797	1.409	0.8613
10	2.863	0.9651	0.5716
11	2.999	1.023	0.7298
12	3.151	1.69	0.804
13	3.129	1.272	0.6196
14	3.676	1.458	0.8047
15	3.54	1.48	1.299
16	3.656	1.41	0.6968
17	4.131	1.446	0.7478
18	3.195	1.408	0.5707
19	3.474	1.827	0.8506
20	3.353	1.491	0.7144
21	4.083	1.77	0.6511
22	4.158	1.929	0.6774
23	4.122	1.97	0.6798
24	4.525	2.087	0.9288
25	4.631	2.197	0.7287
26	3.836	2.158	0.7631
27	4.436	2.297	0.7259

Table L.1 (Cont'd)

28	4.952	2.02	0.6906
29	5.018	2.447	0.7427
30	5.397	2.742	0.9645
31	5.726	2.423	0.9061
32	5.652	2.187	0.8394
33	5.568	2.75	0.8337
34	5.921	2.751	0.8498
35	6.049	2.485	0.7777
36	6.168	2.902	0.8518
37	6.627	2.747	0.7333
38	6.422	3.351	0.783
39	6.346	3.343	0.8769
40	6.904	3.121	0.8006
41	7.103	3.053	0.829
42	6.938	3.053	0.7771
43	6.562	3.034	0.6702
44	7.074	3.173	0.712
45	7.534	3.165	0.6572
46	7.809	3.386	0.7662
47	8.385	3.63	0.7813
48	8.447	3.669	0.7561
49	8.332	3.579	0.69
50	8.167	3.668	0.7674
51	9.097	3.675	0.9162
52	8.222	4.233	0.7632
53	8.611	4.106	0.7121
54	8.854	4.511	0.9944
55	9.318	3.941	0.7298
56	9.441	4.651	0.8425

Table L1 (Cont'd)

57	9.184	4.664	0.7411
58	9.292	4.811	0.7381
59	9.052	4.851	0.7715
60	8.767	4.713	0.7221
61	9.644	4.835	0.8683
62	9.84	4.654	0.7148
63	9.745	4.883	0.7813
64	9.766	5.064	0.72
65	9.979	4.911	0.8844
66	9.962	5.229	0.8401
67	9.595	5.132	0.7777
68	9.959	5.538	0.7788
69	10.67	5.191	0.7919
70	10.81	5.608	0.8093
71	10.78	5.015	0.7241
72	10.99	5.459	0.7324
73	11.27	5.559	0.7485
74	11.25	6.057	0.847
75	11.22	5.864	0.7913
76	11.36	5.456	0.7143
77	11.4	5.607	0.8284
78	11.65	6.152	0.7808
79	12.26	5.718	0.8019
80	12.67	5.908	0.6969
81	11.97	5.984	0.7468
82	12.69	6.346	0.8148
83	12.14	6.382	0.7867
84	11.9	6.013	0.7619
85	12.92	6.513	0.7477

Table L1 (Cont'd)

86	13.3	6.603	0.7786
87	13.26	6.909	0.7383
88	12.77	6.592	0.73
89	13.37	6.722	0.7456
90	13.28	6.692	0.7828
91	13.12	6.522	0.7396
92	13.26	6.711	0.704
93	13.85	6.627	0.6856
94	14.25	6.961	0.7504
95	14.15	6.921	0.7708
96	14.44	6.991	0.6107
97	14.84	6.323	0.7311
98	14.61	7.117	0.7672
99	15.02	6.789	0.7157
100	15.01	7.195	0.6779
101	14.48	7.951	0.8231
102	14.91	8.023	0.7761
103	15.62	7.672	0.7781
104	15.49	7.298	0.7174
105	15.82	7.865	0.7325
106	15.53	7.432	0.6858
107	15.44	7.906	0.7178
108	15.31	7.424	0.6548
109	16.11	8.024	0.7407
110	16.29	8.106	0.7412
111	16.23	7.631	0.7759
112	16.51	8.315	0.7614
113	16.83	7.609	0.7697
114	16.87	7.939	0.7293

Table L1 (Cont'd)

115	16.67	8.027	0.7116
116	17.2	8.386	0.6861
117	17.33	8.146	0.7764
118	17.41	8.16	0.8005
119	17.59	7.96	0.7627
120	17.53	8.306	0.7516
121	17.35	8.951	0.6844
122	17.27	8.436	0.7448
123	18.05	8.683	0.7149
124	18.26	8.686	0.7957
125	18.21	8.903	0.715
126	18.3	9.169	0.7608
127	18.61	9.232	0.7003
128	18.11	9.179	0.8898
129	18.4	9.214	0.713
130	18.7	9.072	0.7785
131	18.56	9.352	0.7343
132	18.62	9.57	0.7947
133	19.64	9.183	0.8185
134	19.63	9.343	0.6786
135	19.32	9.634	0.7845
136	19.88	9.819	0.7011
137	19.89	9.561	0.7241
138	19.55	9.772	0.7953
139	19.63	9.808	0.7724
140	19.99	9.9	0.7334
141	20.67	10.33	0.703
142	20.46	10.28	0.6981
143	20.6	10.17	0.802

Table L1 (Cont'd)

144	20.8	10.18	0.6955
145	21.01	10.29	0.7147
146	20.48	10.74	0.7158
147	21.35	10.85	0.8127
148	20.85	10.93	0.6911
149	21.77	10.86	0.7444
150	21.64	11.26	0.7751
151	22.19	10.59	0.6173
152	22.04	10.39	0.7375
153	22.25	11.08	0.7305
154	22.5	10.39	0.7167
155	22.5	10.96	0.7294
156	22.77	10.91	0.7714
157	22.94	10.9	0.7233
158	22.73	11.16	0.6533
159	23.34	11.1	0.6891
160	22.75	11.16	0.6728
161	22.99	11.15	0.6817
162	23	11.6	0.7454
163	23.09	10.91	0.746
164	23.21	11.01	0.6495
165	23.71	12.06	0.734
166	23.66	11.64	0.7041
167	23.03	11.28	0.7256
168	24.08	11.65	0.7122
169	24.27	11.15	0.6586

LIST OF REFERENCES

Abeels, P.F.J. 1976. Tire deflection and contact studies. Journal of Terramechanics 13(3):183-196, ISTVS, Hoboken, NJ.

Ali, O.S. ,McKyes.1978. Traction characteristics of lug for tires. Transactions of the ASAE 21-231-243, 248. St Joseph, MI 49085.

Al-Hamed, S.A., R.D. Grisso, F.M. Zoz and K. Von Bargen. 1990. Tractor performance spreadsheet for radial tires. ASAE Paper No. 90-1576. ASAE, St Joseph, MI 49085.

ASAE. 1994. ASAE Standard: ASAE S296.3. Uniform terminology for traction of agricultural tractors, self propelled implements, and other traction and transport devices. ASAE Standard 1994, pp 141-143. ASAE, St. Joseph, MI 49085.

Bashford, L.L., S. Al-Hamed, C. Jenane. 1992. Effects of tire size and pressure on tractive performance. ASAE Paper No. 92-1011. ASAE, St Joseph, MI 49085.

Bekker, M.G. 1956. Theory of land locomotion. The University of Michigan Press.

Bekker, M.G. 1960. Off-the-road locomotion. Research and developments in Terramechanics. The University of Michigan Press. Ann Arbor, MI.

Bekker, M.G. 1969. Introduction to terrain-vehicle systems. The University of Michigan Press. Ann Arbor, MI.

Brassart, F.P. 1994. Traction and Agricultural Tractor Tire Selection Studies. Unpublished PhD. Thesis, Louisiana State University.

Brixius, W.W., R.D. Wismer. 1978. The role of slip in traction. ASAE Paper No. 78-1538. ASAE, St Joseph, MI 49085.

Brixius, W.W. 1987. Traction prediction equations for bias-ply tires. ASAE Paper No. 87-1622. ASAE. St Joseph, MI 49085.

Burt, E.C., A.C. Bailey, R.M. Patterson and J.H. Taylor. 1979. Combined effects of dynamic load and travel reduction on tire performance. Transactions of the ASAE 22(1): 40-45, St.Joseph, MI 49085.

Burt, E.C., C.A. Reaves, A.C.Bailey, W.D. Pickering. 1980. A machine for testing tractor tires in soil bins. Transactions of the ASAE 23(3):546-547, 552.

Burt E.C., A.C. Bailey. 1982. Load and inflation pressure effects on tires. Transactions of the ASAE. St Joseph, MI 49085.

Chesness, J.L., E.E.Ruiz and C. Cobb. 1970. Quantitative description of soil compaction in peach orchards utilizing a portable penetrometer. Transactions of the ASAE 15(2):217-219, St Joseph, MI 49085.

Clarck, R.L. 1984. Tractive modeling and field data requirements to predict traction. ASAE Paper No. 84-1055. ASAE. St Joseph, MI 49085

Duncan, J.M., C.Y. Chang. 1970. Non-linear analysis of stress and strain in soils. J. Soil. Mech and Foundations Div. Proc. of American Society of Civil Eng. 96(5):1629-1653.

Dwyer, M.J. 1978. Maximising agricultural tractor performance by matching weight, tire size and speed to the power available. Proceedings of the Sixth International Conference of ISTVS, ISTVS, Hoboken, NJ 07030.

Evans, M.D., R.L. Clarck, G. Manor. 1989. A traction prediction and ballast selection model. ASAE Paper No. 89-1054. ASAE. St Joseph, MI 49085.

Faria, L.O., J.M. Bass, J.T. Oden, E.B. Becker. 1989. A three-dimensional rolling contact model for a Reinforced Rubber Tire. Tire Science & Technology, Vol.17, 217-233.

Forrest, P.J., I.F. Reed and G.V. Constantakis. 1962. Tractive Characteristics of Radial-Ply Tires. The Transactions of the ASAE. Vol.5, 108-115.

Gee-Clough, D., M. McAllister, G. Pearson, D.W. Evernden. 1978. The empirical prediction of tractor-implement field performance. Journal of Terramechanics 15(2):81-94. ISTVS, Hoboken, NJ 07030.

Gee-Clough, D., G. Pearson, M. McAllister. 1982. Ballasting wheeled tractors to achieve maximum power output in frictional-cohesive soils. Journal of Agricultural Engineering Research 27(1):1-19. NIAE, Silsoe, England.

Gill, W.R. and G.E. Vanden Berg. 1968. Soil dynamics in tillage and traction. Agricultural Handbook No. 316, ARS, United States Department of Agriculture.

Godbole, R., R.L. Alcock. 1992. A new approach to the traction prediction equation. ASAE Paper No. SD92-111. ASAE. St Joseph, MI 49085.

Gu, Y., R.L. Kushwaha. 1992. Dynamic load distribution and tractive performance of a model tractor. ASAE Paper No. 92-1018. ASAE. St Joseph, MI 49085.

Hu, Y.K., P.F.J. Abeels. 1994a. The Deformation of Agricultural Tire on Rigid Surface by FEM, ASAE Paper No: 94-1043. St. Joseph, Michigan,ASAE.

Hu, Y.K., P.F.J. Abeels. 1994b. Agricultural Tire Deformations in the 2D case by Finite Element methods. Journal of Terramechanics, 31(6):353-370, ISTVS, Great Britain.

International Petrolium Istatistics Report. DOE/EIA. 1995. United States Department of Energy.

Janosi, Z., B. Hanomoto. 961. An analysis of the pull vs slip relationship for track laying vehicles. report #69. Land Locomotion Laboratory. Michigan.

Kaga, H., K. Okamoto., Y. Tozawa. 1977. Stress Analysis of a Tire Under Vertical Load by a Finite Element Method. Tire Science & Technology, Vol. 29, 45-50.

Karafiath, L.L., E.A. Nowatzki. 1978. Soil Mechanics for off-road vehicle engineering. Trans. Tech. Publication. CH-4711, Aedemanssdorf, Switzerland. 515 pp.

Leviticus, L.I., J.F. Reyes. 1983. Tractor performance on concrete, dynamic ratio and tractive quotient.. ASAE paper No: 83-1558. St Joseph, MI 49085.

Macnab, J.E., R.B. Wensink, D.E. Booster. 1977. Modeling wheel tractor energy requirements and tractive performances. Transactions of the ASAE 20(4): 602-605, 609. ASAE. St Joseph, MI 49085.

Marc user's manual. 1996. Marc Analysis Research Coorporation. 260, Palo Alto, Ca 94306.

McRae, J.L. 1967. Theory for a powered wheel in soil. Journal of Terramechanics 4(3):31-43.

Mstat, Crop and soil sciences department, Michigan State University, E.Lansing, MI 48824

Pollock,D.Jr., J.V. perumpral, T. Kuppusamy. 1986. Finite Element analysis of multipass effecs of vehicles on soil compaction. Transactions of the ASAE 29(1):45-50. ASAE, St joseph, MI 49085.

Ramp, D.P., J.C. Siemens. 1990. Tractor/implement matching for performance and productivity. ASAE Paper No. 90-1562. ASAE. St Joseph, MI 49085.

Ridha, R.A. 1980. Computation of Stresses, Strains and Deformations of Tires. Rubber Chemistry and Technology, Vol.53, 849-902.

Rodhert,H., H.Idelberger., W.Jacobi., G. Laging. 1985. On the Contact Problem of Tires Including Friction. Tire Science & Technology, Vol. 13, 111-123.

Schafer, R.L. C.E. Johnson, A.J. Koolen, S.C. Gupta, R. Horn. 1992. Future research needs in soil compaction. Transactions of the ASAE 35(6): 1761-1770. ASAE. St Joseph, MI 49085.

Chofiled, A.N., P.Wroth. 1968. Critical state soil mechanics, McGraw-Hill, New York, N.Y. 310 pages.

Self, K.P., J.D. Summers. 1988. Dynamic load and wheel speed ratio effects on four-wheel drive tractive performance. ASAE Paper No. 88-1516. ASAE. St Joseph, MI 49085.

Srivastava, A.K., C.E. Goering, R.P. Rochrbach. 1993. Engineering principles of agricultural machinery. Published by the ASAE, 600 pp. ASAE, St Joseph, MI 49085.

Taylor, J.H., E.C. Burt, A.C. Bailey. 1976. Radial tire performance in firm and soft soil. Transactions of the ASAE. 1062-1064. ASAE. St Joseph, MI 49085.

Taylor, J.H., A.C. Trouse, E.C. Burt, A.C. Bailey. 1982. Multipass behavior of a pneumatic tire in tilled soils. Transactions of the ASAE 25(5):1229-1231, 1236. ASAE. St Joseph, MI 49085.

Trabbic, G.W., K.V. Lask, W.F. Buchele. 1959. Measurement of Soil-Tire Interface Pressures. Agricultural Engineering, 40(11):678-681.

Turner, R.J. 1993. A simple system for determining tractive performance in the field. ASAE Paper No. 93-1574. ASAE. St Joseph, MI 49085.

Upadhyaya, S.K., D. Wulfsohn., G. Jubbal. 1987. Traction prediction equations for radial ply tires. ASAE Paper No. 87-1625. ASAE. St. Joseph, MI 49085.

Upadhyaya, S.K., D. Wulfsohn., G. Jubbal. 1989. Traction prediction equations for radial ply tires. Journal of Terramechanics 26(2):149-175. ISTVS, Hoboken, NJ 07030.

Upadhyaya, S.K., D. Wulfsohn. 1990. Relationship between Tire Deflection Characteristics and 2-D Tire Contact Area. American Society of Agricultural Engineers, Vol.33 (1), 25-30

Vandenberg, G.E., W.R.Gill 1962. Pressure distribution between a smooth tire and soil. Transactions of the ASAE 5(2): 105-107.

Vesic,A. 1967. Bearing capacity and settlement of foundation proceedings of a syposium. Duke University, Durham.NC.

Vesic,A. 1975. Foundation engineering handbook. Reinhold company.

VandenBerg, G.E., I.F. Reed. 1962. Tractive Performance of radial-ply and conventional tractor tires. Transactions of the ASAE. 126-129, 132. ASAE. St Joseph, MI 49085.

Way, T.R., E.C. Burt, A.C. Bailey, R.L. Raper. 1993. Tire-lug height effect on soil-tire interface pressures. ASAE Paper No: 93-1518. ASAE, St Joseph, MI 49085.

Wismer, R.D., H.J.Luth. 1974. Off-road traction prediction for wheeled vehicles. Transactions of the ASAE 17(1):8-10,14. ASAE. St Joseph, MI 49085.

Wittig, V., R. Alcock. 1990. An empirical method of predicting traction. ASAE Paper No. 90-1570. ASAE. St Joseph, MI 49085.

Wong, J.Y., A.R. Reece. 1966. Soil failure beneath rigid wheels. Proceedings of the Second International Conference of ISTVS, ISTVS, Hoboken, NJ 07030.

Wong, G. and G.G. Zoerb. 1988. Inderect determination of tractive efficieny, ASAE Paper No: 88-1517. ASAE St Joseph, MI 49085.

Wood, R.K., E.C. Burt and C.E. Johnson. 1988. Thrust-dynamic load relationship for a pneumatic drive tire. ASAE Paper No. 88-1642. ASAE. St Joseph, MI 49085.

Wulfsohn, D.1987. Tractive characteristics of radial ply and bias ply tires in a California soil. M.S. thesis, Dept. of Agr. Eng., University of California, Davis.

Wu, T.H. 1976. Soil mechanics, Allyn and Bacon Inc. Boston, Mass.

Yong, R.N., E.A. Fattah., P.Boonsinsuk. 1978. Analysis and Prediction of Tire-Soil Interaction and Performance Using Finite Elements. Journal of Terracmechanics, Vol.15, 43-61.

Zoz, F.M. 1987. Predicting tractor field performance (updated). ASAE Paper No. 87-1623. ASAE. St Joseph, MI 49085.